Glacimarine sedimentary processes and products at fjord-terminating tidewater glacier margins

STREUFF, KATHARINA,TERESA

Glacimarine sedimentary processes and products at fjord-terminating tidewater glacier margins

Katharina Teresa Streuff

A thesis submitted for the degree of Doctor of Philosophy

July 2017

Supervisors: Colm Ó Cofaigh, Jerry Lloyd, Riko Noormets, Tove Nielsen & Antoon Kuijpers

Department of Geography
University of Durham

Abstract

Tidewater glaciers terminate in the ocean and provide an important link between the terrestrial and marine realm, which makes them particularly vulnerable to both atmospheric and oceanographic changes. Tidewater glacier dynamics are affected by sea-level rise, which, in combination with ocean warming, can amplify glacier retreat. Most glaciers that drain the large contemporary ice sheets of Greenland and Antarctica are marine-terminating, fast-flowing outlets, and the dynamics of these glaciers have a large impact on ice sheet stability and sea level. Understanding how such glaciers have responded to climate change in the past therefore provides an important analogue for assessing current and future changes of the large ice sheets in Greenland and Antarctica. Fjords have proven to be very useful in this context, as their protected environment allows for the accumulation of thick, undisturbed sedimentary sequences, which enable the investigation of past ice sheet change at a high temporal resolution.

This study uses multibeam swath-bathymetry, sub-bottom profiler data, and sediment cores from fjords in Spitsbergen and West Greenland to investigate the glacial landforms and sedimentary facies in front of fjord-terminating tidewater glaciers. The identified landform-sediment assemblages are compared to other High-Arctic fjords and are summarised in a new conceptual model. They are used to infer common sedimentary processes in glacimarine environments, to identify the factors controlling them, and to reconstruct Holocene regional ice dynamics. The results demonstrate that while the sedimentary processes are largely similar between the different regions, differences arise in the landform-sediment assemblages, even between adjacent fjords. This implies that glacier dynamics are not simply controlled by changes in the air or ocean temperatures, but can be highly variable in space and time.

Contents

List of Figures

List of Tables

Acknowledgements

First and foremost, my deepest gratitude goes to my supervisor Colm Ó Cofaigh, who has to be, without a doubt, the greatest supervisor one could ask for. I will never quite understand how it is possible to fit so much into a 24-hour day and still be so dedicated to one's PhD students. And even though it may not have seemed like it when running on that beach in Ireland, I was always able to catch up with you, as you always made time for me. You never grew tired of discussing my data or re-reading my papers for what felt like the hundredth time, and provided many ideas, much-needed encouragement and endless support, which I really, really appreciate.

I am equally grateful to my other supervisors Jerry Lloyd, Riko Noormets, Tove Nielsen and Antoon Kuijpers, without whom this thesis would not be what it is. Jerry, your support throughout the project, the encouragement and your help, particularly with the micropalaeontology bit, were much appreciated. Riko, thank you so much for providing me with all the data and taking me onboard the Helmer Hanssen, as without your help and support it would never have been possible to write such a comprehensive thesis on submarine geomorphology and glacimarine sedimentation. Tove and Antoon, thank you very much for hosting me at GEUS during my two secondments, for always making time for me and for discussing my data. You not only provided valuable insight into my Greenland data and allowed me to put it into a larger perspective, but were always so excited about my work that it was contagious, thus providing an extra-boost of motivation.

My colleagues and friends Elena Grimoldi and Kasper Weilbach not only had to put up with my rants in the office and the occasional nervous breakdown when the computer/software was uncooperative, but were also wonderful companions throughout the entire thesis process. Bouncing ideas off of you, showing you figures and asking your advice as well as killing time over coffee were a lot of fun and also extremely helpful. You have been an inspiration on days that I felt unmotivated and were great to have around. Elena, you never got a break from me, as we even talked about work and other problems at home, but it was really great to share a house with you and to have you as a friend. Thank you!

I am really glad that I was able to find so many friends within the GLANAM project; we could not only commiserate over our PhDs but could also have a lot of fun together on all those annual meetings and workshops. Being part of such a great group of people

made being a PhD student an amazing experience, for which I am truly grateful. In this context I also want to sincerely thank all the collaborators of GLANAM, firstly for making this project possible by putting in all the work and securing the funding, and, secondly, for allowing me to be a part of it.

I know that this PhD would not have been possible without the financial support of the People Programme (Marie Curie Actions) of the European Union's Seventh Framework Programme (FP7/2007-2013/ under REA grant agreement n^{o}317217) and would like to offer my thanks to this initiative for providing the necessary research funds via the GLANAM project. Durham University also played a vital role in providing the resources and facilities I needed to conduct my research. Frank Davies, Neil Tunstall and many others of the lab staff were not only very helpful with matters relating to the labs, but also made my time there more fun. I further received assistance from numerous other members of staff at the Geography Department, including Dave Roberts and Dave Evans, which I greatly appreciate.

My parents are a vital part of this thesis also: you never waiver in your support, no matter what crazy ideas I come up with, and all the love I receive from you makes me feel like I can achieve anything. Thank you for being the best parents a kid could wish for! I am truly grateful also to my godmother Susann, for her incredible generosity, for allowing me to finish writing up my thesis from her apartment and for taking me to the Alps every once in a while to reset. You are a great godmother and the only person I would want to have a "generationsuebergreifende WG" with!

I feel very blessed also to have many wonderful friends in my life who provided welcome distractions, much moral support and several shoulders to cry on if the need arose. They also put up with my phases of social hermitage without ever complaining. I want to particularly thank Tom, Marisa, Lou and Kika: you all made my time in Durham so much better, by always being up for something fun, for great conversations and for providing me with much-needed hugs. Tom, the cycling trip last year was probably one of my best ever holidays and I'll always treasure it as such. My best friends Livia and Eugen were always by my side, even from far away, and supported me endlessly!

I feel extremely lucky to have you all in my life! Thank you!

Declaration:

I declare that this thesis contains the results of research carried out by myself. As most chapters have also been published separately as journal articles, some of the results are based on joint research. A detailed break-down of each author's contribution is given at the end of each of these chapters.

Copyright permission was obtained where necessary and references to existing work were made as appropriate. Any errors or omissions are the responsibility of the author.

Copyright Statement:

Katharina Streuff
1st July, 2017

Chapter 1

Introduction

This study is part of the GLAciated North Atlantic Margins (GLANAM) project, which is an EU-funded collaboration between Norway, Denmark, Ireland and the UK. The project aims to reconstruct the glacial history and palaeoclimate of the continental margins of the Northern Atlantic, which are not only crucial to understanding the influence of climate change on ice sheet dynamics, but are also essential for the hydrocarbon industry. Within GLANAM, this study focuses on contemporary glaciated fjords.

1.1 Aims and objectives

This study investigates the glacial geomorphological and sedimentary products in five Spitsbergen fjords and two West Greenland embayments to develop a comprehensive conceptual model for glacimarine sedimentary processes in front of fjord-terminating tidewater glaciers. The model is based on empirical results from this study, supplemented with information from previous investigations from other fjords in Svalbard, Greenland, Canada, and Alaska. It aims to determine the complex evolution of ice-proximal glacimarine sedimentation in High-Arctic fjords.
In order to achieve the above aim, the following objectives have been developed:

1. to determine the nature of the submarine glacial landforms and glacimarine sediments in the fjords of the study areas,

2. to reconstruct the associated sedimentary processes and glacial dynamics in modern tidewater glacier settings,

3. to compare landform assemblages and sedimentary facies from West Greenland and Spitsbergen with other High-Arctic fjords, and

4. to determine the controls on glacimarine sedimentation associated with fjord-terminating tidewater glaciers.

1.2 Rationale

Fjords are glacially-eroded valleys that occur along the coasts of many (previously) glaciated areas. The tidewater glaciers at the heads of contemporary glaciated fjords

not only represent an important link between the terrestrial and the marine realm, but are also particularly susceptible to climate change, as they are directly influenced by variations in air temperatures, ocean currents, and wind patterns (e.g. Cottier *et al.*, 2010). Understanding their dynamics is therefore crucial for understanding their past, and thus, predicting their future response to changes in climate.

Fjords have been described as "miniature oceans" (Thompson & Barkey, 1938) as, like oceans, they serve as accumulation basins for eroded terrestrial material and are subject to complex oceanographic currents. However, their particular physiography not only allows for sediments to be accumulated at higher rates than in the deep ocean, but a sill at the mouth of many fjords prevents the occurrence of high-energy processes (e.g. bottom current winnowing) common on the open shelf (e.g. Howe *et al.*, 2010). As a result, fjords often provide sheltered environments and facilitate the rapid accumulation of thick, largely undisturbed sedimentary sequences, particularly where tidewater glaciers are present. Such glaciers usually form characteristic landforms, which are revealed as the glaciers retreat (e.g. Ottesen & Dowdeswell, 2006; Ottesen *et al.*, 2008). Due to their potential to record ice dynamics as well as former oceanographic conditions, the landforms and sediments in front of fjord-terminating tidewater glaciers serve as excellent environmental proxies to study past climate at a high temporal resolution (e.g. Syvitski & Shaw, 1995; Forwick *et al.*, 2010).

This study investigates the submarine glacial landforms and sediments in fjords of different geographic locations in order to understand what types of products are usually deposited in front of contemporary tidewater glaciers. The landforms and sediments are used to derive the common Holocene depositional processes in glacimarine environments of Spitsbergen and Greenland, which are then compared to those observed in other glacimarine environments of the northern hemisphere. This research is important for a number of reasons. First, tidewater glaciers in Greenland, for example, have received increasing attention in recent decades, because their extensive thinning and accelerated retreat have been linked, at least partially, to a warming climate (Zwally *et al.*, 2002; Holland *et al.*, 2008; Joughin *et al.*, 2008). Since these glaciers serve as major outlets draining the Greenland Ice Sheet into the ocean, ice sheet mass balance is intrinsically linked to glacier outlet stability and ice dynamics. Understanding the behaviour of such glaciers is hence crucial for predicting sea level rise (e.g. Joughin *et al.*, 2004). Despite this, many studies in Greenland have only focused on the short-term evolution of tidewater glaciers rather than investigating their response to past climate change (e.g. Moon & Joughin, 2008; Thomas *et al.*, 2009; Joughin *et al.*, 2014). Conversely, investigating the products and sedimentary processes in front of such glaciers provides valuable information on their long-term evolution, particularly throughout the Holocene, and thus enables us to reconstruct their response to past climate change in more detail. This, in turn, contributes to our understanding of glacier dynamics by providing additional information about what

drives and influences glacier advance and retreat, which will eventually help to improve predictions of the response of ice sheets and glaciers to future climate change. Second, we require ice sheet models to understand our climate system and the complexity of its individual components (e.g. Stokes *et al.*, 2015; Kirchner *et al.*, 2016). Because such models rely on a number of input parameters, among which is the information derived from past ice sheet reconstructions (e.g. Greenwood & Clark, 2009), the British-Irish Ice Sheet, the Svalbard-Barents Sea Ice Sheet and the Eurasian Ice Sheets have received increasing attention (e.g. Landvik *et al.*, 1998; Svendsen *et al.*, 1999; Hubbard *et al.*, 2009; Clark *et al.*, 2012; Patton *et al.*, 2015; Gowan *et al.*, 2016; Hughes *et al.*, 2016). Many Svalbard fjords today host the glacial remnants of the ice streams that once drained the Svalbard-Barents Sea Ice Sheet; studying the landforms and sedimentary deposits both on the continental shelf and in the fjord basins around the archipelago thus provides an opportunity to reconstruct ice sheet behaviour during and since the Last Glacial Maximum (e.g. Ottesen *et al.*, 2005; Dowdeswell *et al.*, 2010a; Winsborrow *et al.*, 2010; Rebesco *et al.*, 2011; Bjarnadóttir *et al.*, 2013; Andreassen *et al.*, 2014). Third, in the ongoing debate of global warming and climate change, there is a tendency to generalise ice dynamics across wide areas of the globe. However, air and ocean temperatures, wind and water currents, geological setting and individual glacier dynamics can be vastly different across glacimarine environments, and, as of yet, we do not fully understand to what extent the behaviour of the glaciers depends on these parameters. Investigating and comparing glacial dynamics in regions of the northern hemisphere with variable climate will therefore give some indication of the type of parameters governing ice dynamics and their relative importance.

This thesis is a compilation of geographically separate, but thematically linked studies concerning tidewater glacier sedimentation. The areas presented were chosen to highlight the similarities and differences between fjords in West and East Spitsbergen (chapters 2 and 3), two climatically diverse areas, and to evaluate how these compare to fjord settings in Greenland. Specific fjords from the different regions were selected to visualise the seafloor and analyse the sediments of thus far uninvestigated fjords, but were also chosen according to accessibility of data. The fjords were grouped according to geographic region and the associated assumption of a similar climate. Chapters 2–4 are articles that have been published in scientific journals. Chapter 2 focuses on West Spitsbergen and presents the seafloor morphology in (1) Ymerbukta, Trygghamna, and Magdalenefjorden. The glacial products on the seafloor of Ymerbukta and Trygghamna are relatively similar to landforms observed in many other West Spitsbergen fjords and the focus of this chapter is therefore set on Magdalenefjorden in northwest Spitsbergen, about which relatively little is known. Using sediment cores, the glacimarine sedimentary processes are reconstructed for this fjord, giving some indication of common glacimarine processes in northwest Spitsbergen, while radiocarbon dates are used to reconstruct recent glacier dynamics in the fjord. Chapter

3 studies the glacial landforms and sediments in East Spitsbergen using Lomfjorden as an example. It is the first study to investigate glacimarine sedimentary processes, glacial landform assemblages and Holocene ice dynamics in an East Spitsbergen fjord, where the climate is thought to be generally colder than in the west. Radiocarbon dates provide detailed information on the dynamics of a trunk glacier since the Last Glacial Maximum. In chapter 4 the Holocene sedimentary record and associated depositional environments and ice dynamics are reconstructed for Jakobshavn Isbræ and adjacent Greenland Ice Sheet outlet glaciers using a large dataset of sediment cores and acoustic data from Disko Bay and the Vaigat Strait in central West Greenland. The study complements previous studies from the area which have focused on reconstructing the relatively short-term dynamics of these glaciers, on the seafloor morphology of the fjords, or few selected sediment cores. Chapter 5 places the results from the previous three chapters into a wider context and introduces swath-bathymetric data and observed landforms from some fjords in Alaska. It then compares the glacimarine sedimentary environments between fjords of different geographic regions, thereby effectively reviewing glacimarine sedimentary processes and products in front of contemporary fjord-terminating tidewater glaciers in the northern hemisphere. The outcome is summarised in a comprehensive conceptual model showing the reconstructed sedimentary processes with associated lithofacies and glacial landforms in High-Arctic fjords.

Chapter A in the appendix is a published paper presenting the seafloor morphology and some lithofacies in Kongsfjorden in central West Spitsbergen. Because the paper is mainly based on data that was previously used in my master's thesis, it is not included in the main body of the thesis. However, because the findings strongly relate to observations made in the other fjords presented here, data and results from Kongsfjorden were included in chapter 5 in order to add value to the discussion of different glacimarine fjord settings and the developed conceptual model.

Chapter 2

Submarine landform assemblages and sedimentary processes in front of Spitsbergen tidewater glaciers

Streuff, K.; Ó Cofaigh, C.; Noormets, R.; Lloyd, J. (in review): Submarine landform assemblages and sedimentary processes in front of Spitsbergen tidewater glaciers. *Marine Geology, GLANAM Special Issue.*

Abstract

New swath-bathymetric data from the inner parts of the three Svalbard fjords Ymerbukta, Trygghamna, and Magdalenefjorden reveal the landform assemblages deposited in front of tidewater glaciers in West and Northwest Spitsbergen. Overridden moraines in Ymerbukta, a tributary of Isfjorden in central West Spitsbergen, record several re-advances of the glacier Esmarkbreen at the head of the fjord after deglaciation, and glacial lineations formed in the seafloor sediments are indicative of fast ice advance during one of these events. A terminal moraine and associated debris lobe mark the maximum ice extent during the Holocene, which, implied by the presence of crevasse-squeeze ridges, is likely related to a previous surge of Esmarkbreen. Several De Geer moraines provide evidence for subsequent slow and step-wise retreat. In the adjacent Trygghamna and in Magdalenefjorden in Northwest Spitsbergen the landforms are similar but the absence of overridden moraines and glacial lineations shows that the glaciers probably only re-advanced once during the Holocene and that ice flow was relatively slow. Terminal moraines and associated debris lobes mark the maximum extent of these advances and formed during the Little Ice Age (LIA). In Magdalenefjorden the relatively small size of the debris lobe suggests that the ice margin was at its maximum position for only a short period of time, or that sediment availability was restricted during the LIA advance. Similar to Esmarkbreen the retreat phase of the glaciers in Trygghamna and Magdalenefjorden was also characterised by periods of stillstand or small re-advances, although the comparatively small number of De Geer moraines in all three fjords shows that these landforms probably formed much less frequently than previously thought.

Sub-bottom profiler data, four sediment cores and six radiocarbon dates from Magdalenefjorden further provide information about the Holocene sedimentary environments in a Northwest Spitsbergen fjord. The main source of sediment is glacial meltwater entering the fjord from the surrounding coastline, which has led to the accumulation of thick sequences of fine-grained mud. Stratified and laminated muds record glacier-proximal conditions, probably related to a LIA re-advance of Waggonwaybreen around 300 cal a BP, where the interplay of a range of glacimarine processes led to the formation of partially rhythmic couplets of one coarser and one finer layer, accumulated at a rate of around 3 cm a^{-1}. Such sediments are often

observed in ice-proximal glacimarine environments and are probably formed from seasonal variations in meltwater and/or sediment supply. Numerous monosulphid layers indicate that the seasonal control on biological productivity may have aided the formation of individual laminae. Multiple sandy layers intercalated with the glacimarine mud provide evidence for the occurrence of gravitational mass-flow events like turbidity currents. In ice-distal settings, the muds are internally massive or weakly stratified, may show traces of bioturbation, and accumulate at a lower rate of 0.04–0.49 cm a^{-1}. Occasional clasts and diamictic layers show that the depositional environment in Magdalenefjorden is also influenced by sedimentation from icebergs and sea ice, but the ubiquitous glacimarine mud underscores the predominance of meltwater-related sedimentation in the fjord.

2.1 Introduction

High-Arctic glaciers have received increasing attention in the scientific literature as their behaviour is often closely linked to climate change (e.g. Lovell, 2000; Holland *et al.*, 2008; Błaszczyk *et al.*, 2009). Svalbard in particular has been the focus of many investigations, as around 60% of the archipelago is still covered by terrestrial (cirque) glaciers, fjord-terminating tidewater glaciers, and ice caps (e.g. Hagen, 1993; Hagen *et al.*, 2003; Kohler *et al.*, 2007; Mangerud & Landvik, 2007). The ongoing thinning and retreat of these glaciers has resulted in the exposure of well preserved glacial landform-sediment assemblages in many fjords (see chapters A and 3; cf. e.g. Plassen *et al.*, 2004; Ottesen *et al.*, 2008; Fransner *et al.*, 2017). The landforms and sediments deposited in front of Svalbard tidewater glaciers therefore serve as an important indicator of past ice dynamics and have led to a better understanding not only of the response of the Svalbard-Barents Sea Ice Sheet to climate change since the Last Glacial Maximum (LGM), but also of individual glacier dynamics throughout the Holocene. The latter is of particular importance for future predictions of the cryosphere as tidewater glaciers can exhibit a wide range of hydrological, thermal, and dynamic regimes (e.g. Blatter & Hutter, 1991; Dowdeswell *et al.*, 1998; Pettersson, 2004). One example of this are surge-type glaciers, which undergo cyclic switches between active phases of ice advance and passive phases of ice retreat, that are believed to occur largely independently of the climate (e.g. Meier & Post, 1969; Sharp, 1988; Hamilton & Dowdeswell, 1996; Sevestre & Benn, 2015).

The glacimarine sedimentary processes in front of tidewater glaciers are usually a function of meltwater, iceberg, and sea ice fluxes and are therefore relatively similar across a wide range of geographic and climatic locations (cf. e.g. Powell, 1981; Elverhøi *et al.*, 1983; Gilbert, 1983; Ó Cofaigh *et al.*, 2001). Conversely, the formation of glacial landforms is mainly controlled by glacial thermal and hydrological regime, bed substrate, available time for deposition, and sediment availability. Consequently, submarine landform assemblages can vary quite substantially (e.g. Dowdeswell *et al.*, 2016d), even within geographically restricted areas (cf. chapters A and 3). Nevertheless, landform assemblages across many Spitsbergen fjords are remarkably similar and often include (1) glacial lineations associated with rapid ice advance, (2) terminal moraines formed from ice push or thrust at the glacier margin marking the maximum extent of ice advance, (3) debris lobes on the distal flanks of terminal moraines, formed from quasi-continuous slope failure, and (4) recessional moraines or annual push moraines formed each year during winter, when the glacier margins experience short periods of stillstand and/or re-advance during overall retreat (chapter A; e.g. Boulton *et al.*, 1996; Plassen *et al.*, 2004; Forwick & Vorren, 2011). Depending on the glaciological regime and the local bathymetry,

these assemblages can include further components, such as eskers, bedrock highs, iceberg ploughmarks and pockmarks (chapter 3; cf. e.g. Ottesen *et al.*, 2008; Forwick *et al.*, 2009; Dowdeswell & Ottesen, 2016). Crevasse-squeeze ridges are thought to occur exclusively in landform assemblages associated with surging glaciers and have thus been suggested to be diagnostic of surge activity (e.g. Sharp, 1985; Ottesen & Dowdeswell, 2006; Farnsworth *et al.*, 2016). Overridden recessional moraines, although not uniquely linked to surge activity, are an indicator of previous ice advances and are therefore also a common feature in front of surge-type glaciers (chapter A; e.g. Ottesen & Dowdeswell, 2006).

In this study we present new swath-bathymetric data from the inner basins of three Spitsbergen fjords, two in central West Spitsbergen, and one in northwest Spitsbergen, in order to compare the seafloor morphology in front of several tidewater glaciers. Our work complements that of Forwick *et al.* (2009), Ottesen & Dowdeswell (2009), and Forwick & Vorren (2012), who documented landforms observed on the bathymetric data from the outer fjord basins. We use sub-bottom profiler as well as lithological data from Magdalenefjorden to correlate landforms with the lithofacies and reconstruct sediment accumulation rates from a suite of radiocarbon dates. Combined, our data enables us to reconstruct the Holocene depositional processes in front of selected Spitsbergen tidewater glaciers.

2.2 Study areas

2.2.1 Physiographic Setting

Three fjords were investigated: (1) Ymerbukta, (2) Trygghamna, and (3) Magdalenefjorden. All three fjords are located on Spitsbergen, the largest island of the Svalbard archipelago (Fig. 2.1). Ymerbukta and Trygghamna are situated between approximately 78°12'N, 13°35'E and 78°19'N, 14°05'E in central West Spitsbergen, and are northern tributaries of Isfjorden, Svalbard's largest fjord (Fig. 2.1b). Together with its many tributaries, Isfjorden forms the Isfjorden fjord system, which has been the subject of many previous investigations (e.g. Mangerud *et al.*, 1992; Svendsen *et al.*, 1996; Ottesen *et al.*, 2007; Forwick & Vorren, 2011; Rasmussen *et al.*, 2012). Ymerbukta and Trygghamna extend approximately north to south, with the former fjord located east and the latter west of the mountain range Värmlandryggen (Fig. 2.2a). Ymerbukta is bounded by Erdmannodden to the east and Selmaneset to the west and influenced by the tidewater glacier Esmarkbreen at its head (Fig. 2.2a). A 20 m-high ridge separates the fjord into an inner, 3.5 km long and 500–2000 m wide ice-proximal basin, and an outer, 6.5 km long and 2000–2700 m wide ice-distal basin (Fig.

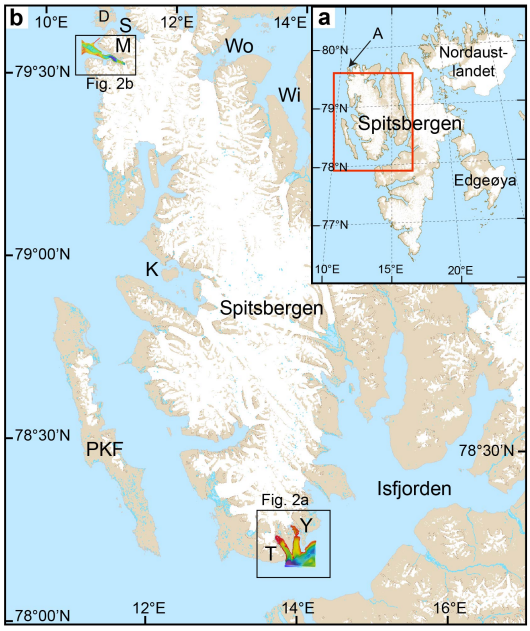

Figure 2.1: *a) Overview map of Svalbard. A = Amsterdamøya. The red rectangle shows the extent of b) map of Northwest Spitsbergen, with bathymetric data available for this study. Y = Ymerbukta, T = Trygghamna, PKF = Prins Karls Forland, K = Kongsfjorden, M = Magdalenefjorden, D = Danskøya, Wo = Woodfjorden, Wi = Wijdefjorden. Map data courtesy of the Norwegian Polar Institute.*

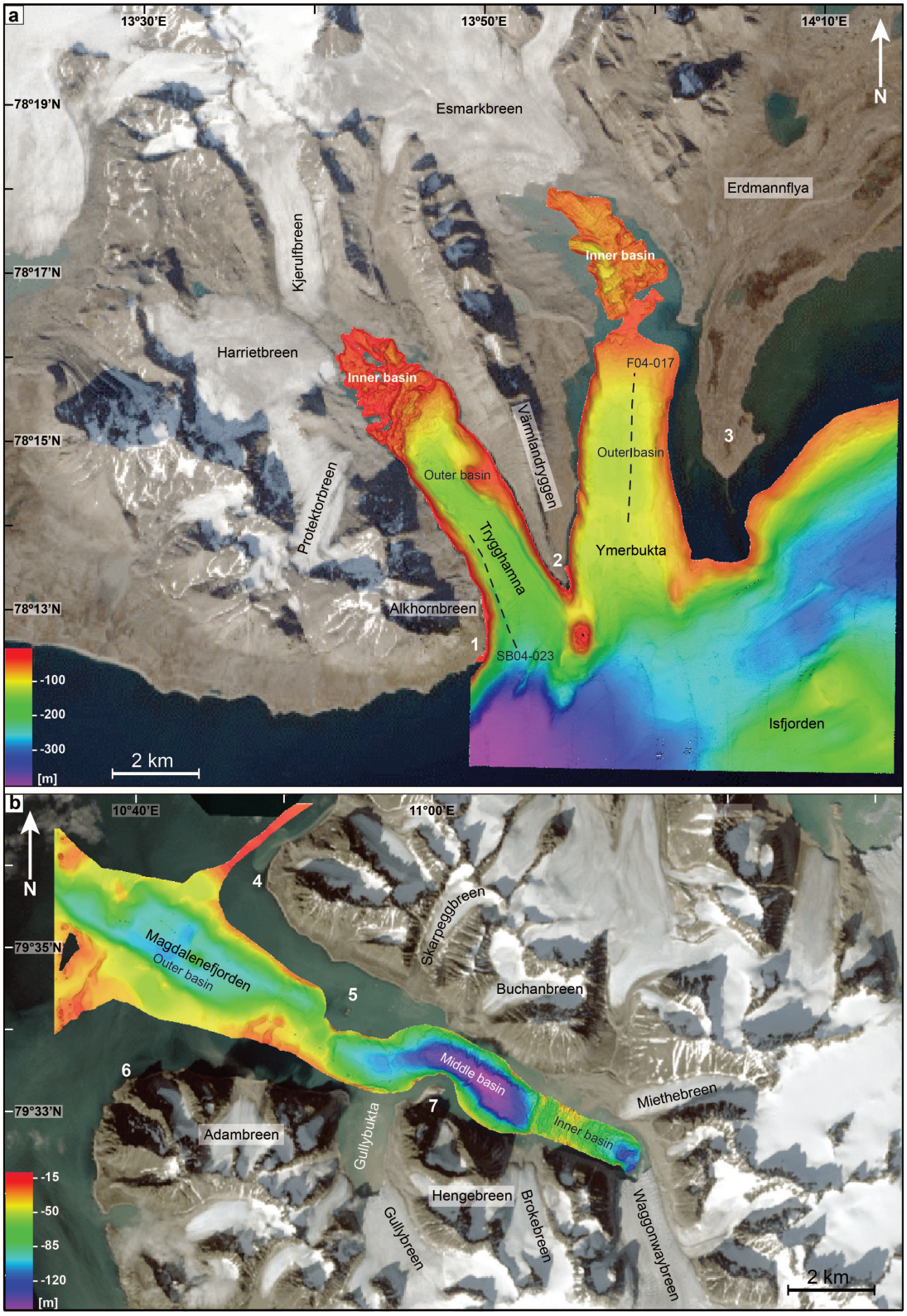

Figure 2.2: *a) Ymerbukta and Trygghamna with their surroundings and the bathymetric data available from the two fjords. 1 = Alkepynten, 2 = Selmaneset, 3 = Erdmannodden. Dashed lines indicate the location of sparker and boomer profiles F04-163 and SB04-023, which were visualised and interpreted in Forwick & Vorren (2011, 2012) and provide the basis for the seismostratigraphy in Ymerbukta and Trygghamna. b) Magdalenefjorden, its surroundings, and the bathymetric data available for this study. 4 = Knattodden, 5 = Fugleholmen, 6 = Magdalenehuken, 7 = Gravneset. For an overview of the study areas' location see also Figure 2.1.*

2.2a). Water depths in Ymerbukta range from 15 to 120 m.

Trygghamna is bounded by Selmaneset to the east and Alkepynten to the west, is approximately 8 km long and between 0.8 and 2.2 km wide (Fig. 2.2a). The tidewater glaciers Kjerulfbreen and Harrietbreen are located at its head and the two terrestrial glaciers Protektorbreen and Alkhornbreen along its western coast (Fig. 2.2a). Trygghamna is between 5 and 50 m deep in its inner, ice-proximal basin, and almost 200 m deep in its outer parts (Fig. 2.2a).

Magdalenefjorden is located in northwest Spitsbergen, between 79°31'N, 10°30'E and 79°37'N, 11°20'E (Fig. 2.2b). The fjord is orientated southeast to northwest and is bounded by Knattodden in the north and Magdalenehuken in the south (Fig. 2.2b). It is 14.5 km long, 700–3200 m wide, between 25 and 135 m deep, and can be subdivided into three basins, the innermost ice-proximal basin at its head, a deep middle basin, and an outer, ice-distal basin (Fig. 2.2b). The two tidewater glaciers Miethebreen and Waggonwaybreen flow into the fjord at its head in the southeast, whereas Gullybreen terminates in the small tributary fjord, Gullybukta, on the southern side of Magdalenefjorden (Fig. 2.2b). The terrestrial glaciers Brokebreen, Hengebreen and Adambreen are situated along Magdalenefjordens southern shore, whereas Buchanbreen and Skarpeggbreen are located along the northern coast (Fig. 2.2b).

2.2.2 Previous work

2.2.2.1 Glacial background

During the LGM Svalbard was covered by a large and dynamic ice sheet, which reached the continental shelf edge (e.g. Elverhøi *et al.*, 1995; Svendsen *et al.*, 1996; Landvik *et al.*, 1998; Mangerud *et al.*, 1998), and was divided into two components: (1) fast-flowing ice streams draining the ice sheet through the major fjord systems, and (2) "inter-ice-stream" areas of slower-moving ice (Landvik *et al.*, 2005; Ottesen *et al.*, 2007; Ottesen & Dowdeswell, 2009; Ingólfsson & Landvik, 2013). Although its glacial history is debated, there is consensus that Isfjorden and its tributaries served as a major pathway for one of these large ice streams, with ice reaching its maximum extent at the continental shelf edge between 24 and 20 ka BP (e.g. Mangerud *et al.*, 1992; Svendsen *et al.*, 1992; Landvik *et al.*, 1998, 2005; Ottesen *et al.*, 2005; Jessen *et al.*, 2010). Around 14.8 ^{14}C ka BP ice began a continuous and rapid retreat from the shelf edge (Elverhøi *et al.*, 1995; Svendsen *et al.*, 1996), and reached the mouth of Isfjorden before 14–12 ka BP, leading to ice-free conditions in coastal areas by 12.3 ka BP (e.g. Mangerud *et al.*, 1992; Landvik *et al.*, 1998; Mangerud *et al.*, 1998; Forwick & Vorren, 2011). Ice recession was interrupted by a re-advance around 12.4 ka BP, but continued until ∼10 ka BP, when ice had retreated to the heads of the tributary fjords (e.g. Svendsen & Mangerud, 1992; Elverhøi *et al.*, 1995; Landvik *et al.*, 1995; Svendsen *et al.*, 1996; Ottesen *et al.*, 2007; Forwick & Vorren, 2009). Geomorphological evidence from Ymerbukta and Trygghamna, as well as lithological evidence from elsewhere in the Isfjorden fjord system suggest that the glaciers underwent a significant re-advance during the Younger Dryas (Mangerud *et al.*, 1992; Svendsen *et al.*, 1996; Forwick & Vorren, 2009, 2011), which is in contrast to other areas in Spitsbergen where glaciers were smaller during the Younger Dryas than during the LIA (Mangerud & Landvik, 2007). In Isfjorden and its tributaries, the glaciers experienced asynchronous regrowth after c. 9 ka BP (e.g. Forwick & Vorren, 2007, 2009; Baeten *et al.*, 2010; Forwick *et al.*, 2010), and their maximum Holocene extents occurred in response to the LIA cooling or due to climatically independent surges (e.g. Plassen *et al.*, 2004; Ottesen & Dowdeswell, 2006; Mangerud & Landvik, 2007; Forwick & Vorren, 2011; and references therein).

In contrast to Isfjorden, Magdalenefjorden was located in an inter-ice-stream area during the LGM, with ice streams located south and east of the fjord, in Kongsfjorden and Woodfjorden (Fig. 2.1b; e.g. Landvik *et al.*, 2005; Ottesen & Dowdeswell, 2009). A distinctive belt of hummocky terrain close to the continental shelf edge was interpreted as the grounding zone of the ice sheet during the LGM and provides evidence that, similar to West Spitsbergen, ice in the northwest reached the shelf edge during this time (Ottesen & Dowdeswell, 2009). However, due to a more alpine topography in the coastal areas, a thinner ice cover and generally reduced ice flux during the LGM, ice flow was inferred to be somewhat slower than in the surrounding fjords (e.g. Landvik *et al.*, 1998; Forman, 1990; Landvik *et al.*, 2003, 2005; Ottesen & Dowdeswell, 2009).

The timing and mode of deglaciation in NW Spitsbergen is still very poorly understood. The only constraint on deglaciation are ^{10}Be exposure dates from the lowlands of the two islands Amsterdamøya and Danskøya (Fig. 2.1), which suggest that these areas were ice-free between 18 and 15 ka BP (Landvik *et al.*, 2005). This may indicate that the mouth of Magdalenefjorden deglaciated around the same time, suggesting that it was probably ice-free much earlier than Isfjorden. Indeed, early deglaciation of northwest Svalbard was also suggested by Forman (1990) and is further supported by Koç *et al.* (2002), who placed the disintegration of the Hinlopen Strait ice in northeast Spitsbergen and possibly the northern margin of the Svalbard-Barents Sea Ice Sheet between 13.9 and 13.7 ka BP. From the geomorphological evidence ice retreat was inferred to be continuous and relatively rapid across the outer shelf, and slower but quasi-continuous across the inner shelf (Ottesen *et al.*, 2007; Ottesen & Dowdeswell, 2009). It is unclear when Magdalenefjorden was deglaciated and the local tidewater glaciers reached the head of the fjord, but a minimum deglaciation age of 8.9–8.5 ka BP from the mouth of the adjacent Smeerenburgfjorden (Velle, 2012) may serve as a rough estimate.

2.2.2.2 Geomorphology

Previous work has been carried out on the landforms in the outer parts of all three fjords. In outer Ymerbukta Forwick *et al.* (2009) documented the abundance of single and composite pockmarks, which were described as up to 250 m wide and 7 m deep. The pockmarks were inferred to have formed from the upward seepage of thermogenic gas, probably predominantly along tectonic faults occurring in the Isfjorden-Ymerbukta Fault Zone (Dallmann *et al.*, 2002; Forwick *et al.*, 2009). Indeed, systematic analysis of seafloor seepage features in the entire Isfjorden fjord system linked the occurrence of pockmarks to the presence of deep bedrock faults and igneous intrusions (Senger *et al.*, 2013; Roy *et al.*, 2015). Further work by Forwick & Vorren (2012) has shown the presence of several sediment lobes, as well as blocks and flow structures in both Ymerbukta and Trygghamna. The majority of the sediment lobes occur in Ymerbukta, are orientated perpendicular to the main fjord axis, and were described as up to 5 m-thick and up to 500 m-long and wide deposits. In Trygghamna, where the presence of sediment lobes is less common, two areas with slide blocks were identified, where individual blocks are up to 150 m wide, up to 100 m long, and up to 8 m high (Forwick & Vorren, 2012). The sediment lobes and slide blocks were interpreted as debris-flow deposits or slump/slide deposits, formed from slope failure during the late Holocene with earthquakes and high sediment accumulation rates as the most likely triggers (Forwick & Vorren, 2012). The presence of terminal moraines, marking the Holocene maximum extent of the local glaciers in Ymerbukta and Trygghamna, was also indicated by Forwick & Vorren (2012). Large-scale sediment lobes on their distal flanks were interpreted as glacigenic debris flows formed from high sediment supply to the glacier margin,

causing repeated slope failure during a period of stillstand.

Ottesen & Dowdeswell (2009) described the seafloor of Magdalenefjorden as generally smooth, and related this to sediment infill and draping by silt and clay settling from suspension in glacial meltwater plumes, with the occurrence of occasionally protruding bedrock in the form of ridges and knobs. On the steep side walls of the central fjord basin the same authors described the occurrence of scars and possibly gullies. In the outer fjord, arcuate sedimentary ridges have a SW-NE orientation and were identified as moraines formed at the retreating ice margin during periods of stillstand (Ottesen & Dowdeswell, 2009). A 40 m-high ridge across the central fjord was interpreted as the terminal moraine marking the maximum extent of Waggonwaybreen during the LIA, which occurs in conjunction with several up to 5 m-high transverse ridges, interpreted as push moraines. The latter are thought to form regularly, possibly annually, during small re-advances of the glacier front during overall ice retreat (Ottesen & Dowdeswell, 2009). The same processes were inferred for a number of similar ridges in front of Gullybreen along the southern shore of the fjord (Ottesen & Dowdeswell, 2009).

2.2.2.3 Seismostratigraphy

While sub-bottom profiler data and sediment cores are available for Magdalenefjorden, and will be investigated here, the seismostratigraphy in Ymerbukta and Trygghamna is derived from seismic interpretations published by Forwick & Vorren (2011, 2012), which were based on a chirp profile through Ymerbukta (F04-017; Fig. 2.2a), and a boomer profile through Trygghamna (SB-04-023 in Fig. 2.2a; for details see Fig. 63.3 in Forwick & Vorren (2012) and Fig. 4b in Forwick & Vorren (2011)). In addition to the acoustic basement, interpreted as bedrock, four acoustic units were described from the two fjords: S2, S4a, S5 and S6 (Forwick & Vorren, 2011, 2012). In Isfjorden at the mouth of the two fjords two additional units, S1 and S3, occur.

Unit S1 was described as (semi-)transparent with few internal reflections and a smooth to hummocky upper boundary. It has a draping character, occurs as basin-fill and on bathymetric slopes, and is present on top of the bedrock in most of Isfjorden (Forwick & Vorren, 2011). The unit was inferred to represent sediment deposited subglacially as till or as cavity infill, with a hummocky appearance ascribed to the presence of glacial lineations (Forwick & Vorren, 2011). The acoustically massive (semi-)transparent unit S2 was determined to represent push or thrust moraines accumulating at the glacier front during recession or minor re-advances during deglaciation, which were inferred to be indicative of episodic retreat (Forwick & Vorren, 2011). Unit S3 appears as mostly wedge-shaped deposits of a stratified to chaotic acoustic appearance (Forwick & Vorren, 2011). The wedges are usually orientated parallel to the direction of (palaeo-) ice flow and were interpreted as products of (1) glacial outwash, (2) repeated slope failures caused by high sedimentation rates, isostatic uplift and seismic activity, or (3) the infill of subglacial cavities (Forwick & Vorren, 2011). The acoustically stratified deposits of unit S4a are characterised by a draping or onlapping geometry and (sub-)parallel internal reflections, and are up to 38 and 40 m thick in Ymerbukta and Trygghamna (Forwick & Vorren, 2011). S4a was found to correlate with stratified glacimarine mud with sandy beds and clasts, which were derived from suspension settling from meltwater, ice rafting, and mass-transport activity in a glacier-proximal environment. The unit probably dates back to the Younger Dryas and was deposited between 14.1 and 11.2 cal ka BP (Forwick & Vorren, 2009, 2011). Unit S5 represents glacimarine deposits from the Early Holocene, which are acoustically (semi-)transparent, conformably overlie S4a, and show occasional onlap geometry. The sediments were sourced from suspension settling and occasional iceberg rafting during the

Holocene Thermal Optimum between 11.2 and 9 cal ka BP (Forwick & Vorren, 2009, 2011). Unit S6 is the stratigraphically youngest facies in Ymerbukta and Trygghamna. It is acoustically stratified and interpreted as Holocene glacimarine pebbly mud deposited after ∼9 cal ka BP, when ice rafting increased due to colder climatic conditions (Forwick & Vorren, 2009, 2011).

2.3 Material and methods

For this study, swath-bathymetric data from Magdalenefjorden, Ymerbukta, and Trygghamna were supplemented with sub-bottom profiler data and four sediment cores from Magdalenefjorden. The data from Magdalenefjorden were gathered in October 2009 on the research vessel *R/V Jan Mayen* (now *Helmer Hanssen*), using a Kongsberg Simrad multibeam EM300 echo sounder for the swath-bathymetric, and an EdgeTech 3300-HM sub-bottom profiler for the chirp data. Swath-bathymetric data from Ymerbukta and Trygghamna were gathered in July 2000 by the Norwegian Hydrographic Survey with a Kongsberg Simrad multibeam EM1002 installed on the research vessel *Sjømaleren* (now *IXPLORER*). Both multibeam echo sounders were calibrated using frequent conductivity-temperature-depth (CTD) measurements from the water column. Bathymetric data were gridded to a cell size of 5x5 m in DMagic, and visualised and interpreted in the Fledermaus v7 3D Software. The chirp sub-bottom profiler was operating at a pulse mode of 2-16 kHz and 3 ms during acquisition and the resulting data were processed using the EdgeTech Software and visualised and interpreted in SMT The Kingdom Suite.

A total of four gravity cores, JM09H-GC01, GC03, GC06, and GC09, were taken from Magdalenefjorden, using a 1900 kg heavy gravity corer with a 6 m-long steel barrel and an inner diameter of ∼110 mm. All cores were cut into up to 1.3 m-long sections, split into working and archive halves, and stored at +4°C. It is important to note that GC01 and GC03 were already split in 2009, whereas GC06 and GC09 were only split in 2016. Thus, certain parameters (e.g. water content) may not be directly comparable between the four cores, although variations within one core are informative. In order to identify the different lithofacies in the fjord, core logs were generated from the visual description of the sediment surface of the working halves, which were supplemented using the information on internal sedimentary structures provided by x-radiographs. The latter were acquired with a GEOTEK Thermo Kevex PSX10-65W-Varian2520DX, running with a voltage of ∼95 kV and a current of around 150 nA. All cores were run through a GEOTEK multi-sensor core logger at Durham University to determine the wet-bulk density and magnetic susceptibility in 1 cm-intervals, the latter of which was measured with a Bartington point-sensor mounted on the system. Magnetic susceptibility values were obtained in SI units (χ x 10^{-5}) but are displayed unitless throughout this article. Bivalve shells located from the x-rays of GC06 and benthic foraminifera from selected sediment depths in GC01 were sent to Beta Analytic for Accelerator Mass Spectrometry (AMS) dating. The obtained conventional ^{14}C ages were calibrated with the MARINE13 calibration (cf. Reimer *et al.*, 2013), using a marine reservoir effect of 400 years and a local ΔR of 61 ± 70 years (Mangerud, 1972). For the water content 1 cm-thick sediment slabs were taken at selected (usually lithofacies-dependent) core depths, weighed, dried at 60°C, and weighed again. The same samples were subsequently soaked overnight in a solution of distilled water and sodium-hexametaphosphate to encourage the disintegration of flocculated clay particles. The sediments were then sieved through mesh sizes of 500, 250, 125 and 63 μm (stacked on top of each other) to determine the grain size distribution within the cores.

2.4 Results

2.4.1 Geomorphology

Based on the swath-bathymetric data from the inner parts of Ymerbukta, Trygghamna, and Magdalenefjorden we identify a total of five different landform types. The distribution of all observed landforms is shown in Fig. 2.3, which incorporates those landforms previously described by Forwick *et al.* (2009), Ottesen & Dowdeswell (2009), and Forwick & Vorren (2012).

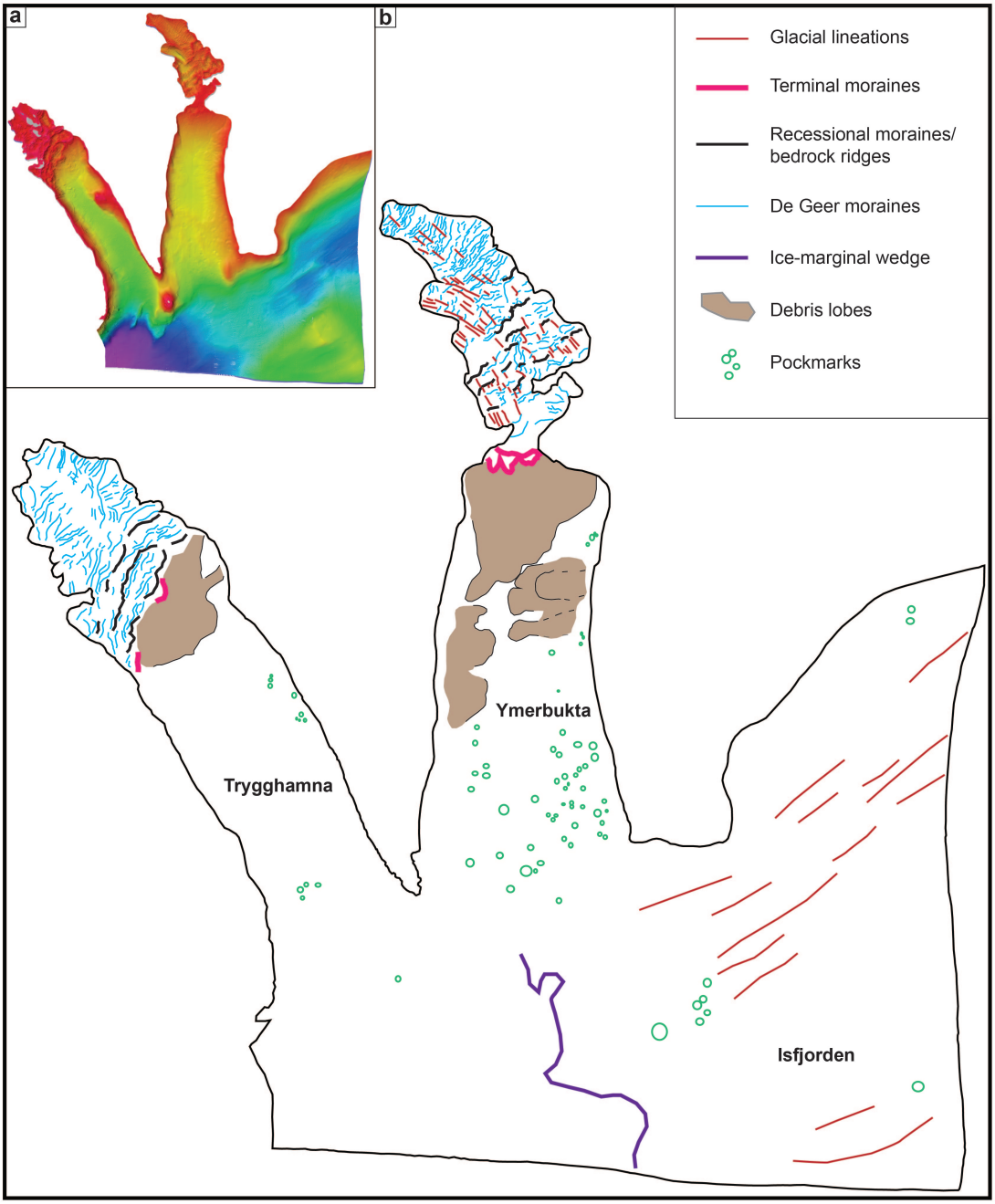

Figure 2.3: *a) Swath-bathymetric data from Ymerbukta and Trygghamna. For the depth scale refer to Figure 2.2. b) Geomorphological map of the landforms in Ymerbukta, Trygghamna and parts of Isfjorden. Pockmarks and debris lobes were previously described and interpreted by Forwick* et al. *(2009); Forwick & Vorren (2012).*

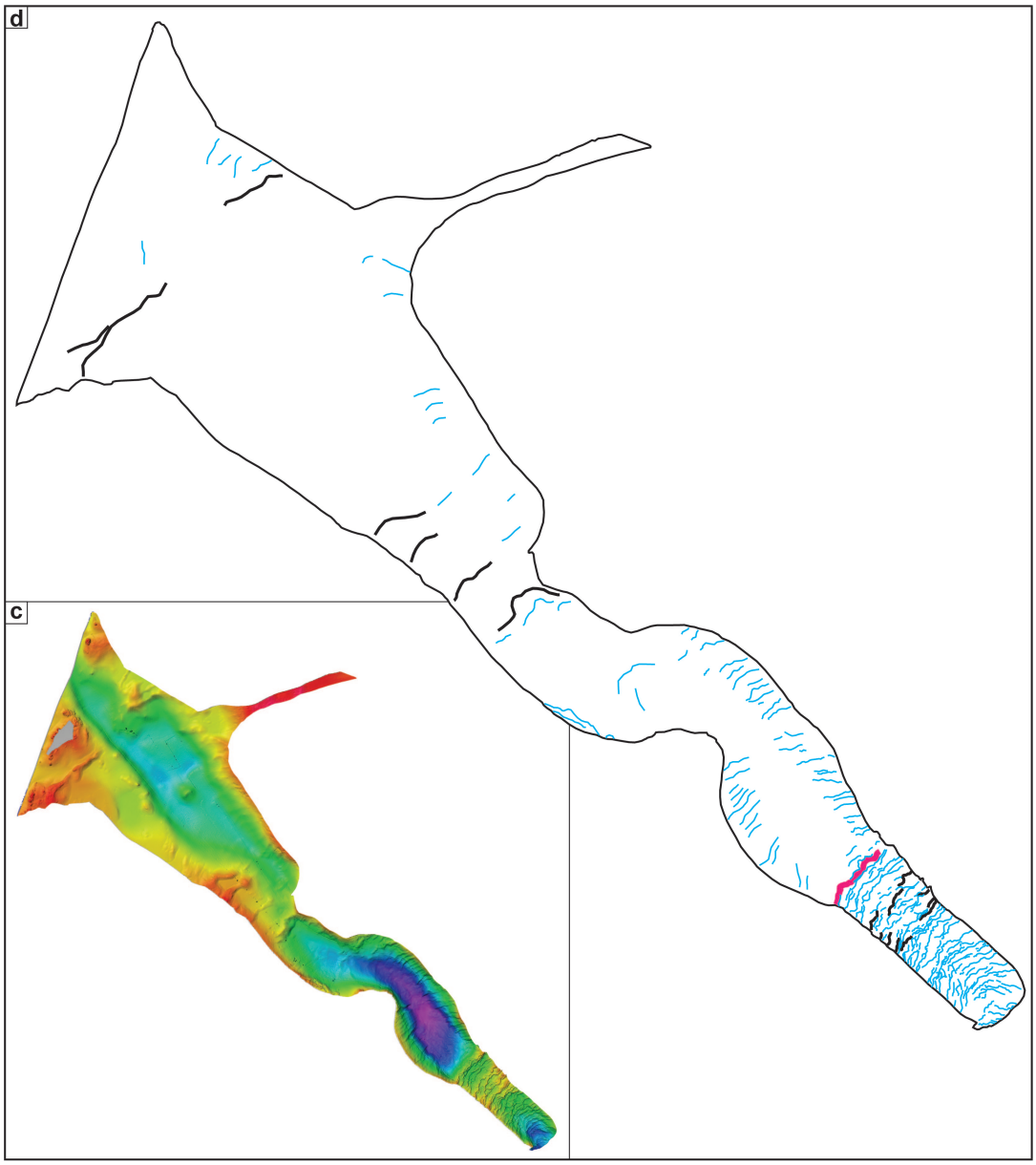

***Figure 2.3** (cont.): c) Swath-bathymetric data from Magdalenefjorden. For the depth scale refer to Figure 2.2. d) Geomorphological map of the landforms in Magdalenefjorden. Part of the moraines/bedrock ridges in the outer and central fjord have been previously documented and interpreted by Ottesen & Dowdeswell (2009).*

2.4.1.1 Groove-ridge features – glacial lineations

Elongate, (sub)parallel ridges and grooves are present in inner Ymerbukta (Fig. 2.4a, b). These features are 25 m high, 150–800 m long, up to 20 m wide and spaced at irregular distances between 50 and several hundred metres (Fig. 2.4a, b). The crests are straight to slightly curved, and round and symmetrical in cross-section. These ridges are orientated parallel to the main fjord axis, i.e. in the direction of ice flow (Fig. 2.3b). The majority of these features are overprinted by small transverse ridges (see section 2.4.1.2 below), indicating that the small elongate ridges were deposited first. Similar, albeit larger ridges (up to 2 km long, ~200 m wide) appear in Isfjorden, where their orientation is northeast-southwest, i.e. almost perpendicular to the ones in Ymerbukta (Fig. 2.3b).

Similar sets of ridges and grooves have previously been described from other Spitsbergen fjords, where they were interpreted as glacial lineations (chapter A; e.g. Ottesen & Dowdeswell, 2006; Ottesen *et al.*, 2008). Indeed, Ottesen *et al.* (2007) already documented the presence of (mega-scale) glacial lineations in Isfjorden. Glacial lineations are formed beneath a glacier or ice stream, where the soft subglacial sediments are deformed into ridges and grooves by processes of erosion and re-deposition (e.g. Tulaczyk *et al.*, 2001; Ó Cofaigh *et al.*, 2005). They are commonly associated with fast ice flow (King *et al.*, 2009).

2.4.1.2 Transverse ridges – recessional moraines

Several large ridges in the innermost fjord basins are orientated transverse to the main fjord axis (Figs. 2.3, 2.4) and extend across the width of the fjords. The ridges are up to 20 m high, 800–2000 m long and 100–300 m wide. Their sometimes multiple crests are sinuous in planform, round, and mostly symmetrical in cross-section (Fig. 2.4d, f). In Ymerbukta some of these ridges are overprinted by the glacial lineations. The most distal ridges in Ymerbukta and Trygghamna are associated with large sediment lobes (see section 2.4.1), which extend down their distal flanks (Fig. 2.3b). In Isfjorden a large feature occurs, which is similar to the transverse ridges in the fjords, but is ∼85 m high, ∼4 km wide and more than 3.8 km long (Fig. 2.4h-j). It is characterised by an asymmetric cross-profile with a steeper distal and a flatter proximal side (Fig. 2.4). In plan-view, it appears more as a plateau with a sharp edge rather than a ridge with a crest (Figs. 2.3a, b, 2.4).

The large transverse ridges are interpreted to be recessional moraines deposited during overall glacier retreat. This is in accordance with e.g. Ottesen & Dowdeswell (2006), Baeten *et al.* (2010) and Streuff *et al.* (2015), who described similar ridges from other Spitsbergen fjords. In Ymerbukta, where these ridges are partially streamlined or overprinted by glacial lineations, they probably represent recessional moraines from an earlier advance of Esmarkbreen, that were overprinted by a later re-advance. The transverse ridges at the outermost edge of the inner basins in Ymerbukta, Trygghamna, and Magdalenefjorden have previously been interpreted as terminal moraines, deposited when the glaciers reached their maximum Holocene extents, either in response to the LIA cooling (Ottesen & Dowdeswell, 2009) or as a result of a surge (Forwick & Vorren, 2012).

We suggest that the ridge-like feature in Isfjorden formed as a sedimentary wedge at or close to the grounding line of an ice stream during a period of stillstand during overall ice retreat. Although formation as a grounding-zone wedge could be feasible in this context, a seismic profile across the feature (SS97-163; Fig. 2.4j) does not show the characteristic reflection pattern (cf. Forwick & Vorren, 2011; Batchelor & Dowdeswell, 2015). We thus support the interpretation of Forwick & Vorren (2011), who, from the seismic profile, inferred the formation of wedge-shaped ice-marginal deposits either from repeated slope failure, as glacial outwash or as sedimentary infill of subglacial cavities.

2.4.1.3 Small transverse ridges – De Geer moraines

Abundant small transverse ridges occur in the inner fjord basins, which extend across the fjords and are between 100 and 2000 m long, around 20 m wide, and ∼3 m high. These ridges overprint the glacial lineations in Ymerbukta, indicating that they are the youngest features. The majority have sharply defined, continuous crests, are largely symmetrical in cross-section, and are spaced at intervals between 10 and 50 m (Fig. 2.4a, c). In places these ridges exhibit branching and may cross-cut each other (Fig. 2.3).

The small ridges are similar to annual push moraines described from other Svalbard fjords (e.g. Ottesen *et al.*, 2008; Flink *et al.*, 2015), which are formed each year during winter, when the presence of shore-fast sea ice causes the generally retreating glaciers to stagnate or even re-advance (Boulton, 1986; Ottesen & Dowdeswell, 2006). The overall regular spacing supports this interpretation. The fact that these ridges exhibit branching and cross-cut each other in places could be indicative of other processes involved, e.g. the squeezing of soft subglacial sediments into basal glacier crevasses (Evans & Orton, 2014; Streuff *et al.*, 2015). This is supported by the presence of terrestrial crevasse-squeeze ridges in the forefield of Esmarkbreen (Farnsworth

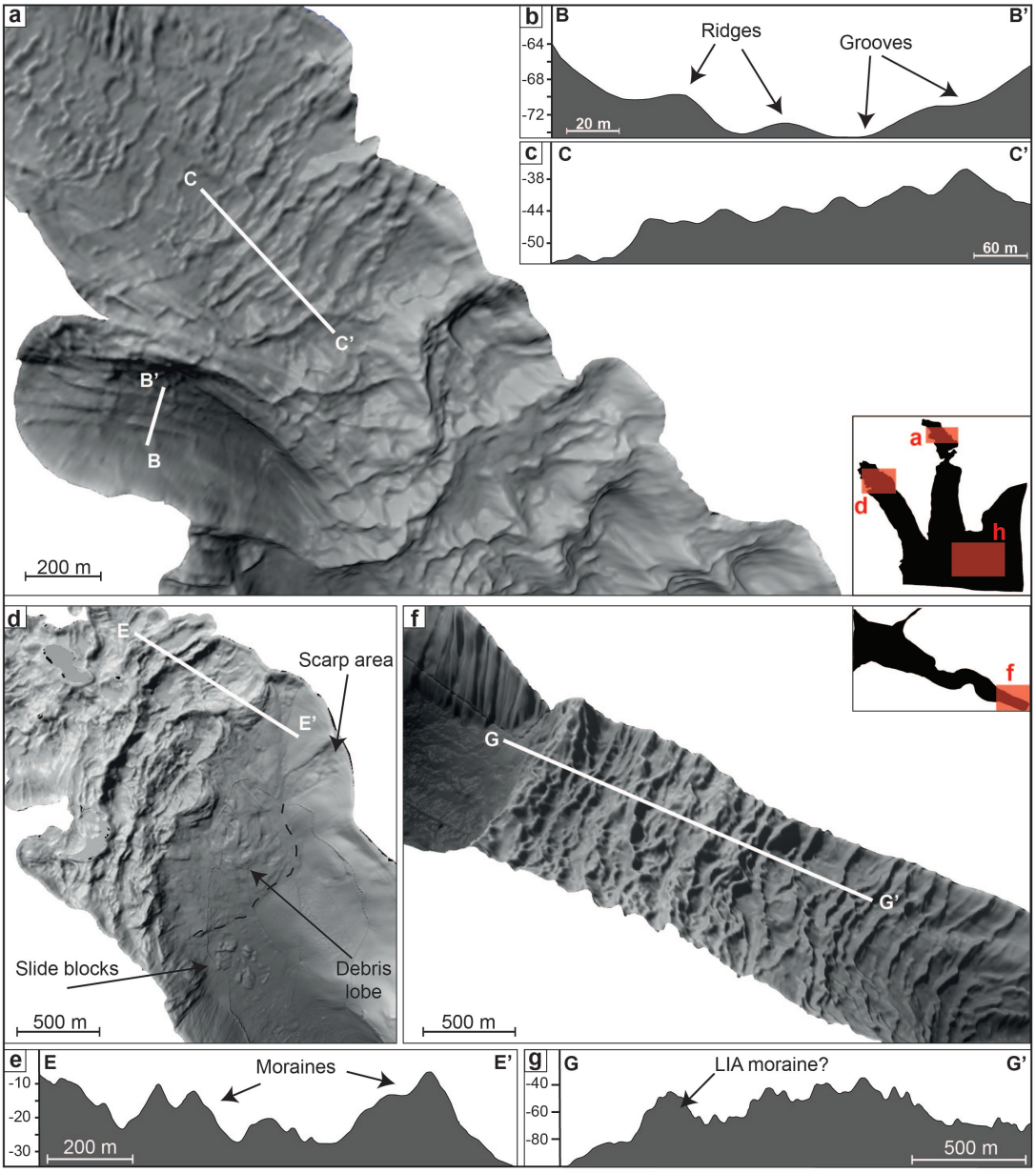

Figure 2.4: *a) Seafloor of the inner fjord basin of Ymerbukta, showing examples of glacial lineations and De Geer moraines. Small red rectangles on the black polygon indicate the location of the subfigures a), d), and h). b) and c) show the cross-sectional profiles B–B' and C–C' across the landforms, respectively. d) Large transverse moraines and an associated debris lobe in Trygghamna. e) Cross-sectional profiles E–E' across Trygghamna moraines. f) De Geer moraines in Magdalenefjorden with g) cross-sectional profile G–G' across them.*

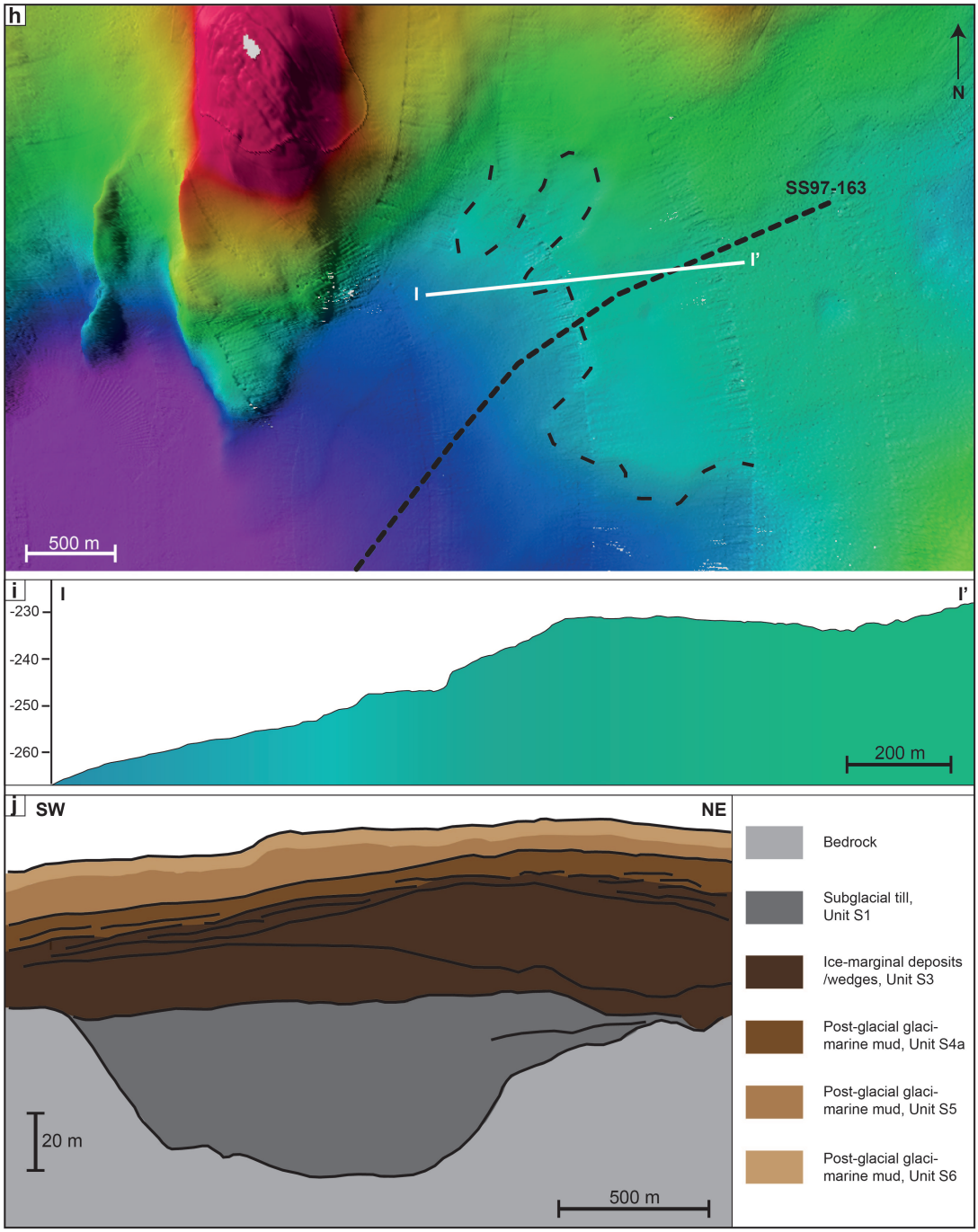

Figure 2.4 *(cont.): h) Ice-marginal deposit in Isfjorden, with i) showing the cross-sectional profile I–I'. j) Acoustic facies interpretation of seismic line SS97-163 (based on, and modified after Forwick & Vorren, 2011).*

et al., 2016). Given the likely mixed origin of the small ridges both as end moraines and as crevasse-squeeze ridges, we interpret these landforms as De Geer moraines (cf. Lundqvist, 1981).

2.4.2 Seismostratigraphy

Description

The chirp data available from Magdalenfjorden reveal a total of five acoustic facies, AF1–AF5 (Fig. 2.5).

AF1 is the stratigraphically lowermost facies in Magdalenefjorden. It is defined by a semi-transparent appearance with very weak and chaotic internal reflections that disappear with depth (Fig. 2.5c). The upper boundary is of variable strength, often hummocky, but discontinuous throughout the fjord (Fig. 2.5). AF1 has a minimum thickness of 10 ms (∼7.5 m).

AF2 directly overlies AF1 in most of the fjord and has a similar acoustic signature with chaotic and semi-transparent internal reflections (Fig. 2.5c). Its top boundary is usually strong and opaque, but can disappear in places. Because of the similar acoustic characteristics and the discontinuous upper boundary of AF1, the transition between AF1 and AF2 is not always clear. The upper boundary of AF2 is sometimes accompanied by strong diffraction hyperbolae (Fig. 2.5c). AF2 is between 1 and 20 ms (0.75–15 m) thick.

AF3 conformably overlies AF2, or AF1, where AF2 is absent. Its acoustic appearance varies from internally massive and semi-transparent to acoustically stratified (Fig. 2.5c). AF3 is especially common in bathymetric basins, where it is up to 24 ms (18 m) thick. Its upper boundary is strong and opaque and relatively continuous throughout the fjord (Fig. 2.5b, c).

AF4 is acoustically (semi)transparent with weak internal reflections of a massive nature that disappear in places (Fig. 2.5c). The facies occurs as lenses or wedge-shaped deposits, often intercalated into AF3 (Fig. 2.5). AF4 is common at the foot of slopes, where it forms deposits, that are 2–22 ms (1.5–16.5 m) thick and pinch out laterally with increasing distance from the slope (Fig. 2.5c, d).

AF5 is the stratigraphically uppermost facies in Magdalenefjoden, and thus the inferred youngest. It is bounded by the seabed on top and appears acoustically stratified, with numerous parallel internal reflections of an opaque nature (Fig. 2.5c). However, as the majority of these reflections are strictly parallel to the seabed, it is possible that they reflect echoes of the latter and mask the facies' true acoustic signature. AF5 is present in the inner fjord, i.e. in ice-proximal areas, is up to 6 ms (4.5 m) thick, and conformably overlies AF4 (Fig. 2.5).

Interpretation

AF1 is interpreted as the acoustic basement in Magdalenefjorden, the acoustic appearance of which suggests that AF1 represents either glacial till or bedrock (cf. Forwick *et al.*, 2010; Forwick & Vorren, 2012; Kempf *et al.*, 2013; Roy *et al.*, 2014). Its stratigraphic position, the hummocky upper boundary, and the outcropping bedrock visible on the swath-bathymetric data (Fig. 2.5) all indicate that the acoustic basement in Magdalenefjorden comprises bedrock.

AF2 is acoustically similar to AF1 and to acoustic facies from other Spitsbergen fjords, including Unit S2 in Ymerbukta and Trygghamna (cf. Forwick & Vorren, 2011, 2012; Kempf *et al.*, 2013), and is thus interpreted as glacial till. This would imply a diamictic composition for the sediments of AF2, which is supported by the massive acoustic appearance and weakening internal reflections with depth (cf. Stewart & Stoker, 1990; Forwick & Vorren, 2012). In innermost Magdalenefjorden AF2 crops out at the seafloor and its very hummocky appearance here correlates with the occurrence of the recessional moraines (Fig. 2.5), also supporting an interpretation as glacial till.

The (semi-)transparent, partially stratified acoustic signature of AF3 supports an

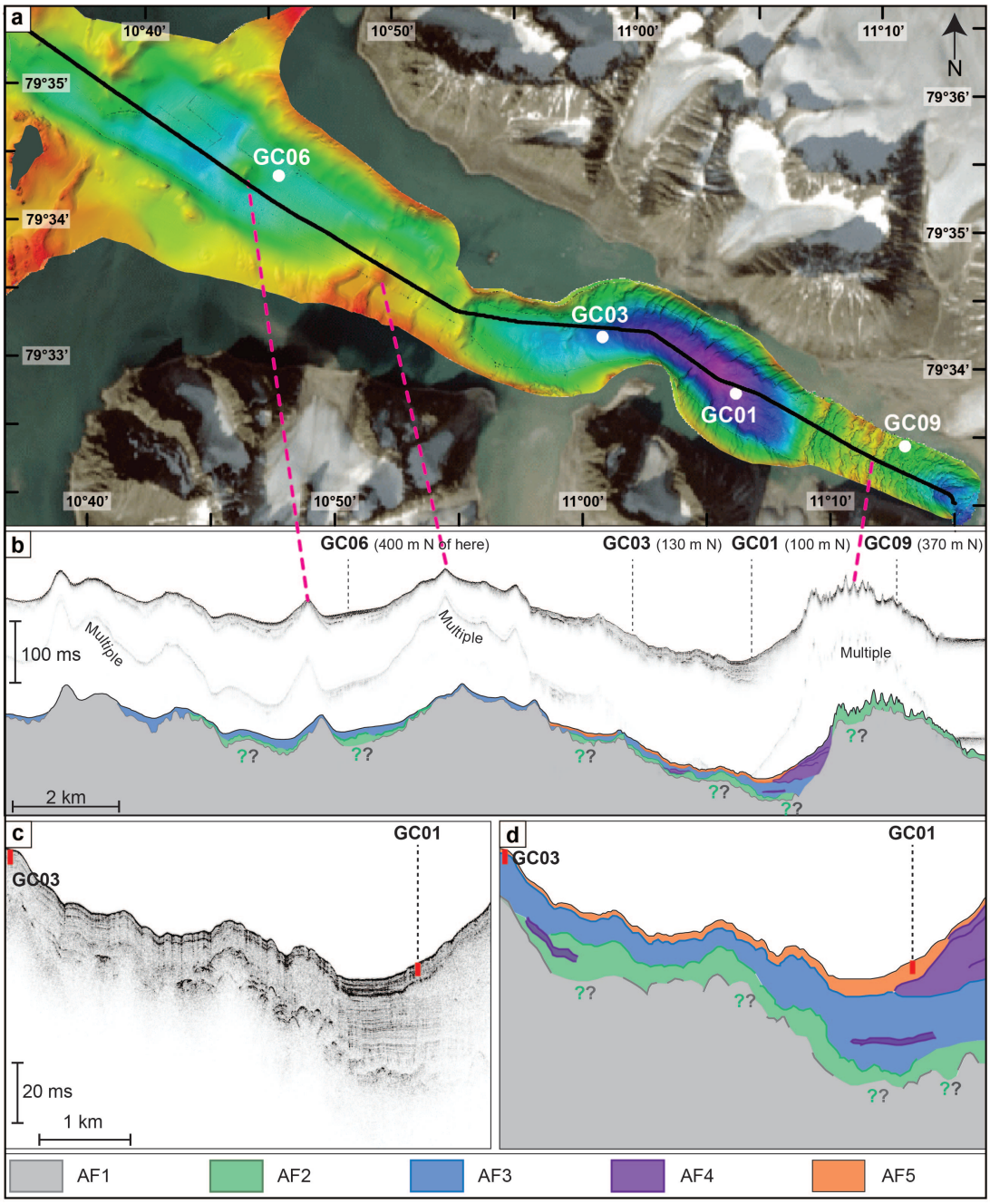

Figure 2.5: *a) Bathymetry in Magdalenefjorden with the location of all cores (white dots) and chirp line 09JM-AG211-006 (black line) indicated. b) Seismic profile of chirp line 006, with approximate locations of the gravity cores. Pink stippled lines correlate bathymetric ridges with the according highs on the seismic profile. The interpretation of the acoustic facies in Magdalenefjorden is shown underneath the seismic profile. The black rectangle marks the extent of c). c) Detailed excerpt from chirp line 006 (black rectangle in b) showing examples of the acoustic facies in Magdalenefjorden. d) Acoustic facies interpretation of c). Red lines in c) and d) illustrate how far GC01 and GC03 penetrate into the seafloor sediments and how they correlate with the acoustic facies in the fjord.*

interpretation as glacimarine sediments derived from suspension settling from meltwater plumes (e.g. Plassen *et al.*, 2004; Kempf *et al.*, 2013; Streuff *et al.*, 2015). Where the facies appears stratified, regular changes in lithology or density are implied, which could indicate a glacier-proximal depositional environment (cf. Syvitski, 1989; Forwick & Vorren, 2012), possibly with the occurrence of turbidity currents or other gravitational mass flows (e.g. Sexton

et al., 1992; Forwick & Vorren, 2012; Streuff *et al.*, 2017). In places the latter is also indicated by the localised appearance of AF4 (see below). AF3 is similar to S4a in Ymerbukta and Trygghamna (cf. Forwick & Vorren, 2011, 2012).

AF4 is interpreted as mass-flow deposits. This is supported by the lenticular appearance, the internally massive semi-transparent acoustic signature, and its similarity with such deposits in other areas around Svalbard (e.g Plassen *et al.*, 2004; Forwick & Vorren, 2007; Hogan *et al.*, 2010; Forwick & Vorren, 2012; Kempf *et al.*, 2013).

AF5 is interpreted as late Holocene glacimarine or hemipelagic sediments delivered into the fjord by meltwater streams (cf. S6 in Ymerbukta and Trygghamna, AF6 in Lomfjorden; Forwick & Vorren, 2011; Streuff *et al.*, 2017). Similar to S5 and S6, the internal reflections could indicate periods of increased iceberg rafting (cf. Forwick & Vorren, 2009, 2011). However, our lithological data suggest that the stratification is probably the result of repeated changes in grain size and possibly mass flow activity (see section 2.4.3 below).

2.4.3 Lithostratigraphy

2.4.3.1 Lithofacies

Description

Based on the sedimentary evidence, we define a total of four lithofacies, LF1–LF4 in Magdalenefjorden (Fig. 2.6).

LF1 contains massive greyish brown to dark greyish brown mud (Munsell codes: 2.5Y 5/2 – 4/2). It only occurs in the top 25 cm of GC01 and GC03, and shows no internal structures and very few clasts. LF1 has a magnetic susceptibility around 20 and contains > 90% clay and silt (Fig. 2.6). The water content is between 25 and 30%, however, this is a minimum content, as both cores were split in 2009, and it is likely that the sediments dried out to some extent since then.

LF2 contains finely laminated to stratified mud with occasional clasts and occurs in GC01 and GC03. Like in LF1, the mud is greyish brown to dark greyish brown (2.5Y 5/2 – 4/2), generally very fine and consists of up to 98% silt and clay (Fig. 2.6). Black mottles appear throughout. We define laminae as thinner than 1 cm (but usually up to only 2 mm in Magdalenefjorden), and strata, which are between 1 and 5 cm thick. The magnetic susceptibility shows only minor variations and is generally low with values between 10 and 20 (Figs. 2.6). The greyscale changes in the x-radiographs suggest that the stratified nature of the sediments is likely caused by differences in grain size or density (Fig. 2.6c, f). The latter is supported by the strong oscillations in bulk density, which varies between ∼1.9 and 2.25 g cm^{-1} (Fig. 2.6). The water content is between 20 and 35%; note, however, that as for LF1, this is a minimum value. We distinguish three subfacies of LF2: LF2a, LF2b, and LF2c. LF2a contains weakly or diffusely stratified, partially bioturbated mud where no significant changes in grain size occur between individual layers (Fig. 2.6f). Occasional clasts within the facies may be accompanied by load structures. In LF2b the stratification is more pronounced and defined by couplets of sharp-bounded coarser and finer layers of variable thickness (Fig. 2.6f). Bioturbation traces are absent. Layers may be inclined with undulating contacts and contain the fine massive sand of LF4 (see below) in places. LF2c contains (diffusely) stratified mud, which appears intercalated with thin layers of a matrix-supported diamict (Fig. 2.6c, f). The boundaries between mud and diamict are gradual and lack load structures (Fig. 2.6f).

LF3 only occurs in GC06 and contains diffusely laminated mud with a relatively high silt and sand content (Fig. 2.6). The sediments are dark grey (5Y 4/1) at the surface, and black

(5Y 2.5/1) in the subsurface, and emit a strong smell of H_2S. Shell fragments and entirely preserved bivalves are common in this facies and may occur in concentrated layers or scattered throughout (Fig. 2.6). LF3 has a relatively low magnetic susceptibility between 5 and ∼10 and a comparably high density >2 g cm^{-3} (Fig. 2.6). The slightly coarser nature of LF3 is reflected in the grain size distribution, which commonly shows 40–80% of the sediments to be finer than 63 μm (Fig. 2.6). Although the water content of 20–35% is similar to the fine-grained mud of LF2a, it is important to note that GC06 was one of the two cores split in 2016; its water

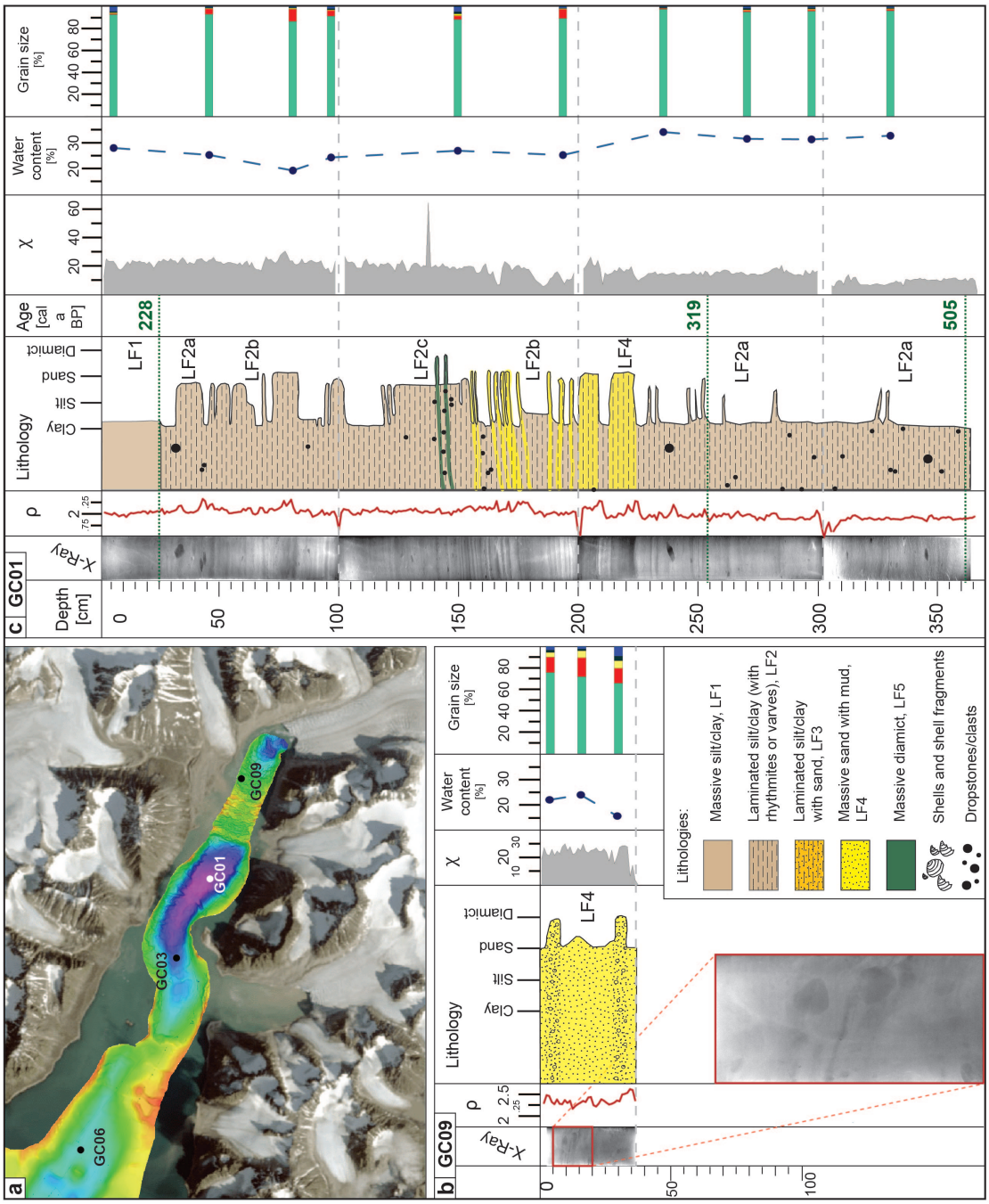

Figure 2.6: *a) Overview of the four core locations in Magdalenfjorden with respect to the bathymetry. b) X-radiographs, lithofacies log and physical properties of core GC09 in the inner fjord. ρ = wet bulk density, χ = magnetic susceptibility in SI x 10^{-5}. c) X-radiographs, lithofacies log and physical properties of core GC01 in the central fjord.*

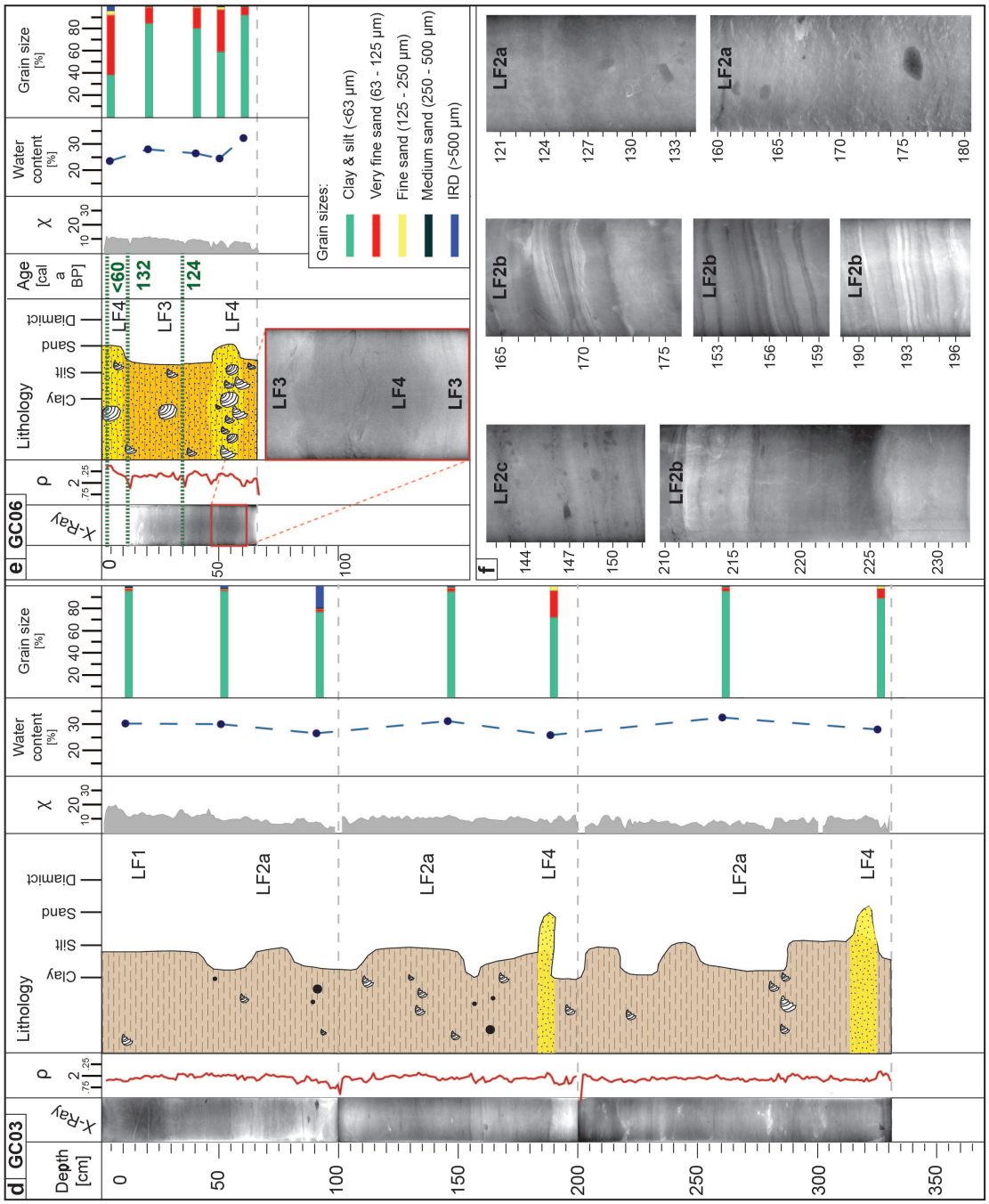

Figure 2.6 *(cont.): d) X-radiographs, lithofacies log and physical properties of core GC03 in the central fjord. e) X-radiographs, lithofacies log and physical properties of core GC06 in the outer fjord. f) Examples of the x-radiographs showing the different types of laminated/stratified sediment in Magdalenefjorden.*

content is thus regarded as more reliable, and the water content of LF2a may consequentially be higher than measured.

LF4 occurs as thin beds or as thick strata and has a massive, unsorted appearance. It contains dark greyish brown (2.5Y 4/2) fine sand, and small, but variable amounts of greyish brown mud (2.5Y 5/2). During core splitting a strong H_2S odour occurred and the sediments' subsurface is characterised by a black colour (5Y 2.5/1). Clasts and shell fragments are sparse. Boundaries to other lithofacies are often sharp (Fig. 2.6). The magnetic susceptibility is

between ∼15 and 30 and the density between 2 and 2.5 g cm^{-3} (Fig. 2.6). LF4 contains less than 25% water and 60–80% clay and silt (Fig. 2.6). GC09 is only composed of LF4 (Fig. 2.6b).

Interpretation

LF1 is similar to massive muds observed in other glacimarine settings and is interpreted as mud settling from suspension in meltwater plumes or the water column. The massive internal structure and the presence of occasional bioturbation structures indicate ice-distal conditions during the accumulation of LF1 (cf. e.g. Elverhøi *et al.*, 1983; Forwick & Vorren, 2009; Baeten *et al.*, 2010).

The stratified muds of LF2 are similar to sediments documented from other fjords in Spitsbergen and are accordingly interpreted as glacimarine mud deposited in a relatively calm, meltwater-dominated depositional environment (cf. e.g. Elverhøi *et al.*, 1983; Plassen *et al.*, 2004; Forwick *et al.*, 2010). Laminated or stratified glacimarine muds commonly occur in Arctic fjords, where they are usually associated with an interplay of depositional processes or sedimentation from multiple sources (cf. e.g. Elverhøi *et al.*, 1980; Ó Cofaigh & Dowdeswell, 2001; Forwick & Vorren, 2009; Streuff, 2013). Stratification and lamination of LF2 and its subfacies in Magdalenefjorden could thus be a consequence of (1) multiple glaciers delivering sediments to the source, (2) tidally controlled release of the suspension load carried in the meltwater plumes, (3) diurnal or seasonal variation in meltwater flux and thus depositional energy, and (4) an interplay between suspension settling from meltwater plumes and repeated gravity flows (e.g. Elverhøi *et al.*, 1983; Mackiewicz *et al.*, 1984; Cowan & Powell, 1990; Ó Cofaigh & Dowdeswell, 2001; Gilbert *et al.*, 2002). This is further discussed in section 2.5.2 below.

LF3 is similar to LF2a with the main differences being darker sediments and coarser grains in LF3. Above, we suggested a number of processes that could lead to the stratified appearance of glacimarine mud for the formation of LF2, and infer that similar processes deposited LF3 (see also section 2.5.2 below). Black mottles and the smell of H_2S are suggested to reflect monosulphid layers, formed from seasonal variations in biological productivity (e.g. Elverhøi *et al.*, 1980, 1983).

The unsorted and massive appearance of LF4 as well as the coarser grain sizes are interpreted as the result of sediment accumulation in a high-energy depositional environment, i.e. from gravity flows. Where LF4 occurs as thin beds or lenses, these flows were probably of relatively small scale and could represent turbidite deposits in a glacier-proximal environment (cf. e.g. Gilbert, 1982; Gilbert *et al.*, 1993). Larger packages of LF4, such as at the top of GC06, may accordingly result from large-scale mass-transport deposits, which commonly occur in Svalbard fjords, especially along the fjord walls (e.g. Forwick & Vorren, 2007, 2012; Streuff *et al.*, 2017; this study).

2.4.3.2 Radiocarbon dates and sediment accumulation rates

Six radiocarbon dates were obtained from foraminifera and molluscs from GC01 and GC06 in Magdalenefjorden. The dates are displayed in Table 2.1 and Figure 2.7.

The results from the AMS dating show that the sediments in GC01 reflect recent deposition, with a basal date of ∼505 cal ka BP, an age of ∼319 cal ka BP for a sediment depth of 254 cm, and an age of ∼228 cal ka BP at a sediment depth of 25 cm (Table 2.1, Fig. 2.7). As all dates stem from around 6 mg of generally well-preserved benthic foraminifera we consider the

Table 2.1: *Radiocarbon dates from this study, calibrated using a ΔR of 61 ± 70 (Mangerud, 1972). Note that the reported age for Beta–434937 indicates an age of post 1950 AD and is therefore given in percent modern carbon (pMC) of the modern reference standard.*

Core ID	Depth [cm]	Lab Code	Sample	Reported age [^{14}C a BP]	Median [cal a BP]	2σ [cal a BP]
GC01	25	Beta–447123	Foraminifera	660 ± 30	228	0–20; 49–410
GC01	254	Beta–447124	Foraminifera	730 ± 30	319	131-472
GC01	359-363	Beta–448203	Foraminifera	950 ± 30	505	360-640
GC06	3.5	Beta–434937	Bivalve	106.2 pMC ± 0.3	NA	∼0–60
GC06	12	Beta–434938	Single valve	560 ± 30	132	0–262
GC06	35	Beta–434939	Fragmented bivalve	550 ± 30	124	0–257

foraminifera in GC01 to reflect in-situ conditions and infer that the obtained ages are reliable. Assuming a linear rate of sediment accumulation, the dates from GC01 suggest that LF2a in the lower parts of the core accumulated at a rate of ∼0.49 cm a^{-1}, whereas LF2b, between 254 and ∼50 cm sediment depth, accumulated at a rate of around 3.3 cm a^{-1}. LF1 in the topmost 25 cm of the core was deposited at a sediment accumulation rate (SAR) of 0.04 cm a^{-1} (Fig. 2.7). The relatively high SAR in the central parts of the core suggests that an interpretation of LF2b as ice-proximal sediments is reasonable (cf. e.g. Elverhøi *et al.*, 1980, 1983). Similarly, the lower SAR of the topmost 25 cm supports a distal glacimarine environment. The sediments in GC06 are younger than those in GC01, as the AMS dating shows ages of ∼124 cal ka BP for a sediment depth of 35 cm, ∼132 cal ka BP for a sediment depth of 12 cm, and an age of <60 years for the sediments around 3.5 cm core depth. The age reversal between the two lowermost dates in GC06 may indicate that the single valve at 12 cm was reworked, but considering the very young ages of the sediments at both depths, the large error range may easily account for the older age at 12 cm. Furthermore, the weakly stratified nature of LF3 and the good preservation of the shells sampled suggest that sediment reworking is unlikely in this part of the core. The two ages at 12 and 35 cm could thus suggest that the shells were deposited simultaneously and that LF3 in GC06 accumulated quasi-instantaneously. However, as there is

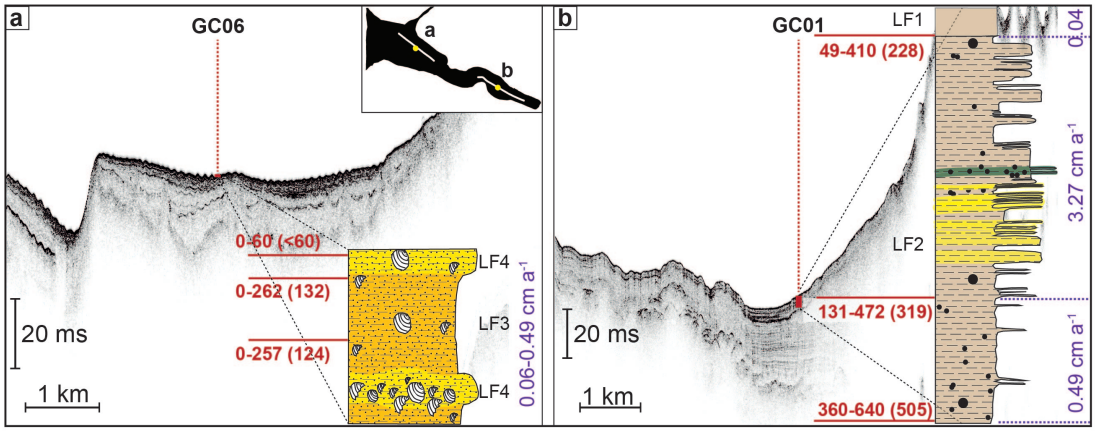

Figure 2.7: *a) Detail of chirp line 09JM-AG211-003 with core location and log of GC06. White lines and dots on the black polygon in the top-right hand corner show the locations of a and b with respect to the bathymetric outline. b) Detail of chirp line 09JM-AG211-006 with the core location and log of GC01. Red lines and numbers show the 2-σ range and the median radiocarbon age in brackets at respective sediment depths, while purple labels refer to sediment accumulation rates.*

some evidence of bioturbation in the core, it is also possible that the age reversal at 12 cm was caused by post-depositional upward migration of an older shell into younger sediments. If this were the case, LF3 was deposited at a SAR of 0.25–0.49 cm a^{-1} in GC06, indicating that this lithofacies was probably deposited in a similar environment to LF2a.

2.5 Discussion

2.5.1 Landform assemblages in Ymerbukta, Trygghamna and Magdalenefjorden

The landforms described from Ymerbukta, Trygghamna, and Magdalenefjorden include (1) bedrock highs, (2) overridden recessional moraines, (3) glacial lineations, (4) terminal moraines, (5) deposits from gravitational mass flows, (6) unmodified recessional moraines, (7) De Geer moraines, and (8) pockmarks. While there is some variability in the landforms observed in the outer fjord basins, the landform assemblages in the ice-proximal basins adjacent to the present glacier fronts are remarkably similar. In Ymerbukta and Trygghamna the more distal fjord basins are characterised by a relatively smooth seafloor with pockmarks and debris flow deposits as the only landforms. In Magdalenefjorden, pockmarks and mass flow deposits are absent and bedrock highs and partially buried recessional moraines are the only features observed. The smooth seafloor in all three fjords suggests some degree of sediment draping, possibly masking underlying landforms (cf. Ottesen & Dowdeswell, 2009), which is confirmed by the thick sedimentary sequences observed on the sub-bottom profiler data (Forwick & Vorren, 2011, 2012; this study). The presence or absence of debris flows could be related to local differences in sediment availability, accumulation rates, exposure to earthquakes, and/or the presence or absence of gaseous fluids beneath the seafloor (cf. e.g. Hovland & Judd, 1988; Forwick *et al.*, 2009; Forwick & Vorren, 2012).

Based on the presence of the landforms in the inner fjord basins and their relationship with each other, we define three landform assemblages, one for each fjord. All assemblages are named after their inferred source glacier. The Esmarkbreen Assemblage occurs in Ymerbukta and comprises overridden recessional moraines, glacial lineations, a terminal moraine and associated debris lobes on its distal flank, and a number of De Geer moraines. The Kjerulfbreen-Harrietbreen Assemblage in Trygghamna is made up of a terminal moraine and an associated debris lobe, three recessional moraines, and a sequence of De Geer moraines. The three recessional moraines and the De Geer moraines in inner Magdalenefjorden form the Waggonwaybreen Assemblage. Their formation is discussed in section 2.5.3 below.

2.5.2 Sedimentary environments

From the lithological data in Magdalenefjorden, we identify three main sedimentary processes in the fjord: (1) suspension settling of fine-grained glacimarine mud from glacial meltwater, (2) delivery of clasts to the fjords as ice-rafted debris melting out from icebergs and sea ice, and (3) abundant gravitational processes reworking the accumulated sediments. The first process, i.e. the rainout of suspension load from meltwater, is the most dominant process in Magdalenefjorden, where the seafloor is covered by a relatively thick sequence of glacimarine muds. These muds are massive at the top of GC01 and GC03 (LF1), where they overlie the (diffusely) stratified mud of LF2. While the depositional process is the same for both lithofacies, the different internal structure indicates slight changes in the depositional environment. Massive mud as recorded in LF1 could reflect more distal conditions, in which there is insufficient energy to transport coarser grains to the core sites and gravitational processes are rare. Ice-distal

conditions and thus lower energy during the accumulation of LF1 are further supported by the low SAR of 0.04 cm a^{-1} and the scattered bioturbation traces (cf. e.g. Elverhøi *et al.*, 1980; Lønne & Mangerud, 1991; Sexton *et al.*, 1992; Baeten *et al.*, 2010).

Similar conditions are inferred for the diffusely stratified sediments of LF2a. In contrast, more pronounced lamination or stratification characteristic of LF2b is considered to be consistent with a more glacier-proximal setting (e.g. Elverhøi *et al.*, 1983; Ó Cofaigh & Dowdeswell, 2001; Forwick & Vorren, 2009), where individual strata were formed due to regular variations in depositional energy. Thinner, more rhythmic laminae, for instance, probably derive from semi-regular changes in meltwater supply or suspension release from the meltwater plumes, which could be tidally or seasonally controlled (e.g. Elverhøi *et al.*, 1980; Mackiewicz *et al.*, 1984; Cowan *et al.*, 1997; Ó Cofaigh & Dowdeswell, 2001). Given the sedimentation rate of 3.7 cm a^{-1} in GC01 we can infer that two such couplets occur per year (in 4 cm of sediment), providing evidence that some of these laminations are indeed seasonally controlled. The abundance of black mottles in LF2 supports this, as it is possibly related to seasonal variations in biological productivity, where black layers reflect diatom blooms in spring (Elverhøi *et al.*, 1980, 1983). Where the lamination or stratification is more irregular, and sandy beds occur, the deposition of glacimarine mud from meltwater is probably influenced by punctuated single events, such as turbidity currents. This is supported by the sharp-based, sometimes undulating boundaries of the sand layers and their downward inclination (see Fig. 2.6f), which are common features of turbidite deposits from glacier-proximal environments (e.g. Kuenen, 1948; Gilbert, 1982; Powell & Molnia, 1989; Gilbert *et al.*, 1993). The relatively high SAR around 3 cm a^{-1} and the absence of bioturbation traces within this facies further supports a glacier-proximal origin for LF2a.

The clasts scattered throughout the glacimarine muds in Magdalenefjorden likely represent IRD and therefore imply that sedimentation from icebergs and sea ice is another process influencing the depositional environment in the fjord. However, the relatively low number of clasts emphasises the importance of sedimentation from meltwater, which partly masks the input from IRD. Individual clasts in lithofacies LF2a are probably dropstones, as indicated by the occasional presence of load structures. The rare diamictic and clast-rich layers embedded into the weakly stratified mud of LF2c on the other hand probably originate from concentrated melting events, either related to iceberg turnover or to the meltout of IRD from shore-fast sea ice and entrapped icebergs during summer, while the surrounding mud was deposited during winter when IRD supply was suppressed (cf. Syvitski *et al.*, 1996; Jennings & Weiner, 1996; Dowdeswell *et al.*, 2000). Considering the nearly stratified appearance of the diamict layers, the gradual, quasi-horizontal contacts (see Fig. 2.6f), and the absence of load clasts, seasonally-controlled sedimentation appears to be more likely than iceberg dumping.

Similar to LF2a, LF3 is interpreted as relatively ice-distal glacimarine mud. The colour difference between the two facies could indicate a different meltwater source, i.e. variable sediment provenance (cf. Forwick & Vorren, 2009; Forwick *et al.*, 2010), an assumption that seems reasonable when considering the location of the core sites. GC01 and GC03, which predominantly contain LF1, are located in the inner and central fjord and are thus likely influenced by meltwater supplied by the four glaciers at the head of the fjord, Buchanbreen, Waggonwaybreen, Miethebreen, and Brokebreen. The core site of GC06 in the outer fjord, on the other hand, may additionally be influenced by sediment supply from Gullybreen, Adambreen, and Skarpeggbreen (see Fig. 2.2). The strong smell of H_2S and the generally darker sediment colour is probably related to a relatively high organic content, which, again, could contribute to the diffuse stratification in the form of annual monosulphid layers formed

by spring algal bloom (Elverhøi *et al.*, 1980, 1983).

The massive sand intermixed with glacimarine mud in LF4 is interpreted as a product of glacier outwash, especially in the inner fjord, or of larger-scale mass-transport events. The latter is more likely, as the frequent occurrence of such events in all fjords is also attested to by the sedimentary lobes visible on the bathymetric data and by the appearance of the lenticular bodies of AF4 and S4a, which were at least partially interpreted as gravity-flow deposits (Forwick & Vorren, 2011; this study). The fact that GC09 and GC06 only contain LF3 and LF4 shows that these core sites are located in a relatively high-energy depositional environment, where such events are frequent, which is a logical consequence of their relatively ice-proximal location.

Although we have no lithological evidence from Ymerbukta and Trygghamna, we suggest that similar sedimentary processes to those in Magdaleneforden also operate in the two Isfjorden tributaries. This is based on the sub-bottom profiler data, showing that sedimentary facies in the three fjords are very similar, and that sedimentation is controlled by glacial meltwater, occasional icebergs, and occasional to frequent gravitational mass flows (Forwick & Vorren, 2011, 2012; this study). This corroborates the findings of previous studies, which showed that the sedimentary processes in front of tidewater glaciers are generally similar, and that it is more the magnitude and the different factors controlling sedimentation rather than the individual processes themselves that vary with climate and locality (e.g. Elverhøi *et al.*, 1983; Cowan *et al.*, 1999; Ó Cofaigh & Dowdeswell, 2001; Ó Cofaigh *et al.*, 2001; Gilbert *et al.*, 2002; Streuff *et al.*, 2017).

2.5.3 Evolution of the landform-sediment assemblages and associated glacier dynamics

From the different landform assemblages observed in the three fjords, we infer regionally variable glacier dynamics. In Ymerbukta, the Esmarkbreen Assemblage is consistent with submarine landform assemblages deposited from glacier surges (e.g. Solheim & Pfirman, 1985; Ottesen *et al.*, 2008; Flink *et al.*, 2015; Streuff *et al.*, 2015), not least because the crevasse-squeeze component in the De Geer moraines may be indicative of surge activity (cf. e.g. Sharp, 1985; Ottesen & Dowdeswell, 2006; Farnsworth *et al.*, 2016). The presence of overridden moraines indicates that Esmarkbreen experienced at least one re-advance after deglaciation. Given that Esmarkbreen was not part of the original surge-type glacier inventory put forward by Hagen et al. in 1993, but was recently identified as surge-type based on the presence of crevasse-squeeze ridges observed in the glaciers terrestrial foreland (Farnsworth *et al.*, 2016), Esmarkbreen probably only surged recently, suggesting that most of the landforms in the Ymerbukta assemblage are relatively young. The exception are the overridden moraines, that must have formed prior to the surge and thus provide evidence for episodic ice retreat during deglaciation or after a LIA advance of Esmarkbreen. A later re-advance, likely related to a surge of Esmarkbreen, formed the glacial lineations during the active phase of rapid advance, the terminal moraine and the associated debris lobe during the transition from active to passive phase, and a sequence of De Geer moraines during subsequent episodic retreat. If we assume that the De Geer moraines were formed each year during winter as suggested for other Spitsbergen fjords (e.g. Ottesen & Dowdeswell, 2006; Ottesen *et al.*, 2008; Flink *et al.*, 2016b) the total number of such moraines in Ymerbukta should indicate that Esmarkbreen surged around 50 years ago. However, given the crevasse-squeeze component of some of these ridges, the fact that Esmarkbreen did not show surge-like behaviour until ∼2010 (Heidi Sevestre, pers. comm.), and the comparatively small number of De Geer moraines in Trygghamna and

Magdalenefjorden (see below), we suggest that the moraines form much less regularly than previously thought and may not necessarily be related to winter re-advances.

Glacier dynamics such as those suggested here for Esmarkbreen have been documented for a large number of Spitsbergen surge-type glaciers (cf. Solheim & Pfirman, 1985; Solheim, 1991; Boulton *et al.*, 1996; Christoffersen *et al.*, 2005; Ottesen *et al.*, 2008; Kristensen *et al.*, 2009; Flink *et al.*, 2015; Streuff *et al.*, 2015), supporting the hypothesis that Esmarkbreen is indeed a surging glacier (Farnsworth *et al.*, 2016). The sub-bottom profiler data from the fjord show that sedimentation was largely similar throughout the Holocene with mud settling from glacial meltwater, IRD melting out from icebergs and or sea ice, and occasional mass transport events reworking the accumulated deposits (Forwick & Vorren, 2009, 2011).

In Trygghamna we identified 29 De Geer moraines and a large debris lobe on the flank of the outermost moraine (see Figs. 2.3, 2.4d) as part of the Kjerulfbreen-Harrietbreen Assemblage. This outermost moraine could represent a terminal moraine marking the Holocene maximum ice extent in the fjord. Despite the similarities in landforms between Trygghamna and Ymerbukta, and although both Kjerulfbreen and Harrietbreen at the head of Trygghamna have recently been identified as surge-type glaciers (Farnsworth *et al.*, 2016), we hesitate to ascribe a definitive surge origin to the submarine landforms in Trygghamna. This is mainly because the absence of overridden moraines indicates only one Holocene re-advance of the glaciers in the fjord, which could also be related to the LIA cooling rather than a surge (cf. e.g. Plassen *et al.*, 2004; Ottesen & Dowdeswell, 2006; Forwick *et al.*, 2010), and because the absence of glacial lineations suggests relatively slow ice flow (cf. King *et al.*, 2009), which is atypical for the active phase of a surging glacier (e.g. Meier & Post, 1969; Raymond, 1987; Sharp, 1988; Benn & Evans, 2010). The landform assemblage in Trygghamna could thus be a product of ice retreat, either during deglaciation or after the LIA, with the outermost moraine indicative of a prolonged period of stillstand related to either (i) shoaling waters and accordingly slowed glacier retreat (e.g. Oerlemans & Nick, 2006; Benn *et al.*, 2007a; Kehrl *et al.*, 2011), or (ii) the transition between ice advance and ice retreat during the LIA. Nevertheless, if crevasse-squeeze ridges are indeed surge-diagnostic landforms, their presence in the terrestrial forelands of both glaciers (Farnsworth *et al.*, 2016), and the variable orientations of some of the submarine De Geer moraines should suggest that the entire landform assemblage formed from a glacier surge. Based on the absence of overridden moraines and glacial lineations, we suggest that formation of the terminal moraine and the associated debris lobe in Trygghamna occurred as a result of a re-advance of Harrietbreen and Kjerulfbreen during the LIA cooling (cf. Ottesen & Dowdeswell, 2006), but note that glacier advance and subsequent landform formation could have occurred from both glacier surging or LIA advances. Similar conclusions have also been drawn for the adjacent Borebukta and Yoldiabukta (Ottesen & Dowdeswell, 2006).

The debris lobes and pockmarks in the outer parts of both Ymerbukta and Trygghamna must have formed during the Holocene after the fjord was ice free, as a grounded glacier would have prevented the deposition of large mass-transport deposits along the fjord walls and the escaping of fluids from the seafloor (cf. Forwick *et al.*, 2009; Forwick & Vorren, 2012).

Glacial lineations in Isfjorden are transverse to the direction of inferred ice flow through Ymerbukta and Trygghamna and are thus likely the product of ice streaming through the fjord during the LGM (cf. e.g. Landvik *et al.*, 1998; Ottesen *et al.*, 2005). The ice-marginal wedge provides evidence for an extended period of stillstand during overall glacier retreat.

In Magdalenefjorden, the presence of a deep bathymetric basin in the central fjord complicates the reconstruction of the local ice dynamics, as it is difficult to ascertain whether

a lack of glacial landforms within the central parts of this basin is related to (i) partial ungrounding of the retreating ice margin during deglaciation, or (ii) post-glacial sediment masking. The De Geer moraines in the fjord could thus have formed during episodic ice retreat related to either deglaciation or a LIA re-advance of the local glaciers. As the moraines or parts thereof occur within the entire fjord and along the steep side walls of the bathymetric basin, it is likely that at least the moraines in the outer fjord, and possibly those within the basin, were deposited during deglaciation when ice retreated from its maximum position at the continental shelf edge (cf. Ottesen & Dowdeswell, 2009). In the inner fjord, the moraines could also be a product of Holocene glacier re-advance and subsequent retreat. Indeed, the most distal of the De Geer moraines here is slightly larger than the rest and was previously interpreted as a terminal moraine marking the maximum ice extent of Waggonwaybreen during the LIA (Ottesen & Dowdeswell, 2009). This interpretation is supported by our lithological evidence and sub-bottom profiler data which show the presence of a small and localised debris flow down the moraine's distal flank. We note, that in this instance the assumption of annual formation for the De Geer moraines would also be unreasonable, as the total number of 37 would suggest that Waggonwaybreen reached its LIA maximum less than 40 years ago.

From the lithological data in Madalenefjorden we summarise the following chronology for the sediments in the fjord: LD2a is the oldest recovered facies in the cores and was deposited during relatively ice-distal conditions. Based also on the AMS date of around 500 cal ka BP, it is likely that this subfacies was deposited during glacier retreat during deglaciation, probably before the LIA. The fact that GC03 mostly contains LF2a shows that the sedimentary processes at this core site were largely the same throughout the Holocene. In GC01 LF2a is overlain by LF2b, which was interpreted as proximal glacimarine sediment. The stratification, the high SAR and the accumulation of this facies relatively soon after ∼320 cal ka BP could suggest that Waggonwaybreen re-advanced in response to the LIA cooling. The increasingly more diffuse stratification up-core of GC01 and the re-appearance of LF2a before ∼230 cal ka BP implies that retreat after the LIA advance was already underway at this point. The ice-distal sediments of LF1 at the top of both GC01 and GC03 indicate that the glacier front had retreated relatively far back from the core sites by ∼230 cal ka BP.

Lithofacies LF3 reflects the contemporary sedimentary environment at the core site of GC06, where the input from many different sources maintains a high SAR and causes occasional small-scale changes in the depositional environment. As LF4 was interpreted as deposits from gravitational mass-flow events, this lithofacies is chronologically independent, as such events can occur at any point in time. Nevertheless, where the facies occurs as thin beds in the mud of LF2b in GC01, the deposition of LF4 was likely related to the possible re-advance of Waggonwaybreen during the LIA.

2.6 Conclusions

Swath-bathymetric data from three fjords reveal the landform assemblages in front of several Spitsbergen tidewater glaciers. While the main processes forming the landforms are somewhat similar, individual glacier dynamics control the occurrence of different types of landforms. In Ymerbukta, one or more surges of Esmarkbreen are indicated by the presence of overridden moraines and glacial lineations, formed during retreat followed by relatively fast glacier re-advance. A terminal moraine and associated debris lobe mark the maximum extent of the glacier

during the Holocene, and the occurrence of numerous De Geer moraines provides evidence for subsequent step-wise retreat. Processes of crevasse-squeezing are implied by the variable orientation and occasional cross-cutting of these moraines. In the adjacent Trygghamna a terminal moraine and debris lobe were probably formed as a result of a LIA re-advance of the two glaciers Kjerulfbreen and Harrietbreen at the head of the fjord, after which retreat was similarly episodic as in Ymerbukta.

In Magdalenefjorden in northeast Spitsbergen a slightly larger moraine at the edge of the innermost basin is probably related to a re-advance of Waggonwaybreen in response to the LIA around 300 cal a BP. The characteristic debris lobe often associated with the distal flank of such terminal moraines in Svalbard fjords appears to be unusually small in Magdalenefjorden, suggesting that the glacier front halted there for only a short period of time, or that sediment availability was restricted. Retreat, as indicated by numerous De Geer moraines, was also episodic. Our data show, that contrary to previous assumptions, De Geer moraines can form much less frequently than once a year. The transition from distal to proximal to distal glacimarine mud in one of the gravity cores from Magdalenefjorden reflects a sequence of glacier retreat, likely related to deglaciation after the LGM, glacier re-advance probably related to the LIA cooling, and subsequent retreat of the glacier front. Distal glacimarine muds are massive to weakly stratified with occasional evidence of bioturbation, and were deposited at relatively low rates of 0.04–0.49 cm a^{-1}. Ice-proximal glacimarine muds are distinctly laminated or stratified and contain couplets of one coarser and one finer layer, which probably derive from seasonally controlled suspension rainout from meltwater plumes. The occurrence of turbidity currents is indicated by the presence of several thin sandy layers in the glacimarine mud. The proximal stratified muds accumulated at a rate of around 3 cm a^{-1}.

The lithofacies observed in the gravity cores reveal that suspension settling from meltwater plumes and the water column is the dominant sedimentary process in Magdalenefjorden, with very occasional input of IRD from icebergs and sea ice. These sediments are reworked as a consequence of turbidity currents close to the glacier fronts and of other mass-flow events such as slides and slumps down steep submarine slopes. Our data show that components of landform assemblages as well as sedimentary processes in glacimarine environments are largely similar and that small variations across wider areas are controlled by localised changes in glacier hydrology, thermal regime, sediment availability, bathymetry and air/ocean temperatures, rather than different geographic location and climate.

Acknowledgements

This work, as part of the GLANAM project "Glaciated North Atlantic Margins", was funded by the People Programme (Marie Curie Actions) of the European Union's Seventh Framework Programme FP7/2007-2013/ under REA grant agreement n^o 17217. We thank the captain and crew of *R/V Helmer Hanssen* (previously *Jan Mayen*).

Author contributions

This chapter in its current form is based on a team effort of the individual co-authors. Data acquisition was organised by Riko Noormets, who made the data accessible to me and helped me with the coordinate conversion of the raw files. All analyses and interpretations including the visualisation of acoustic data, the description and sub-sampling of sediment cores and the isolation and preparation of radiocarbon samples were carried out by the lead author, who

also prepared all figures and the large majority of the text. Colm Ó Cofaigh did most of the reviewing, providing feedback and suggestions for improvement on the manuscript as a whole. Jerry Lloyd and two anonymous reviewers also helped improve the manuscript by providing several suggestions for editing. Author contributions to the manuscript in its current form are estimated as follows (not considering data acquisition processes): Katharina Streuff 85%, Colm Ó Cofaigh 10%, Riko Noormets 3% and Jerry Lloyd 2%.

Chapter 3

Submarine landforms and glacimarine sedimentary processes in Lomfjorden, East Spitsbergen

Streuff, K.; Ó Cofaigh, C.; Noormets, R.; Lloyd, J. M. (2017a): Submarine Landforms and Glacimarine Sedimentary Processes in Lomfjorden, East Spitsbergen. *Marine Geology.* DOI: 10.1016/j.margeo.2017.04.014.

Abstract

Understanding the role of fjords in modulating the long-term interaction between ice sheets and glaciers with the surrounding ocean requires the investigation of glacigenic landform and sediment archives. In Svalbard, there is a wealth of data from fjords in West Spitsbergen that constrains the glacial history of this sector of the Svalbard-Barents Sea Ice Sheet (SBIS) since the Last Glacial Maximum (LGM), and the nature and timing of subsequent ice retreat. In contrast, however, very little is known about the glacial history of fjords in East Spitsbergen.

This paper combines multibeam swath-bathymetry, sub-bottom profiles, lithological data and radiocarbon dates from Lomfjorden, Svalbard, to provide the first insights into the dynamics of tidewater glaciers and associated glacimarine sedimentary processes in a northeast Spitsbergen fjord. At the LGM, a fast-flowing ice stream drained the SBIS through Lomfjorden, serving as a tributary to a south-north flowing ice stream in Hinlopenstretet. Ice advance is recorded by streamlined bedrock, glacial lineations and drumlins. A radiocarbon date of ∼9.7 ka BP from the outer fjord provides a minimum date for retreat of this ice stream, and suggests that Lomfjorden was ice-free earlier than fjords in West Spitsbergen. Ice retreat occurred in a slow and step-wise manner, indicated by the presence of recessional moraines and De Geer moraines. By 4.5 ka BP the local tidewater glaciers had probably retreated inland of their present positions. The limited extent of glacigenic landform assemblages in front of these glaciers implies that any Holocene re-advances were probably restricted.

The principal sedimentary processes during deglaciation were suspension settling from meltwater, causing deposition of weakly stratified, bioturbated mud in ice-distal settings at rates of 0.02–0.08 cm a^{-1}, and gravitational mass flows forming sandy turbidites in ice-proximal areas. Iceberg ploughmarks and ice-rafted debris provide evidence for the presence of large icebergs during deglaciation.

Our data suggest an early and extensive deglaciation in East Spitsbergen fjords and show that previous reconstructions of the extent of the SBIS need to be revised as new data emerges from East Spitsbergen. The data confirm that tidewater glaciers from different regions of Spitsbergen behaved differently since the LGM, and that variations in landform-sediment assemblages occur even within geographically adjacent fjords.

3.1 Introduction

The landforms and sediments deposited beneath and in front of modern glaciers are an important archive of past glacial dynamics and of glacier response to climatic forcing (e.g. Cottier *et al.*, 2010; Forwick *et al.*, 2010), but glacier beds and submarine forelands are often relatively inaccessible due to the presence of overlying glacier ice or sea ice in fjords. In this context Svalbard is of particular interest, as the ongoing retreat of many fjord-terminating tidewater glaciers has recently exposed well-preserved glacial and glacimarine landform-sediment assemblages (e.g. Plassen *et al.*, 2004; Ottesen & Dowdeswell, 2006; Ottesen *et al.*, 2008; Forwick *et al.*, 2010; Kempf *et al.*, 2013; Flink *et al.*, 2015; Streuff *et al.*, 2015). Furthermore, fjords in Spitsbergen, the largest island of the archipelago, are usually ice-free during summer and thus enable the acquisition of high-resolution seismic data and sediment cores. These data provide valuable insights into the nature of the glacial deposits, and thus, by inference, into the associated glacigenic processes (e.g. Syvitski, 1989; Sexton *et al.*, 1992; Boulton *et al.*, 1996; Cai *et al.*, 1997; Forwick *et al.*, 2010). Fjords along the west coast of Spitsbergen have received increasing attention during the last two decades and resulting studies have documented characteristic landform assemblages in front of many tidewater glaciers. These include (overridden) recessional moraines, glacial lineations, eskers, terminal moraines, debris flow lobes, in some cases crevasse-squeeze ridges, and annual push moraines (e.g. Ottesen & Dowdeswell, 2006; Ottesen *et al.*, 2008). Terminal moraines in the fjords commonly mark the extent of glacier advances during the Holocene, which occurred either due to climatic cooling, particularly during the Little Ice Age (LIA), or as a consequence of glacier surges (e.g. Plassen *et al.*, 2004; Ottesen & Dowdeswell, 2006; Ottesen *et al.*, 2008; Forwick & Vorren, 2011; Flink *et al.*, 2015; Streuff *et al.*, 2015; Burton *et al.*, 2016). Conversely, very little is known about the fjords along Spitsbergen's eastern coast, where, to our knowledge, only Hambergbukta in the south has been studied in detail (Noormets *et al.*, 2016a,b). Hence, our limited understanding of oceanography, glaciology, glacigenic landform assemblages and sedimentary processes in east Spitsbergen fjords inhibits the development of accurate ice sheet models, which are crucial to understanding the complex climatic system and the role of its individual components on ice sheet dynamics and deglaciation history in Svalbard and the Barents Sea (Patton *et al.*, 2015; Stokes *et al.*, 2015; Gowan *et al.*, 2016; Kirchner *et al.*, 2016).

This study is the first to address in detail the glacimarine environment, including oceanography, sedimentary processes, and landforms in a northeast Spitsbergen fjord, and is the first to provide constraints on the timing of ice retreat in this area. We present and analyse multibeam swath-bathymetric and sub-bottom profiler data, sediment cores, CTD data and a suite of radiocarbon dates from Lomfjorden, Northeast Spitsbergen, from which we reconstruct the Holocene dynamics of the local tidewater glaciers and evaluate whether glaciers in East Spitsbergen behaved differently to those in the west.

3.2 Study area and background

3.2.1 Physiographic setting

Lomfjorden is located in Northeast Spitsbergen between ~79°21'N, 17°40'E and 79°43'N, 18°20'E. It is orientated south to north, opens into Hinlopenstretet, a strait between Spitsbergen and Nordaustlandet, and is located in a relatively protected environment (Fig. 3.1). Lomfjorden is 35 km long, 2–10 km wide and up to 200 m deep. A major fault zone, the Lomfjorden-

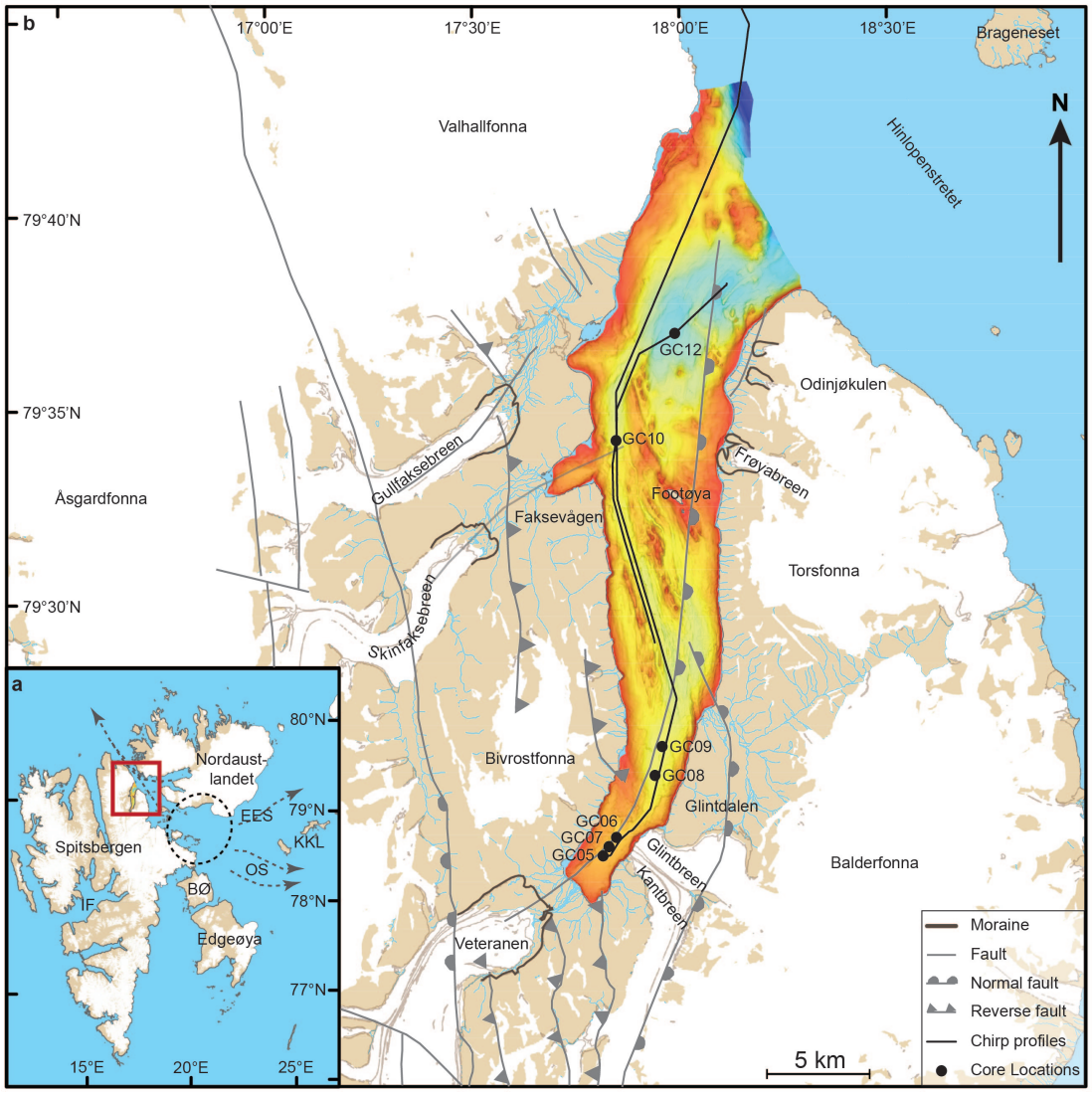

Figure 3.1: *a) Overview map of Svalbard with red rectangle indicating the area presented in b. EES = Erik Eriksenstretet, OS = Olgastretet, KKL = Kong Karls Land, BØ = Barentsøya, IF = Isfjorden. Black circle and grey arrows indicate position of a suggested ice dome and ice flow directions, respectively, during the Late Weichselian (Landvik* et al.*, 1998; Dowdeswell* et al.*, 2010a). b) Study area with multibeam swath-bathymetry, chirp lines (black lines) and core locations (black dots) available for this study. Brown lines on the glaciers represent moraines. Basemap data are courtesy of the Norwegian Polar Institute (geodata.npolar.no).*

Agardhbukta Fault Zone, runs through the centre of the fjord, with Palaeozoic and Mesozoic sediments defining Lomfjorden's eastern coast, and Neoproterozoic basement rocks defining the west (Dallmann *et al.*, 2002). There are three tidewater glaciers along Lomfjorden's shore, Glintbreen and Kantbreen in the east, and Valhallfonna in the northwest (Fig. 3.1). At the head of Lomfjorden, the Veteranen glacier previously reached tidewater but has now retreated onto land where it formed several moraines (Fig. 3.1). Other currently terrestrial glaciers are Odinjøkulen and Frøyabreen along the eastern shore and Bivrostfonna, Frostbreen, Skinfaksebreen and Gullfaksebreen along the western shore (Fig. 3.1). Two small embayments are located along the fjord's western shore, Faksevågen in the south and De Geerbukta in the north, which host Skinfaksebreen and Gullfaksebreen, respectively (Fig. 3.1). The catchment areas of the tidewater glaciers are mainly underlain by carbonate bedrock (dolomites and limestones) with lesser quartzites and metagreywacke (Dallmann *et al.*, 2002).

In terms of oceanographic setting, little is known about Lomfjorden. Investigations from the

eastern side of Svalbard document that the waters there are mostly fed by relatively cold and fresh Arctic Water and that the inflow of warm and saline Atlantic water, so common in West Spitsbergen, is absent in the east (cf. e.g. Svendsen *et al.*, 2002; Hald *et al.*, 2004; Ślubowska-Woldengen *et al.*, 2007). Nevertheless, inflow of warmer Atlantic water into Hinlopenstretet was indicated by lithological records from the northern Svalbard margin (e.g. Koç *et al.*, 2002; Ślubowska *et al.*, 2005).

3.2.2 Glacial background

Contrary to the well-investigated history of the SBIS in West Spitsbergen and north and east of Svalbard (e.g. Mangerud *et al.*, 1992; Elverhøi *et al.*, 1995; Landvik *et al.*, 1995, 1998; Ottesen *et al.*, 2005; Ingólfsson & Landvik, 2013), very little is known about the glaciological evolution of fjords in East Spitsbergen, including Lomfjorden. Only recently have summer sea ice conditions allowed the acquisition of geophysical and lithological data in eastern Svalbard and thus enabled the reconstruction of the glacial history around Kong Karls Land and Edgeøya (Dowdeswell *et al.*, 2010a; Hogan *et al.*, 2010). General consensus is that large parts of the Barents Sea and all of Svalbard were glaciated during the LGM, ∼20 ka BP, when the large fjord systems on Svalbard channelled fast-flowing ice streams that extended to the continental shelf edge (e.g. Elverhøi *et al.*, 1993; Landvik *et al.*, 1998; Svendsen *et al.*, 2004; Ottesen *et al.*, 2005; Ingólfsson & Landvik, 2013). During this time ice flowed eastwards through Olgastretet and Erik Eriksenstretet, westwards towards Isfjorden, and northwestwards through Hinlopenstretet and Wijdefjorden from a large ice dome located just west of Kong Karls Land at the southern entrance of Hinlopenstretet (Fig. 3.1a; Landvik *et al.*, 1998; Dowdeswell *et al.*, 2010a; Hogan *et al.*, 2010). The timing of the onset of deglaciation in this part of the Barents Sea is still debated, with ages ranging from 15 ka BP to 13.4 ka BP (Jones & Keigwin, 1988; Elverhøi *et al.*, 1995; Kleiber *et al.*, 2000). During deglaciation ice retreated relatively slowly and in a step-wise manner, depositing recessional moraines in Erik Eriksen Strait (Dowdeswell *et al.*, 2010a; Hogan *et al.*, 2010). Edgeøya and Barentsøya southeast of Spitsbergen became ice-free around 10.3 ka BP, when a major calving event resulted in the disintegration of the marine-based sector of the SBIS (Landvik *et al.*, 1995).

3.3 Material and methods

Multibeam swath-bathymetry, subbottom profiler (chirp) data, and seven sediment cores provide the basis for this study. Bathymetric data were collected by the Norwegian Hydrographic Survey in July and August 2011, using a Kongsberg Simrad Multibeam EM3002 on the vessel *Hydrograf*. The data were processed in DMagic, gridded to a resolution of 5 m and visualised and interpreted in the Fledermaus v7 Software. Chirp data were acquired by the University Centre in Svalbard on *R/V Helmer Hanssen* in September 2014, using an EdgeTech 3300-HM subbottom profiler operating at a pulse mode of 2–16 kHz bandwidth and 3 ms pulse length. The data were processed using the EdgeTech Software and visualised in IHS The Kingdom Software. Seven gravity cores were taken during the same cruise and provide the basis for the lithology section (Table 3.1). At two of the core sites and one additional site conductivity-temperature-depth (CTD) information was obtained from the water column (Table 3.1). Gravity cores were retrieved with a 1900 kg heavy gravity corer with a 6 m long steel barrel. Upon retrieval the cores were cut into sections of up to 110 cm long and run through a loop sensor to measure the magnetic susceptibility of the sediments. The cores were

then split into working and archive halves. For the water content 1 cm-thick sediment slabs were taken in 8 cm-intervals, weighed, dried at 60°C and weighed again. The samples were subsequently wet-sieved through mesh sizes of 500, 250, 125 and 63 μm to determine the grain size distribution within the cores. Core logs were generated based on the visual description of the sediment surface aboard the ship and at the University Centre in Svalbard. The archive halves (in some cases the working halves) were subsequently x-rayed using a GEOTEK Thermo Kevex PSX10-65W-Varian2520DX with a voltage of ∼95 kV and a current of around 150 μA. Correlation between seismo- and lithostratigraphy and calculation of acoustic facies thickness were done by converting sediment core depth from m to ms, and facies thickness from ms to m, assuming an average p-wave velocity of 1500 m s^{-1} (two-way travel time). Conversions are estimates only and may lead to slight inaccuracies concerning core penetration depth and actual facies thickness. Foraminifera and, where present, bivalves, were collected from strategic locations in two of the gravity cores, GC12 in the outer fjord and GC08 in the inner fjord, and were submitted to Beta Analytic for Accelerator Mass Spectrometry radiocarbon dating. The obtained conventional ^{14}C ages were calibrated using the MARINE13 calibration with a marine reservoir effect of 400 years and a Delta R of 100 ± 39 years (Table 3.2; cf. Long *et al.*, 2012).

Table 3.1: *Gravity cores and CTD data used in this study.*

Sample ID	CTD	Recovery [cm]	Water depth [m]	Latitude (N)	Longitude (E)
GC05 + CTD	St611	263	68	79°23.033'	17°43.325'
GC06		88.5	75	79°23.488'	17°45.283'
GC07		294	70	79°23.265'	17°44.163'
GC08		276	116	79°25.037'	17°51.073'
GC09 + CTD	St612	305	119	79°25.773'	17°52.310'
GC10		105	118	79°33.702'	17°47.905'
GC12		339	200	79°36.392'	17°57.003'
CTD	St613		205	79°37.571'	18°04.736'

3.4 Results

3.4.1 Seafloor morphology

Based on the available swath-bathymetric data, we define (1) streamlined bedrock highs, (2) glacial lineations, (3) drumlins, (4) recessional moraines and, in some cases, associated debris lobes, (5) De Geer moraines, (6) submarine channels, (7) mass-transport deposits, and (8) iceberg ploughmarks in Lomfjorden. Their distribution in the fjord is shown in Figure 3.2.

3.4.1.1 Large longitudinal ridges – bedrock

Four large, straight to slightly sinuous ridges, R1, R2, R3, and R4 occur in inner and central Lomfjorden (Fig. 3.2). They are orientated NNW–SSE, obliquely to the main fjord axis, and are composed of several segments, which are 60–100 m high, up to 1.2 km wide and 150–2500 m long. These segments generally have sharply defined crests which are composed of multiple peaks (Fig. 3.3b). The ridges occur in water depths between 20 and 120 m and reach overall lengths between 2 and 5.5 km. They appear streamlined in the inner fjord, where they are also

overprinted by drumlins (see Figs. 3.2, 3.3 and section 3.4.1.3 below). R4 is the submarine extension of the island Footøya (Fig. 3.2) and its most distal segment has three crests along its main axis. In addition to the ridges in the central and inner fjord, several large bathymetric highs occur in the outer fjord (Fig. 3.2). These are around 60 m high and 0.5–3 km wide.

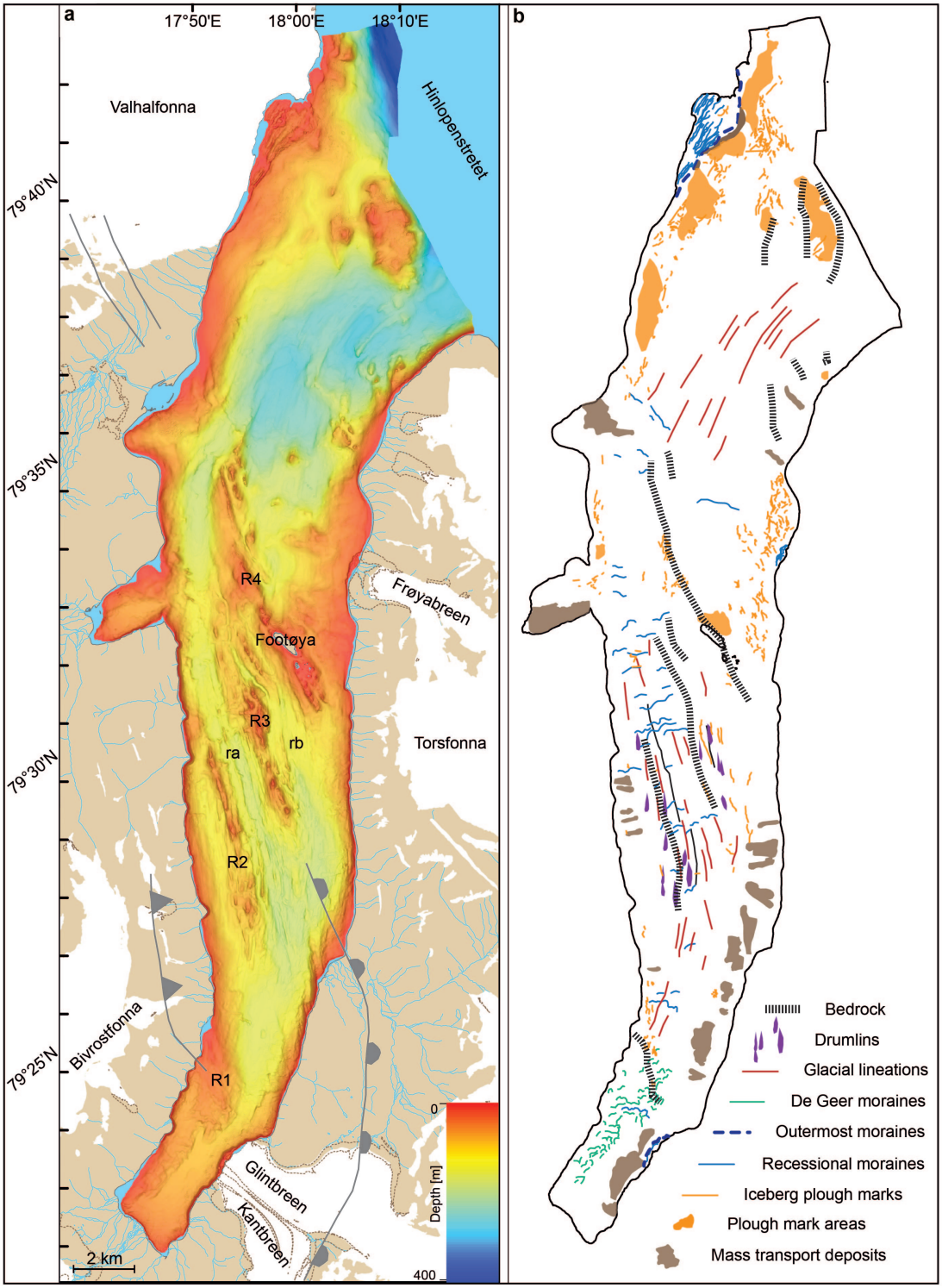

Figure 3.2: *a) Bathymetry of the study area with faults (grey lines; information from geodata.npolar.no) and larger ridges (R1–R4, ra, rb) indicated. See Figure 3.1 for full legend. b) Morphological map of the landforms observed in Lomfjorden.*

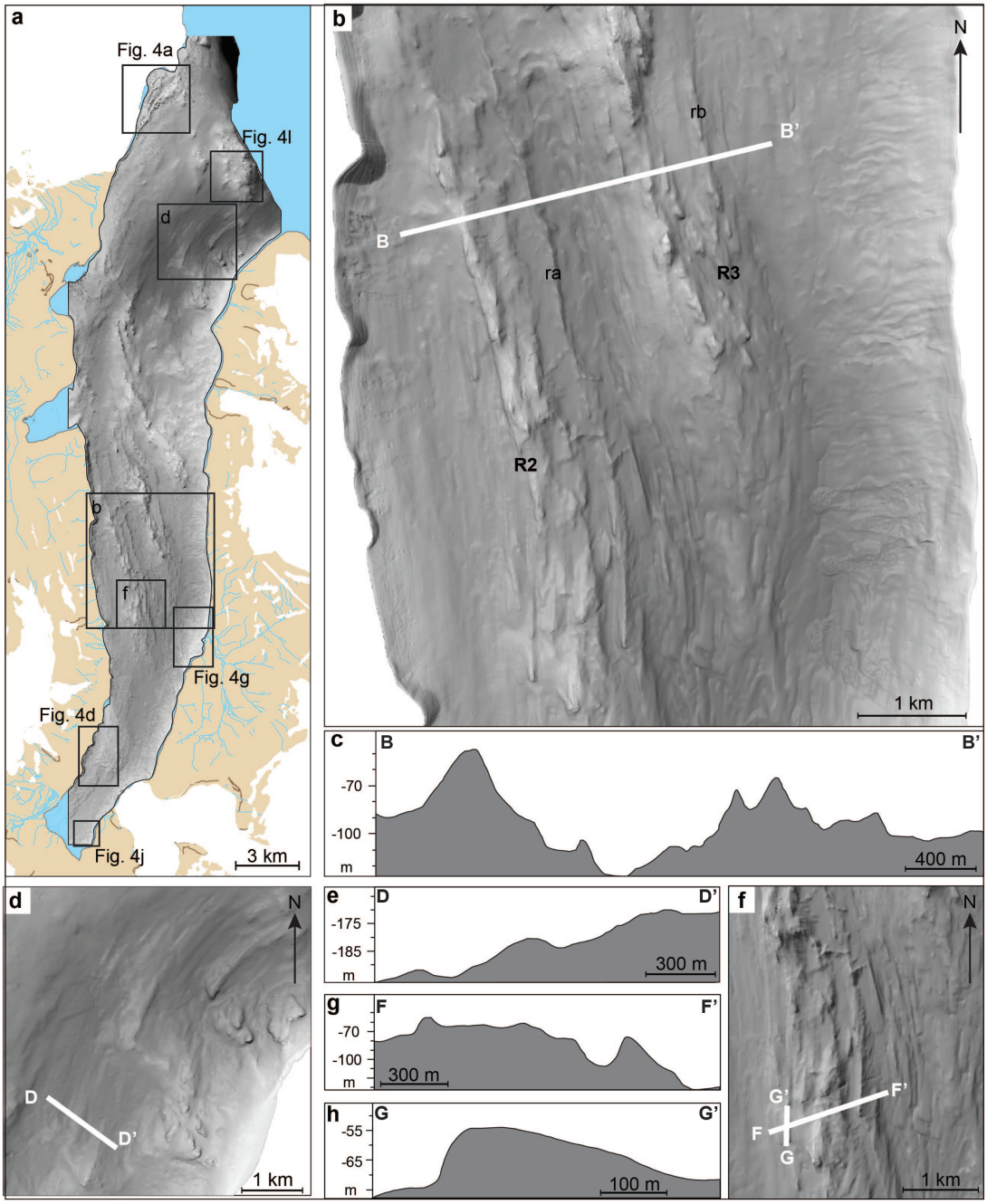

Figure 3.3: *a) Overview of the bathymetric data and the locations for subfigures of this figure and Figure 4. b) Example of the bedrock ridges in Lomfjorden with cross-sectional profile B-B' shown in c). d) Glacial lineations in the outer fjord with cross-sectional profile D-D' shown in e). f) Drumlins in the inner fjord with two cross-sectional profiles F-F' and G-G' displayed in g) and h), respectively.*

The irregular and discontinuous character of the ridge crests as well as their large scale is unlike any glacially-derived submarine ridges in Spitsbergen (cf. e.g. Solheim & Pfirman, 1985; Boulton *et al.*, 1996; Ottesen *et al.*, 2008). Furthermore, we would expect pro- or subglacial ridges to be formed either perpendicular or (sub-)parallel to the direction of ice flow. The ridges' oblique orientation, their morphology, and their location in the fjord is therefore at odds with a solely glacial origin and we suggest that the ridges and, in the outer fjord, the bathymetric highs, are composed of bedrock that has been partially streamlined. This is based on the following: (1) the ridges' orientation is similar to some of the faults in the area (Figs.

3.1, 3.2), (2) R4 is the submarine extension of the island Footøya (Fig. 3.2), and (3) the ridges are similar to bedrock ridges in Van Keulenfjorden (Kempf *et al.*, 2013).

Two small longitudinal, streamlined ridges (ra and rb) follow the bathymetric contours of R1-R4 (Figs. 3.2, 3.3b). They are morphologically similar to the bedrock ridges, as ra and rb are also composed of several segments, which have straight to slightly sinuous crests with multiple peaks. However, their segments are much longer (up to 3.5 km) and lower (2–15 m high) than those of R1–R4, and are up to 150 m wide (Fig. 3.3b). In a few places ra and rb are overprinted by, or confluent with, the small transverse ridges described in section 3.4.1.4 below.

Based on similarities in morphology and orientation, these ridges could represent the small-scale equivalent of the bedrock ridges R1–R4. However, ra and rb are also, at least partially, of glacial origin, as they are streamlined and similar to the glacial lineations and drumlins observed in the fjord (see sections 3.4.1.2 and 3.4.1.3 below).

3.4.1.2 Elongate, streamlined grooves and ridges – glacial lineations

Elongate grooves and ridges in the outer fjord are 2–10 m high, 700–3000 m long, up to 200 m wide and spaced at distances of between 200 and 400 m (Figs. 3.2, 3.3d, e). Their elongation ratios, in most cases, exceed 10:1. Their crests are straight to slightly curved and are mostly round and symmetrical in cross-section (Fig. 3.3).

The elongate features in outer Lomfjorden appear similar to groove-ridge features described from other Spitsbergen fjords, and are thus interpreted as (mega-scale) glacial lineations (cf. Ottesen & Dowdeswell, 2006; Ottesen *et al.*, 2008). Glacial lineations, especially those with length:width ratios exceeding 10:1 are exclusively associated with fast ice flow (Stokes & Clark, 2002; King *et al.*, 2009). They are formed beneath a (surging) glacier or ice stream, where the soft subglacial sediments are deformed into ridges and grooves by a combination of erosion and re-deposition (Smith, 1997; Tulaczyk *et al.*, 2001; Clark *et al.*, 2003; Ó Cofaigh *et al.*, 2005).

Segments of similar streamlined grooves and ridges occur around the three bedrock ridges R2–R4 in the central part of Lomfjorden (Fig. 3.2). They are up to 700 m long, 100 m wide, and ∼5 m high, with maximum elongation ratios of 7:1. The grooves and ridges are orientated (sub-)parallel to each other and spaced at variable distances between 50 and 100 m. They follow the contours of the bedrock ridges (Figs. 3.2, 3.3) and have thus slightly variable orientations.

These groove-ridge segments are similar to the glacial lineations in the outer fjord and were presumably formed by the same processes, i.e. sediment deformation beneath the glacier. Nevertheless, the discontinuous character and the much smaller elongation ratios of the streamlined segments indicate that the conditions during their formation may have been different. Possible explanations for the short lengths could be (1) insufficient sediment, (2) a less deformable glacier bed, and/or (3) slower ice flow. The outcropping bedrock highs at the seafloor may, for example, have acted as "sticky spots" or obstacles and thus slowed glacier flow.

3.4.1.3 Small, streamlined ridges – drumlins

Small, elongate (sub-)parallel ridges occur in close proximity to the bedrock ridges in central Lomfjorden (Fig. 3.2), and are between 250 and 1500 m long, up to 200 m wide, and ∼10 m high. They have straight, sharply defined crests and are spaced at distances between 50 and 200 m (Fig. 3.3b, f–h). The ridges are orientated in the direction of the main fjord axis and appear slightly broader and blunter at their ice-proximal (stoss) sides, where they often have a small bulge (Fig. 3.3h). Their distal ends appear tapered and terminate in a point.

Although some of the small ridges in central Lomfjorden appear similar to glacial lineations from other Spitsbergen fjords (Flink *et al.*, 2015; Streuff *et al.*, 2015), the blunt stoss sides, tapered lee ends, dimensions and 'tear-drop' shape in planform are more consistent with these features being drumlins (cf. Clark *et al.*, 2009; Spagnolo *et al.*, 2010).

3.4.1.4 Transverse ridges – recessional moraines

Small ridges in front of Valhallfonna in the outer fjord (Fig. 3.2) are parallel to the ice margin and to each other, are continuous, and up to 3 km long (Fig. 3.4a–c). They are orientated transverse to the inferred direction of ice flow, are 2–5 m high, around 30 m wide and occur in water depths of around 10 m (Fig. 3.4a, b). The ridges are generally symmetrical in cross-section and have well-defined, sharp, and slightly sinuous crests. Several of these ridges are observed to merge in places and exhibit branching. They are spaced at distances of approximately 50, 100, or 150 m. The outermost ridge furthest away from the current ice margin is slightly larger and is up to 20 m high, 3.6 km long, and ∼400 m wide (Fig. 3.4a, b).

In front of Glintbreen/Kantbreen in inner Lomfjorden, two of these ridges are ∼1 km long and occur spaced at ∼50 m in a water depth of around 10 m. Again, the outermost ridge is slightly higher (10 m) than the inner one (5 m). In front of both Valhallfonna and Glintbreen/Kantbreen lobate landforms occur on the outermost ridges' distal flank and cover areas of approximately 200 x 1500 and 250 x 850 m^2. In front of Frøyabreen in the east, four of the small ridges occur (Fig. 3.2) and are up to 1 km long, ∼5 m high and spaced at approximately 50 m.

Ridges in the central fjord are morphologically similar to those in front of the tidewater glaciers, but are slightly wider (∼100 m) and much shorter (∼500 m). These shorter ridges are predominantly sub-perpendicular to the main fjord axis, parallel to each other, and are, in some cases, closely associated with ridge ra described in section 3.4.1.1; either as perpendicular "branches" to one side of the ridge or cross-cutting the ridge at a ∼90°-angle. They are irregularly spaced, with distances of 700–2000 m between individual ridges (Figs. 3.3b, 3.4d).

In terms of dimensions, morphology and orientation, the transverse ridges in Lomfjorden are similar to annual push moraines described from other fjords in Spitsbergen (Ottesen & Dowdeswell, 2006; Ottesen *et al.*, 2008), which suggests that the ridges in Lomfjorden were also formed as end moraines at a glacier grounding line. Annual push moraines result from small winter re-advances or stillstands of the glacier during overall retreat, and are often the result of shore-fast sea ice preventing iceberg calving and thus further retreat of the glacier margin (e.g. Boulton, 1986; Ottesen & Dowdeswell, 2006; Flink *et al.*, 2015). The symmetrical form of the Lomfjorden ridges may reflect formation from debris meltout at the grounding line rather than actual sediment push, and we therefore favour the more general interpretation of these ridges as recessional moraines.

In front of Valhallfonna in the outer fjord, the spacing at ∼50, ∼100, or ∼150 m implies that the ridges were deposited on a somewhat regular basis, but as the ridges are not spaced at equal distances throughout, they were either not always formed annually or retreat distances between subsequent years were variable. Based on the slightly larger dimensions of the outermost ridges in front of Valhallfonna and Glintbreen/Kantbreen, these ridges may have formed as terminal moraines during an advance of the respective glacier during the LIA (cf. Plassen *et al.*, 2004; Ottesen & Dowdeswell, 2006; Ottesen *et al.*, 2008). They could, however, also have formed from a slightly prolonged period of glacier stillstand. The lobate deposits on the distal flanks are interpreted as glacier outwash fans or glacigenic debris lobes, formed from continuously

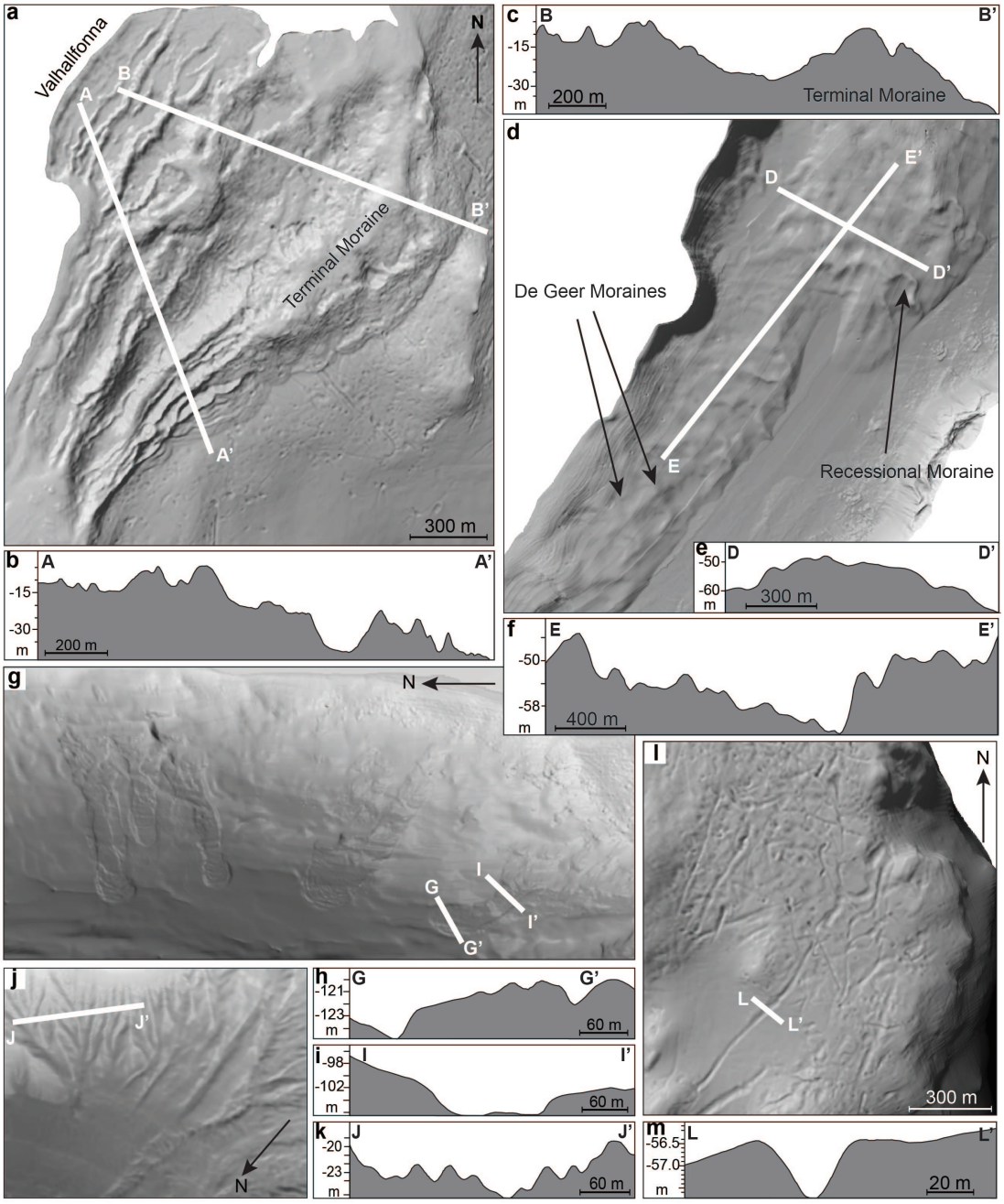

Figure 3.4: *a) Moraines in front of Valhallfonna with cross-sectional profile A–A' displayed in b), and profile B–B' shown in c). d) Example of De Geer moraines in the inner fjord with cross-sectional profiles D–D' and E–E' shown in e) and f). g) Example of mass-transport deposits in Lomfjorden, with cross-sectional profile G-G' (deposit) in h) and I-I' (Type-A trough) in i). j) Example of submarine channel (Type-B trough) along the fjord walls with cross-sectional profile J-J' shown in k). l) Example of iceberg ploughmarks in the outer fjord with cross-sectional profile L-L' displayed in m).*

high sediment influx either supplied from glacial meltwater streams or extruded from beneath the glacier at its grounding line (cf. e.g. Boulton, 1986; Kristensen *et al.*, 2009). Such debris lobes are often associated with LIA advances and may thus support an interpretation of the outermost ridges as terminal moraines (Plassen *et al.*, 2004; Ottesen & Dowdeswell, 2006; Forwick & Vorren, 2011). This is further discussed in section 3.5.3 below.

The much shorter ridges in the central fjord may have formed at the grounding line of an ice stream or tidewater glacier (Veteranen) retreating through the fjord, with the larger spacing

indicating faster ice flow and/or irregular intervals of deposition. The shorter lengths could be linked to (1) a narrower grounding line, and/or (2) post-depositional sediment masking of parts of the ridges. The latter is supported by the abundance of glacimarine sediments in the fjord, as shown by the subbottom profiler data (section 3.4.2).

3.4.1.5 Small and short ridges – De Geer moraines

Small ridges on the western flank of the innermost fjord basin are up to 2 m high and have poorly defined, smooth and indistinct crests, which appear to be interconnected in places. The ridges are orientated obliquely to each other and, in places, form a sort of diffuse ridge network (Fig. 3.4d). Ridge segments are up to 500 m long and around 100 m wide. The connection and variable orientation of the crests to each other is different to the strictly (sub-)parallel recessional moraines described above (Fig. 3.4d).

These small ridges are interpreted as De Geer moraines (cf. Lundqvist, 1981), which usually occur as sets of ∼3 m high, up to 30 m wide and several hundred metres long, submarine, mainly transverse, and irregularly-spaced ridges (Zilliacus, 1989; Lundqvist, 2000). The formation of De Geer moraines is attributed to either (1) pushing up of subglacial sediments at the grounding line (e.g. De Geer, 1940; Boulton, 1986; Larsen *et al.*, 1991; Blake, 2000), a process analogous to the formation of annual push moraines, or (2) the squeezing of soft subglacial sediments into basal glacier crevasses (e.g. Hoppe, 1957; Strömberg, 1965; Zilliacus, 1989; Beaudry & Prichonnet, 1991), analogous to the formation of crevasse-squeeze ridges (e.g. Solheim & Pfirman, 1985; Boulton *et al.*, 1996; Ottesen & Dowdeswell, 2006). Both processes are possible for the formation of the ridges in inner Lomfjorden, as their indistinct appearance is different to the well-developed, sharp-crested crevasse-squeeze ridges in other Spitsbergen fjords (Ottesen *et al.*, 2008; Flink *et al.*, 2015). This could be related to the presence of an undersaturated, less deformable subglacial till in Lomfjorden (cf. e.g. Lovell *et al.*, 2015), to poorly-developed crevasses within the glacier, or to post-glacial sediment infill between individual ridges masking their true appearance. The predominantly transverse orientation of the ridges and the lack of cross-cutting relationships between individual ridges are consistent with formation of the ridges as glacier end moraines. This is further supported by the limited number of well-developed superficial crevasses on Glintbreen, Kantbreen, and Veteranen, which suggests that these glaciers are not subject to the stress regime necessary to form crevasses (cf. Van der Veen, 1999; Benn & Evans, 2010). Although no guarantee, this, in turn, implies that basal crevasses are also relatively scarce. Notwithstanding this, the distribution of the ridges as a diffuse network of partially interconnected crests appears to be more consistent with crevasse-squeezing. We therefore suggest that the ridges formed from debris-meltout at the grounding line of a retreating ice margin with some degree of crevasse-squeezing during periods of longer stillstand (e.g. Solheim & Pfirman, 1985; Boulton *et al.*, 1996; Ottesen & Dowdeswell, 2006; Ottesen *et al.*, 2008).

3.4.1.6 Steep elongate channels and lobate deposits – submarine channels and mass-transport deposits

Elongate U- or V-shaped channels can be found along the steep fjord walls of Lomfjorden and are orientated (sub-)perpendicular to the main fjord axis. We distinguish two kinds of channels: Type-A channels with lobate deposits at their flat ends (Figs. 3.2, 3.4g–i) and Type-B channels dissociated from such deposits (Fig. 3.4j, k). Type-A channels are normally ∼3 m deep, up to 1 km long and usually ∼200 m wide, with slope angles of 10–20°. Lobate-shaped deposits at their

mouths are up to 700 m long, 1–3 m high and match the approximate width of their associated channel. The lobes generally have slopes of around 1 or 2° and hummocky surfaces. In front of the Kantbreen ice margin some larger lobes occur independently of any channels. The lobes are up to 700 m long, partly superimpose each other and have a cumulative width of 1800 m. Type-B channels are between 50 and 150 m wide, between 2 and 5 m deep, and 100–500 m long. They are mostly symmetrical in cross-section with rounded edges and along-channel slopes of around 10° (Fig. 3.4j, k). They often occur in clusters where they cross-cut or merge with each other.

The channels are commonly associated with meltwater streams exiting the glaciers and ice caps around Lomfjorden, which makes it likely that they represent channels formed from erosion by downslope processes. The Type-A channels and their associated lobe-deposits are interpreted as products of mass-transport events occurring along the fjord walls, comparable to those documented in Isfjorden in West Spitsbergen (Forwick & Vorren, 2011). The slope failures are likely triggered by the high supply of relatively fine-grained sediments, delivered into the fjord by rivers and meltwater streams, which rapidly settle and cause slope oversteepening (e.g. Gilbert, 1982; Forwick & Vorren, 2011). The Type-A channels in Lomfjorden probably represent the head scarp, where the slide or slump originated, and the slippery zone of transport, where sediment was continuously eroded. This sediment was then re-deposited at the foot of the slope as large sediment lobes once flow momentum ceased. The hummocky surface of these lobes might derive from the formation of pressure ridges, or from the transport and re-deposition of larger sediment blocks (cf. Prior *et al.*, 1984). In front of Kantbreen the lobes probably represent glacier contact fans formed by the same processes as their adjoining debris lobes in front of Glintbreen (see section 3.4.1.4). The absence of sediment lobes at the foot of the Type-B channels indicates that the main formation mechanism for these channels is the erosion of the fjord walls by the inflowing meltwater streams, although excavation may have been aided by occasional mass-transport events.

3.4.1.7 Small circular depressions and elongate furrows – iceberg ploughmarks

Abundant small circular depressions in Lomfjorden are up to 2 m deep with diameters of between 20 and ∼80 m. These depressions are U- or V-shaped in cross-section and can be symmetrical or asymmetrical with predominantly gentle slopes (Fig. 3.4l, m). They often show an up-standing rim on one side. The majority of these features have smooth, defined edges. A few occur as single features or small clusters, but the majority appear at one end of elongated furrows, which commonly occur on bathymetric highs (Fig. 3.2). These furrows form criss-crossing patterns and appear in water depths down to 50 m (Fig. 3.4l). Single furrows are up to 700 m long, <1 m deep and up to 30 m wide (Fig. 3.4l, m). The furrows have random orientations and often show a linear or curvilinear appearance in planform (Figs. 3.2, 3.4l).

The furrows are interpreted as iceberg ploughmarks, formed when the keels of grounded icebergs erode the seafloor into elongate furrows (e.g. Belderson *et al.*, 1973; Dowdeswell *et al.*, 1993; Dowdeswell & Bamber, 2007). This process is frequently observed in front of marine-terminating glaciers (Barnes & Lien, 1988; Woodworth-Lynas & Guigné, 1990). As iceberg drift is largely dependent on wind and ocean currents, changes in the icebergs' direction are common and account for the curvilinear appearance of the ploughmarks (e.g. Dowdeswell & Bamber, 2007; Andreassen *et al.*, 2008). Their occurrence in water depths down to 50 m suggests that the keels of icebergs in Lomfjorden are generally shallower than 50 m (cf. Dowdeswell & Forsberg, 1992; Dowdeswell *et al.*, 1993). The circular depressions at the end of the furrows probably

record the in-situ melting of grounded icebergs when movement ceased. Nevertheless, especially where these depressions are detached from the furrows, they could also be pockmarks, which are defined as concave, subaquatic depressions formed as a result of gas or pore fluid seepage (e.g. Harrington, 1985; Hovland & Judd, 1988; Forwick *et al.*, 2009; Roy *et al.*, 2015).

3.4.2 Seismostratigraphy

Six acoustic facies AF1–AF6 are distinguished in Lomfjorden (Fig. 3.5).

AF1, is stratigraphically the lowermost facies and inferred to be the oldest. It is acoustically semi-opaque to transparent with only rare internal reflections and is bounded by a hummocky upper reflection of variable strength (Fig. 3.5). Facies AF1 occasionally crops out on the seafloor, where it is overprinted by 1–3 m high bumps of Facies AF2. The minimum thickness is ∼7.5 m.

Its stratigraphic position, its acoustic appearance and its hummocky upper boundary indicate that AF1 represents the acoustic basement in Lomfjorden, which could either reflect bedrock or glacial till (cf. Forwick *et al.*, 2010; Forwick & Vorren, 2011; Kempf *et al.*, 2013; Roy *et al.*, 2014). Based on the frequent appearance of bedrock on the seafloor as imaged on the multibeam data (section 3.4.1.1), we consider it more likely that AF1 represents bedrock.

AF2 occurs mostly as small mounds overprinting Facies AF1 (Fig. 3.5). AF2 is acoustically semi-opaque to transparent, with very weak, chaotic internal reflections that weaken and disappear with depth. AF2 is acoustically similar to AF1, but is bounded by a strong, sharp, and mostly continuous upper reflection and is up to 26 m thick. It directly overlies AF1 (Fig. 3.5).

AF2 is acoustically similar to subglacial till in other Spitsbergen fjords (cf. Forwick & Vorren, 2011; Kempf *et al.*, 2013). The overall massive acoustic appearance as well as the loss of internal reflections with depth are thought to indicate uniformly mixed material, possibly of diamictic composition (cf. Stewart & Stoker, 1990; Forwick & Vorren, 2011), which is consistent with an interpretation as glacial till. Furthermore, the bumps of AF2 on the chirp data correlate with the small recessional moraines, some of the De Geer moraines, and glacial lineations on the bathymetric data, also supporting an interpretation as glacial till.

AF3 is acoustically (semi-)transparent with occasional diffuse internal reflections. Based on geometry and appearance, AF3 is sub-divided into two subfacies, AF3a and AF3b. AF3a occurs as lens-shaped bodies in the inner and central fjord (Fig. 3.5), which can be up to 350 m wide and around 8 m thick. AF3a often pinches out laterally and appears interbedded with AF4, particularly in the inner fjord. AF3b is characterised by a strong, continuous, undulating bottom reflection and is laterally extensive over large areas in Lomfjorden (Fig. 3.5). It is more common in the central and outer fjord where it appears as 1–3 m thick packages.

The massive, (semi-)transparent acoustic signature of AF3 is in accordance with mass-transport deposits documented on subbottom profiler data from other areas around Svalbard (e.g. Plassen *et al.*, 2004; Forwick & Vorren, 2007; Hogan *et al.*, 2010; Streuff *et al.*, 2015). We thus interpret the lenticular bodies of AF3a as the mass-transport-derived sediment lobes described in section 3.4.1.6, an interpretation supported by the correlation of the chirp and bathymetric data. The erosional lower contact of AF3b indicates that this subfacies is also a product of mass transport. The orientation and undulating appearance of this lower boundary in the central fjord suggests that the deposits may be related to ice-marginal processes from the tributary glaciers Skinfaksebreen or Gullfaksebreen, and mass transport from side-walls in the central fjord.

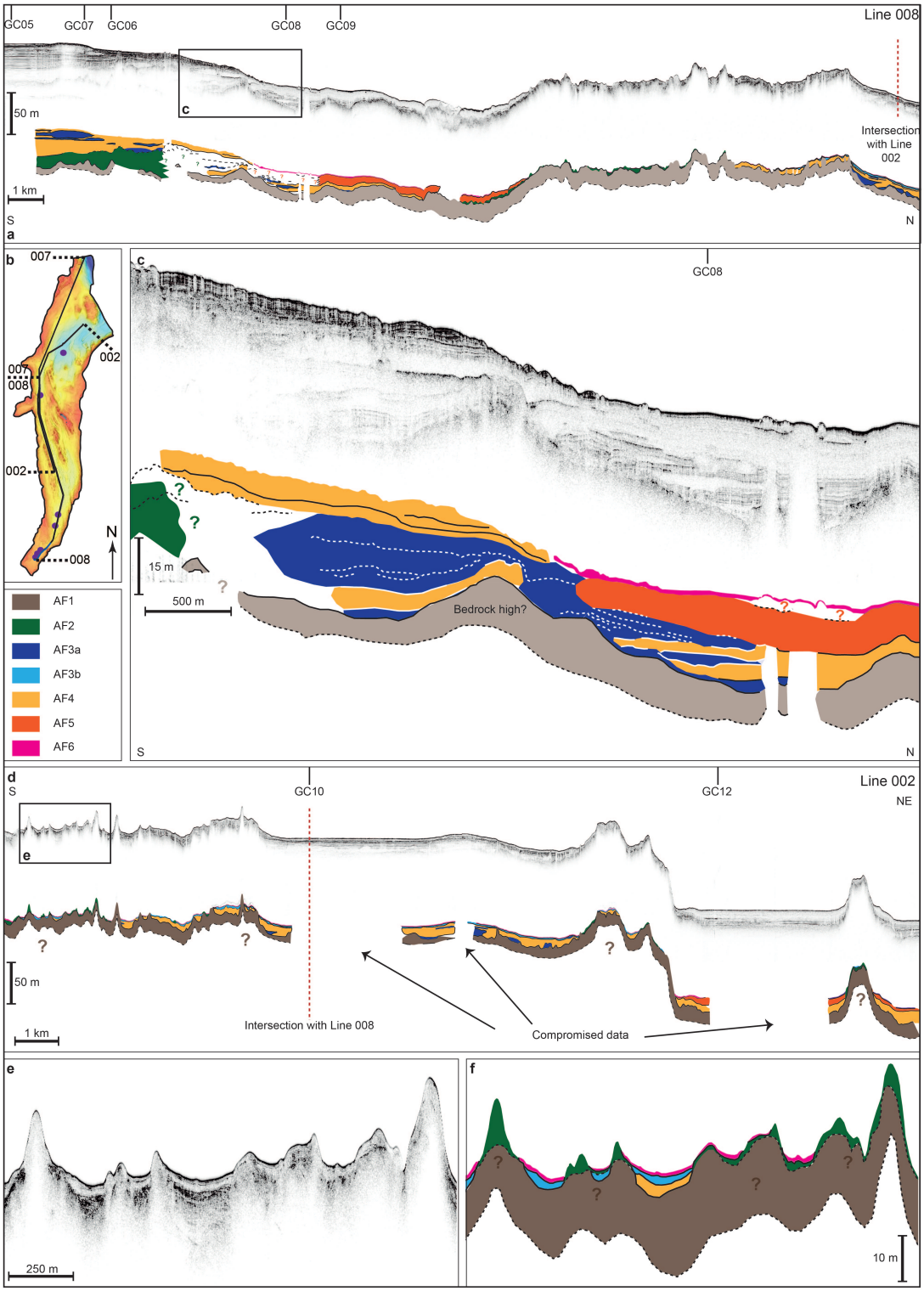

Figure 3.5: *a) Chirp line 008 from south to north with the interpretation of acoustic facies underneath. Locations of gravity cores are indicated. The black rectangle shows the extent of c). Conversion between m and ms was based on an assumed p-wave velocity of 1500 m* s^{-1}*. b) Location of the chirp lines (002, 007, 008) and core sites with respect to the bathymetric data. c) Detail figure of Line 008 and the associated acoustic facies interpretation. d) Line 002 through the outer fjord with the according interpretation of the acoustic facies. The black rectangle indicates the extent of e), detail figure of Line 002 with the acoustic facies interpretation shown in f).*

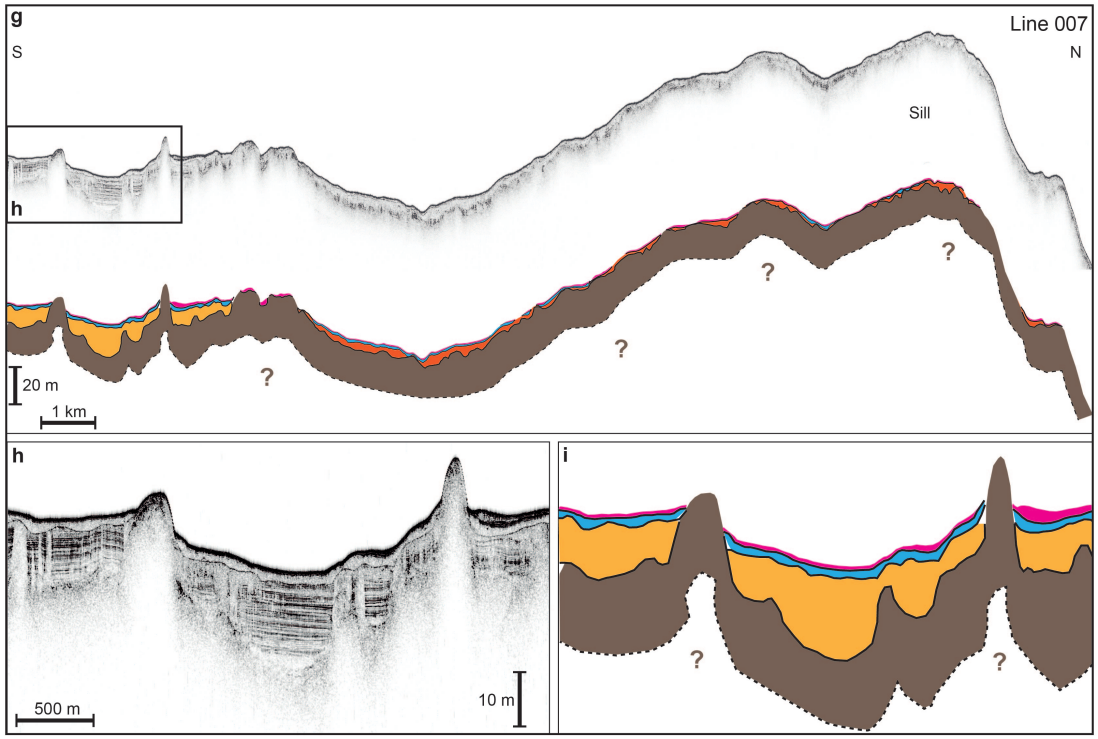

Figure 3.5 *(cont.): g) Line 007 through the outer fjord and associated facies interpretation. The black rectangle shows the extent of h), a detail figure of Line 007 with its acoustic facies interpretation in i).*

AF4 is acoustically stratified due to the presence of very regular, mostly continuous, parallel internal reflections (Fig. 3.5). AF4 occurs in the entire fjord, but is particularly common in proximal areas and in bathymetric depressions where it is up to 12 m thick and conformably overlies AF1 or AF3a (Fig. 3.5).

The stratified acoustic appearance of AF4 suggests regular changes in lithology or density (cf. Syvitski, 1989; Forwick & Vorren, 2011). Similar sediments described from other Spitsbergen fjords have been interpreted as glacimarine sediments derived from suspension settling from meltwater plumes (e.g. Plassen *et al.*, 2004; Kempf *et al.*, 2013; Streuff *et al.*, 2015), or as ice-proximal glacimarine fans in which suspension settling alternates with turbidity currents and gravitational downslope processes (e.g. Sexton *et al.*, 1992; Forwick & Vorren, 2011). Based on the lithological evidence, we favour the latter interpretation as the most likely mode of formation of this acoustic facies, and suggest an ice-proximal origin for AF4 (see also section 3.4.4 below).

AF5 is similar to AF3 with an acoustically semi-transparent appearance and very weak chaotic internal reflections. AF5 occasionally shows a draping character and is common in basins, where it generally overlies AF4 (Fig. 3.5). It is up to 13 m thick and lacks distinct contacts.

The chaotic internal reflections and acoustic transparency of AF5 indicate fairly homogeneous, possibly fine-grained, material (e.g. Forwick & Vorren, 2011). The draping character and large thickness of AF5 is consistent with sediments deposited in a relatively low-energy glacimarine environment. Although the sediments could also derive from the suspension load carried in rivers or from normal hemipelagic sedimentation from the water column, we consider the rainout of the fine-grained suspension load from meltwater plumes most likely (see also section 3.4.4 below). AF5 is particularly thick in proximal areas of the fjord, thus supporting a glacigenic origin.

AF6 is bounded by the seabed on top and has a stratified acoustic appearance imparted by parallel, opaque internal reflections, whose strength decreases with depth (Fig. 3.5). AF6 is bounded by a strong bottom reflection in places, which is orientated obliquely to the seabed, but as this reflection cannot be traced for long distances, AF6 can only be unambiguously identified in the central fjord, close to core GC09 (Fig. 3.5; see also Fig. 3.9 below).

The stratigraphic position of AF6 directly beneath the seabed indicates that this facies was only deposited recently and we therefore interpret it as Holocene glacimarine or hemipelagic sediments delivered into the fjord by meltwater streams and tidal processes. Indeed, AF6 is acoustically and lithologically similar to AF4 (see also section 3.4.4 below). This suggests a similar origin for both facies and would indicate that AF6 was also deposited in a relatively ice-proximal environment.

3.4.3 Oceanography

CTD data were obtained at three sites in Lomfjorden (see Table 3.1) and are shown in Figure 3.6. Generally, predominant water masses are colder and fresher in the inner fjord, but warmer and more saline in the outer fjord (Fig. 3.6), which is likely related to increased run-off of relatively fresh, cold meltwater in the inner fjord. Towards the outer fjord, further away from the glacier fronts, a decreasing influence of meltwater on the water column is seen in the warmer and more saline waters. Water masses with a salinity of <34.4 psu and between 34.4 and 34.9 psu are defined as Polar and Arctic Surface Water, respectively (Ślubowska-Woldengen *et al.*, 2007) and characterise bottom waters in central Lomfjorden (Fig. 3.6). In the outer fjord Arctic Surface water overlies the warmer, more saline bottom water, whose characteristics are

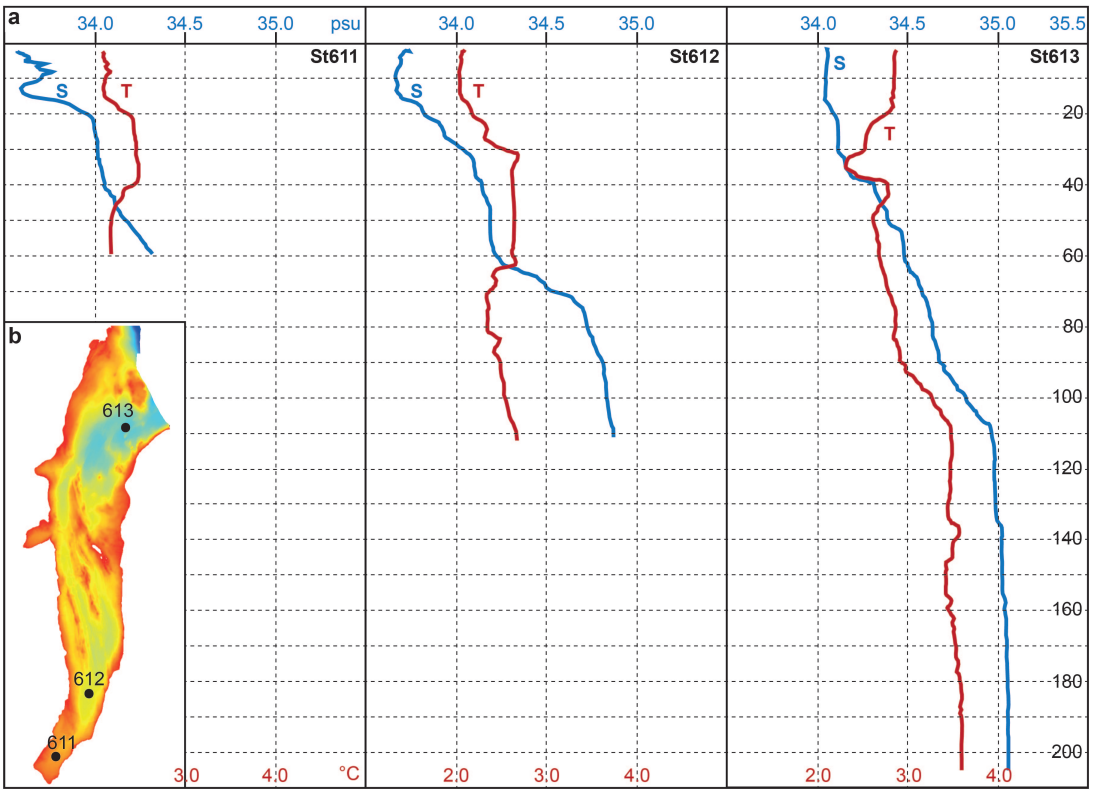

Figure 3.6: *a) Conductivity-Temperature-Depth data from the water column at three different sites in Lomfjorden. Y-axis shows water depth in metres, whereas the x-axes show S = salinity in psu and T= temperature in °C. b) Location of the three CTD sites.*

comparable to those reported from the Atlantic Layer in northern Svalbard (part of the Svalbard branch; Aagaard *et al.*, 1987; Pfirman *et al.*, 1994; Ślubowska *et al.*, 2005). A relatively thin superficial layer of colder and fresher water in the outer fjord (Fig. 3.6) may represent meltwater inflow from Valhallfonna. The inflow of Atlantic water into the inner fjord is probably prevented by the shoaling seafloor. The data suggest (1) that Atlantic water flows into Hinlopenstretet and into Lomfjorden from the northern Svalbard shelf (Ślubowska *et al.*, 2005) and (2) that oceanographically Lomfjorden is not much colder than the fjords in West Spitsbergen (cf. e.g. Svendsen *et al.*, 2002; Ślubowska-Woldengen *et al.*, 2007; Rasmussen *et al.*, 2012).

3.4.4 Lithostratigraphy

Based on variations in colour, grain size and geographical distribution of sediment in the seven gravity cores analysed, five lithofacies (LF1–LF5) are distinguished in Lomfjorden. Their occurrence in the sediment cores, along with water content, magnetic susceptibility and grain size distribution, is shown in Figure 3.7, while examples of x-radiographs and colour photographs are displayed in Figure 3.8.

LF1 is composed of finely stratified silt with a small but variable clay component and a water content around 30%. Grain size analysis shows that >90% of the sediment is finer than 63 μm and the magnetic susceptibility shows minor variations between overall values from 20 to 40 x 10^{-5} SI (Fig. 3.7). The sediments are heavily bioturbated and occasional clasts, shells and shell fragments are scattered throughout. Black mottles are abundant (Fig. 3.8). The silt of LF1 varies in colour between dark grey and dark greyish brown, but very dark grey to black mottles make the sediments appear darker in places (Fig. 3.8).

The high amount of bioturbation and biogenic activity, indicated by the mottles and shell fragments, suggest favourable living conditions for marine fauna, while the clasts reflect ice-rafted debris settling from melting sea ice and/or icebergs. We thus interpret LF1 as distal glacimarine sediment deposited from suspension rainout from meltwater plumes and/or the water column (hemipelagic sedimentation), combined with bioturbation. A similar lithofacies was also reported in other Spitsbergen fjords by Elverhøi *et al.* (1983), Plassen *et al.* (2004), Baeten *et al.* (2010), and Forwick *et al.* (2010). LF1 correlates with AF5 (Fig. 3.9).

LF2 contains massive sand intermixed with variable amounts of silt (Figs. 3.7, 3.8). All grain sizes from very coarse sand to silt appear in an upward-fining succession, but the sediments are generally poorly sorted. Coarser components appear slightly darker than finer grains with colours between very dark and dark grey (Fig. 3.8). The water content is ∼15% and the magnetic susceptibility around 30 x 10^{-5} SI (Fig. 3.7).

The sand is inferred to have been deposited in an environment with initially high (coarser grains) but increasingly low depositional energy (finer grains). A succession such as the one observed in LF2 is, for example, common for turbidites (e.g. Gilbert, 1982; Andersen *et al.*, 1996; Syvitski *et al.*, 1996; Lønne, 1997). LF2 is confined to the lowermost centimetres of GC10, and its thickness as well as inaccuracy between time-depth conversion (see section 3.3) makes unambiguous correlation to an acoustic facies difficult. We tentatively suggest that LF2 forms part of AF3b, which would be in accordance with the previous interpretations of AF3 as mass-transport deposits.

LF3 contains partly compacted, massive, dark grey, fine to medium sand which occurs as lenses, thin horizons, or larger sand bodies in all cores from Lomfjorden except GC12 (Figs. 3.7, 3.8). Contacts with surrounding facies range from sharp to gradational. The sand may contain various amounts of silt, but is generally well-sorted with up to 90% of the sediment

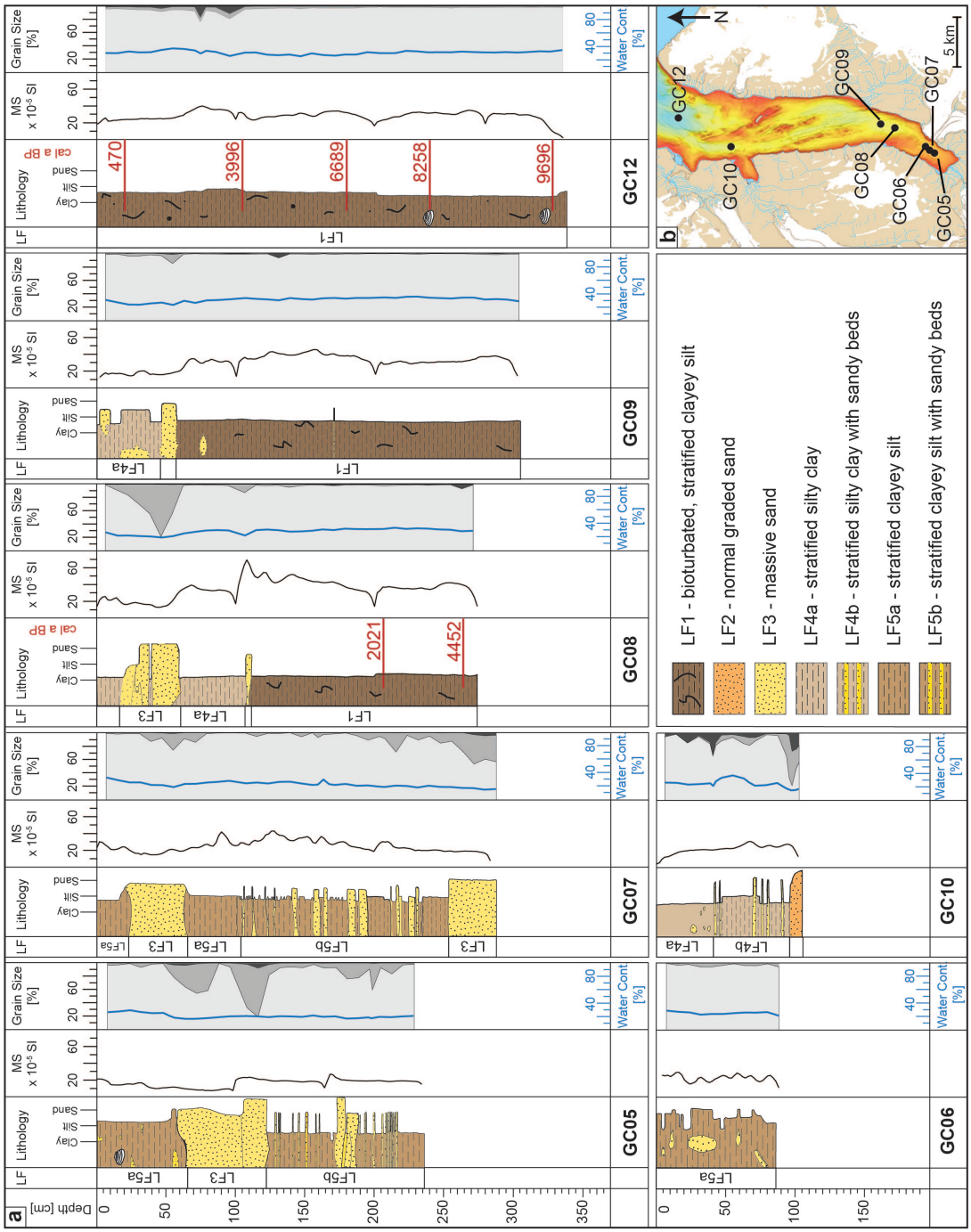

Figure 3.7: *a) Lithofacies logs of all gravity cores with magnetic susceptibility (MS), water content and grain size distribution in weight percent. For the grain size plots, light grey areas = sediment fraction <63 µm, medium grey areas = sediment fraction 63–250 µm, and dark grey areas = sediment fraction >250 µm, the latter classified as IRD. b) Overview of the core locations in Lomfjorden.*

finer than 63 μm. The water content is <20% and the magnetic susceptibility between 10 and 20 x 10^{-5} SI (Fig. 3.7).

LF3 is interpreted as a product of downslope gravitational processes. The massive appearance and the presence of silt may indicate intermixing of coarser and finer material and could thus be evidence for sediment reworking, which, in addition to the often sharp contacts, is in good agreement with an interpretation as mass-transport deposits (e.g. Forwick & Vorren, 2007). Where contacts are more gradual, emplacement of the sand could relate to non-eroding

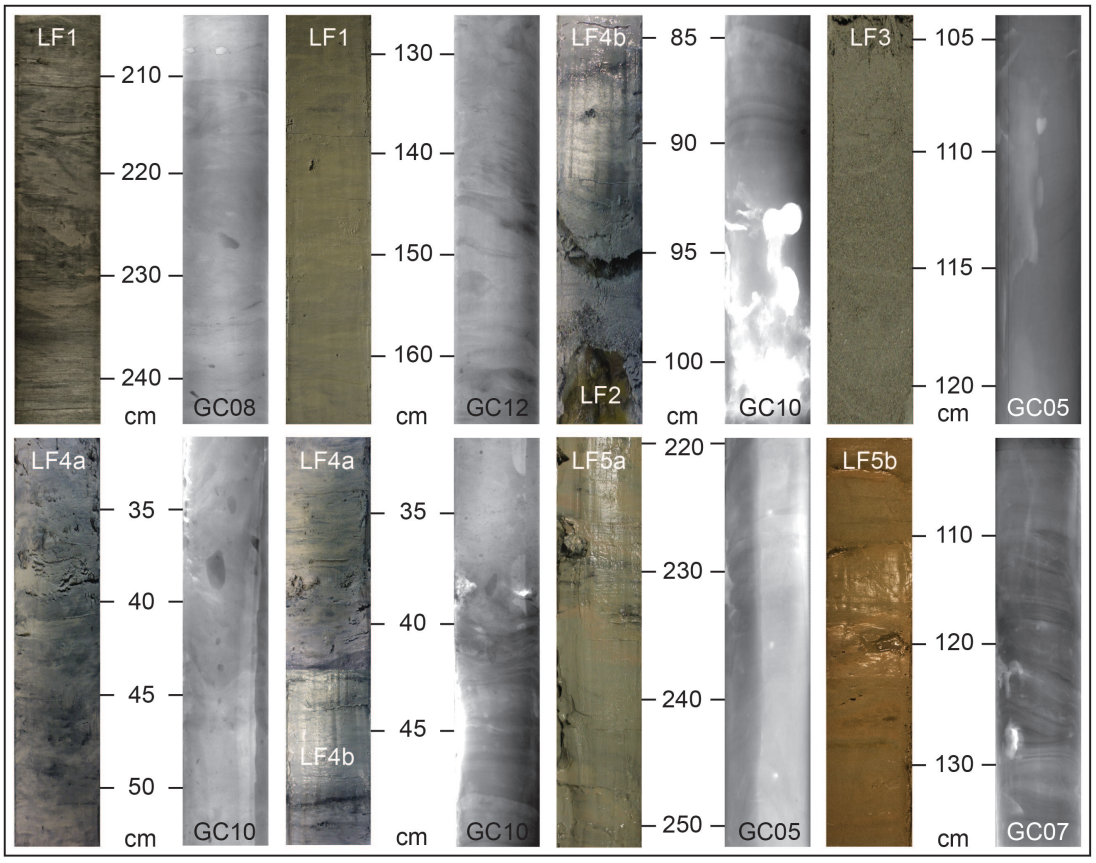

Figure 3.8: *Examples of core photos and x-radiographs of each of the lithofacies in Lomfjorden. On the x-radiographs darker areas represent denser material.*

turbidity flows or hydroplaning debris flows (cf. e.g. Elverhøi *et al.*, 2000; Mulder & Alexander, 2001; Forwick & Vorren, 2007, 2011). Sand appearing as thicker packages probably derives from larger-scale events, such as slope failures along the fjord walls or glacier outwash (cf. e.g. Boulton, 1986; Forwick & Vorren, 2007), whereas thinner strata may represent small-scale events, such as turbidites. We correlate LF3 with acoustic facies AF3 (Fig. 3.9).

LF4 is divided into subfacies LF4a and LF4b. LF4a comprises very weakly stratified clay with variable amounts of silt which occasionally contain lenses of LF3 (Fig. 3.7). The stratification is mainly imparted by colour changes from grey to (dark) greyish brown. Grain size analyses reveal that >95% of the sediment is finer than 63 μm (Fig. 3.7). LF4a contains occasional clasts and abundant mottles (Fig. 3.8). Its magnetic susceptibility is generally between 10 and 20 x 10^{-5} SI, and the water content is around 50% (Fig. 3.7). LF4b occurs only in GC10, and contains the clay from LF4a interbedded with thin sandy beds of LF3 (Fig. 3.8). The latter have relatively sharp bottom and graded top contacts, can appear contorted, are relatively well-sorted, and show a weak tendency of cross-bedding (Figs. 3.7, 3.8).

LF4a is similar to glacimarine muds documented from other Spitsbergen fjords (e.g. Forwick & Vorren, 2009; Kempf *et al.*, 2013; Streuff *et al.*, 2015), which suggests that the clay and silt originate from the rainout of suspension load carried in glacial meltwater plumes. The weak stratification is indicative of a depositional environment with low energy, which could stem from regular variations in sediment source, sediment delivery and discharge, or glacier front oscillations (e.g. Ó Cofaigh & Dowdeswell, 2001; Szczuciński & Zajaczkowski, 2012). The regularity of the lamination suggests seasonal changes to be the cause for such variations. Based

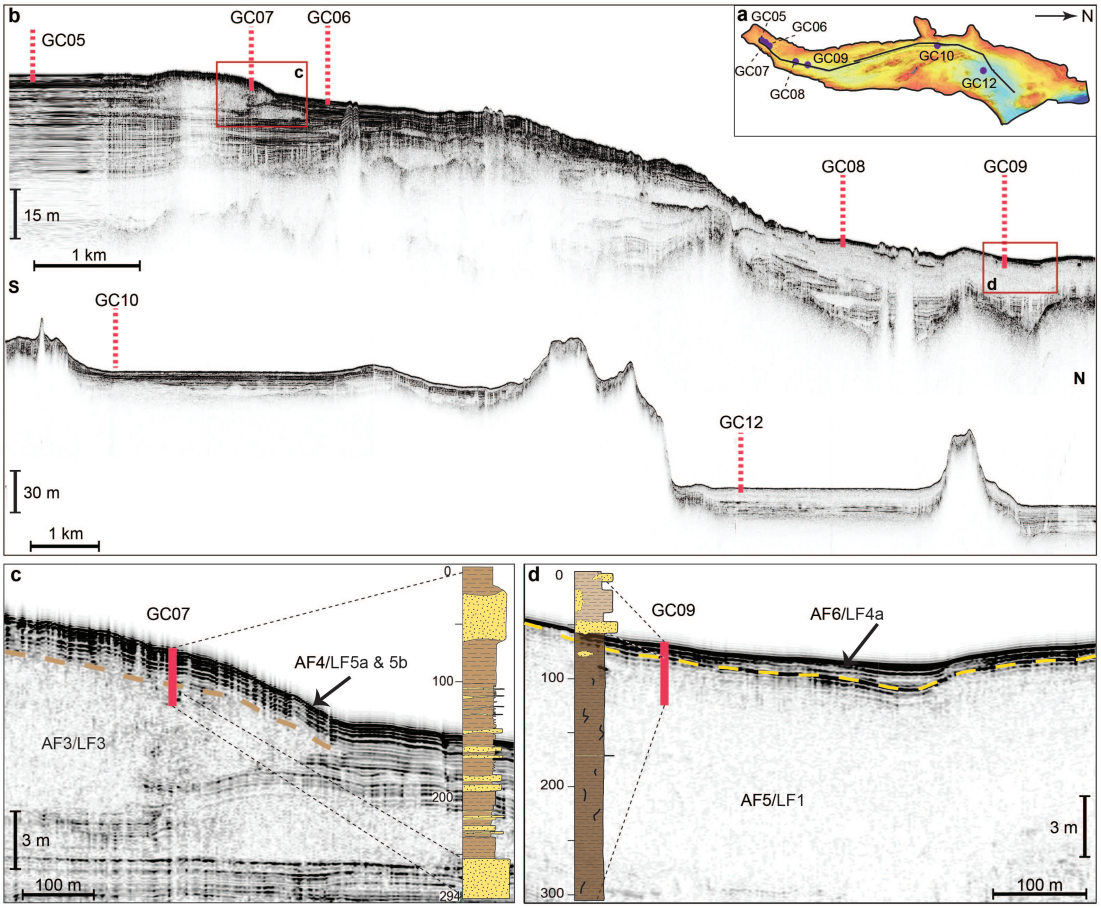

Figure 3.9: *a) Overview of bathymetry, chirp lines 008 (left) and 002 (right) and sediment cores from Lomfjorden. b) Chirp lines 008 (top) and 002 (bottom) with approximate penetration depths of the sediment cores. Conversion between m and ms was based on an assumed p-wave velocity of 1500 m s^{-1}. c) Sediment core GC07 and its lithological units with respect to the acoustic facies. d) Sediment core GC09 and its lithological units with respect to the acoustic facies.*

on the characteristics of the sand layers, LF4b is interpreted as suspension rainout alternating with turbidites (e.g. Gilbert, 1982; Mackiewicz *et al.*, 1984; Ó Cofaigh & Dowdeswell, 2001). LF4a correlates with acoustic facies AF6, whereas LF4b probably reflects the stratified nature of AF4 (Fig. 3.9).

LF5 is subdivided into LF5a and LF5b. LF5a consists of soft, weakly laminated, brown to dark grey clayey silt. Laminations occur due to minor colour variations between brown and dark grey, as well as density variations (Fig. 3.8), the latter probably related to small changes in clay content. More than 90% of the sediment is finer than 63 μm. The water content is between 20 and 30% and the magnetic susceptibility shows minor oscillations with values between 10 and 30 x 10^{-5} SI. LF5a is prominent in inner Lomfjorden and occurs in the proximal cores (Fig. 3.7). Occasional shells, shell fragments and abundant mottles appear throughout. In GC05 and GC07 the silt from LF5a is interbedded with several mm- to cm-thick well-sorted sand horizons of LF3, which have sharp bottom boundaries and show occasional cross-bedding (Fig. 3.8). This subfacies is defined as LF5b (Fig. 3.7).

The fine grain size of the sediments in LF5a indicates a low-energy depositional environment and is similar to LF4a, and to glacimarine muds from other Spitsbergen fjords. We therefore interpret this lithofacies as glacimarine sediment deposited by suspension rainout from meltwater plumes exiting a tidewater glacier (cf. Elverhøi *et al.*, 1980, 1983; Plassen

et al., 2004; Forwick & Vorren, 2009). Similar to LF4a, the laminations may reflect regular, probably seasonal changes in meltwater and sediment supply (cf. Cowan & Powell, 1990; Powell & Domack, 1995). LF5a is slightly coarser than LF4a, with an increased proportion of silt, which suggests that LF5a was deposited in a slightly higher-energy environment than LF4a and thus reflects more proximal conditions. We infer similar processes of formation for LF5b as for LF4b and suggest that LF5b consists of glacimarine muds deposited from suspension settling alternating with turbidites and/or other mass-transport deposits. LF5 forms part of the acoustic facies AF4, with the acoustic stratification probably reflecting the common occurrence of turbidites in LF5b (Fig. 3.9).

3.4.5 Radiocarbon dates and sediment accumulation rates

AMS radiocarbon dating was carried out on foraminifera and bivalves from five sediment depths in core GC12 in outer Lomfjorden, and from two sediment depths from GC08 in the central fjord (Table 3.2, Fig. 3.10). All radiocarbon dates were taken from lithofacies LF1. A basal age of 9.7 cal ka BP from GC12 shows that the sedimentary record in this core covers a large part of the Holocene. Conventional radiocarbon ages were used to calculate sediment accumulation

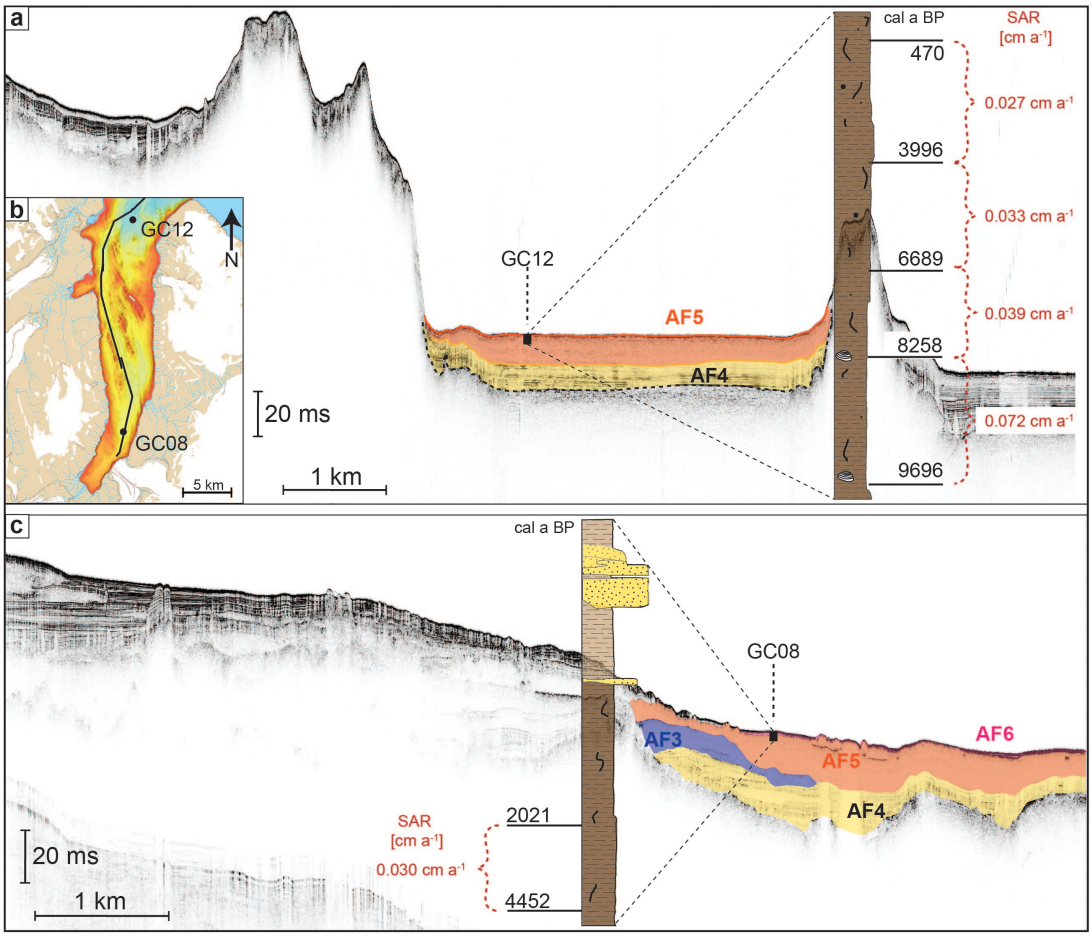

Figure 3.10: *a) Chirp line 002 from the outer fjord showing the approximate location of GC12 with the core log, radiocarbon dates and calculated sediment accumulation rates. Note that the chirp line does not cover the core site of GC12 and the sedimentary environment for this core can thus only be inferred. Conversion between m and ms was based on an assumed p-wave velocity of 1500 m* s^{-1}*. b) Overview of the location of the chirp lines in a) and c) and the core sites of GC08 and GC12. c) Chirp line 008 through the inner and central fjord and the sedimentary environment of GC08. The core log with radiocarbon dates and calculated sediment accumulation rates is also shown.*

rates (SARs), which, in GC12, decrease up-core, and range from 0.72 to 0.21 mm a^{-1} (Fig. 3.10). In GC08, a basal date of ∼4.5 cal ka BP at 265 cm and a date of ∼2 cal ka BP at 207 cm provide a low SAR of 0.3 mm a^{-1} (Fig. 3.10), which indicates relatively ice-distal conditions during the accumulation of LF1 in this core (cf. e.g. Elverhøi *et al.*, 1980, 1983). Note that these rates are based on an assumption of linear sediment accumulation.

Table 3.2: *Radiocarbon dates and calibrated ages used in this study.*

Core ID	Depth [cm]	Lab Code	Sample	Reported age [^{14}C a BP]	Mean probability age [cal a BP]	2σ [cal a BP]
GC08	207	Beta–441327	Bivalve	2490 ± 30	2021	2146–1882
GC08	265	Beta–441328	Foraminifera	4420 ± 30	4452	4595–4293
GC12	20	Beta–441322	Foraminifera	940 ± 30	470	543–357
GC12	105	Beta–441323	Foraminifera	4090 ± 30	3996	4139–3849
GC12	180	Beta–441324	Foraminifera	6340 ± 30	6689	6824–6555
GC12	240	Beta–441325	Bivalve	7890 ± 30	8258	8360–8156
GC12	328	Beta–441326	Bivalve	9120 ± 30	9696	9872–9540

3.5 Discussion

3.5.1 Glacial geomorphology and landform assemblages in Lomfjorden

Swath-bathymetric data from Lomfjorden reveal (1) bedrock highs, (2) glacial lineations, (3) drumlins, (4) recessional moraines with, in some cases, associated debris lobes, (5) De Geer moraines, (6) submarine channels, (7) mass-transport deposits, and (8) iceberg ploughmarks. Except for the bedrock highs, which have been at least partly modified by glacial streamlining, all of the landforms are regarded as glacigenic, i.e. formed from subglacial, ice-marginal, or glacimarine processes. They are common components of glacial landform assemblages documented in other Svalbard fjords (cf. Boulton, 1986; Solheim & Pfirman, 1985; Solheim, 1991; Plassen *et al.*, 2004; Ottesen & Dowdeswell, 2006; Ottesen *et al.*, 2008; Baeten *et al.*, 2010; Forwick & Vorren, 2011; Kempf *et al.*, 2013; Flink *et al.*, 2015; Streuff *et al.*, 2015). Based on their orientation within the fjord, the landforms in Lomfjorden can be divided into two separate assemblages: (1) the Trunk Glacier Assemblage, formed from an extended Veteranen glacier flowing through the fjord, parallel to the fjord long axis, and (2) the Tributary Glacier Assemblage, formed from glaciers flowing into the fjord from the sides, i.e. perpendicular to the fjord long axis (Fig. 3.11).

3.5.1.1 Trunk Glacier Assemblage

The glacial lineations, drumlins, De Geer moraines, and recessional moraines in central Lomfjorden are part of the Trunk Glacier Assemblage (Fig. 3.11). Their orientation is parallel or transverse to the main fjord axis, which implies that these landforms are related to trunk ice flowing through the fjord from south to north, and were thus deposited by an extended Veteranen glacier. The absence of terminal moraines in this assemblage suggests only one glacial advance-retreat sequence, and we infer that the glacial lineations and drumlins formed during ice advance, possibly beneath fast-flowing ice (cf. King *et al.*, 2009), and that the recessional and De Geer moraines formed during episodic ice retreat (cf. Dowdeswell *et al.*, 2010a; Hogan *et al.*, 2010).

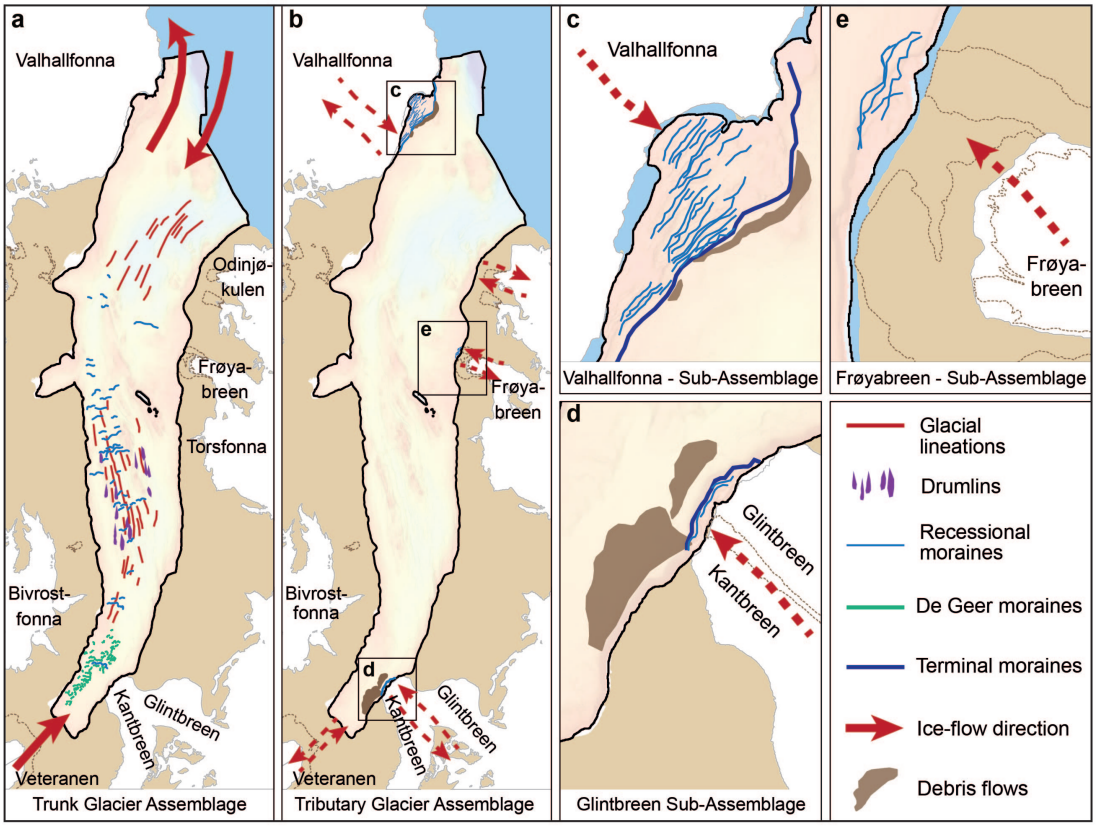

Figure 3.11: *Landform assemblages distinguished in Lomfjorden. a) Trunk Glacier Assemblage related to trunk ice streaming through the fjord; b) Tributary Glacier Assemblage with c), d), e) detailed maps of individual assemblages in front of the three tributaries Valhallfonna (c), Glintbreen/Kantbreen (d), and Frøyabreen (e). The Tributary Assemblages could have formed during ice advance or retreat (dashed red arrows).*

3.5.1.2 Tributary Glacier Assemblage

The Tributary Glacier Assemblage contains all recessional moraines located in front of the tributary glaciers and, in some cases, debris lobes associated with the outermost moraine (Fig. 3.11). It can be further sub-divided into three individual landform assemblages related to the three tributary glaciers Valhallfonna in the outer fjord, Frøyabreen on the eastern shore and Glintbreen/Kantbreen in the inner fjord (the "tributaries", Fig. 3.11). The landforms are orientated transverse to the respective glacier's direction of ice flow, i.e. (sub-)parallel to the main fjord axis, and are therefore likely a product of individual glacier dynamics, with ice flow occurring more or less perpendicular to that of the trunk glacier. The timing of formation for all landform assemblages is discussed in section 3.5.3 below.

3.5.2 Sedimentary environments

From the lithological record in Lomfjorden we infer two main sedimentary processes: (1) suspension rainout from meltwater plumes and/or the water column, and (2) sediment reworking by downslope gravity flows and iceberg ploughing. Delivery of IRD by icebergs and sea ice occurred to some degree, but was relatively minor compared to the other two processes. In outer and central Lomfjorden, the laminated clayey silt of facies LF1 shows signs of intense biological activity in the form of bioturbation, black mottles, and shell fragments, indicating a distal glacimarine environment (cf. Ó Cofaigh & Dowdeswell, 2001). Ice-distal conditions are further supported by the very low SARs between ~0.2 and 0.7 mm a^{-1} (cf. Elverhøi *et al.*, 1983; Forwick & Vorren, 2009; Szczuciński *et al.*, 2009). Note that these rates are up to one order of

magnitude lower than rates suggested for glacier-distal environments in other Spitsbergen fjords (Elverhøi *et al.*, 1980, 1983), and are more similar to SARs documented from East Greenland. This could indicate that meltwater availability was much lower during the Holocene, that glacial erosion was too weak to produce sufficient "rock flour", and/or that the glacimarine environment of East Spitsbergen is indeed colder and more polar compared to that of the warmer, more temperate, West Spitsbergen (cf. Mackiewicz *et al.*, 1984; Dowdeswell *et al.*, 1998; Ó Cofaigh & Dowdeswell, 2001). As colder conditions in Lomfjorden are inconsistent with the CTD data, which record the inflow of warm Atlantic water into the fjord, based on the assumption that glaciers in West and East Spitsbergen would produce similar amounts of rock flour (cf. Dallmann *et al.*, 2002), a low SAR during the Holocene must thus be a consequence of decreased meltwater runoff. The occurrence of only LF1 in GC12 and its basal date of 9.7 cal ka BP shows that the sedimentary processes at this location remained largely unchanged throughout the Holocene. In the central fjord, the laminated silts of LF1 at the base of GC08 also reflect ice-distal conditions until after ∼2.0 cal ka BP, deposited at a SAR of 0.3 mm a^{-1}. The upwards fining of LF1 in the central and inner fjord into the weakly laminated clay of LF4a could suggest increasingly distal conditions and thus continuous glacier retreat, which is also indicated by the decreasing SARs in GC12 (cf. Syvitski & Murray, 1981; Gilbert, 1982; Elverhøi *et al.*, 1983; Sexton *et al.*, 1992). However, occasional sand bodies with sharp bounding contacts attest to the occurrence of downslope mass-transport processes in Lomfjorden: the concurrent occurrence of LF4a with larger bodies and smaller lenses of LF3 at the top of GC08 and GC09 thus shows an increasing frequency of mass-transport events in recent times. This could be related to a more proximal depositional environment, possibly related to a late Holocene glacier re-advance, which is also implied by the presence of the acoustically stratified sediments of AF6 (see section 3.4.2).

In cores GC05, GC06, and GC07 in the inner fjord clayey silt is interbedded with sandy turbidites, providing evidence for relatively proximal conditions (e.g. Gilbert, 1982; Gilbert *et al.*, 1993). The decreasing frequency of sandy layers up-sequence could be related to decreasing depositional energy and increasingly ice-distal conditions as a consequence of ice retreat. Nevertheless, a lack of turbidites could also be related to decreasing meltwater and thus sediment availability (cf. Mackiewicz *et al.*, 1984; Stevens, 1990; Laberg & Vorren, 1995; Ó Cofaigh & Dowdeswell, 2001), which may be a consequence of a period of generally cooler conditions and glacier advance.

Most areas in the fjord are influenced by intense sediment reworking, either due to erosion and re-deposition from meltwater streams along the submarine channels, due to downslope gravitational flows forming mass-transport deposits, or due to ploughing by icebergs calved from the local tidewater glaciers. However, as icebergs are absent on recent aerial photos from the fjord, iceberg ploughing does not appear to play a major role in contemporary sediment reworking.

3.5.3 Glacial evolution in Lomfjorden

The Trunk Glacier Assemblage records a single glacial advance-retreat event related to the flow of an extended Veteranen glacier along the length of Lomfjorden. Fjord-parallel glacial lineations occurring throughout the fjord indicate formation during a time when Lomfjorden was fully glaciated. We infer that all the landforms in the Trunk Glacier Assemblage were formed from ice-streaming during and after the LGM. This interpretation is supported by the fact that the sediment core GC12 in the outer fjord provides evidence for continuously ice-distal conditions since at least 9.7 cal ka BP, and that the landforms in the Trunk Glacier Assemblage

are consistent with those formed by other palaeo-ice streams in eastern Svalbard (Dowdeswell *et al.*, 2010a; Hogan *et al.*, 2010; Ingólfsson & Landvik, 2013). Lomfjorden may thus have served as one of the larger fjord systems channelling a fast-flowing ice stream from the SBIS during the LGM, the latter presumably serving as a tributary to the ice stream draining the ice sheet from south to north through Hinlopenstretet (e.g. Landvik *et al.*, 1998; Ottesen *et al.*, 2007; Ingólfsson & Landvik, 2013). The basal date from GC12 also provides the first documented age for the deglaciation of Northeast Spitsbergen and indicates that deglaciation was underway by 9.7 cal ka BP. It is important to note, however, that this is a minimum age for two reasons: (1) by this time the ice margin must have already retreated far into the fjord, as shown by the presence of only ice-distal sediments in GC12, and (2) GC12 only covers the uppermost 3.36 m of a ∼18 m-thick sedimentary basin infill sequence (Fig. 3.10). This strongly suggests that Lomfjorden was ice-free much earlier than other Spitsbergen fjords, which is also indicated by recent work from Ingólfsson *et al.* (2016), who suggest that De Geerbukta (see Fig. 3.1) must have been deglaciated before 12 cal ka BP. The succession of the ice-proximal stratified sediments from AF4 at the bottom of the basin, which are overlain by the ice-distal massive sediments of AF5 at the core site of GC12 (Fig. 3.10), suggests that retreat from the core site was relatively continuous and unlikely to have been interrupted by a glacier re-advance during the Holocene. This is supported by the continuous, roughly exponential decrease in sediment accumulation rate in GC12 (Fig. 3.10). The latter also shows that the assumption of linear sediment accumulation would be incorrect, preventing the calculation of a more accurate deglaciation age. The basal age of ∼4.5 cal ka BP in ice-distal sediments from GC08 shows that the glaciers must have been well south of the core site by this time. Considering the very limited fjord width (<3 km) at the core site of GC08 and, as a consequence, the concentrated sediment input from a minimum of three glaciers, this implies that the margins of most of the glaciers were located on land, likely at considerable distances from the coast, during the deposition of LF1.

An early and extensive deglaciation of Lomfjorden yields two major implications: (1) If the outer parts of Lomfjorden were indeed ice-free before 12 cal ka BP (cf. Ingólfsson *et al.*, 2016), the inferred position of the ice margin would be somewhere in the central part of Lomfjorden or even further south around that time. This is at odds with previous reconstructions of the extent of the SBIS, which place the ice margin ∼60 km north at the northern entrance of Hinlopenstretet around 12 cal ka BP (e.g. Landvik *et al.*, 1998; Ingólfsson & Landvik, 2013). This suggests that these reconstructions need to be revised as more data emerges from East Spitsbergen. (2) As the onset of deglaciation in West Spitsbergen was dated to around 15 cal ka BP, with ice having receded into the fjords around 12 cal ka BP and fjords being ice-free around 10 cal ka BP (e.g. Landvik *et al.*, 1998; Ingólfsson & Landvik, 2013), our data imply that the deglacial evolution of Lomfjorden could have been similar to that of fjords from West Spitsbergen. This seems reasonable, given the apparent similarity in their oceanography (see section 3.4.3). A warmer setting than originally thought for Lomfjorden is also supported by the very extensive retreat of the glaciers documented from our sediment cores. Although the latter is at odds with glaciers in West Spitsbergen, one explanation could be that Lomfjorden is located further inland than most West Spitsbergen fjords, and has a presumably drier climate. This may have led to reduced precipitation and, as a consequence, to increasingly negative glacier mass balances throughout most of the deglaciation.

In contrast to the Trunk Glacier Assemblage, the landforms of the Tributary Glacier Assemblage must have formed in an ice-free fjord, as the presence of a trunk glacier in the

fjord would presumably have prevented formation of the observed landforms. The Tributary Assemblages are consistent with landform assemblages observed in front of other Spitsbergen tidewater glaciers, where large outer moraines and a succession of recessional or annual push moraines are generally associated with Holocene re-advance, followed by slow and step-wise retreat, either related to a glacier surge, or to the LIA cooling (e.g. Plassen *et al.*, 2004; Ottesen & Dowdeswell, 2006; Forwick & Vorren, 2011; Flink *et al.*, 2015; Streuff *et al.*, subm.). It is thus possible that the Lomfjorden tributaries underwent re-advance during the Holocene, which also seems to be indicated by the lithological evidence. We note that none of the Lomfjorden glaciers are recognised as surge-type at present (Hagen, 1993), and, hence, the slightly larger outer moraines could represent the glaciers' maximum extents during the LIA (Forwick & Vorren, 2011; and references therein). However, the presence of the outermost recessional moraines at 1500 m (Valhallfonna), 200 m (Frøyabreen), and 220 m (Glintbreen/Kantbreen) from the present glacier termini show that such glacier advances cannot have been very extensive. This is further supported by the relatively small dimensions of the terminal moraines. Alternatively, small terminal moraines and the relative lack of turbidites in the upper parts of all proximal cores could also be related to moraine formation during deglaciation and associated ice retreat as the tributary glaciers decoupled from the Veteranen ice stream. This explanation seems reasonable as all landforms in the Tributary Glacier Assemblage occur in shallow waters very close to the present coast. The larger moraines and associated debris lobes in front of Glintbreen/Kantbreen and Valhallfonna could then have been formed during a prolonged stillstand related to ice grounding close to the shallow coastline (cf. e.g. Crossen, 1991; Seramur *et al.*, 1997; Ó Cofaigh, 1998; Ó Cofaigh *et al.*, 1999).

Considering that most Svalbard glaciers experienced at least one, usually relatively extensive, re-advance during the Holocene, and that these advances left distinct geomorphological imprints in the submarine record (cf. Plassen *et al.*, 2004; Ottesen & Dowdeswell, 2006; Baeten *et al.*, 2010; Forwick & Vorren, 2011; Kempf *et al.*, 2013; Flink *et al.*, 2015; Streuff *et al.*, 2015), the absence of similarly distinct and extensive assemblages in Lomfjorden is notable. However, the glaciers in Lomfjorden likely retreated far behind their present positions during deglaciation, as indicated by the large proportion of distal sediments in GC08. Hence the glacier margins would not necessarily have advanced far into the fjord during their respective LIA advances. Indeed, the presence of terrestrial moraines in front of most land-terminating glaciers in the area (see Fig. 3.1) shows that the minority of glaciers reached tidewater during the LIA. Alternatively, the generally drier continental climate in eastern Spitsbergen may not have supplied sufficient precipitation, causing any LIA advances in Lomfjorden to be restricted.

3.6 Conclusions

Swath-bathymetric data from Lomfjorden provide the first insights into glacigenic landform-sediment assemblages in an East Spitsbergen fjord. The landforms are: (1) streamlined bedrock highs, (2) glacial lineations, (3) drumlins, (4) recessional moraines and, in some cases, associated debris lobes, (5) De Geer moraines, (6) submarine channels, (7) mass-transport deposits, and (8) iceberg ploughmarks. We suggest that Lomfjorden was fully glaciated during the LGM and channelled a fast-flowing ice stream, which coalesced with the ice stream flowing through Hinlopenstretet at the mouth of the fjord. Drumlins and lineations record the advance of the ice stream through the fjord with recessional moraines and De Geer moraines recording slow

and step-wise retreat. A radiocarbon date of ∼9.7 cal ka BP in ice-distal sediments from the outer fjord suggests that deglaciation was well underway by this time. The inner parts of the fjord were ice-free before ∼4.5 cal ka BP and by this time all glaciers had retreated far into the hinterland. Our findings indicate that the glaciers in Lomfjorden may have undergone more extensive retreat during deglaciation than glaciers in West Spitsbergen. We suggest that this was likely caused by a drier climate and the resulting negative mass balances.

The principal sedimentary processes after deglaciation were (1) suspension settling from meltwater (plumes) and from the water column, and (2) reworking of the sediments by (a) gravitational mass-flow events and (b) iceberg ploughing. Deposition of partly bioturbated clayey silt occurred from suspension settling in ice-distal areas at decreasing sediment accumulation rates from 0.7 to 0.2 mm a^{-1}; the clayey silts are overlain by silty clay recording progressive glacier retreat. Silty clay interbedded with frequent sandy turbidites in the inner fjord indicates a higher-energy depositional environment, possibly related to more proximal glacimarine conditions. Ice-rafting played a minor role and delivered occasional lonestones to the outer fjord. Throughout the Holocene submarine channels formed from erosion by meltwater streams flowing into the fjord, which led to the deposition of numerous mass-transport deposits. The reworking of glacimarine sediment by grounded iceberg keels resulted in the formation of abundant iceberg ploughmarks during deglaciation. During the LIA, the local tidewater glaciers underwent (restricted) re-advances, and either formed terrestrial moraines, or submarine terminal moraines very close to the coast.

Acknowledgements

This work, as part of the GLANAM project "Glaciated North Atlantic Margins", was funded by the People Programme (Marie Curie Actions) of the European Union's Seventh Framework Programme FP7/2007-2013/ under REA grant agreement n^{o}317217. We thank the captain and crew of *R/V Helmer Hanssen*, Kelly Hogan, the students of the UNIS course AG211, and Oscar Fransner and Anne Flink for their help with data acquisition. Discussions with Anne Flink, Elena Grimoldi and Wesley Farnsworth as well as the comments of two anonymous reviewers were greatly appreciated and further helped to improve the manuscript.

Author contributions

This chapter in its current form is based on a team effort of the individual co-authors. Data acquisition was organised by Riko Noormets, and achieved by him, members of the crew of the research vessel, several colleagues and the lead author. All analyses and interpretations including the visualisation of acoustic data, the description and sub-sampling of sediment cores and the isolation and preparation of radiocarbon samples were carried out by the lead author, who also prepared all figures and the large majority of the text. Colm Ó Cofaigh did most of the reviewing, providing feedback and suggestions for improvement on the manuscript as a whole. Riko Noormets also corrected the text on several occasions, providing vital suggestions for the final structure. Jerry Lloyd helped with advice on the radiocarbon dating and, together with two anonymous reviewers, also helped improve the manuscript by providing several suggestions for editing. Author contributions to the manuscript in its current form are estimated as follows (not considering data acquisition processes): Katharina Streuff 85%, Colm Ó Cofaigh 10%, Riko Noormets 3%, and Jerry Lloyd 2%.

Chapter 4

Seafloor geomorphology and glacimarine sedimentation associated with fast-flowing ice sheet outlet glaciers in Disko Bay, West Greenland

Streuff, K.; Ó Cofaigh, C.; Hogan, K. A.; Jennings, A.; Lloyd, J. M.; Noormets, R.; Nielsen, T.; Kuijpers, A.; Dowdeswell, J. A.; Weinrebe, W. (2017b): Seafloor geomorphology and glacimarine sedimentation associated with fast-flowing ice sheet outlet glaciers in Disko Bay, West Greenland. *Quaternary Science Reviews.* DOI: 10.1016/j.quascirev.2017.05.021.

Abstract

Fast-flowing outlet glaciers currently drain the Greenland Ice Sheet (GIS), delivering ice, meltwater and debris to the fjords around Greenland. Although such glaciers strongly affect the ice sheet's mass balance, their glacimarine processes and associated products are still poorly understood. This study provides a detailed analysis of lithological and geophysical data from Disko Bay and the Vaigat Strait in central West Greenland. Disko Bay is strongly influenced by Jakobshavn Isbræ, Greenland's fastest-flowing glacier, which currently drains ∼7% of the ice sheet. Streamlined glacial landforms record the former flow of an expanded Jakobshavn Isbræ and adjacent GIS outlets through Disko Bay and the Vaigat Strait towards the continental shelf. Thirteen vibrocores contain a complex set of lithofacies including diamict, stratified mud, interbedded mud and sand, and bioturbated mud deposited by (1) suspension settling from meltwater plumes and the water column, (2) sediment gravity flows, and (3) iceberg rafting and ploughing. The importance of meltwater-related processes to glacimarine sedimentation in West Greenland fjords and bays is emphasised by the abundance of mud preserved in the cores. Radiocarbon dates constrain the position of the ice margin during deglaciation, and suggest that Jakobshavn Isbræ had retreated into central Disko Bay before 10.6 cal ka BP and to beyond Isfjeldsbanken by 7.6–7.1 cal ka BP. Sediment accumulation rates were up to 1.7 cm a^{-1} for ice-proximal glacimarine mud, and ∼0.007–0.05 cm a^{-1} for overlying distal sediments. In addition to elucidating the deglacial retreat history of Jakobshavn Isbræ, our findings show that the glacimarine sedimentary processes in West Greenland are similar to those in East Greenland, and that variability in such processes is more a function of time and glacier proximity than of geographic location and associated climatic regime.

4.1 Introduction

Tidewater glaciers terminate in the ocean at a grounded ice front (Meier & Post, 1987), represent an important link between terrestrial and marine environments, and are particularly susceptible

to climate change. Along the coast of Greenland many fast-flowing outlet glaciers drain the interior of the Greenland Ice Sheet (GIS), terminating as tidewater margins in the surrounding fjords. The associated glacial landforms and glacimarine sediments are revealed as the glaciers retreat, and provide important archives for understanding the long-term glacial evolution of the ice sheet and its future role with respect to sea-level rise (cf. e.g. Alley *et al.*, 2005; Bamber *et al.*, 2007; Nick *et al.*, 2009; Ó Cofaigh *et al.*, 2013; Dowdeswell *et al.*, 2014; Lane *et al.*, 2014; Joughin *et al.*, 2014; Hogan *et al.*, 2016; Sheldon *et al.*, 2016). Jakobshavn Isbræ, in central West Greenland, is of particular interest in this context, as it is the fastest-flowing of these outlets, currently flowing at velocities >17 km a^{-1} and draining ∼7% of the GIS, and thus exerts a strong influence on the ice sheet's mass balance (e.g. Bindschadler, 1984; Joughin *et al.*, 2004; Rignot & Kanagaratnam, 2006; Joughin *et al.*, 2014). Indeed, the increasing retreat speed and break-up of the glacier tongue has led to a rise in global sea level of almost 1 mm between 2000 and 2011 (Howat *et al.*, 2011; Joughin *et al.*, 2014). Although a number of investigations have focussed on the short-term dynamics of GIS outlet glaciers (e.g. Joughin *et al.*, 2004; Moon & Joughin, 2008; Joughin *et al.*, 2014), knowledge about their longer-term flow dynamics, their glacimarine processes, and the overall interaction of the glaciers with the marine environment since the Last Glacial Maximum (LGM) is only just emerging (e.g. Long & Roberts, 2003; Young *et al.*, 2011a; Jennings *et al.*, 2013; Ó Cofaigh *et al.*, 2013; Dowdeswell *et al.*, 2014; Hogan *et al.*, 2016; Sheldon *et al.*, 2016). This study uses sediment cores, multibeam bathymetry, sub-bottom profiler data, and radiocarbon dates from Disko Bay and the Vaigat Strait (Fig. 4.1) to (1) investigate the Holocene glacimarine sedimentary processes and products in Disko Bay and (2) to elucidate the deglacial history of Jakobshavn Isbræ in order to see how this particular outlet responded to environmental changes since the LGM.

4.2 Study area

4.2.1 Physiographic setting

Disko Bay is a marine embayment in central West Greenland, which is separated from the Vaigat Strait, a relatively narrow deep water trough, by Disko Island (Fig. 4.1). Disko Bay is located between ∼68°30'–69°40'N and 50°50'–55°00'W, and is roughly 100 km wide and between 50 and 500 m deep. It covers an area of ∼18000 km^2 and is bounded by Isfjorden and the Greenland mainland to the east, and Baffin Bay to the west (Fig. 4.1). A large, relatively shallow ridge, Isfjeldsbanken, is located at the entrance of the smaller Isfjorden and serves as a sill between the latter and Disko Bay. The Vaigat Strait is situated between ∼69°40'– 70°50'N and 50°50'-55°00'W (Fig. 4.1), is 10–30 km wide, and 200–650 m deep. It is bounded by the Nuussuaq Peninsula to the north and east and Disko Island to the south and west (Fig. 4.1). Three larger basins are present in the study area, one in the Vaigat Strait (up to 650 m deep) and two in western Disko Bay. The latter are ∼800 m deep and part of Egedesminde Dyb, a large trough, which is orientated northeast-southwest linking Disko Bay with the continental shelf (Fig. 4.1b). The local geology is dominated by Precambrian basement, including crystalline rocks such as granites and orthogneisses along the western shore of the Greenland mainland, Palaeogene basalts on Disko Island and western Nuussuaq, and Palaeogene and Upper Cretaceous sediments exposed at the seafloor and on parts of Disko Island and the Nuussuaq Peninsula (Chalmers *et al.*, 1999; Larsen & Pulvertaft, 2000; Weidick & Bennike, 2007).

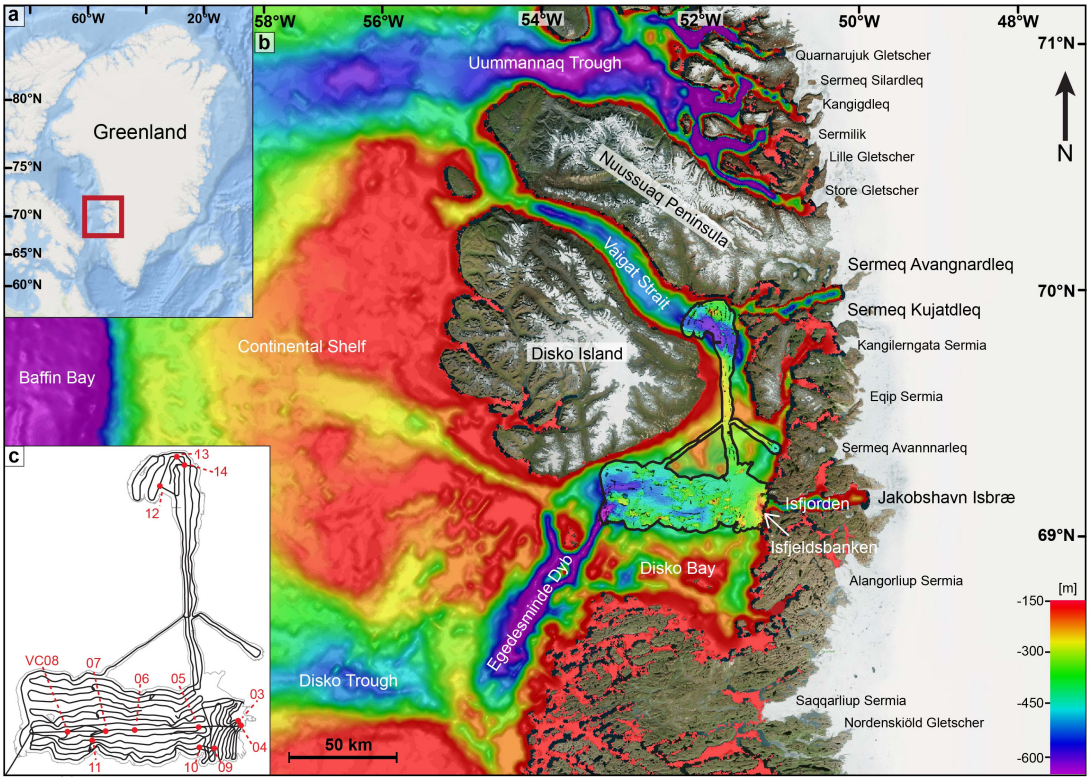

Figure 4.1: *a) Overview of Greenland with red rectangle indicating the extent of b). b) Study area and local bathymetry (IBCAO). The black outline shows the extent of the bathymetric data available for this study. Purple areas indicate bathymetric troughs. c) Distribution of TOPAS lines and location of the vibrocores.*

4.2.2 Glacial background

Although there are still gaps in our understanding of the long-term evolution of the GIS and its outlet glaciers (cf. Funder *et al.*, 2011), recent studies have outlined the Pliocene-Pleistocene glacial development of the Disko Bay margin (Hofmann *et al.*, 2016), and established that during the LGM an extended Jakobshavn Isbræ and several other glaciers in the area drained the GIS via Disko Bay and the Vaigat Strait, and extended to the outer shelf edge (Ó Cofaigh *et al.*, 2013; Jennings *et al.*, 2013; Hogan *et al.*, 2016). Radiocarbon dates from reworked shells from the Disko trough-mouth fan and tills on the adjoining shelf suggest that retreat of Jakobshavn Isbræ was underway by at least 13.8 ka BP and was briefly interrupted around 12.3–12 ka BP when the ice sheet underwent a re-advance in Disko Trough during the Younger Dryas (Ó Cofaigh *et al.*, 2013). Two modes of ice retreat have been suggested, (1) fast and relatively continuous retreat from the continental shelf and through Disko Bay (e.g. Long & Roberts, 2003; Lloyd *et al.*, 2005; Hogan *et al.*, 2012; Kelley *et al.*, 2013), and (2) step-wise retreat, where Jakobshavn Isbræ experienced short periods of stillstand at bedrock highs (e.g. Weidick, 1996; Rasch, 2000; Hogan *et al.*, 2016). The general consensus is that retreat across the continental shelf and through Disko Bay was relatively fast, but slowed once the ice stream entered Isfjorden in the east (cf. Funder & Hansen, 1996; Lloyd *et al.*, 2005; Hogan *et al.*, 2012; Kelley *et al.*, 2013; Ó Cofaigh *et al.*, 2013).

Deglaciation of western Disko Bay commenced around 10.8 ka BP, and the bay's eastern part was ice-free by 10.2 ka BP (Lloyd *et al.*, 2005; Kelley *et al.*, 2013). The grounded margin of Jakobshavn Isbræ most likely reached Isfjeldsbanken in eastern Disko Bay around 10.1 ka BP, pausing there until ~7.9 ka BP, when it retreated into Isfjorden (see Fig. 4.1b; Lloyd

et al., 2005; Weidick & Bennike, 2007; Kelley *et al.*, 2013). At present the Jakobshavn Isbræ margin is located approximately 50 km east of Isfjeldsbanken and discharges 90–100 km^3 a^{-1} of ice into Isfjorden (Joughin *et al.*, 2014). Due to a shorter calving line, the calving flux from Jakobshavn Isbræ was suggested to be significantly reduced around 9-10 ka BP, when the glacier margin was at Isfjeldsbanken, and the glaciers in northeast Disko Bay were inferred to be the dominant source of ice-rafted debris (IRD; Weidick, 1994; Long & Roberts, 2003; McCarthy, 2011). Retreat of the outer parts of the GIS outlets was asynchronous along Greenland's western coast (Ó Cofaigh *et al.*, 2013; Sheldon *et al.*, 2016), and deglaciation in the Vaigat was underway by 12.4 ka BP, with its western part ice-free before 11.8 ka BP and its eastern part deglaciated before 10.0 ka BP (Weidick, 1968; Bennike, 2000).

4.2.3 Oceanography

During deglaciation and the early Holocene, ocean waters in Disko Bay and the Vaigat Strait were mainly dominated by cold and fresh meltwater from the GIS (e.g. Lloyd *et al.*, 2005; Jennings *et al.*, 2013). By approximately 10 ka BP, the West Greenland Current (WGC) started to bring warmer and more saline waters into the bay, influencing the coastal areas around 7.8 ka BP, when ice had retreated into Isfjorden and the meltwater flux into Disko Bay had decreased (Lloyd *et al.*, 2005; Lloyd, 2006). After c. 6 ka BP the regional circulation pattern started to resemble modern conditions (Perner *et al.*, 2013), and today the modern tidewater glaciers still influence the surface waters in Disko Bay and the Vaigat Strait, which are cold and fresh (Andersen, 1981; Ribergaard & Buch, 2008). The bottom waters, however, contain warmer and more saline waters from the WGC (Lloyd *et al.*, 2005; Perner *et al.*, 2013). These waters are advected through Disko Bay from west to east and flow northwards around Disko Island and through the Vaigat Strait (e.g. Andresen *et al.*, 2010). They not only influence iceberg calving rates, but have also been linked to increased thinning and melting of GIS outlet glaciers (Holland *et al.*, 2008; Rignot *et al.*, 2010; Kelley *et al.*, 2013).

4.2.4 Acoustic stratigraphy of marine sediments

The sub-bottom profiler data available for this study were previously described and interpreted by Hogan *et al.* (2011, 2012), who identified four acoustic facies in Disko Bay, AD1–AD4, culminating in a total maximum thickness of up to 258 ± 8 m (calculated using a p-wave velocity of 1610 m s^{-1}; Fig. 4.2a, b). Facies AD1, with a stratified acoustic signature and a strong upper reflection (Fig. 4.2a), is 16–64 m thick, has onlap-fill geometry, and forms wedges in places (Hogan *et al.*, 2012). Facies AD2 generally overlies and locally cuts into AD1, is composed of acoustically transparent sub-units, and shows tapered or wedge-shaped geometry. It is 4–32 m thick and its upper boundary generally occurs as a continuous reflection of high amplitude (Fig. 4.2a; Hogan *et al.*, 2012). Facies AD3, like AD1, is acoustically stratified with internal reflections of medium strength (Fig. 4.2a). AD3 conformably overlies AD2, drapes some of the bedrock highs in the area and is up to 13 m thick. Facies AD4 only occurs in parts of Disko Bay, where it appears acoustically transparent with weak and chaotic internal reflections protruding into AD1 and AD2, and a strong, hummocky and chaotic upper boundary (Fig. 4.2a; Hogan *et al.*, 2012).

In southern Vaigat, Hogan *et al.* (2012) distinguished a total of five acoustic facies, AV1-AV5, with a cumulative thickness of up to 109 ± 3 m (Fig. 4.2c, d). Facies AV1, AV2, AV3, and AV4 are acoustically homogeneous with generally weak, discontinuous to chaotic internal reflections and are bounded by medium-strong, mostly continuous upper, in places hummocky,

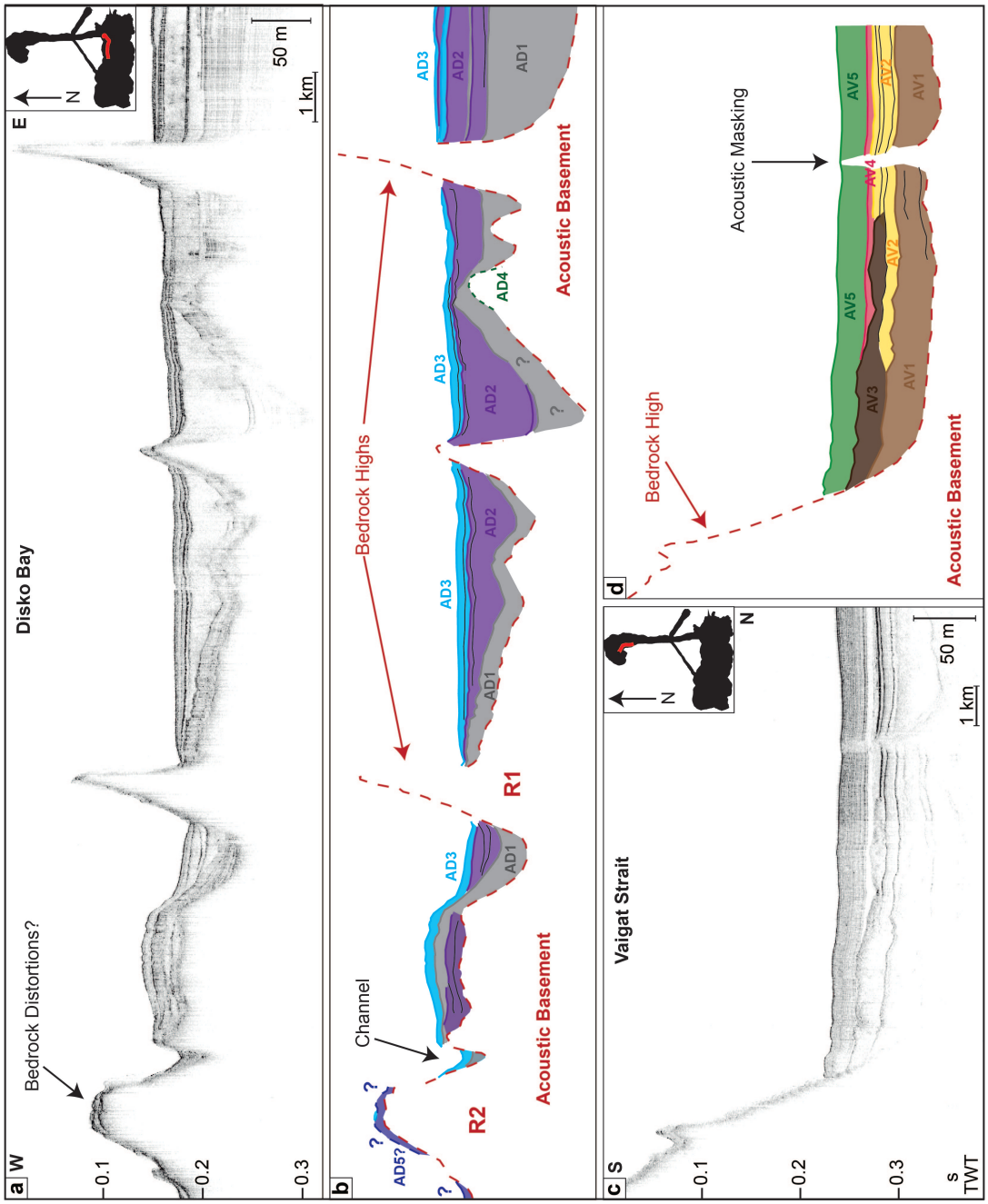

Figure 4.2: *a) TOPAS profile showing an example of the acoustic facies in Disko Bay. b) Interpretation of acoustic facies in Disko Bay, after Hogan* et al. *(2012). c) TOPAS profile with examples of acoustic facies occurring in the Vaigat Strait. d) Acoustic facies interpretation in the Vaigat Strait based on Hogan* et al. *(2012). The red lines on the black polygons indicate the respective location of the profiles.*

reflections. A distinction into four acoustic facies was mostly based on different morphologies; while AV1 represents the deepest basin-infill strata in the Vaigat, AV2 has a distinct wedge-shape, AV3 occurs as lenticular bodies, and AV4 infills surface depressions of AV2 and AV3 (Fig. 4.2c, d). AV5 is acoustically weakly stratified. It is the topmost facies in the Vaigat Strait and forms a conformable drape over the existing topography (Hogan *et al.*, 2012).

Facies AD1 was inferred to contain sediment deposited from turbid meltwater plumes, from the water column, icebergs, and sediment gravity flows in an ice-proximal environment in the eastern bay and in an ice-distal environment in the western bay (Hogan *et al.*, 2011, 2012).

From the tapered/wedge-shaped geometry and the acoustic transparency, the sub-units of AD2 were interpreted to also reflect gravity-flow deposits. These are occasionally interbedded with thin sediment strata derived from hemipelagic sedimentation, bottom currents, and smaller-scale or more dilute gravity flows (Hogan *et al.*, 2012). Hogan *et al.* (2011, 2012) interpreted Facies AD3 as ice-distal sediments settling from hemipelagic sedimentation and icebergs and/or sea ice. The internal reflections were associated with variations in input of IRD and/or bottom current activity. Facies AD4 was interpreted as a facies representing the upward migration of fluids through the sediment column (Hogan *et al.*, 2012).

Facies AV1–AV4 in the Vaigat were interpreted as partly erosive gravity-flow deposits derived from: (i) the deposition and remobilisation of glacimarine sediment settling from turbid meltwater plumes in the case of AV1 and AV4; (ii) an interplay of suspension settling and bottom currents in the case of AV2; and/or (iii) slumps down bedrock slopes in the case of AV3 (Hogan *et al.*, 2012). Facies AV5 was inferred to be deposited by post-glacial hemipelagic sedimentation with variable input of IRD by icebergs and sea ice (Hogan *et al.*, 2012).

4.3 Materials and methods

Nine vibrocores (VC03–VC11) from Disko Bay and three from the Vaigat (VC12–VC14; Fig. 4.1c) were collected in August 2009 during cruise JR175 of the *RRS James Clark Ross* to the West Greenland continental margin. Together with swath-bathymetric data (Fig. 4.1b), these sediment cores provide the basis for this study. The cores were acquired using the British Geological Survey vibrocorer with a 6 m-long barrel and an inner diameter of approximately 9 cm. Core recovery was excellent in soft sediments to moderate in diamicts. Upon retrieval, all sediment cores were divided into ∼1 m long sections, split into working and archive halves, and stored at +4°C. Core locations and lengths are summarised in Table 4.1. In order to identify the lithofacies, core logs of all working halves were generated from the core sections, and x-radiographs were used to provide supplementary information on sub-surface sedimentary structures and quantification of clasts larger than 2 mm, classified as IRD (sensu Grobe, 1987). A GEOTEK multi-sensor core logger (MSCL) was used to measure physical properties such as wet-bulk density, p-wave velocity (only VC05, VC07, VC09) and magnetic susceptibility (MS), which was acquired with a Bartington point-sensor mounted on the GEOTEK system. Shear strength measurements were taken with a Durham Geo Slope Indicator torvane and, for most cores, were carried out directly after splitting in 2009. For VC03 and VC04, however, the shear strength was only determined in 2016; hence values for these cores should be treated as estimates. Grain-size distribution and water content were measured by sampling approximately 1 cm-thick sediment slices in 8 cm-intervals, which were weighed, dried at 60°C and subsequently weighed and sieved through mesh sizes of 500, 250, 125, and 63 μm.

Samples for radiocarbon dating were collected from as close to distinct lithological boundaries in the cores as possible. Accelerator Mass Spectrometry (AMS) radiocarbon dates were measured at Beta Analytic on ∼6 mg of mixed species benthic foraminifera, and additional radiocarbon dates were obtained from molluscs and seaweed at the INSTAAR NSRL laboratory. The conventional radiocarbon ages were calibrated into cal a BP using Calib 7.1 with the MARINE13 curve and a reservoir correction of ΔR=140±25 (Stuiver & Reimer, 1993; Lloyd *et al.*, 2011; Reimer *et al.*, 2013). The same calibration was applied to already published ^{14}C dates from marine shells in Disko Bay (Lloyd *et al.*, 2005; McCarthy, 2011; Ó Cofaigh *et al.*, 2013), in order to make dates directly comparable.

Table 4.1: *Core locations and recovery.*

Core ID	Latitude	Longitude	Area	Depth [m]	Length [m]
VC03	69°10.81' N	51°11.61' W	Disko	545	1.57
VC04	69°09.97' N	51°10.15' W	Disko	263	1.10
VC05	69°09.60' N	51°31.63' W	Disko	389	5.87
VC06	69°08.94' N	52°04.14' W	Disko	439	4.94
VC07	69°08.62' N	52°18.88' W	Disko	439	5.46
VC08	69°08.35' N	52°38.24' W	Disko	429	3.91
VC09	69°05.79' N	51°23.65' W	Disko	294	5.98
VC10	69°05.95' N	51°31.22' W	Disko	351	4.86
VC11	69°06.90' N	52°25.60' W	Disko	410	3.25
VC12	69°53.12' N	51°53.15' W	Vaigat	616	3.66
VC13	69°58.46' N	51°44.47' W	Vaigat	341	3.40
VC14	69°56.97' N	51°40.35' W	Vaigat	386	4.66

Swath-bathymetric data were acquired during the JR175 cruise, using a hull-mounted Kongsberg Maritime Simrad EM120 multibeam echo sounder. The system operates at a frequency of 12 kHz and was calibrated using sound velocity profiles for the water column obtained from XBTs. The data were processed using MB-System Software and QPS Fledermaus, gridded to a cell size of 30x30 m in QPS DMagic, and visualised and interpreted in Fledermaus. The data were supplemented with swath-bathymetric data collected during two additional cruises to Disko Bay, one on *RV Maria S. Merian* in June 2007, and the other on the private fishing vessel *MV Smilla* in August 2008. The *Merian* data were acquired with a hull-mounted Kongsberg Maritime EM120 multibeam echo sounder in deep water and a Kongsberg Maritime EM1002 in shallow water, with the former operating at a frequency of 12 kHz and the latter at 95 kHz. The data were processed in the MB-System software (sensu Caress & Chayes, 1996) and gridded to a cell size of 24x24 m. The *MV Smilla* data were collected using a temporarily installed Sea Beam 1180 shallow water swath echo sounder system at a nominal frequency of 180 kHz, and gridded to a cell size of 15x15 m. Sub-bottom profiler data are also available for this study (Fig. 4.1c) and were gathered simultaneously with the swath-bathymetry from the 2009 *James Clark Ross* cruise, using a Kongsberg Maritime TOPAS PS18 sub-bottom profiler, which operated at a frequency of 3.5 kHz. These data were played out in near-real time with an EPC chart recorder installed on board the vessel, providing high-resolution (30–40 cm) acoustic profiles, post-processed in the TOPAS Software, and subsequently loaded into IHS The Kingdom Software 2015. Conversion between milliseconds and metres was done using a p-wave velocity of 1610 m s^{-1}, the combined average velocity measured in unconsolidated sediments from the three cores from Disko Bay. The TOPAS data and parts of the swath-bathymetric data were already analysed and interpreted by Hogan *et al.* (2012) and TOPAS profiles are thus only used for correlation purposes in this study. Bathymetric data from the *Merian* and *Smilla* vessels were previously interpreted by Schumann *et al.* (2012).

4.4 Results

4.4.1 Swath-bathymetry

A geomorphological map of the landforms in Disko Bay and the Vaigat Strait is shown in Figure 4.3. Earlier mapping from the easternmost part of Disko Bay (Hogan *et al.*, 2012; Schumann *et al.*, 2012) is incorporated into this map.

4.4.1.1 Large transverse ridges

The most prominent characteristic of the seafloor is its rugged, irregular topography, imparted by a number of transverse ridges, which are generally orientated in a north-south direction (Fig. 4.3). Most of these ridges are relatively discontinuous and between 1 and 2 km long. They have sharp crests imparted by steep eastern, and more gradual western flanks, the majority of which

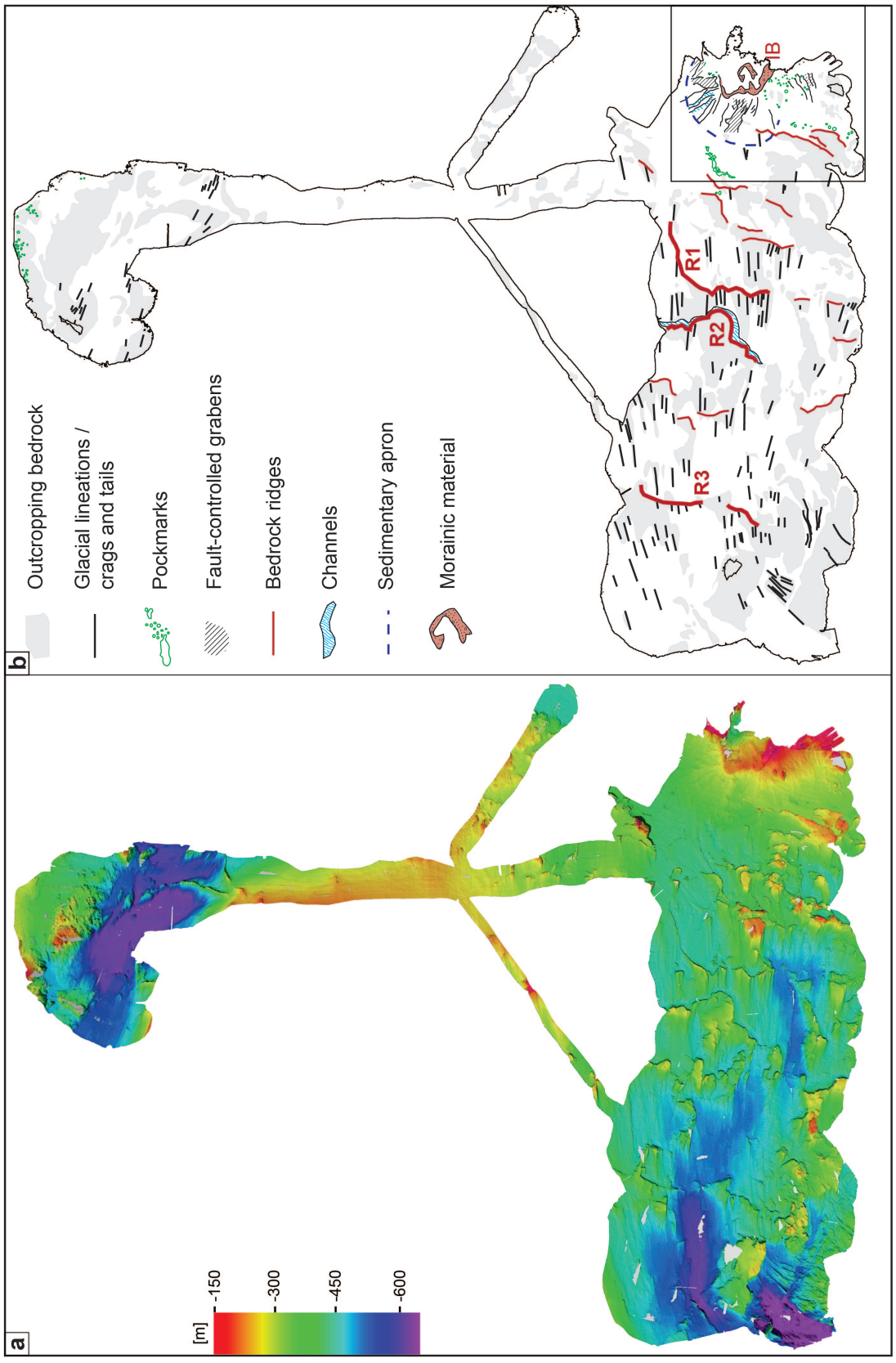

Figure 4.3: *a) Bathymetry in Disko Bay and the Vaigat Strait. b) Geomorphological map of all the landforms in Disko Bay. Landforms in the black rectangle indicate those already mapped by Hogan* et al. *(2012) and Schumann* et al. *(2012). IB = Isfjeldsbanken. Detailed examples are shown in Fig. 4.4.*

are intensely streamlined in the direction of ice flow (generally east-west). Three ridges, R1–R3, stand out morphologically (Fig. 4.3). R1 is the most proximal ridge, concave in planform with respect to the ice margin, and located approximately 20 km west of Isfjeldsbanken. It is ∼4.5 km long, 40 m high, and up to 500 m wide. R2, at 26 km from Isfjeldsbanken, is 20 km long, 200–1000 m wide, and 10–120 m high, with a generally convex crest forming a slight zig-zag pattern (Fig. 4.4). The distal flanks of R1 and parts of R2 are intensely streamlined (Fig. 4.4). R3 is curvilinear in plan view, 20 km long, up to 4 km wide and 20–120 m high.

The large dimensions and the rugged appearance of R1–R3 indicate that a purely glacial origin is unlikely (cf. Ottesen & Dowdeswell, 2006; Ottesen *et al.*, 2008; Hogan *et al.*, 2011; Flink *et al.*, 2015; Streuff *et al.*, 2015), and the sub-bottom profiler data show that the majority of the topographically distinct highs are formed in bedrock (e.g. Fig. 4.4d). We therefore interpret these ridges as bedrock highs that were overridden and streamlined by glacial ice.

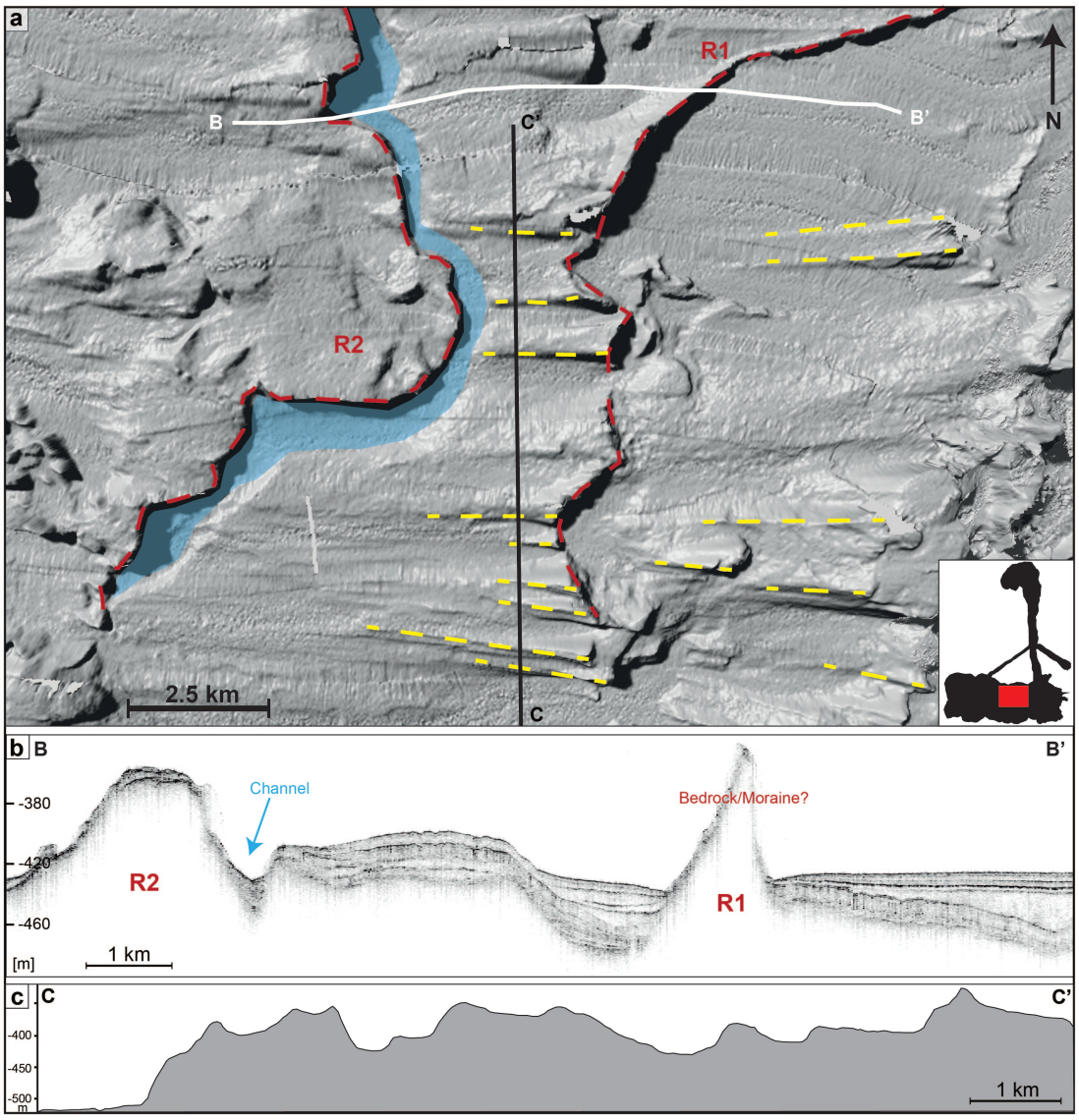

Figure 4.4: *a) Shaded-relief image of the bathymetry in Disko Bay. Red lines show the location of bedrock ridges, while yellow stippled lines follow the long-axes of the crag-and-tails. The blue polygon shows the location and extent of C1, and the red rectangle on top of the black polygon in the bottom-right hand corner shows the extent and location of a). b) TOPAS profile B–B' across a submarine channel and a ridge. c) Bathymetric profile C–C' across crag-and-tails.*

4.4.1.2 Elongate hills

The north-south orientated bedrock ridges in Disko Bay are closely associated with east-west orientated elongate hills (Figs. 4.3, 4.4). The latter are 1.5–7 km long, 100–1000 m wide, and around 10 m high with typically broader, steeper stoss sides and gently tapering lee ends (Fig. 4.4). The characteristics of these landforms are consistent with formation as crag-and-tails, the presence of which in Disko Bay was also documented by Ó Cofaigh *et al.* (2013). Crag-and-tails form subglacially and in association with bedrock highs, where the crag consists of bedrock with a lee-side tail forming from deposition of unconsolidated subglacial sediment (Dionne, 1987; Stokes *et al.*, 2011).

4.4.1.3 Submarine channels

A large channel, C1, occurs about 25 km west of Isfjeldsbanken and is ∼16 km long, around 800 m wide and up to 40 m deep. It follows the eastern edge of R2 and is sinuous in planform (Fig. 4.4). Several similar, generally smaller depressions have also been observed along the western flank of Isfjeldsbanken (Fig. 4.3; Hogan *et al.*, 2012). The large channel C1 is interpreted to be a subglacial channel eroded by meltwater flowing beneath an extended Jakobshavn Isbræ (cf. e.g. Walder & Hallet, 1979). The depth and shape of the channel imply that its formation took some time, during which meltwater erosion must have been focussed along R2. Assuming that meltwater disperses with increasing distance from the ice margin, concentrated meltwater routing implies that the ice margin was relatively close. As the channel is located on the proximal side and follows the line of R2, it seems plausible that the glacier front grounded on the bedrock high for an extended period of time and subglacial meltwater was routed around the bedrock obstacle, thereby eroding the channel. The smaller channels on the western flank of Isfjeldsbanken formed in the sediment pile and are interpreted as submarine channels eroded from downslope sediment-gravity flows, occasionally promoted by the presence of faults (Hogan *et al.*, 2012).

4.4.1.4 Sediment gravity flows

A large sedimentary apron on the western flank of Isfjeldsbanken was described by Schumann *et al.* (2012) and several smaller incisions along the same flank were interpreted as sediment slumps from downslope-gravity flows (Hogan *et al.*, 2012). Although such landforms do not always appear clearly on our bathymetric data, the sub-bottom profiler data indicate the abundance of such deposits in Disko Bay and the Vaigat Strait (see AD2 and AV1–AV4 in Fig. 4.2). Common triggers of gravity-flows are, for example, continuously high sediment accumulation and regional seismicity, the latter possibly related to isostatic rebound (e.g. Hunt & Malin, 1998; Forwick & Vorren, 2012).

4.4.1.5 Pockmarks

Several circular depressions occur in Disko Bay, and are especially common in the eastern part of the bay and on the distal flank of Isfjeldsbanken (Figs. 4.3, 4.5; see also Figs. 6 and 8 in Hogan *et al.*, 2012). The depressions often occur in clusters, are between 5 and 300 m in diameter, and 7–30 m deep. On the sub-bottom profiler data, the depressions are associated with a drawdown of the overlying reflections and occasional acoustic masking (Fig. 4.5; Hogan *et al.*, 2012). These depressions are interpreted as pockmarks (Hogan *et al.*, 2012), which are formed as a result of gas or pore fluid seepage (e.g. Harrington, 1985; Hovland & Judd, 1988; Forwick *et al.*, 2009; Nielsen *et al.*, 2014; Dowdeswell *et al.*, 2016f). Acoustic masking on the

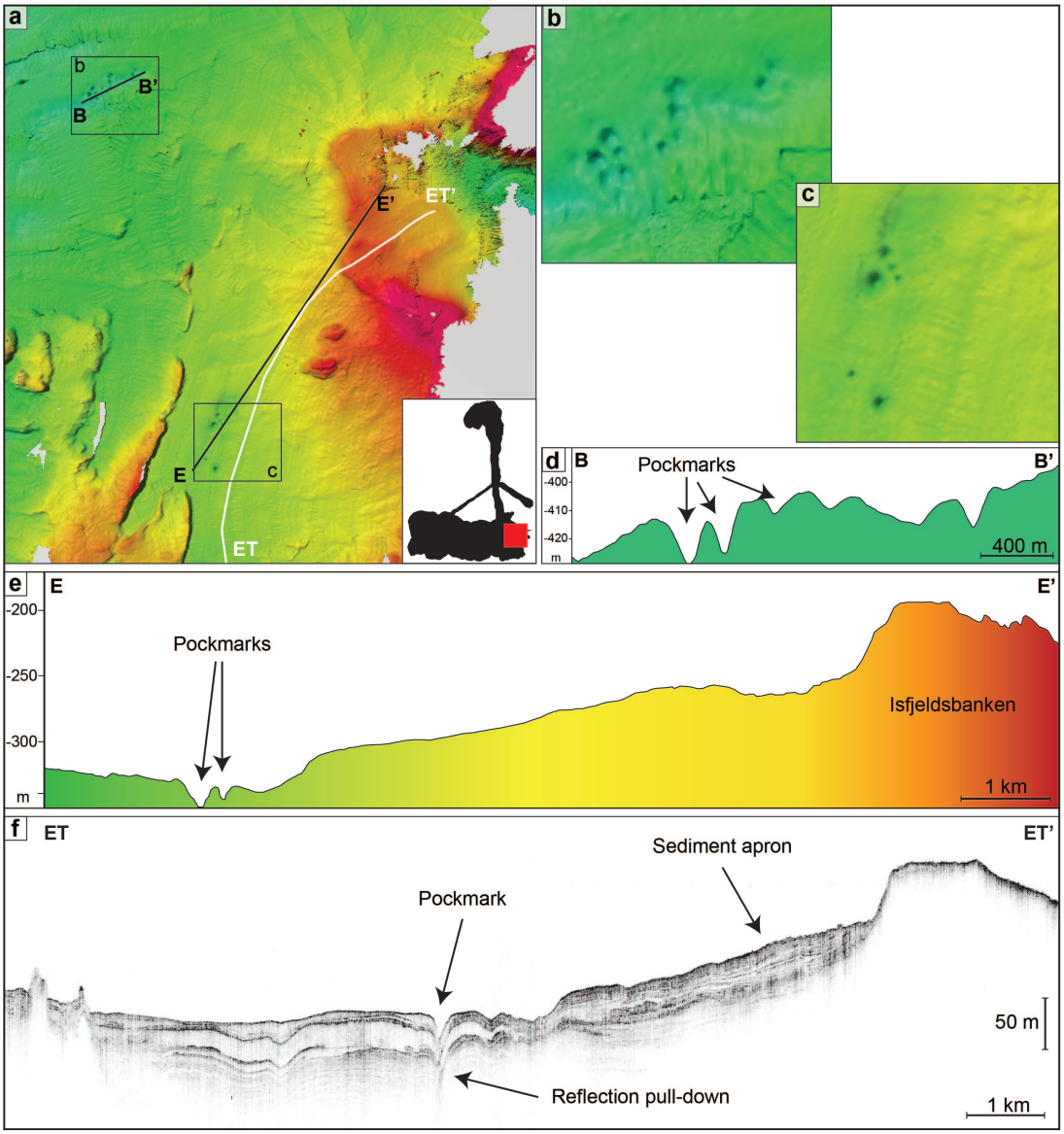

Figure 4.5: *a) Bathymetry around Isfjeldsbanken. Black polygon in the bottom-right hand corner shows location of a). b), c) Zoom-in on pockmark areas indicated in a). d) Bathymetric profile B–B' across pockmark area. e) Bathymetric profile E–E' across Isfjeldsbanken and pockmarks. f) TOPAS profile ET–ET' of e).*

sub-bottom profiler data supports this interpretation.

4.4.2 Sub-bottom profiler data

Description

Our seismostratigraphic findings support previous work from Hogan *et al.* (2012), who identified four acoustic facies in Disko Bay, AD1–AD4. Although difficult to discern, we identify one additional acoustic facies, AD5, which conformably overlies and occasionally onlaps the acoustic basement in localised areas of Disko Bay (see Figs. 4.2a, b, 4.6c, f). AD5 is characterised by chaotic, semi-transparent internal reflections of variable strength and is 11 ms (∼9 m) at its thickest. It can be bounded by a strong upper reflector and can appear slightly distorted by bedrock echos (Fig. 4.2a). AD5 differs from AD2 by a slightly more opaque acoustic character with a larger number of internal reflections. Furthermore, unlike in AD2, the TOPAS signal weakens with increasing depth and quickly disappears beneath the upper boundary of AD5.

Interpretation

The semi-transparent and internally massive acoustic appearance of Facies AD5 as well as a decreasing signal strength with depth have sometimes been attributed to uniformly mixed sediments of possibly diamictic composition (Stewart & Stoker, 1990; Forwick & Vorren, 2011). AD5 could thus represent a diamict deposited either at or beneath the glacier grounding line as glacial till, or from increased iceberg-rainout. Our sedimentary data indicate that the diamict is more likely related to deposition from glacimarine processes (see LD1, section 4.4.3 below), but based on the partly distorted signal on the sub-bottom profiler data and a limited penetration depth of the cores into AD5, a clear distinction cannot be made.

4.4.3 Lithological data

4.4.3.1 Lithofacies

From the sedimentary record preserved in the vibrocores we define five lithofacies in Disko Bay (LD1–LD5), and one in the Vaigat (LV1). The correlation between lithology and sub-bottom profiler data is shown in Figure 4.6. Physical properties of the lithofacies and their stratigraphic distribution within the cores are displayed in Figures 4.7 and 4.9, while examples of the x-radiographs for each facies are shown in Figure 4.8.

LD1 is a dense (2–3 g cm^{-3}), matrix-supported diamict with a predominantly sandy matrix, and a majority of sub-angular to sub-rounded clasts (Fig. 4.8). Based on differences in shear strength and sediment structure, we distinguish LD1a and LD1b. LD1a shows some contortions on x-radiographs (Fig. 4.8), has a shear strength of up to 40 kPa, and only occurs in VC08 (Fig. 4.7). LD1b is massive, has a shear strength of up to 70 kPa, and only occurs in VC03 and VC04. The water content and the proportion of clay and silt in both lithofacies of LD1 are low with values around 20% and 40%, respectively (Fig. 4.7). Around 30-40% of the grains are >250 μm, with generally 5–10 clasts >2 mm occurring per 2 cm-window. The MS is around 100 x 10^{-5} SI on average and shows distinct peaks. LD1b is part of AD5 (Fig. 4.6), but strong bedrock reflection hyperbolae on the TOPAS signal around the core site of VC08 prevented a direct correlation between LD1a and its acoustic counterpart.

Lithofacies LD2 contains mud with highly variable amounts of clasts and is present in all cores from Disko Bay (Fig. 4.7). Clasts are pebble- to gravel-sized, mainly sub-angular to sub-rounded and of predominantly granitic composition, presumably sourced from the Precambrian basement (Fig. 4.8; cf. Chalmers *et al.*, 1999; Larsen & Pulvertaft, 2000; Weidick & Bennike, 2007). The matrix is composed of clay and silt and varies in colour between (dark) greenish grey (Munsell colour code: GLEY 1 4/10Y to 5/10Y) and greenish grey (GLEY 1 5/10Y to 6/10Y) or dark to olive grey (5Y 4/1 to 4/2). The muds have a density of 1–2 g cm^{-3} and a shear strength between 2 and 10 kPa, which slightly increases down-core (Fig. 4.7). LD2 has a water content between 30 and 60% (Fig. 4.7) and standing water was observed on localised areas of the sediment surface. The mud fraction generally exceeds 90% but can drop to 80% where clasts are abundant (Fig. 4.7). Clast concentrations are up to 25 clasts per 2 cm-window. The facies has a highly variable MS between ~15 and 150 x 10^{-5} SI (Fig. 4.7). We distinguish subfacies LD2a, LD2b, and LD2c. In LD2a, which only occurs at the bottom of VC09, the mud appears diffusely stratified with some pebble-sized clasts and occasional bioturbation burrows at the top of the facies (Figs. 4.7, 4.8). LD2b contains internally massive mud in stratified sequences, with strata between ~4 and 15 cm thick. The strata have generally sharp contacts in the lower parts of LD2b, and more diffuse boundaries, partly promoted by bioturbation, in the upper parts (Figs. 4.7, 4.8). LD2c contains massive, occasionally bioturbated mud (Fig.

4.8). LD2 correlates with acoustic facies AD2 and AD3 (Fig. 4.6).

Lithofacies LD3 is composed of massive and partly contorted mud, interspersed with massive fine sand-rich units (Fig. 4.7). These units are occasional to frequent, mostly inclined, and occur as mm-thick laminae or cm-thick layers with sometimes sharp, but mostly diffuse lower boundaries (Fig. 4.8). In places the sandy beds are heavily contorted (Fig. 4.8). The overall density of LD3 is around 1.6 g cm^{-3} with minor variations, whereas the shear strength is highly variable (0.5 and 12 kPa; Fig. 4.7). Water content is around 20–30%, and grain size distribution varies according to the sub-sampled lithology, with >95% clay and silt in the matrix, and ~80% clay and silt in the sandy layers (Fig. 4.7). IRD grains >2 mm are rare. The MS is ~100–120

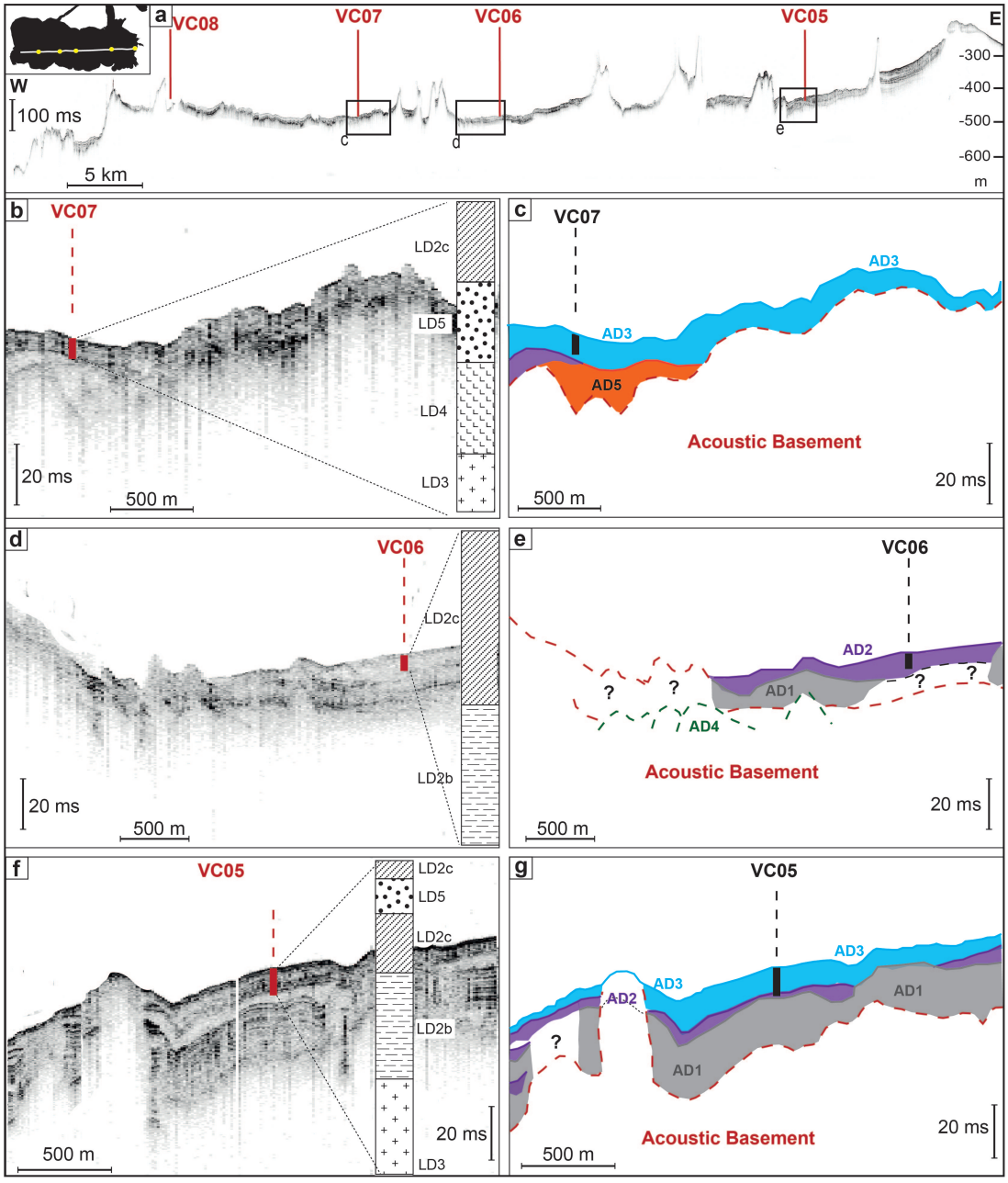

Figure 4.6: *a) TOPAS profile across the core locations. The black polygon indicates location and extent of the profile. b), d), f) TOPAS lines across VC07, VC06, and VC05, respectively, with c), e), g) showing the according acoustic facies interpretation with respect to core penetration.*

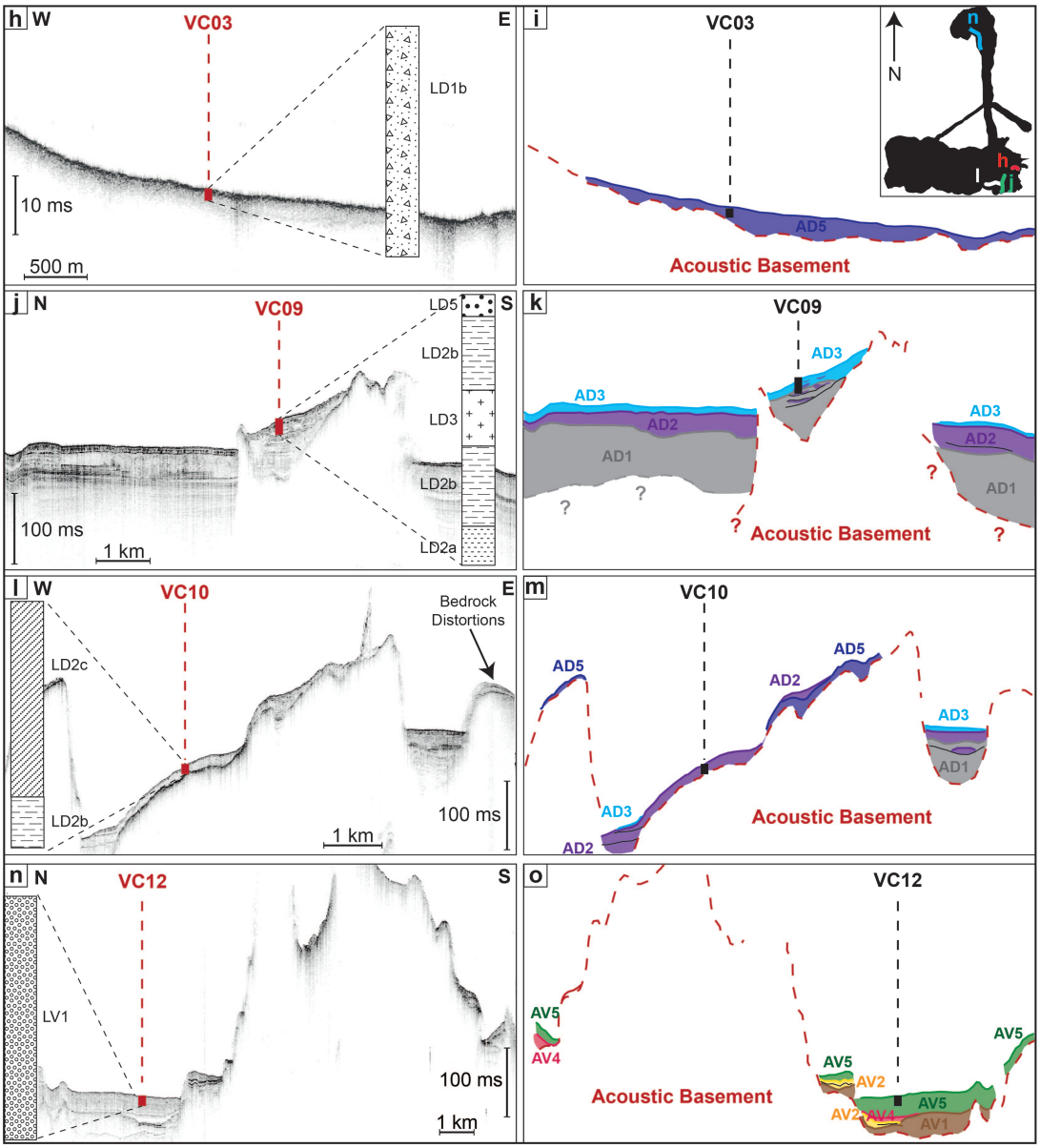

Figure 4.6 *(cont.): TOPAS lines across and acoustic facies interpretation at the core sites of h), i) VC03, j), k) VC09, l), m) VC10, and n), o) VC12 from the Vaigat Strait. Black polygon in the top right-hand corner of i) shows the location of the TOPAS lines with respect to the bathymetry.*

x 10^{-5} SI with few localised and distinct peaks. The facies occurs in either the basal or middle parts of VC05, VC07, and VC09 (Fig. 4.7). LD3 forms part of the acoustic facies AD2 (Fig. 4.6).

Lithofacies LD4 contains diffusely laminated mud interbedded with diamictic layers (Figs. 4.7, 4.8). The diamict layers are up to 4 cm thick, contain fines, sand, and pebbles, and normally have a very gradual and diffuse lower boundary, but a sharper upper contact, which is especially pronounced in the bottom parts of LD4 (Fig. 4.8). The shear strength is around 8 kPa, the water content ~40%, and >90% of the sediment are <63μm. The increased clast content in the diamictic layers is reflected in a variable IRD count of up to 21 clasts per 2 cm (Fig. 4.7). Minor oscillations in MS, which is generally ~50 x 10^{-5}, are interrupted by several pronounced peaks to values between 125 and 225 x 10^{-5} SI (Fig. 4.7). LD4 is present only in VC07 (Fig. 4.7).

Lithofacies LD5 is a matrix-supported diamict, with a mud-dominated matrix (rather than sand-dominated as for LD1) and abundant angular to sub-angular clasts of variable diameter (Fig. 4.8). Smaller pebbles are sometimes concentrated in dense, cm-thick beds, which have sharp contacts with the surrounding sediments. The density is around 1.5 g cm^{-3}, the shear strength between 5 and 10 kPa, and the water content between 10 and 40%. LD5 has a variable proportion (20–80%) of fines (<63 μm) and a high IRD count of up to 25 clasts per 2 cm-

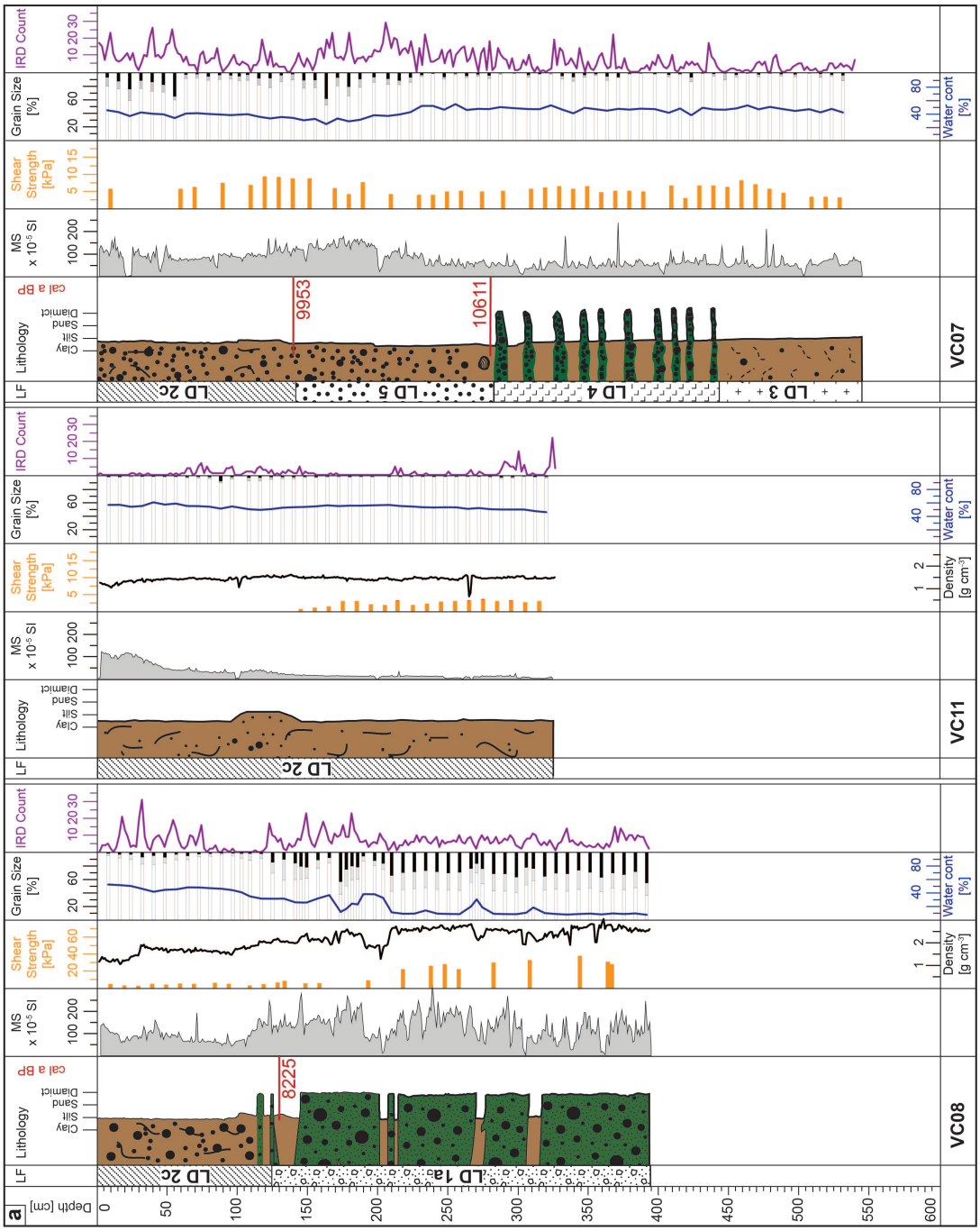

Figure 4.7: *a) Lithofacies and lithological logs with physical properties of and radiocarbon dates from vibrocores VC08, VC11, and VC07 from Disko Bay (west to east). MS = magnetic susceptibility. Note the different scales for the shear strength. Grain-size distribution results were grouped thus: white bars = grains <63 μm, grey bars = 63–250 μm, black bars = grains >250 μm.*

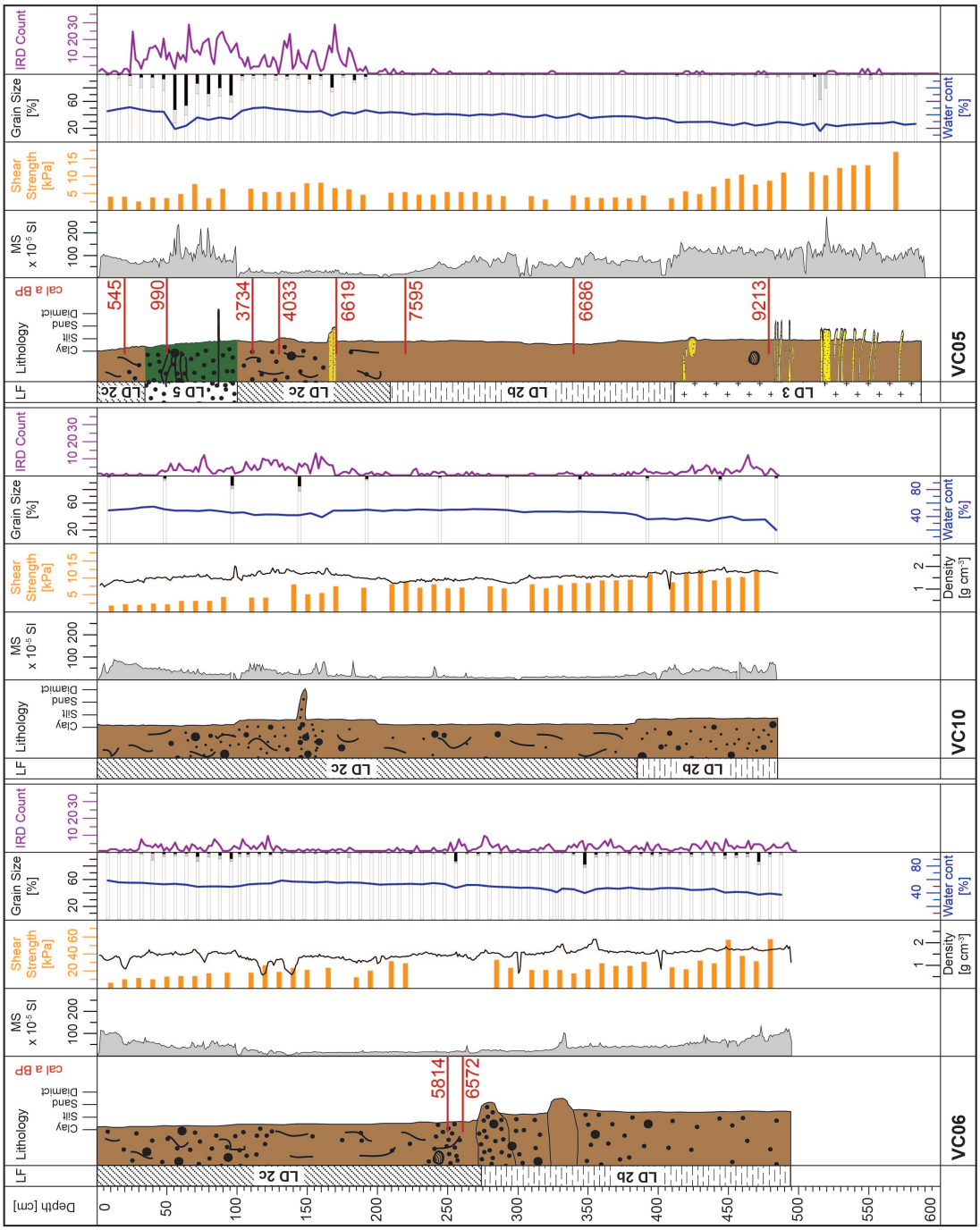

Figure 4.7 *(cont.): Lithofacies and lithological logs with physical properties of and radiocarbon dates from vibrocores VC06, VC10, and VC05 from Disko Bay (west to east). MS = magnetic susceptibility. Grain-size distribution: white bars = grains <63 µm, grey bars = 63–250 µm, black bars = grains >250 µm.*

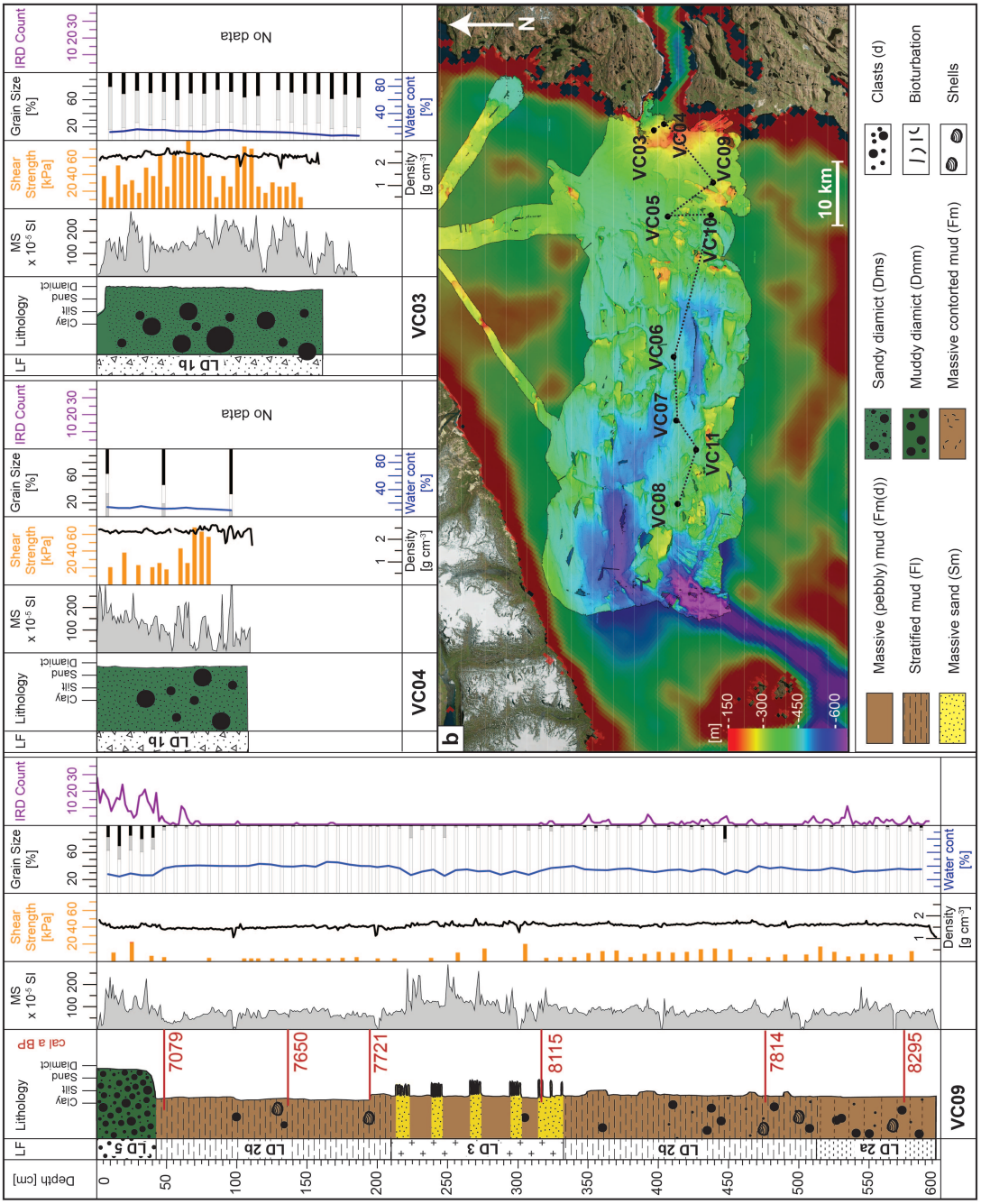

***Figure 4.7** (cont.): Lithofacies and lithological logs with physical properties of and radiocarbon dates from vibrocores VC09, VC04, and VC03 from Disko Bay (west to east). MS = magnetic susceptibility. b) Core locations. The black stippled line indicates the order in which cores are shown. Grain-size distribution: white bars = grains <63 µm, grey bars = 63–250 µm, black bars = grains >250 µm.*

window. A spiky appearance with numerous well-pronounced peaks defines the MS, which, in most cases, exceeds 80 x 10^{-5} SI.

The cores from the Vaigat contain a single lithofacies, LV1, which comprises massive, dark grey to dark olive grey mud (5Y 4/1 to 3/2) with a moderate clast abundance (Figs. 4.8, 4.9). It is similar to LD2a from the cores in Disko Bay, but the matrix contains low amounts of sand and there is no evidence of bioturbation. Internal sedimentary structures are absent, with the exception of occasional laminae of coarser grains (medium sand to pebble-sized; Fig. 4.8). The

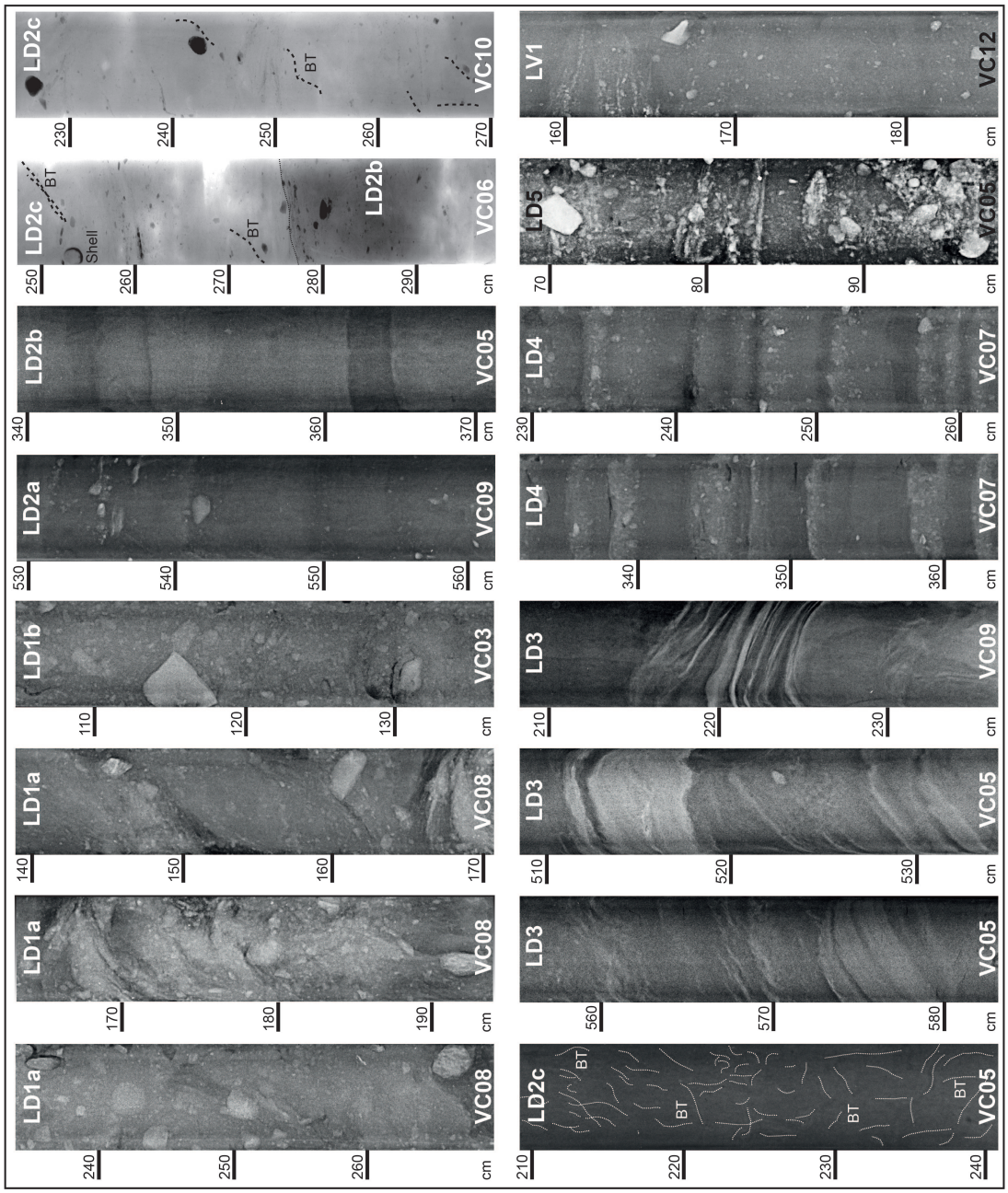

Figure 4.8: *Examples of the x-radiographs from the six lithofacies LD1–LD5, and LV1 from different vibrocores (VC) and sediment depths in Disko Bay and the Vaigat Strait. Generally denser parts appear lighter, except for in the two x-radiographs from VC10 and VC06, where colours are reversed. BT = bioturbation.*

density is around 1.5 g cm^{-3} and the shear strength 4–12 kPa, with a slight increasing trend down-facies (Fig. 4.9). LV1 has a water content of ∼50% and >95% fines and occurs in all three cores from the Vaigat (Fig. 4.9). The IRD count is highly variable with 0–22 clasts per 2 cm-window, and the MS is generally around 200–250 x 10^{-5} SI with relatively minor variations (Fig. 4.9). LV1 forms part of acoustic facies AV5 (Fig. 4.6).

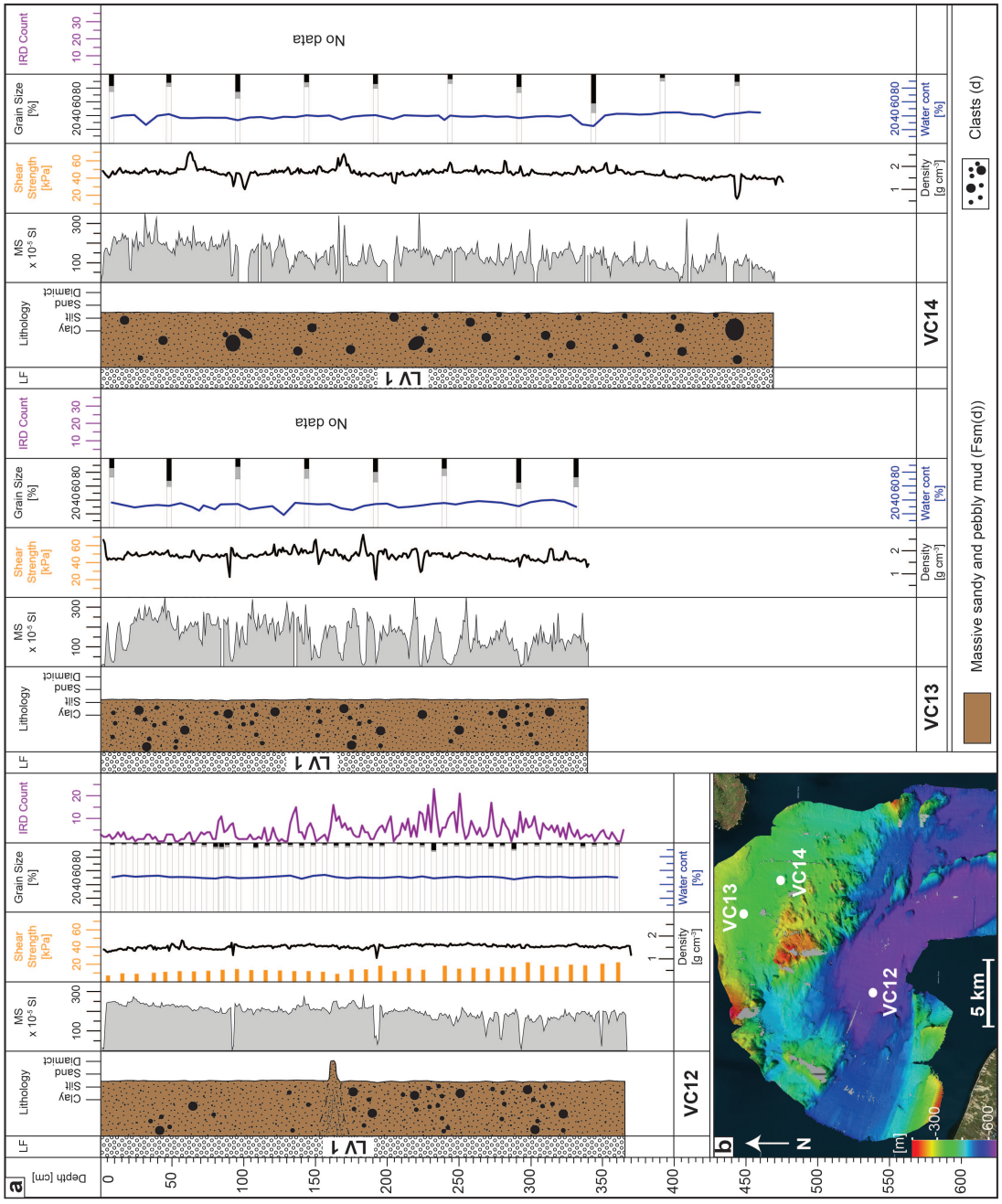

Figure 4.9: *Lithofacies and lithological logs of the three vibrocores from the Vaigat Strait and their physical properties. MS = magnetic susceptibility. Grain-size distribution: white bars = grains <63 µm, grey bars = 63–250 µm, black bars = grains >250 µm.*

4.4.3.2 Radiocarbon dates and sediment accumulation rates

Radiocarbon dates presented here are rounded to the closest 100 years and are shown in detail in Table 4.2 and Figure 4.10. AMS measurements were carried out on paired or whole bivalve shells (Table 4.2) or mixed benthic foraminifera taken from seemingly undisturbed sediment sections to ensure accuracy of the radiocarbon dates. The exception is the date at 316 cm in VC09, where the frequent sandy deposits most likely represent turbidites and the obtained date may hence derive from reworked material (see section 4.4.3.3 below). Other AMS measurements were carried out on seaweed taken from near the centre of the split cores to reduce the risk of

Table 4.2: *Radiocarbon dates and calibrated ages used in this study. Unless otherwise specified all bivalves were intact and did not show evidence of being re-worked.*

Core ID	Depth [cm]	Lab Code	Sample	Reported age [^{14}C a BP]	Mean probability age [cal a BP]	2σ [cal a BP]
VC05	20–21	AA–90391	Seaweed	1079 ± 78	545	418–668
VC05	50–51	AA–90392	Seaweed	1575 ± 88	990	778–1190
VC05	112–113	Beta–434927	Seaweed	3930 ± 30	3734	3612–3845
VC05	130–131	AA–90393	Seaweed	4159 ± 50	4033	3872–4210
VC05	170–171	AA–90394	Seaweed	6322 ± 60	6619	6451–6776
VC05	220–221	AA–90395	Seaweed	7250 ± 380	7595	6788–8355
VC05	340–341	AA–90396	Seaweed	6370 ± 180	6686	6294–7119
VC05	478–479	AA–90396	Paired Bivalve	8710 ± 50	9213	9045–9383
VC06	250	Beta–434928	Single Bivalve	5580 ± 30	5814	5711–5905
VC06	272–273	Beta–434929	Seaweed	6280 ± 30	6572	6456–6672
VC07	140–142	Beta–434930	Foraminifera	9300 ± 30	9953	9772–10118
VC07	280–281	Beta–434931	Paired Bivalve	9850 ± 30	10611	10503–10723
VC08	130–132	Beta–434932	Foraminifera	7890 ± 30	8225	8130–8326
VC09	48	Beta–434933	Seaweed	6700 ± 30	7079	6955–7184
VC09	137	Beta–434934	Paired Bivalve	7330 ± 30	7650	7570–7743
VC09	195	Beta–434935	Paired Bivalve	7400 ± 30	7721	7631–7821
VC09	316–318	Beta–434936	Foraminifera	7800 ± 30	8115	8001–8214
VC09	476	Beta–265208	Paired Bivalve	7490 ± 50	7814	7684–7928
VC09	575	Beta–265209	Paired Bivalve	7970 ± 50	8295	8171–8394

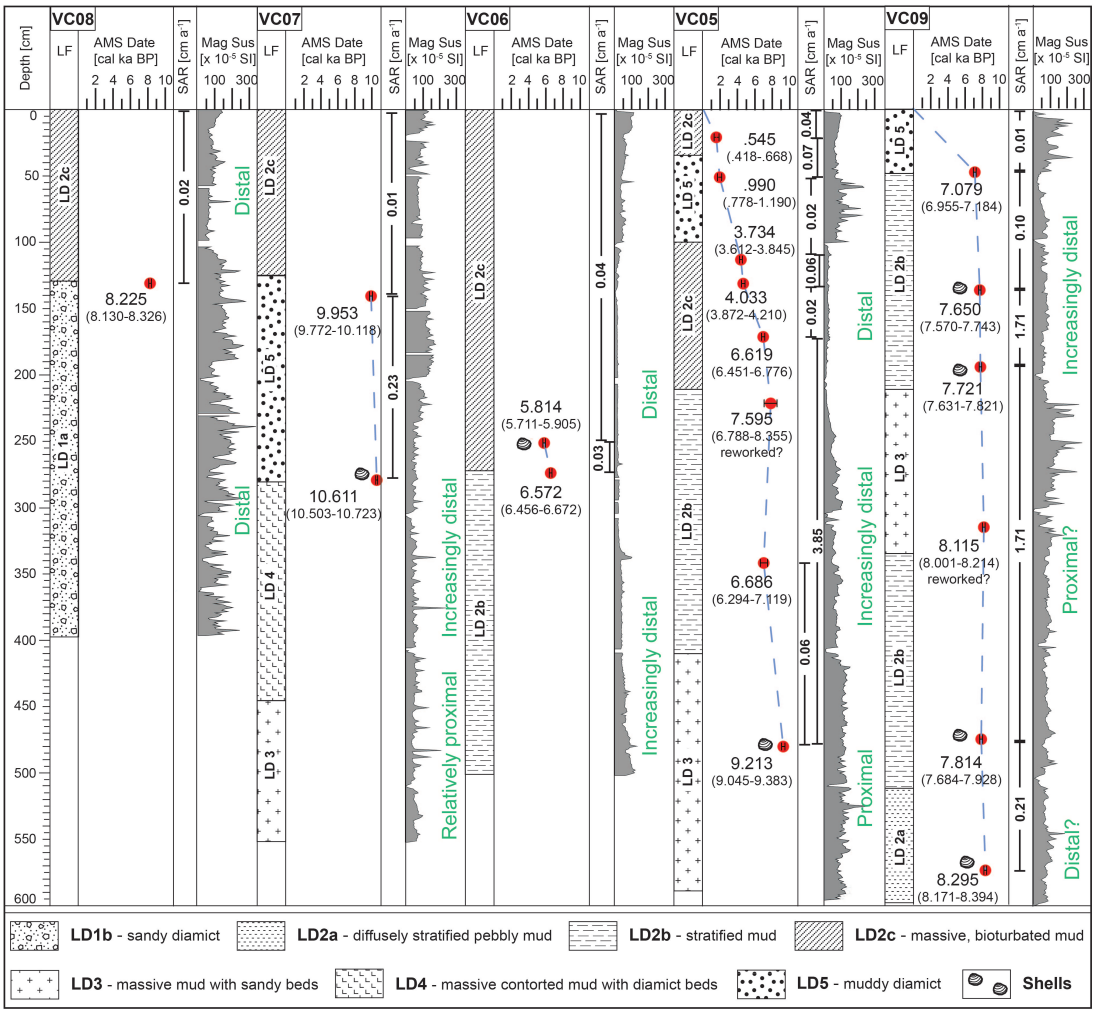

Figure 4.10: *Lithofacies logs with radiocarbon dates (error bars indicate 2σ-range) and calculated SARs from a core transect across Disko Bay from west to east (see Fig. 4.7b for core locations). Note that facies signatures are only used as a means to visually differentiate between lithofacies, not to describe the actual lithology. For details on the lithological composition of the cores and lithofacies see also Fig. 4.7 and section 4.4.3. Together with the MS these values give an idea about the glacimarine environment the lithofacies were deposited in.*

material having been dragged down-core during the coring process. Notwithstanding this, the age reversal and the large error margin for the sample from 340 cm in VC05 indicate that the seaweed at this depth was not in-situ. Sediment accumulation rates (SARs; Fig. 4.10) were calculated from the mean radiocarbon ages and assume constant accumulation between each date.

Radiocarbon dating suggests that LD1a at the base of VC08 was deposited prior to ∼8.2 cal ka BP and that the overlying LD2c accumulated at an average rate of 0.02 cm a^{-1} (Fig. 4.10). Basal sediments in VC07 contain LD3 and LD4 and are the oldest recovered from Disko Bay, deposited before 10.6 cal ka BP. The top of the overlying LD5 dates to ∼9.9 cal ka BP, implying a SAR of 0.23 cm a^{-1} for this facies (Fig. 4.10). The same date suggests that the topmost facies in VC07, LD2c, was deposited afterwards at a SAR of 0.01 cm a^{-1}. Two dates from VC06 indicate that its bottom part (LD2b) is older than ∼6.5 cal ka BP, and that the overlying LD2c accumulated at a rate of 0.03–0.04 cm a^{-1} (Fig. 4.10). LD3 at the bottom of VC05 was deposited around 9.2 cal ka BP. Assuming that the date of 7.6 cal ka BP at the top of the overlying LD2b is indeed unreliable, LD2b accumulated from before 6.7 to just before 6.6 cal ka BP at a rate of ∼0.05 cm a^{-1} (Fig. 4.10). The overlying LD2c was deposited until today, at a rate of 0.02–0.06 cm a^{-1}, but deposition was interrupted from ∼3.7 until after 0.99 cal ka BP, during which time LD5 formed (Fig. 4.10). The bottom half of VC09 (LD2a, LD2b and LD3) was deposited between 8.3 and 7.7 cal ka BP at an SAR of 0.21–1.71 cm a^{-1} (Fig. 4.10). In the top half of the core LD2b accumulated between 7.7 and 7.0 cal ka BP at decreasing rates between 1.72 and 0.10 cm a^{-1}, and is overlain by LD5, deposited since 7.0 cal ka BP at a very low SAR of 0.01 cm a^{-1} (Fig. 4.10).

4.4.3.3 Interpretation

LD1 – sandy diamict

Although x-radiographs of LD1 are similar to glacial till documented from outer Disko Bay and the continental shelf in the Disko and Uummannaq Troughs (Ó Cofaigh *et al.*, 2013; Dowdeswell *et al.*, 2014; Hogan *et al.*, 2016; Sheldon *et al.*, 2016) and the shear strength of ∼40–80 kPa exceeds that of subglacial tills from Antarctica (cf. Ó Cofaigh *et al.*, 2005), the absence of planar structures or indications of clast alignment in both, LD1a and LD1b appear to be at odds with an interpretation as glacial till. Furthermore, in the case of LD1a, we would expect glacial till to be significantly older than the given age of 8.2 cal ka BP, considering that the bay was probably ice-free around 10 cal ka BP (Lloyd *et al.*, 2005; Young *et al.*, 2011a). In the case of LD1b, we would expect any sequence of glacial till to be covered by a succession of Holocene sediments, as till could only have formed at the core sites when the ice margin last paused at Isfjeldsbanken, around 10 ka BP. We therefore favour an interpretation of LD1a as a mass-flow deposit and of LD1b as post-glacial glacimarine sediments, where deposition occurred from meltwater and/or the water column and melting icebergs (e.g. Elverhøi *et al.*, 1980, 1983; Gilbert, 1983; Hogan *et al.*, 2016). The partly contorted appearance of LD1a in VC08 and the occurrence of mud strata within the facies indicate sediment reworking and suggest that LD1a was formed as a gravity-flow deposit reworking glacimarine mud and IRD (cf. e.g. Kuenen, 1948; Shanmugam *et al.*, 1994; Forsberg *et al.*, 1999). This seems reasonable, as the core site of VC08 is located in a submarine basin between two bedrock highs, the steep slopes of which could have promoted repeated mass flows. Indeed, the sub-bottom profiler data show abundant mass-flow deposits in Disko Bay, supporting an interpretation of LD1a as a gravity-flow deposit. This interpretation is also consistent with the low shear strength and the comparatively young age of LD1a. An

interpretation of LD1b as post-glacial IRD-rich sediment is based on the fact that VC03 and VC04, containing LD1b, were taken from the top of Isfjeldsbanken, where the high accumulation of IRD is likely, because (1) all icebergs calved off Jakobshavn Isbræ pass through Isfjorden into Disko Bay, and (2) the sill traps larger icebergs inside the fjord due to the shallow water depth (Echelmeyer *et al.*, 1991; Hogan *et al.*, 2011). These bergs need to melt considerably before passing into Disko Bay (Echelmeyer *et al.*, 1991; Hogan *et al.*, 2011), and thus probably deposit the majority of their debris at or near Isfjeldsbanken. Although no distinct iceberg ploughmarks were observed on the swath-bathymetric data, the relatively high shear strength in LD1b indicates that icebergs may have grounded at the core sites, scouring, compacting and homogenising the deposited sediments. Indeed, LD1b is macroscopically similar to diamicts in East Greenland, which have been interpreted as "iceberg turbates" (Vorren *et al.*, 1983; Marienfeld, 1992; Dowdeswell *et al.*, 1994b; Linch & Dowdeswell, 2016).

LD2 – massive to stratified mud

LD2 is interpreted as glacimarine mud settling from suspension in glacial meltwater plumes and the water column (cf. e.g. Gilbert, 1983; Elverhøi *et al.*, 1983; Dowdeswell *et al.*, 1998; Ashley & Smith, 2000). Clasts record the deposition of IRD from icebergs and/or sea ice. The low shear strength and high water content of this facies support this interpretation.

Stratification in LD2a and LD2b is likely related to changes in depositional environment or sediment source. These are controlled by a number of factors, including e.g. regional warming and melting of the ice sheet, variability in the position of meltwater efflux, inter-annual variations in meltwater flux due to seasonal or tidal controls or floods from glacial lakes, or by ice-margin fluctuations controlling the proximity of the core site to the ice margin. The diffuse nature of the stratification in LD2a is thought to reflect a relatively ice-distal environment, where such changes have a smaller impact on the sedimentary record. An upward increase in bioturbation and the low SAR of 0.2 cm a^{-1} support an interpretation of LD2a as glacimarine mud deposited under (increasingly) distal conditions. Conversely, the distinct stratification in LD2b is thought to be indicative of a more glacier-proximal depositional environment. Ice-proximal conditions are supported by a high concentration of meltwater-derived fines, also reflected in SARs of up to 1.7 cm a^{-1}, an increased MS suggesting a predominantly terrestrial input (Robinson, 1993; Møller *et al.*, 2006; Seidenkrantz *et al.*, 2013), and the lack of IRD, as under these conditions the input from icebergs is often masked by the fast accumulation of meltwater-derived fines (e.g. Elverhøi *et al.*, 1980; Dowdeswell & Dowdeswell, 1989; Cowan *et al.*, 1997; Gilbert *et al.*, 2002). Radiocarbon dates show that LD2a was deposited some time after 8.2 cal ka BP, and accordingly the change from more distal to more proximal conditions between LD2a and LD2b in VC09 possibly reflects a re-advance of Jakobshavn Isbræ in response to the 8.2 ka cooling event (Weidick & Bennike, 2007; Young *et al.*, 2011a, 2013). LD2b was deposited prior to 7.6 cal ka BP in VC05 and between ∼7.8 and 7.1 cal ka BP in VC09 (interrupted by deposition of LD3 just before 7.7 cal ka BP, Fig. 4.10). During this time Jakobshavn Isbræ was at Isfjeldsbanken and began retreating into Isfjorden, which could have resulted in minor oscillations in the position of the ice margin causing the stratification in LD2b. However, deposition of LD2b also coincides with a period of strongly increased meltwater discharge, presumably caused by extensive thinning of the ice sheet prior to 8.3 ka BP (Rinterknecht *et al.*, 2009; Seidenkrantz *et al.*, 2013). Stratification would then have been imparted by inter-seasonal variations in meltwater flux to the core site, as the large variability in strata thickness within LD2b is at odds with the rhythmic stratification usually observed

in seasonally-controlled meltwater deposits (cf. e.g. Domack, 1984; Mackiewicz *et al.*, 1984; Ó Cofaigh & Dowdeswell, 2001). Although both scenarios are possible for the deposition of LD2b, we favour the former possibility and suggest that LD2b was deposited in a glacier-proximal environment where stratification was caused by minor ice-front oscillations. This is based on several reasons, including that: (1) the occurrence of presumably distal glacimarine mud (LD2a) at the bottom of VC09 around 8.2 cal ka BP is strange given that enhanced meltwater release started as early as 8.6 ka BP in some regions, (2) lithological evidence from Disko Bay showed that the meltwater event had ceased by 7.7–7.5 ka BP (Seidenkrantz *et al.*, 2013), yet deposition of LD2b and hence a strong meltwater signal prevailed until 7.0 cal ka BP in VC09, and even until 6.6 cal ka BP in VC06, and (3) if the meltwater event was responsible for the deposition of LD2b, the deposition of LD3 in between two packages of LD2b in VC09 (Fig. 4.10) would be difficult to understand (see also below). Furthermore, the traces of bioturbation at the top of LD2b and the declining MS and SARs up-facies are more easily accounted for by gradual ice-margin retreat rather than a drastic reduction in meltwater flux. Ongoing retreat could also have led to an increasing amount of sediment being trapped behind the sill in Isfjorden, thus causing additional variability in the depositional environment at the core sites.

Based on its massive structure and the presence of bioturbation burrows suggesting favourable living conditions for some benthic organisms, LD2c is interpreted as ice-distal glacimarine mud. This is in accordance with the radiocarbon dates, which provide evidence for deposition of LD2c after ∼6.7 cal ka BP in VC05, during which time ice was retreating through Isfjorden (e.g. Lloyd *et al.*, 2005; Weidick & Bennike, 2007; Hogan *et al.*, 2011). The switch from ice-proximal (LD2b) to ice-distal conditions (LD2c) between ∼6.7 and 7.6 cal ka BP in VC05 and around 7.1 cal ka BP in VC05 and VC09, respectively, show that by this time Jakobshavn Isbræ had retreated so far into Isfjorden, that meltwater sedimentation was no longer the dominant process at the core sites. The stratigraphic position of LD2c at the top of most cores from Disko Bay, the low SAR of ∼0.2 cm a^{-1}, and the low MS indicating a predominantly hemipelagic origin (cf. Møller *et al.*, 2006; Seidenkrantz *et al.*, 2013) support this interpretation (e.g. Syvitski & Murray, 1981; Gilbert, 1982; Boulton, 1990; Sexton *et al.*, 1992). Indeed, the ice margin is thought to have retreated behind its present position during the mid-Holocene, where it remained until ∼2.2 ka BP (Weidick & Bennike, 2007). However, the gradual increase in MS in the top 50 cm of LD2c in most cores from Disko Bay, and the simultaneous increase in SARs in VC05 and VC06 (Fig. 4.10) suggest a terrestrial origin for the youngest sediments in Disko Bay and a relatively higher availability of meltwater-derived fines. This could be related to the westward re-advance of the ice margin after 2.2 ka BP and/or the recent increase of thinning and subglacial melting of Jakobshavn Isbræ and adjacent GIS outlets (Holland *et al.*, 2008; Rignot *et al.*, 2010).

LD3 – stratified mud with sand laminae

The stratified fine-grained mud in lithofacies LD3 is interpreted as glacimarine mud from meltwater, with the sand laminae deposited from downslope gravity flows, e.g. turbidity currents (e.g. Gilbert, 1982; Elverhøi *et al.*, 1983; Mackiewicz *et al.*, 1984; Sexton *et al.*, 1992; Ó Cofaigh & Dowdeswell, 2001). Where the sand and mud layers appear contorted, accumulation likely relates to gravitational slump events that acted to rework and re-deposit the sediments downslope (e.g. Kuenen, 1948; Shanmugam *et al.*, 1994; Forsberg *et al.*, 1999). Turbidites are often associated with proximal glacimarine conditions (e.g. Gilbert, 1982; Gilbert

et al., 1993), suggesting that during the deposition of LD3 the margin of Jakobshavn Isbræ was relatively close. Although the turbidites could simply be a product of the abundant mass flows occurring in Disko Bay due to the very irregular topography, an ice-proximal origin for LD3 is also supported by the radiocarbon dates, which provide evidence that LD3 was deposited around 9.2 cal ka BP in VC05, and between 7.8–7.7 ka BP in VC09 (the date of 8.1 ka BP in VC09 is considered unreliable, see section 4.4.3.2), during which time the ice margin was at or near Isfjeldsbanken (Lloyd *et al.*, 2005; Long *et al.*, 2006; Weidick & Bennike, 2007; Kelley *et al.*, 2013). An ice-proximal origin for LD3 is further supported by the overall constant, relatively high MS, the close stratigraphic relationship of LD3 to the proximal sediments of LD2b (Fig. 4.7), and the lack of IRD, as large amounts of fresh glacial meltwater may have promoted debris retention in icebergs, or high SARs of mud may have swamped the input of IRD.

LD4 – stratified mud and diamict

The inter-stratified muds and diamicts of lithofacies LD4 are similar to deposits described from the continental shelf west of Disko Bay, which were linked to variations in meltwater-derived sediment flux, likely related to seasonal cycles (Hogan *et al.*, 2016). As also argued by Hogan *et al.* (2016), such deposits can form in two ways: (1) the fine-grained layers form during summer, when IRD flux to the core sites is overwhelmed by increased influx of meltwater-derived fines. In winter, sedimentation from icebergs dominates over the reduced influx of fine-grained mud associated with lower melt rates, and the diamictic layers form (cf. Cowan *et al.*, 1997; Hogan *et al.*, 2016). (2) The fine-grained sediments are deposited during winter, when shore-fast sea ice traps icebergs and prevents the meltout and deposition of IRD, while subglacial meltwater delivers fine-grained mud to the core sites. In summer the sea ice breaks up and releases the icebergs, and their incorporated IRD melts out and forms the diamict layers (cf. Syvitski *et al.*, 1996; Dowdeswell *et al.*, 1998, 2000). The generally sharper upper boundaries of the diamict units in the lower parts of LD4 indicate an abrupt increase in meltwater discharge at the start of the summer season and/or increased sediment concentrations in the meltwater plumes (cf. Ó Cofaigh & Dowdeswell, 2001; Knudsen *et al.*, 2007) and we thus suggest that the mud layers in LD4 were more likely deposited from a meltwater plume (cf. Hogan *et al.*, 2016). The change to noticeably more diffuse boundaries towards the upper part of LD4 likely represents a transition from a more proximal glacimarine environment lower in LD4 to more distal conditions higher up in the facies (cf. Hogan *et al.*, 2016). A radiocarbon date from LD4 indicates that this facies was deposited prior to 10.6 ka BP (Fig. 4.10), which supports this interpretation as the ice margin was probably slightly west of Isfjeldsbanken during this time (Lloyd *et al.*, 2005). The date further provides an important constraint for the retreat of Jakobshavn Isbræ through Disko Bay (see section 4.5.2).

LD5 – pebbly mud

The muddy matrix in facies LD5 is interpreted as the product of hemipelagic or distal glacimarine suspension settling, with the predominantly angular clasts likely deposited from icebergs (cf. Dowdeswell & Dowdeswell, 1989). The high clast abundance points to (1) increased iceberg calving rates, (2) concentrated dumping events (i.e. overturning icebergs), (3) increased iceberg melt, or (4) a decreasing accumulation of fine-grained sediments from a retreating ice margin emphasising the IRD input (e.g. Elverhøi *et al.*, 1980, 1983; Dowdeswell & Dowdeswell, 1989; Moros *et al.*, 2002; Andresen *et al.*, 2010; Seidenkrantz *et al.*, 2013). The occurrence of LD5 in VC07 and VC09 does not seem to be linked to a specific climatic warming event, which

suggests iceberg dumping to be the most likely cause of formation. Conversely, the deposition of LD5 dates to ∼3.7 ka BP in VC05 during which time the Jakobshavn ice margin was located east of its present position (Weidick & Bennike, 2007). As some authors have suggested a late Holocene Thermal Maximum in Disko Bay and other West Greenland fjords lasting until at least ∼3.5 ka BP (Moros *et al.*, 2006; Møller *et al.*, 2006; Seidenkrantz *et al.*, 2007), the deposition of LD5 in this core could be linked to enhanced glacier and/or iceberg melting during the late stages of this climatic amelioration. As argued by Long & Roberts (2003), Roberts & Long (2005), and Lloyd (2006), warmer conditions would have led to reduced coupling between the glacier and its bed, and thus reduced supply of meltwater-derived fines to the core sites. The latter could be reflected in the low SARs (∼0.02 cm a^{-1}) of LD5. Incidentally, although not specifically mentioned in the literature, such brief periods of climatic warming, or, alternatively, strengthened inflow of warm WGC waters, seem plausible in a system as climatically complex as Disko Bay and could thus also account for the occurrence of LD5 in VC07 and VC09. Notwithstanding this, the high concentration of IRD in LD5 could also imply a re-advance of Jakobshavn Isbræ, possibly related to the onset of Neoglaciation, which would have caused the ice to be subjected to the increasing influence of warm Atlantic water, leading to enhanced calving rates. The high flux of IRD would then have outpaced the flux of meltwater, leading to the deposition of a clast-rich mud. A higher iceberg availability was one of the reasons suggested for the high amounts of IRD in the lithological record from the Vaigat Strait (Andresen *et al.*, 2010).

LV1 – massive mud with clasts

Based on its similarity to LD2a and sediments from the same area investigated by Andresen *et al.* (2010) and McCarthy (2011), we interpret LV1 from the Vaigat Strait as glacimarine mud deposited from meltwater plumes and/or the water column, and clasts settling from icebergs and sea ice drifting over the core sites. Large-scale re-working of the sediments downslope into the Vaigat Strait probably led to the massive internal structure. The comparatively large number of clasts in LV1 can be explained by the fact, that, in addition to the icebergs from the local glaciers, icebergs calved from Jakobshavn Isbræ are also transported to the Vaigat Strait by the local ocean currents (Lloyd *et al.*, 2005; Andresen *et al.*, 2010; McCarthy, 2011).

4.5 Discussion

4.5.1 Landforms and sediment facies signature of Jakobshavn Isbræ and adjacent fast-flowing GIS outlets

The submarine landform assemblage in Disko Bay and the Vaigat Strait includes (1) streamlined bedrock ridges, (2) crag-and-tails, (3) submarine channels, and (4) pockmarks. TOPAS profiles further indicate the abundance of (5) deposits from gravitational mass transport. The streamlined bedrock and crag-and-tails record the flow of an extended Jakobshavn Isbræ and adjacent GIS outlets across the bay during the LGM and are indicative of relatively fast ice flow (cf. King *et al.*, 2009). The absence of recessional moraines, which are commonly observed in glaciated areas (e.g. Landvik, 1994; Ottesen *et al.*, 2005; Ottesen & Dowdeswell, 2009; Dowdeswell *et al.*, 2010a; Hogan *et al.*, 2010), suggests that retreat was so rapid that there was insufficient time for recessional moraines to form, or that the ice margin retreated as a floating ice shelf. An interpretation of rapid retreat is supported by the reconstructed high retreat rates from the continental shelf and from Disko Bay (discussed in section 4.5.3 below).

In terms of the Holocene sedimentary environments and the associated depositional processes in front of Jakobshavn Isbræ and adjacent GIS outlet glaciers, we identify four main processes: (1) suspension settling of glacimarine muds from meltwater and the water column, (2) meltout of coarser grains from icebergs and sea ice (3) sediment gravity flows, reworking both fine- and coarse-grained deposits down the slopes of submarine basins, and (4) ploughing of sediments by grounded iceberg keels. Meltwater-derived sedimentation is the dominant process, as indicated by the exceptionally well-sorted muds (usually >95% of the muds have a grain size <63 μm) and their overall strong terrestrial signal.

4.5.2 Timing of ice retreat and deglacial ice sheet dynamics

In order to reconstruct a retreat chronology for Jakobshavn Isbræ, we integrate the radiocarbon dates presented in this study with previously published data from both marine and terrestrial settings in West Greenland (Fig. 4.11). An extended Jakobshavn Isbræ and its adjacent GIS outlets flowed through Disko Bay and through the Vaigat Strait onto the continental shelf during the LGM (cf. Ó Cofaigh *et al.*, 2013; Dowdeswell *et al.*, 2014). The ancestral Jakobshavn Isbræ commenced retreat from the outer continental shelf around 13.8 ka BP or before, and underwent a short-lived re-advance during the Younger Dryas on the shelf west of Disko Bay, at ∼12.3–12.0 ka BP (re-calibrated from Ó Cofaigh *et al.*, 2013). Deglaciation of the inner continental shelf and the western parts of Disko Bay was underway by 10.9 and 10.8 ka BP, respectively (Fig. 4.11; McCarthy, 2011; Hogan *et al.*, 2012; Kelley *et al.*, 2013). Our date of 10.6 ka BP from relatively proximal glacimarine sediments in central Disko Bay serves as a minimum age for deglaciation of the central bay and demonstrates that the ice margin had retreated to a position east of VC07 by this time. The 2.8 m-thick sequence of proximal sediments at the base of VC07 must have been deposited before this date and could indicate that the ice margin retreated very slowly (see also section 4.5.3 below) or paused close to the core site of VC07. A radiocarbon date published by Lloyd *et al.* (2005) from core POR18 showed that the ice margin was located at or somewhere within 6 km west of Isfjeldsbanken at 10.2 ka BP (re-calibrated; Fig. 4.11), and is in good agreement with findings from Young *et al.* (2011a), who place the ice margin at or close to Isfjeldsbanken at 10.2 ka BP. Sub-bottom profiler data presented by Hogan *et al.* (2011) suggest a prolonged stillstand of the ice margin at Isfjeldsbanken, which led to the accumulation of thick sedimentary basin infills immediately west of the sill. The radiocarbon dates from thick ice-proximal sedimentary sequences from inner Disko Bay (VC09 and VC05, this study; DA00-06, Lloyd *et al.*, 2005) further support this. Two re-advances of Jakobshavn Isbræ occurred in response to climatic cooling events around 9.3 and 8.2 ka BP (e.g. Young *et al.*, 2013), the latter of which may be reflected in the transition from more distal (lithofacies LD2a) to more proximal glacimarine muds (LD2b) in VC09. The change from relatively proximal glacimarine (LD2b) to predominantly hemipelagic sediments (LD2c) in VC05 and VC09 implies that Jakobshavn Isbræ had retreated into Isfjorden sometime around 7.6–7.1 ka BP. This is consistent with work from Lloyd *et al.* (2005) and Hogan *et al.* (2011), who concluded that the ice stream retreated from Isfjeldsbanken into Isfjorden at c. 7.9–7.8 ka BP. Although Corbett *et al.* (2011) and Young *et al.* (2011a,b, 2013) suggested slightly earlier deglaciation of the coastal areas in eastern Disko Bay, it is possible that Jakobshavn Isbræ remained grounded at Isfjeldsbanken longer than the surrounding ice masses. During subsequent retreat the ice margin withdrew to a position behind that of the present terminus, where it remained throughout the mid-Holocene (Young *et al.*, 2011a, 2013; Kelley *et al.*, 2013), before it re-advanced westwards to its present position after 2.2 ka BP (cf. Weidick & Bennike,

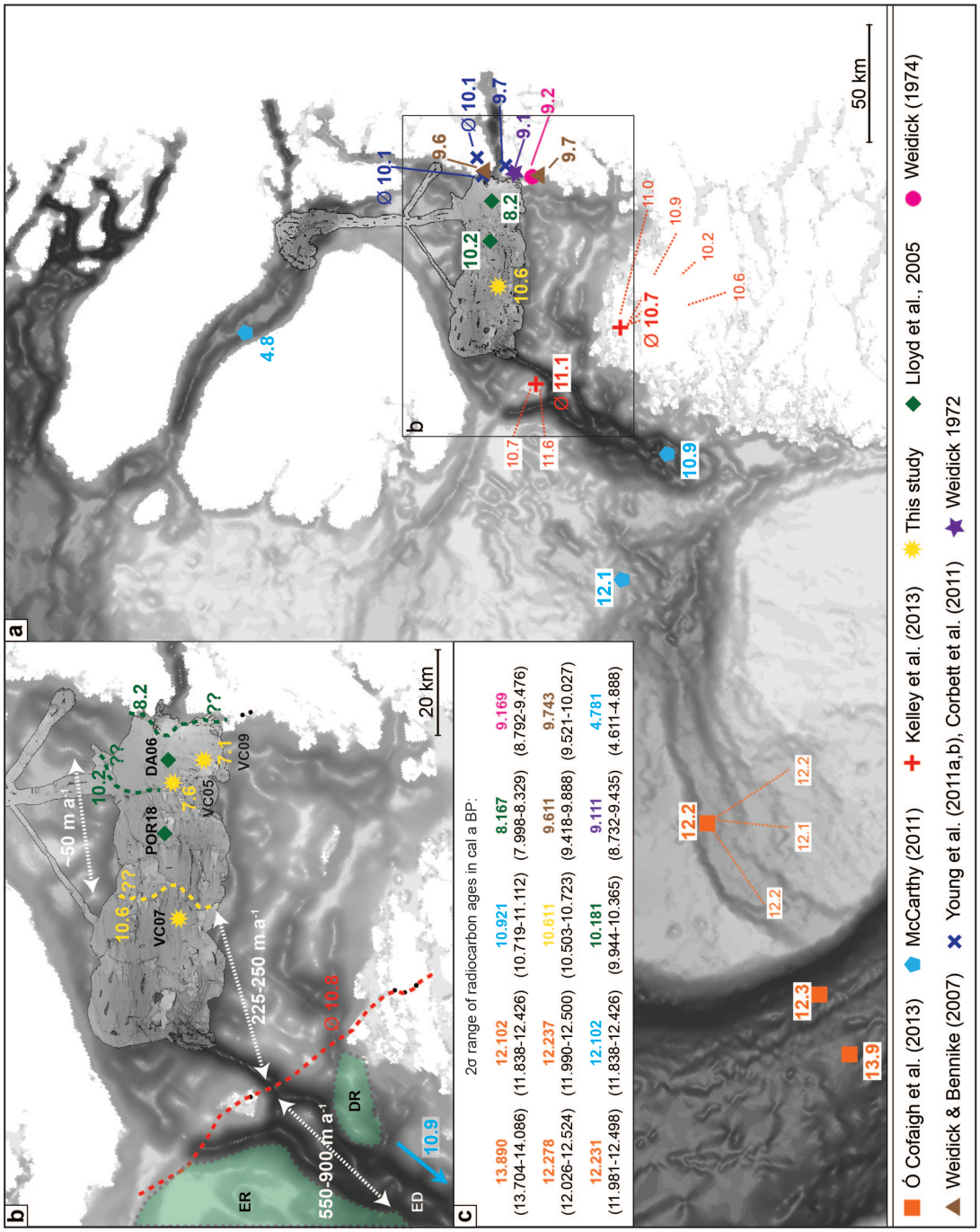

Figure 4.11: *a) Summary of radiocarbon (median) and* ^{10}*Be dates available from marine organisms on the continental shelf and Disko Bay, and from bedrock from adjacent land areas in (cal) ka BP. Radiocarbon dates from previously published studies were re-calibrated using a* ΔR *of* 140 ± 25 *years (Lloyd* et al.*, 2005). b) Zoom-in on the study area according to the rectangle indicated in a). Stippled red, yellow and green lines show an estimation of where the ice front could have been positioned, based on the dates from boulders/bulk sediment (red; Kelley* et al.*, 2013) and sediment cores (yellow for this study and green for Lloyd* et al.*, 2005). White arrows and numbers imply possible retreat rates. Green shaded areas show Egedesminde Ridge (ER). ED = Egedesminde Dyb, DR = Disko Gneiss Ridge (cf. Hofmann* et al.*, 2016). c) Summary of the* 2σ *ranges obtained from re-calibration of the radiocarbon ages.*

2007).

In the Vaigat Strait, the chronology of deglaciation is less clear, reflecting a lack of data

from this region but also the very thick post-glacial sediment cover, which makes it difficult to obtain radiocarbon ages relating to ice retreat through the strait. In fact, to our knowledge, the oldest date of 4.8 cal ka BP (re-calibrated) was obtained at a depth of 435 cm from a core from the central Vaigat Strait (Fig. 4.11; McCarthy, 2011), and is regarded as a minimum age for ice retreat.

4.5.3 Retreat rates

From the above constraints on the timing of ice retreat, minimum rates of retreat can be estimated for the ice sheet outlet glaciers, which retreated relatively quickly across the continental shelf, accelerated through Egedesminde Dyb, slowed slightly through western Disko Bay, and significantly slowed through the eastern bay. Note that the rates presented here are average rates, based on the assumption of linear ice retreat. The geomorphological and lithological evidence presented in this study suggests that the margin of Jakobshavn Isbræ was grounded during retreat. This is based on the implication of meltwater-dominated sedimentation with moderate input from icebergs and sea ice in the cores from Disko Bay and the Vaigat Strait, as sediment facies associated with ice shelves tend to be diamictic and coarse-grained close to the grounding line, and, in the case of the more distal sub-ice shelf sediments, tend to lack IRD (cf. e.g. Anderson *et al.*, 1991; Powell *et al.*, 1996; Domack *et al.*, 1999; Kilfeather *et al.*, 2011). Furthermore, the presence of a large submarine channel (C1, see section 4.4.1 and Figs. 4.3, 4.4) in the central bay is thought to support a grounded ice margin, because its depth, shape, and the close association with a transverse bedrock ridge seem consistent with subglacial meltwater excavation at the grounding line of a stagnating ice margin over an extended period of time. Nevertheless, the absence of recessional features on the seafloor in Disko Bay and the periodic appearance of coarse-grained diamicts (LD1 in VC03, VC04, and VC08) may reflect transient decoupling of the ice stream from its underlying bed. Indeed, a lightly grounded and relatively thin ice margin with predominantly hydrostatic support was already proposed by Hofmann *et al.* (2016), who further suggested that the ice stream may have grounded intermittently at bedrock highs. It is therefore possible, that, while our data mainly imply grounded ice, the ice stream experienced occasional periods of ungrounding, at least locally.

The ancestral Jakobshavn Isbræ retreated at rates between 22–275 m a^{-1} across the continental shelf after its Younger Dryas re-advance around 12.3–12.0 ka BP (Ó Cofaigh *et al.*, 2013). A retreat of up to 90 km between c. 10.9 ka BP (re-calibrated radiocarbon date from McCarthy, 2011) and 10.8 ka BP (^{10}Be date from Kelley *et al.*, 2013; Fig. 4.11) implies accelerated retreat through Egedesminde Dyb at rates between 550 and 900 m a^{-1}. Although these rates are much higher than those for the continental shelf, more extensive calving and thus faster ice retreat has often been linked to bathymetric overdeepening (e.g. Meier & Post, 1987; Seramur *et al.*, 1997; Oerlemans & Nick, 2006; Benn *et al.*, 2007a; Ó Cofaigh, 1998; Kehrl *et al.*, 2011). Furthermore, Egedesminde Ridge west of the trough (Fig. 4.11), could have served as a pinning point during ice retreat (Hofmann *et al.*, 2016). Once the ice stream detached from this ridge, fast retreat would have occurred due to increased glacier bottom melting caused by the inflow of warm Atlantic water into the trough (cf. Andersen, 1981; Lloyd *et al.*, 2005; Lloyd, 2006; Holland *et al.*, 2008). The subsequent retreat across outer Disko Bay occurred over a minimum distance of 45 km between ∼10.8 and 10.6 ka BP to a position east of VC07, suggesting minimum rates between 225 and 250 m a^{-1} from the western to the central bay (Fig. 4.11). This shows that retreat either slowed, or that Jakobshavn Isbræ temporarily

paused upon entering Disko Bay, which is likely, given the sudden shoaling from >1100 to 400 m water depth at the eastern end of Egedesminde Dyb and a sudden widening of the retreat basin (e.g. Oerlemans & Nick, 2006; Benn *et al.*, 2007a). Retreat was even slower through the eastern parts of the bay, as shown by dates of 10.6 ka BP from proximal glacimarine sediments in VC07 and 10.2 ka BP from similar sediments in POR18, which indicate a retreat of approximately 20 km at a rate of ∼50 m a^{-1} (Fig. 4.11; Lloyd *et al.*, 2005; this study). Similar rates were obtained from the cosmogenic dates in the area, thus supporting slow or intermittent retreat through eastern Disko Bay (Kelley *et al.*, 2013).

4.5.4 Comparison between West Greenland and other glacimarine environments

Suspension settling, ice rafting, sediment gravity flows, and iceberg ploughing were identified as the key sedimentary processes during deglaciation of Disko Bay and the Vaigat Strait. Although these four processes reflect those commonly observed in High-Arctic fjord environments (e.g. Elverhøi *et al.*, 1983; Powell & Molnia, 1989; Andrews *et al.*, 1994; Syvitski *et al.*, 1996; Dowdeswell *et al.*, 1998; Ó Cofaigh & Dowdeswell, 2001; Forwick *et al.*, 2010), the variable magnitude of each of these has important implications for our understanding of glacimarine sedimentation. Thus far, depositional environments in front of tidewater glaciers have been categorised according to climatic and glaciological regime (Dowdeswell *et al.*, 1998). Southeast Alaska forms the warmer end of the spectrum, with predominantly fine-grained mud deposited from glacial meltwater (Powell & Molnia, 1989; Cowan & Powell, 1991). Antarctica forms the other extreme, defined as a polar and climatically severe setting, where sedimentation occurs mainly at the grounding line (e.g. Domack *et al.*, 1999; Powell *et al.*, 1996; Ashley & Smith, 2000). Fjords around Svalbard and Baffin Island are in between these two end members (Dowdeswell *et al.*, 1998) with high amounts of meltwater-derived muds close to the glacier fronts (e.g. Elverhøi *et al.*, 1983; Gilbert, 1983; Gilbert *et al.*, 1990; Forwick *et al.*, 2010; Streuff *et al.*, 2015), but increasing amounts of ice-rafted material towards ice-distal areas (e.g. Elverhøi *et al.*, 1983; Forwick & Vorren, 2009; Kempf *et al.*, 2013). East Greenland was initially defined as an environment with low meltwater availability, where sedimentation is dominated by iceberg rafting and debris meltout from sea ice (e.g. Marienfeld, 1991; Syvitski *et al.*, 1996; Dowdeswell *et al.*, 1993, 1994b, 1998). However, subsequent work by Smith & Andrews (2000) and Ó Cofaigh *et al.* (2001) showed that large amounts of fine-grained stratified sediments in proximal areas of East Greenland fjords record sedimentation predominantly from meltwater, and that deposition of IRD only becomes important in more ice-distal environments. Large amounts of silt and clay derived from meltwater were also observed in other East Greenland fjords (Andrews *et al.*, 1994). Accordingly, Ó Cofaigh *et al.* (2001) proposed that glacimarine sedimentary processes can be very similar despite different climatic, glaciological and oceanographic settings, and that their variability may rather be a consequence, at least in part, of local controls, such as distance to the ice margin (see also section 6.5 in chapter 6 below).

There has been limited research investigating glacimarine sedimentary processes in West Greenland and it has not been considered in the spectrum outlined above, perhaps due to the only recently emerging data (e.g. McCarthy, 2011; Jennings *et al.*, 2013; Ó Cofaigh *et al.*, 2013; Dowdeswell *et al.*, 2014; Hogan *et al.*, 2016; Sheldon *et al.*, 2016). The abundance of meltwater-derived sediments in the cores from Disko Bay and the Vaigat Strait emphasise the importance of meltwater sedimentation in proximal areas of GIS outlets here and suggest that the ice-proximal sedimentary processes in West Greenland are comparable with those from warmer settings like Svalbard and Alaska (e.g. Powell & Molnia, 1989; Cowan & Powell, 1991;

Cai *et al.*, 1997; Forwick & Vorren, 2009; Forwick *et al.*, 2010; Streuff *et al.*, 2015). Considering the nearly identical mean annual air temperatures and annual precipitation between Svalbard and West Greenland and that both are influenced by relatively warm and saline Atlantic water, similar depositional processes may not be surprising. Similarity in sedimentary processes also suggests that in terms of depositional environment Disko Bay acts more like a fjord than a marine embayment on the continental shelf. However, the increasingly hemipelagic and diamictic sediments and the associated reduction in meltwater flux in the distal areas of Disko Bay (VC08 and VC07) are different from Svalbard and Alaska, where sedimentation from meltwater remains the dominant process throughout the entire glacimarine setting (Elverhøi *et al.*, 1983; Cowan & Powell, 1991; Streuff, 2013; Streuff *et al.*, 2017). This strongly implies that glacimarine processes and their associated facies are not simply a function of climate. In fact, Disko Bay appears to be more similar to the glacimarine depositional environments of East Greenland fjords, which is notable given the classification of East Greenland as a polar, meltwater-restricted glacimarine environment, and the extensive sea ice in most of its fjords. The comparatively low SARs in Disko Bay with respect to those in East Greenland fjords may be related to differences in the availability of meltwater or glacial debris, or to the different fjord morphology compared to Spitsbergen and East Greenland fjords (wide open bay vs. narrow constricted fjords). It follows that even within geographically-constrained areas glacimarine sedimentary processes and their magnitude can vary significantly over distance and time. We conclude that variability between meltwater-dominated and iceberg-dominated glacimarine sedimentation is not necessarily related only to climate and glaciology but is also dependent on local factors including distance to the ice margin, seafloor topography and glacier size (cf. Ó Cofaigh *et al.*, 2001).

4.6 Conclusions

Lithological data integrated with swath-bathymetry and TOPAS sub-bottom profiler data provide new insights into the Holocene glacimarine sedimentary processes in Disko Bay and the Vaigat Strait in West Greenland. Vibrocores comprise diamict, (diffusely) stratified mud, massive mud with sharp-based sand layers, IRD-rich massive mud, and massive bioturbated muds. These lithofacies show that suspension settling of fine-grained sediment from turbid meltwater plumes and the water column, sediment gravity flows, and iceberg rafting and ploughing were the dominant sedimentary processes during and following ice retreat, with meltwater sedimentation dominant in ice-proximal areas, and hemipelagic suspension settling and IRD-rainout from icebergs dominant in distal areas.

Our findings show that despite similar climate and oceanography glacimarine sedimentary processes differ between Svalbard and West Greenland, but are similar between East and West Greenland in spite of different oceanographic conditions. This confirms that such processes vary more as a function of local controls such as distance from the ice margin and geomorphological setting rather than climate and geographic location. Radiocarbon dates provide the basis for estimated SARs between 0.1 and 1.7 cm a^{-1} in proximal areas, and ~0.007–0.05 cm a^{-1} in distal areas, which are lower than SARs documented for East Greenland. The radiocarbon dates further constrain the retreat dynamics of Jakobshavn Isbræ during deglaciation. Streamlined glacial landforms, including crag-and-tails and glacial lineations, record the former flow of an expanded Jakobshavn Isbræ and adjacent GIS outlets through Disko Bay and the Vaigat Strait towards the adjoining continental shelf. During deglaciation, retreat was relatively fast

across the continental shelf (22–250 m a^{-1}), through Egedesminde Dyb (∼550–900 m a^{-1}), and the western parts of Disko Bay (∼225–250 m a^{-1}), all of which were deglaciated before 10.6 ka BP. Subsequent retreat through eastern Disko Bay was much slower (∼50 m a^{-1}), and likely interrupted by at least one stillstand due to pinning of the grounded glacier margin on submarine bedrock ridges. The ice margin paused again at Isfjeldsbanken before retreating into Isfjorden. Around 7.6–7.1 ka BP the ice margin had probably retreated far back into Isfjorden, as at this point sediment delivery to the core sites from meltwater plumes became significantly reduced. The variable retreat rates and sedimentary facies we document here underscore the importance of local morphology and glacier proximity for the palaeo-retreat dynamics and associated glacimarine sedimentary processes of marine-terminating Greenland Ice Sheet outlet glaciers.

Acknowledgements

This research has received funding from the UK Natural Environment Research Council (Grants NE/D001986/1 and NE/ D001951/1) and the People Programme (Marie Curie Actions) of the European Union's Seventh Framework Programme FP7/2007-2013/ under REA grant agreement n^{o}317217. Some of the radiocarbon dates were acquired with the NSF-OPP-0713755 grant awarded to Anne Jennings by the National Science Foundation, USA. We thank the participants and crew of the JR175 research cruise for their help with data acquisition and Aiobheann Kilfeather for her help with the shear strength analysis. Neil Tunstall and Frank Davies kindly assisted with the use of the MSCL. Discussions with Elena Grimoldi, Louise Callard and Kasper Weilbach and the comments from two anonymous reviewers further helped to improve the manuscript.

Author contributions

This chapter in its current form is based on a team effort of the individual co-authors. Data acquisition was organised by Colm Ó Cofaigh, who was assisted by Riko Noormets, Julian Dowdeswell, and Anne Jennings. The majority of the analyses and interpretations including the visualisation of acoustic data, the description and sub-sampling of sediment cores and the isolation and preparation of radiocarbon samples were carried out by the lead author, who also prepared all figures and the large majority of the text. Kelly Hogan post-processed and visualised the multibeam swath-bathymetry and parts of the sub-bottom profiler data and was immensely helpful with providing advice and answering questions I had regarding the data. Wilhelm Weinrebe acquired and allowed me to include the multibeam swath-bathymetry gathered onboard the *Maria S. Merian* and *MV Smilla*. Anne Jennings sub-sampled and provided all radiocarbon dates for core VC05 and two dates for VC09. Tove Nielsen and Antoon Kuijpers hosted me at the Geological Survey of Denmark and Greenland in Copenhagen for several weeks, providing many useful suggestions and improvement tips. Colm Ó Cofaigh did most of the reviewing, providing feedback and suggestions for improvement on the manuscript as a whole. Jerry Lloyd and two anonymous reviewers also helped improve the manuscript by providing several suggestions for editing. Author contributions to the manuscript in its current form are estimated as follows (not considering data acquisition processes): Katharina Streuff 70%, Kelly Hogan 10%, Anne Jennings 5%, Colm Ó Cofaigh 10%, and 5% between Julian Dowdeswell, Jerry Lloyd, Tove Nielsen, Antoon Kuijpers, Riko Noormets and Wilhelm Weinrebe.

Chapter 5

Submarine landform-sediment assemblages in front of Arctic fjord-terminating tidewater glaciers and their implications for glacimarine sedimentation

5.1 Introduction

The principal rationale for conducting the research presented in this thesis is that, despite their importance for climatic research, the Holocene evolution of and associated sedimentary processes in front of many tidewater glaciers are still poorly understood. As a result, there is relatively little information regarding the similarities and differences between glacimarine environments across wider geographic areas. The previous three chapters and chapter A in the appendix investigated the glacimarine sedimentary processes and products in front of individual tidewater glaciers in Spitsbergen and West Greenland. In line with the aims and objectives presented in section 1.1, the submarine glacial landforms and glacimarine sediments in Kongsfjorden, Magdalenefjorden, Ymerbukta, Trygghamna, Lomfjorden, Disko Bay, and the Vaigat Strait were determined independently and were used to reconstruct the regional Holocene ice dynamics. This chapter aims to compare the identified landform-sediment assemblages with those previously documented from East Greenland, other parts of Svalbard, Alaska, and the Canadian Arctic in order to develop a comprehensive conceptual model, that summarises the complex evolution of ice-proximal glacimarine sedimentation and associated products in High-Arctic fjords.

5.2 Background

It is generally assumed that a warming climate drives glacier retreat, and it has indeed been found that the inflow of increasingly warmer ocean waters into glacier-dominated fjords promotes glacier melt and, hence, faster retreat (e.g. Holland *et al.*, 2008; Rignot *et al.*, 2010; Straneo *et al.*, 2010). Ice dynamics are further controlled by the climate, as the latter defines the hydrological and thermal composition of a glacier (Benn & Evans, 2010), according to which Arctic fjords are classified as temperate, sub-polar, or polar (Dowdeswell *et al.*, 1998; Howe *et al.*, 2010). In maritime areas with high winter precipitation and high summer melt, glaciers are mainly temperate, and the majority of the ice mass is at the pressure melting point, with only the uppermost section of the glacier varying with seasonal air temperatures (Hambrey, 1994; Benn & Evans, 2010). Here, meltwater is available in large quantities, which leads to high sediment accumulation rates dominated by fine-grained material (e.g. Elverhøi *et al.*, 1983; Cowan & Powell, 1990; Dowdeswell *et al.*, 1998). Conversely, in colder sub-

polar and polar glacimarine environments with little precipitation and low air temperatures, cold glaciers dominate. These comprise ice that is below the pressure melting point, as heat sources are scarce (Hambrey, 1994; Benn & Evans, 2010). Accordingly, these glaciers tend to produce limited meltwater volumes and deposition of mainly coarse-grained material occurs from icebergs or directly from the glacier ice (e.g. Dowdeswell *et al.*, 1994b, 1998; Ashley & Smith, 2000; Hambrey & McKelvey, 2000). In between these two end members are sub-polar glacimarine environments, where glaciers are polythermal, and comprise both cold and warm ice. A variable configuration of the two within the glaciers leads to a range of thermal structures (Blatter & Hutter, 1991; Pettersson, 2004), and causes these glaciers to occur in both cold areas with low summer melt (predominantly cold glaciers) and in warmer polar-maritime climates (predominantly warm glaciers; Benn & Evans, 2010).

Glaciated fjords of the northern hemisphere are mostly temperate and sub-polar and occur in Alaska, Iceland, Norway, Svalbard, Greenland and Canada. In these environments, the relative importance of the individual glacimarine sedimentary processes changes due to the variable glacier regimes, which leads to a complex interplay of processes forming different lithological records. Svalbard is a good example, as, similar to temperate settings, meltwater-derived sedimentation dominates ice-proximal areas, but iceberg-derived sedimentation, typical of polar environments, becomes more important with increasing distance from the glacier margins (e.g. Elverhøi *et al.*, 1983; Boulton, 1990; Dowdeswell *et al.*, 1998; Forwick & Vorren, 2009). Furthermore, many of the Svalbard tidewater glaciers, which account for ∼60% of the total glaciated area in this region (e.g. Hagen, 1993; Błaszczyk *et al.*, 2009), have been found to undergo climatically-independent cycles of advance and retreat. These so-called "surges" are mainly a function of the glacier's hydrological and thermal regime (Meier & Post, 1969; Sevestre & Benn, 2015), and may further influence the glacial sedimentary products (e.g. Sharp, 1985; Solheim & Pfirman, 1985; Ottesen *et al.*, 2008). Observations like this led to the understanding that sedimentary processes in glacier-dominated fjords are more complex than originally thought, and, in addition to climate, are subject to a range of external factors (e.g. Powell & Molnia, 1989; Powell, 1991; Smith & Andrews, 2000; Ó Cofaigh *et al.*, 2001). In order to test this theory, different fjord settings across the northern hemisphere are compared throughout this chapter. From this, the common lithofacies and landforms in front of Arctic tidewater glaciers are identified and their similarities and differences evaluated.

5.3 Study areas

5.3.1 Geographic setting

Six fjords and one marine embayment (which for simplicity will also be referred to as a fjord throughout this chapter) were investigated in detail, based on acoustic and lithological

Table 5.1: *Characteristics of the seven fjords in the study area. Sp = Spitsbergen, Gr = Greenland. W = width, L = length, D = depth. TG = number of tidewater glacier termini in each fjord. As several glaciers can share one ice front, the number of actual glaciers may differ and is displayed in parentheses.*

Fjord	Location	Lat	Long	W [km]	L [km]	D [m]	TG
Ymerbukta	W Sp	78°12'–78°19'N	13°52–14°05'E	0.5–2.7	10	15–120	1
Trygghamna	W Sp	78°12'–78°19'N	13°38'–13°52'E	0.8–2.2	8	5–200	1 (2)
Kongsfjorden	W Sp	78°50'–79°04'N	11°40'–12°40'E	4–10	20	10–350	6 (7)
Magdalenefjorden	NW Sp	79°31'–79°37'N	10°30'–11°20'E	0.7–3.2	14.5	25–135	1
Lomfjorden	E Sp	79°21'–79°43'N	17°40'–18°20'E	2–10	35	0–200	3 (4)
Disko Bay	W Gr	68°30'–69°40'N	50°50'–55°00'W	100	3865	50–500	1
Vaigat Strait	W Gr	69°40'–70°50'N	50°50'–55°00'W	10–30	3600	200–650	2

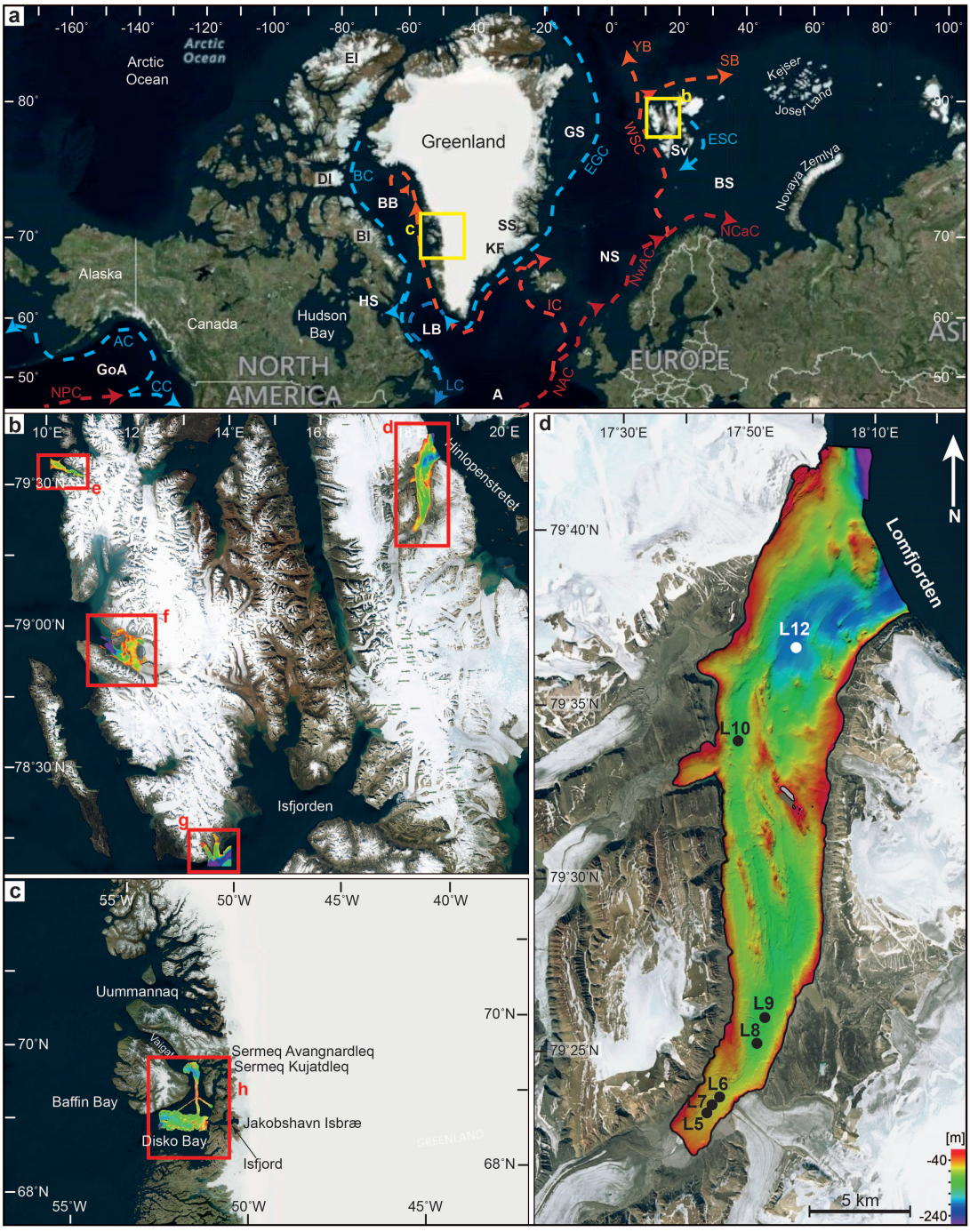

Figure 5.1: *a) Overview map of the areas of focus in the northern hemisphere with the main oceanographic currents shown by the arrows. NPC = North Pacific Current, CC = Coastal Current, AC = Alaska Current, GoA = Gulf of Alaska. EI = Ellesmere Island, DI = Devon Island, BI = Baffin Island, BC = Baffin Current, BB = Baffin Bay, HS = Hudson Strait, WGC = West Greenland Current, SS = Scoresby Sund, KF = Kangerdlussuaq Fjord, GS = Greenland Sea, EGC = East Greenland Current. LB = Labrador Bay, LC = Labrador Current, A = Atlantic, IC = Irminger Current, NAC = North Atlantic Current, NwAC = Norwegian Atlantic Current, NS = Norwegian Sea, NCaC = North Cape Current, BS = Barents Sea, WSC = West Spitsbergen Current, YB = Yermak Branch, SB = Svalbard Branch, ESC = East Spitsbergen Current, Sv = Svalbard. For details on oceanography see for example Aagaard & Coachman (1968), Royer (1983), Koç* et al. *(2002), Lloyd* et al. *(2005), and Ślubowska* et al. *(2005). Map data courtesy of Bing maps. The yellow rectangles indicate the locations of b) and c). b) Northern Spitsbergen showing the bathymetric data used for this study. The red rectangles show the locations and extents of the swath-bathymetric data and the sediment cores used in this study from d) Lomfjorden, e) Kongsfjorden, f) Magdalenefjorden, and g) Ymerbukta and Trygghamna. c) Overview of West Greenland with the bathymetric data available for this study. Red rectangle shows the extent of h).*

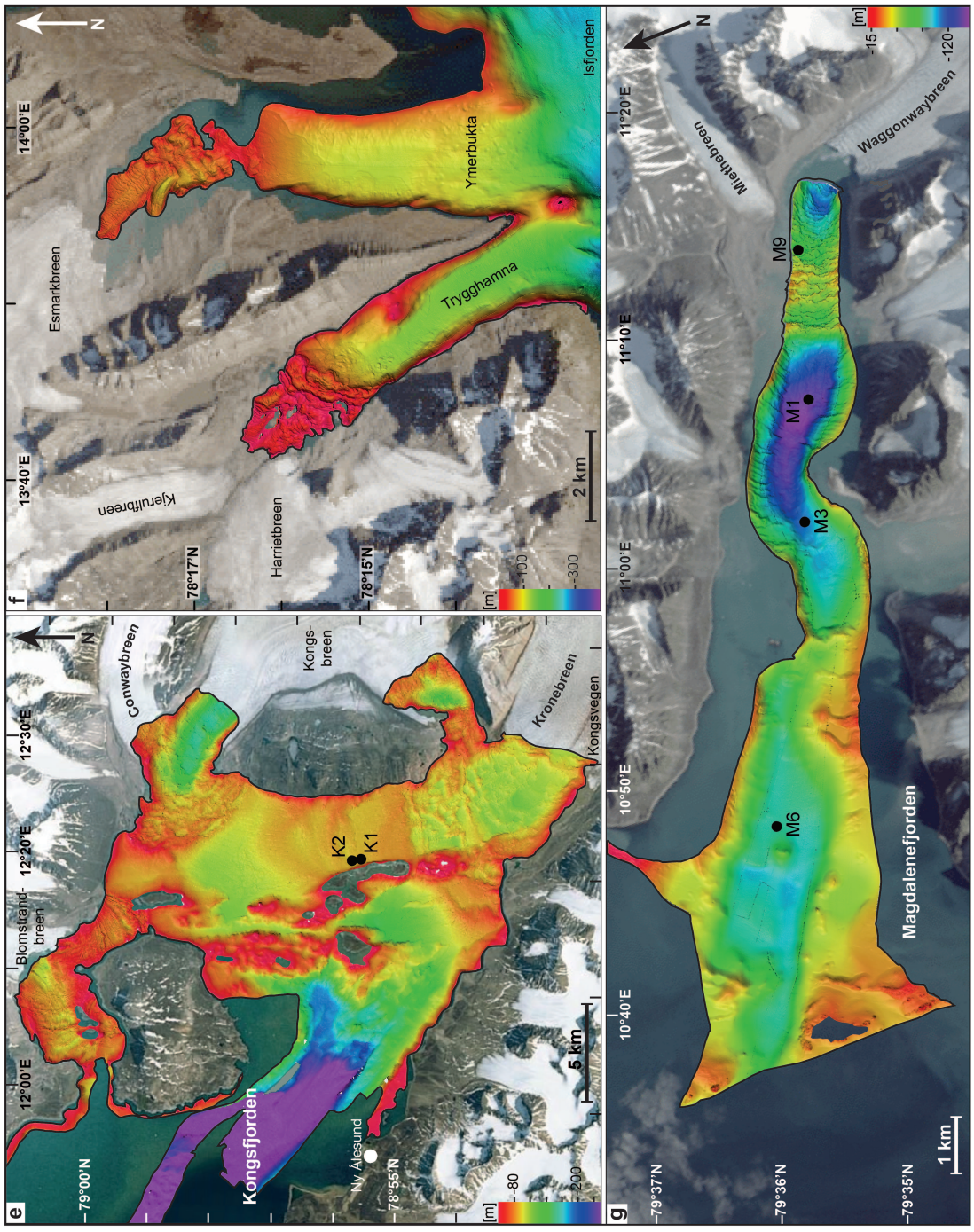

Figure 5.1 *(cont.):* *Swath-bathymetric data and core locations from e) Kongsfjorden, f) Ymerbukta and Trygghamna, and g) Magdalenefjorden in Spitsbergen.*

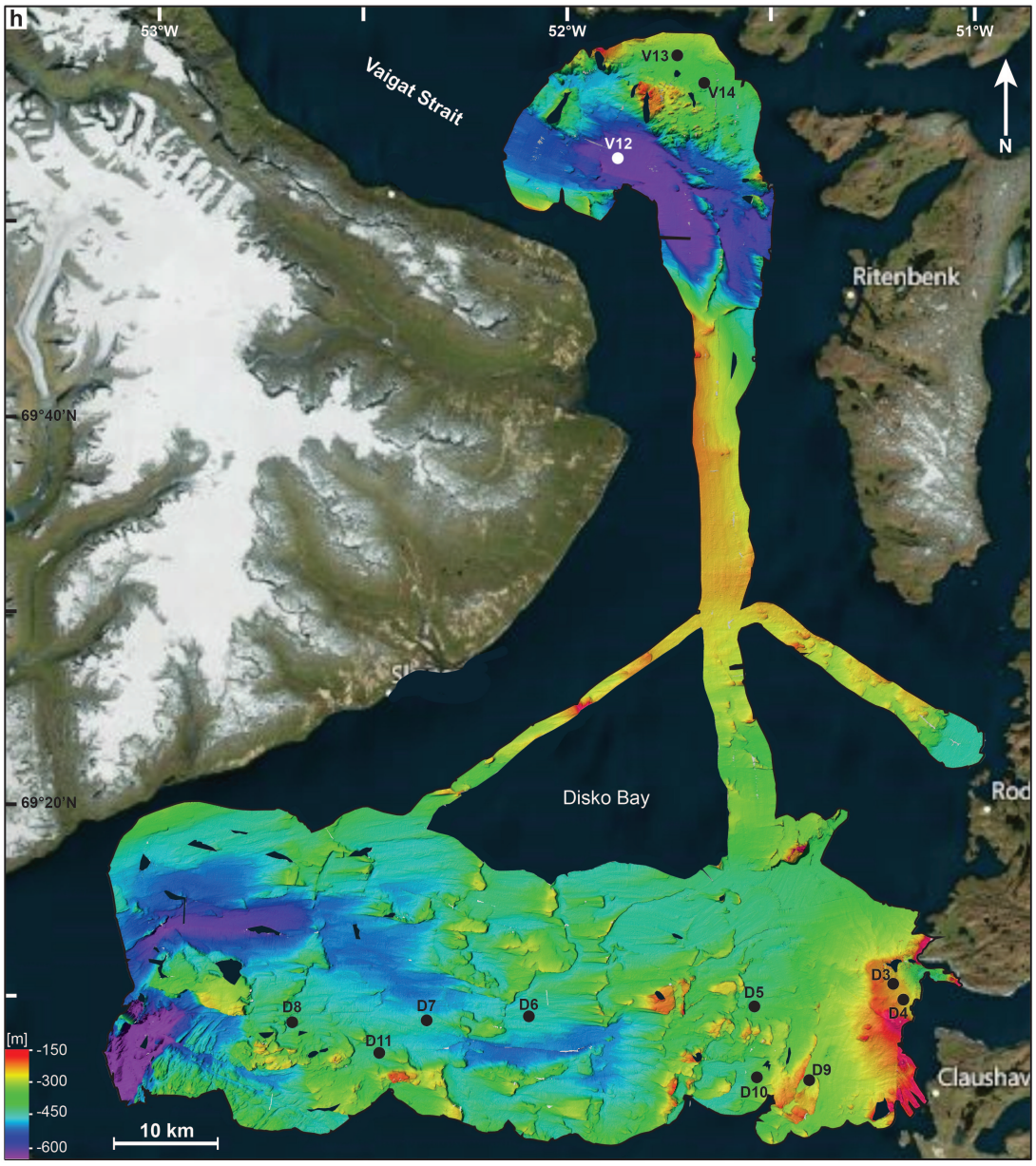

Figure 5.1 *(cont.): g) Swath-bathymetric data and core locations from Disko Bay and the Vaigat Strait, West Greenland.*

data. These are situated in various geographic locations and are characterised by different morphologies (Table 5.1). Five of the fjords are located around the coast of Spitsbergen, the largest island of the Svalbard archipelago, with Ymerbukta, Trygghamna and Kongsfjorden in the central western part, Magdalenefjorden in the northwest, and Lomfjorden in the east (Fig. 5.1b). The two remaining fjords, Disko Bay (technically an embayment) and the Vaigat Strait, are situated in central West Greenland (Fig. 5.1a, c; Table 5.1). Previously published observations from other Arctic fjords are integrated with the results from this thesis in order to compare the landform-sediment assemblages. With the exception of the fjords in West Greenland, this study puts emphasis on fjords that still have tidewater glaciers at their heads, to ensure that the reconstructed processes are reflective of a tidewater glacier setting. As glaciers in Norway and Iceland have retreated from tidewater, it is assumed that the sediments in those fjords are no longer directly representative of ice-contact glacimarine environments.

These areas are therefore not considered here.

5.3.2 Oceanography and climate

The fjords selected for this study as well as those used for comparison are climatically and oceanographically diverse. Their main climate characteristics are summarised in Table 5.2. Air temperatures, oceanographic conditions and precipitation volumes appear remarkably similar, particularly when comparing West with East Greenland and Greenland with Spitsbergen. Note, however, that due to the locations of available weather stations, values may be locally biased. In Svalbard, for example, the northernmost weather station is located in central West Spitsbergen (Ny Ålesund; Fig. 5.1e), so that air temperatures and precipitation volumes for the northern part of the archipelago look identical to the central western part, but may, in reality, differ quite substantially. The vast size of Greenland also leads to considerable variations in air temperature, precipitation and sea ice cover, and a comparably small number of weather stations likely leads to large uncertainties in climatic parameters.

Fjords in Alaska are at the warmest end of the glacimarine spectrum, with a cool-temperate glacimarine environment and mean annual air temperatures (MATs) around +4° (Cowan, 1992; USC, 2017). Water masses are predominantly fresh and cold (0–12°, 4–32 psu) dominated by

Table 5.2: *Climate characteristics of glaciated fjords across the northern hemisphere. Class. = Climatic regime classification, T = Mean Annual Air Temperature, PV = Precipitation Volume, WM = Water Masses, WT = Water Temperatures, Sal = Salinity. Canada refers to the Canadian Arctic Archipelago, covering Baffin Island and Ellesmere Island. Sp. = Spitsbergen, Gr. = Greenland. Temp. = temperate, cont. = continental. ACC = Alaska Coastal Current, SW = Surface Water, BC = Baffin Current, WGC = West Greenland Current, WSC = West Spitsbergen Current, AW = Atlantic Water, TAW = Transformed Atlantic Water, WCW = Winter Cooled Water, ArSW = Arctic Surface Water, PW = Polar Water, ESC = East Spitsbergen Current, EGC = East Greenland Current, AIW = Atlantic Intermediate Water, FW = Fjord Waters. Note that SW is a descriptive term only, refers to different water masses across the Arctic, and may therefore have variable characteristics. Values are approximations obtained from the closest weather stations and may show discrepancies between individual fjords.*

Location	**Lat**	**Long**	**Class.**	**T** [°C]	**PV** [mm/a]	**WM**	**WT** [°C]	**Sal** [psu]	**References**
Alaska	51°N 71°N	172°E 141°W	temp.	+4	≤ 2000	ACC SW	+7–12 0–8	26–32 4–32	Royer (1983) Hoskin & Burrell (1972) Cowan *et al.* (1988) Cowan (1992); USC (2017)
Canada	61°N 83°N	61W 126°W	marine Arctic– polar desert	-35 +10	150–220	BC WGC SW	-1.8–0 -2–8	31–33.7 15–23	met (2017); Cli (2017) Gilbert (1978, 1982) Lemmen (1990) Syvitski & Hein (1991)
W Sp.	76°N 81°N	∼10°E 17.5°E	cont.– maritime	-6	45–100	WSC AW TAW WCW ArSW	 >3 >1 <0.5 ∼1–6	 >34.9 >34.7 ∼34–35 <34	Svendsen *et al.* (2002) Førland *et al.* (2009) Rasmussen *et al.* (2012)
E Sp.	76°N 80°N	17.5°E 21.5°E	cont.	-6	95	AW ArSW PW SW	>3 2.5–3.5 ∼2.5 ∼2–2.5	>34.9 34–34.9 <34.4 33–34.4	Ślubowska-Woldengen *et al.* (2007) Streuff *et al.* (2017)
W Gr.	59°N 84°N	44°W 73°W	Arctic	-3.9	270	WGC	3.5– 4°C	34.2– 34.4	Cappelen *et al.* (2001) Lloyd *et al.* (2005) Weidick & Bennike (2007)
E Gr.	59°N 84°N	11° 44°W	Arctic	-4	500–800	EGC AIW PW FW	 0–1 -1–0 -1.8–4	 ≥34 28–33 >31	Aagaard & Coachman (1968) Andrews *et al.* (1994) Syvitski *et al.* (1996) Smith & Andrews (2000)

the large amounts of meltwater and precipitation entering the ocean from the coast (Table 5.2; e.g. Hoskin & Burrell, 1972; Royer, 1983; Cowan, 1992).

Fjords along the western Svalbard coast are strongly influenced by the inflow of warm Atlantic water in the form of the West Spitsbergen Current, causing the climate to be relatively mild (e.g. Svendsen *et al.*, 2002; Hald *et al.*, 2004; Ślubowska-Woldengen *et al.*, 2007). The glacimarine environments there are classified as sub-polar with predominantly polythermal glaciers (e.g. Schytt, 1969; Dowdeswell *et al.*, 1998; Benn & Evans, 2010) and a continental–maritime climate (MATs ∼–6° C, Table 5.2; cf. Førland *et al.*, 2009). Water masses are cold and fresh at the surface (1–6°C, <34 psu), caused by high meltwater flux, and warmer, more saline, at the bottom, representing the Atlantic component (>1–3°, >34.7 psu; Svendsen *et al.*, 2002; Ślubowska-Woldengen *et al.*, 2007; Rasmussen *et al.*, 2012).

In East Spitsbergen and Nordaustlandet climatic conditions are less well known, but the presence of sea ice in eastern Svalbard for 8 to 9 months per year[1] suggests somewhat colder conditions than in the west. Nevertheless, oceanographic settings appear to be similar to West Spitsbergen, with meltwater at the surface and warm Atlantic water inflow at depth also recorded in Hinlopenstretet, Lomfjorden and a fjord in West Nordaustlandet (water temperatures between 2–4°C, salinities between 33.5–35.2 psu; see section 3.4.3 and Pfirman *et al.*, 1994; Koç *et al.*, 2002; Ślubowska-Woldengen *et al.*, 2007; Kubischta *et al.*, 2010; Chauhan *et al.*, 2016). Conversely, the coast of East Nordaustlandet is likely to be significantly colder than the west, as it lacks the North Atlantic component in the water masses and is instead influenced by cold Arctic water.

The eastern coast of Greenland (MAT = -4°C; Andrews *et al.*, 1994; Syvitski *et al.*, 1996) is influenced by the East Greenland Current, which transports a mixture of cold, fresh, Polar Water (∼-1–0°C, ∼28–33 psu), warm, saline, Atlantic Intermediate Water (∼0–1°C, ≥34 psu), and ice southwards along the East Greenland shelf (Aagaard & Coachman, 1968; Syvitski *et al.*, 1996). Many fjord heads in the region are "covered" by a semi-permanent mixture of sea ice and icebergs ('sikkusaqs'), which can effectively trap icebergs in the fjords for up to two years (e.g. Andrews *et al.*, 1994; Syvitski *et al.*, 1996). The ensuing cooling effect is further enhanced by meltwater run-off from the local outlet glaciers (cf. Jennings & Weiner, 1996; Syvitski *et al.*, 1996; Andrews *et al.*, 1997), leading to water temperatures between –1.8 and +4°C and salinities of >31 psu (Table 5.2; cf. Smith & Andrews, 2000).

The West Greenland Current (3.5–4°C, 34.2–34.4 psu; Lloyd *et al.*, 2005) is the main oceanographic current influencing the fjords along Greenland's western coast and is composed of the East Greenland Current and the Irminger Current, a branch of the North Atlantic Current, which transports warm and saline waters northwestwards to Southeast Greenland before flowing along the Greenland shelf into Baffin Bay (Fig. 5.1a; cf. e.g. Lloyd *et al.*, 2005; Knutz *et al.*, 2011). The MAT in Disko Bay is ∼ -3.9°C and most fjords are ice-free during summer (e.g. Cappelen *et al.*, 2001; Buch, 2002; Weidick & Bennike, 2007).

The climate on the islands north of Hudson Strait in Canada (see Fig. 5.1a) where most glaciated fjords occur, varies between polar desert (MAT = -18° C; Lemmen, 1990) and marine Arctic conditions (Syvitski & Hein, 1991) with both cold-based and warm-based glaciers at the fjord heads (Ó Cofaigh *et al.*, 1999). Water masses tend to be cold and fresh (-2 to +8° C, 12–34 psu) aided by meltwater inflow and/or the presence of floating glacier tongues and sea ice (Gilbert, 1978, 1982, 1990; Lemmen, 1990; Gilbert *et al.*, 1993).

[1] www.npolar.no

5.4 Material and methods

This study uses swath-bathymetric data from Kongsfjorden, Ymerbukta and Trygghamna in central West Spitsbergen, Magdalenefjorden in northwest Spitsbergen, Lomfjorden in northeast Spitsbergen, and Disko Bay and the Vaigat Strait in central West Greenland (Fig. 5.1; see also chapters 2–5). The data were gathered by the Norwegian Hydrographic Survey, the University in Tromsø, the University Centre in Svalbard and Durham University on a range of cruises between 2000 and 2014, utilising different types of equipment. Acquisition specifics are summarised in Table 5.3. Swath-bathymetric data were gathered with different models of Kongsberg Simrad multibeam echo sounders (Table 5.3) and were gridded, visualised and interpreted in QPS DMagic and Fledermaus 3D Visualisation and Analysing Software.

For five of the fjords additional sub-bottom profiler and lithological data were available and include TOPAS and chirp data as well as thirteen gravity cores from Spitsbergen and twelve vibrocores from West Greenland (Table 5.3). Gravity cores were obtained with a gravity corer with a 6 m long steel barrel and an inner diameter of 11 cm, whereas cores from Disko Bay were taken with the British Geological Survey vibrocorer, also with a 6 m-long barrel but an inner diameter of approximately 9 cm. Where available, radiocarbon dates were determined from isolated bivalves or mixed species benthic foraminifera and seaweed. The results were used to calculate sediment accumulation rates within the fjords and to infer regional ice dynamics. The data displayed in Table 5.3 provide the basis for this study and were integrated with extensive literature on the sedimentary processes and products in Arctic fjords.

5.5 Results

5.5.1 Submarine glacial landforms in High-Arctic fjords

5.5.1.1 Spitsbergen and West Greenland

The swath-bathymetric data from the study area reveal a total of nine types of landforms. Examples of each type are shown in Figure 5.2.

1. Overridden moraines

Overridden moraines are terminal moraines or recessional moraines that were glacially modified and develop when a glacier re-advances and overrides terminal or recessional moraines formed during a previous advance. Overridden moraines tend to be superimposed by sets of newer landforms, often in the form of streamlined bedforms and/or small transverse ridges (Fig. 5.2a,b; sections A.5.1.1 and 2.4.1.2; cf. Ottesen & Dowdeswell, 2006). Because the formation of overridden moraines is solely dependent on the presence of overriding glacier ice, their presence can be used to infer multiple glacier re-advances.

2. Streamlined bedforms

Streamlined bedforms occur in all fjords. They appear as sets of grooves and ridges, up to 3 km long, 200 m wide, and 2–10 m high, as small-scale ridges up to 800 m long, ∼20 m wide, and 1–3 m high, or as elongate hills with a broader stoss side and a tapering lee end (Fig. 5.2c–f). The latter features are variable in size, between 250–7000 m long, up to 1000 m wide, and around 10 m high (section 3.4.1.2; Howe *et al.*, 2003; MacLachlan *et al.*, 2010).

Table 5.3: *Datasets used for this study with acquisition specifics. Lat. = Latitude min., max.; Long. = Longitude min., max.; Depth = Water depth min., max.; Op = Operator; GC = Gravity core, VC = Vibrocore; Specs. = Instrument specifics and, for multibeam data: grid size; for chirp = ping rate when available; for cores = depth of recovery. * R/V Jan Mayen is now R/V Helmer Hanssen. ** Sjømaleren is now IXPLORER. UiT = University in Tromsø; UNIS = The University Centre in Svalbard; NHS = Norwegian Hydrographic Survey; DurU = Durham University. EMxxx = Kongsberg Simrad model; SBP = Sub-bottom profiler; C = Corer; f = frequency. After this table core IDs will be referred to as the first letter of the fjord with the core number, e.g. HH14-GC05 will be L5.*

Data	Location	Lat.	Long.	D [m]	Vessel	Op.	Date	Instrument	Specs.
Multibeam	Kongsfjorden	78°51'35"N 79°03'28"N	11°41'48"E 12°40'50"E	0 360	*Jan Mayen**	UiT	September 2010	EM300	f = 30 kHz 5x5 m
Chirp	Kongsfjorden	78°52'14"N 78°59'12"N	11°51'34"E 12°31'55"E	25 360	*Jan Mayen**	UiT	September 2010	3300-HM SBP	2–12 kHz & 3 ms 1.9 Hz
10JM-GB-GC01	Kongsfjorden	78°55'50"N	12°20'49"E	50	*Jan Mayen**	UiT	September 2010	Gravity Core	286 cm
10JM-GB-GC02	Kongsfjorden	78°55'59"N	12°20'36"E	53	*Jan Mayen**	UiT	September 2010	Gravity Core	339 cm
Multibeam	Magdalenefjorden	79°32'18N 79°37'19"N	10°34'31"E 11°15'46"E	0 110	*Jan Mayen**	UNIS	October 2009	EM300	f = 30 kHz 5x5 m
Chirp	Magdalenefjorden	79°31'21"N 79°42'43"N	09°22'29"E 11°15'18"E	40 110	*Jan Mayen**	UNIS	October 2009	3300-HM SBP	2–16 kHz & 3 ms
JM09H-GC01	Magdalenefjorden	79°33'39"N	11°05'32"E	134	*Jan Mayen**	UNIS	October 2009	Gravity Core	364 cm
JM09H-GC03	Magdalenefjorden	79°34'00"N	10°59'59"E	108	*Jan Mayen**	UNIS	October 2009	Gravity Core	331 cm
JM09H-GC06	Magdalenefjorden	79°35'01"N	10°46'25"E	84	*Jan Mayen**	UNIS	October 2009	Gravity Core	65 cm
JM09H-GC09	Magdalenefjorden	79°33'21"N	11°12'32"E	71	*Jan Mayen**	UNIS	October 2009	Gravity Core	37 cm
Multibeam	Trygghamna/ Ymerbukta	78°11'09"N 78°18'15"N	13°41'23"E 14°14'52"E	0 360	*Sjømaleren***	NHS	July 2000	EM1002	f = 95 kHz 5x5 m
Multibeam	Lomfjorden	79°21'28"N 79°43'08"N	17°32'37"E 18°21'57"E	0 400	*Hydrograf*	NHS	July – August 2011	EM3002	f = ∼300 kHz 5x5 m
Chirp	Lomfjorden	79°22'56"N 79°34'27"N	17°43'19"E 18°04'49"E	35 400	*Helmer Hanssen*	UNIS	Sept 2014	3300-HM SBP	2–16 kHz & 3 ms
HH14-GC05	Lomfjorden	79°23'02"N	17°43'20"E	68	*Helmer Hanssen*	UNIS	September 2014	Gravity Core	236 cm
HH14-GC06	Lomfjorden	79°23'29"N	17°45'17"E	75	*Helmer Hanssen*	UNIS	September 2014	Gravity Core	88.5 cm
HH14-GC07	Lomfjorden	79°23'16"N	17°44'10"E	70	*Helmer Hanssen*	UNIS	September 2014	Gravity Core	294 cm
HH14-GC08	Lomfjorden	79°25'02"N	17°51'04"E	116	*Helmer Hanssen*	UNIS	September 2014	Gravity Core	276 cm
HH14-GC09	Lomfjorden	79°25'46"N	17°52'19"E	119	*Helmer Hanssen*	UNIS	September 2014	Gravity Core	305 cm
HH14-GC10	Lomfjorden	79°33'42"N	17°47'54"E	118	*Helmer Hanssen*	UNIS	September 2014	Gravity Core	105.5 cm
HH14-GC12	Lomfjorden	79°36'24"N	17°57'00"E	200	*Helmer Hanssen*	UNIS	September 2014	Gravity Core	339 cm
Multibeam	Disko Bay	69°01'39"N 70°00'19"N	50°58'16"W 53°11'01"W	180 850	*James Clark Ross*	DurU	August 2009	EM120	f = ∼12 kHz 30x30 m
Topas	Disko Bay	69°00'18"N 69°59'17"N	51°00'18"W 53°14'44"W	200 800	*James Clark Ross*	DurU	August 2009	PS18 SBP	f = 3.5 kHz
JR175-VC03	Disko Bay	69°10'49"N	51°11'37"W	545	*James Clark Ross*	DurU	August 2009	Vibrocore	157 cm
JR175-VC04	Disko Bay	69°09'58"N	51°10'09"W	263	*James Clark Ross*	DurU	August 2009	Vibrocore	110 cm
JR175-VC05	Disko Bay	69°09'36"N	51°31'38"W	389	*James Clark Ross*	DurU	August 2009	Vibrocore	587 cm
JR175-VC06	Disko Bay	69°08'56"N	52°04'08"W	439	*James Clark Ross*	DurU	August 2009	Vibrocore	494 cm
JR175VC07	Disko Bay	69°08'37"N	52°18'53"W	439	*James Clark Ross*	DurU	August 2009	Vibrocore	546 cm
JR175-VC08	Disko Bay	69°08'21"N	52°38'14"W	429	*James Clark Ross*	DurU	August 2009	Vibrocore	391 cm
JR175-VC09	Disko Bay	69°05'47"N	51°23'39"W	294	*James Clark Ross*	DurU	August 2009	Vibrocore	598 cm
JR175-VC10	Disko Bay	69°05'57"N	51°31'13"W	351	*James Clark Ross*	DurU	August 2009	Vibrocore	486 cm
JR175-VC11	Disko Bay	69°06'54"N	52°25'36"W	410	*James Clark Ross*	DurU	August 2009	Vibrocore	325 cm
JR175-VC12	Vaigat Strait	69°53'07"N	51°53'09"W	616	*James Clark Ross*	DurU	August 2009	Vibrocore	366 cm
JR175-VC13	Vaigat Strait	69°58'28"N	51°44'28"W	341	*James Clark Ross*	DurU	August 2009	Vibrocore	340 cm
JR175-VC14	Vaigat Strait	69°56'58"N	51°40'21"W	386	*James Clark Ross*	DurU	August 2009	Vibrocore	466 cm

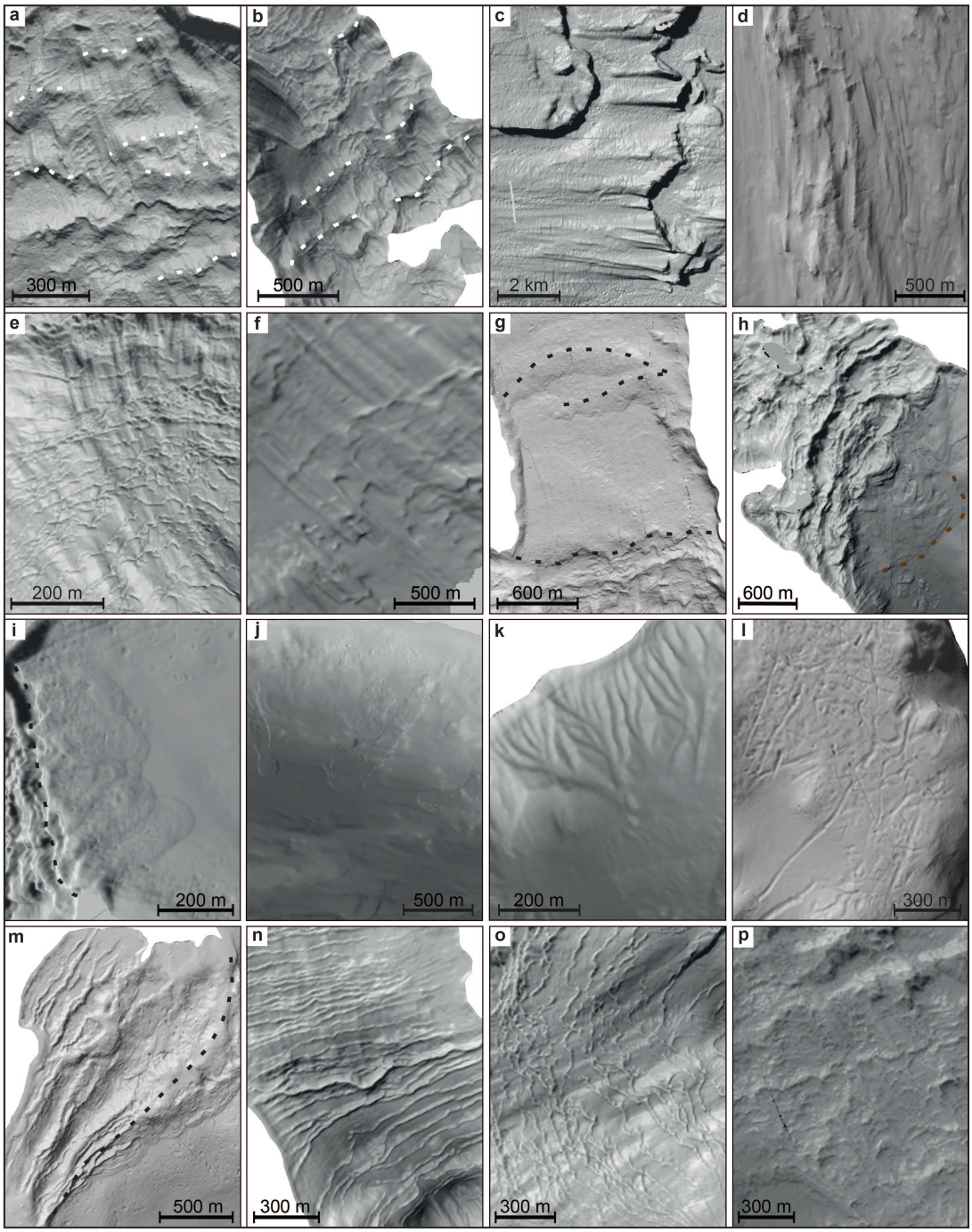

Figure 5.2: *a) Overridden moraines (indicated by white dashed lines) in front of Kronebreen/Kongsvegen, Kongsfjorden. b) Overridden moraines (white dashed lines) in front of Esmarkbreen, Ymerbukta. c) Crag-and-tails in Disko Bay, Greenland. d) Drumlins and crag-and-tails in Lomfjorden, Spitsbergen. e) (Mega-scale) glacial lineations in front of Blomstrandbreen, and f) in front of Conwaybreen, Kongsfjorden. g) Terminal moraines in front of Kronebreen/Kongsvegen, Kongsfjorden. h) Terminal moraine and debris lobe in front of Kjerulfbreen/Harrietbreen, Trygghamna. i) Sets of superimposing debris flows in front of Blomstrandbreen, Kongsfjorden. j) Mass-transport deposits in Lomfjorden. k) Gullies in Lomfjorden. l) Iceberg ploughmarks in Lomfjorden. m) De Geer moraines and terminal moraine in front of Valhallfonna, Lomfjorden. n), o) De Geer moraines and one recessional moraine (white dashed line) in front of Blomstrandbreen, Kongsfjorden. p) De Geer moraines in front of Kronebreen/Kongsvegen, Kongsfjorden.*

The streamlined bedforms are interpreted as glacial lineations, and crag-and-tails or drumlins. Glacial lineations are commonly associated with fast ice flow, particularly when their elongation ratios are high (>10:1; Stokes & Clark, 2002; King *et al.*, 2009), and form

from processes of erosion and re-deposition of soft sediments beneath glaciers or ice streams (Tulaczyk *et al.*, 2001; Ó Cofaigh *et al.*, 2005). The characteristic "tear-drop" shape of crag-and-tails and drumlins in particular evolves from subglacial sediments being deposited around and downstream of a bedrock obstacle (e.g. Dionne, 1987; Stokes *et al.*, 2011). I suggest that their morphology depends on the size of the outcropping bedrock obstacle, the amount of sediment available to form the tail and the velocity of ice flow.

3. Terminal moraines

Large arcuate ridges, orientated perpendicular to the direction of ice flow, are 10–35 m high, several 100 m wide, and 500–2000 m long (Fig. 5.2g, h). These features are interpreted as terminal moraines pushed up at the glacier front during ice advance and subsequent small-scale oscillations in the position of the ice front before retreat commenced (e.g. Boulton, 1986; Boulton *et al.*, 1996). Terminal moraines mark the maximum extent of the Holocene re-advances of many Spitsbergen tidewater glaciers, which are related to glacier surging or to Little Ice Age cooling (see also sections A.6 and 2.5.3; e.g. Plassen *et al.*, 2004; Ottesen *et al.*, 2008; Forwick & Vorren, 2011).

4. Mass-flow deposits

Lobe-shaped deposits occur on the distal flanks of the terminal moraines and along the steep fjord walls where they are commonly associated with chutes and gullies (Fig. 5.2i, j). They are between a few hundred and several thousand metres wide, up to 4.5 km long and up to 45 m thick and are interpreted as debris flows and other gravitational mass flows forming from repeated slope failure. In the case of the debris lobes on the terminal moraines, slope failure occurs either quasi-continuously during moraine formation or from steadily high sediment accumulation rates (e.g. Boulton, 1986; Powell, 1990; Kristensen *et al.*, 2009). Depending on the main formation mechanism, such lobes form during ice advance or while the glacier is quasi-stationary over extended periods of time. Slope failure along the fjord walls may also be triggered by high sediment accumulation; other triggers are earthquakes, regionally high seismic activity, or instability caused by escaping pore fluids (Forwick & Vorren, 2012).

5. Recessional moraines

Transverse ridges, several 100 m wide, 500–2000 m long, and commonly ∼5 m high (up to 20 m in places) are interpreted as recessional moraines, formed during intermittent periods of stillstand in overall glacier retreat (Fig. 5.2m, n). In front of surge-type glaciers these moraines are sometimes overridden by landforms formed during a later re-advance of the glacier (see also sections A.5.1.1 and 5.5.1.1; e.g. Ottesen & Dowdeswell, 2006).

6. De Geer moraines

Well-developed suites of predominantly transverse ridges occur in all investigated Spitsbergen fjords with individual features smaller and more randomly orientated than the recessional moraines (Fig. 5.2o, p). These ridges are only a few metres high and few tens of metres wide, but up to several kilometres long. They have continuous, slightly arcuate crests or appear discontinuous with bifurcating crests of variable orientations that occasionally cross-cut each other. The ridges tend to overprint glacial lineations, indicating that they were formed during ice retreat. They are similar to annual push moraines, which are landforms deposited from meltout of subglacial debris and/or from glacier push at the glacier grounding line during smaller stillstands or re-advances of the glacier front during winter (e.g. Boulton, 1986; Ottesen

& Dowdeswell, 2006; Flink *et al.*, 2016b). In contrast to most annual push moraines, however, the ridges in the study area are normally symmetrical in cross-section, which could indicate that glacier push, if present, played a subsidiary role during their formation (cf. Boulton, 1986). Furthermore, the variable orientation of some of the crests, the occasional cross-cutting, and the more discontinuous character suggest that other processes were active during their formation and the ridges are therefore interpreted as De Geer moraines (see also section 5.6.3 below; cf. Lundqvist, 2000).

7. Submarine gullies and channels

Abundant troughs occur in the study area, particularly along the steep fjord walls, where they are relatively linear, inclined at angles of 10–20°, and up to 1 km long, ∼3 m deep and ∼200 m wide (Fig. 5.2k). These features are interpreted as gullies eroded by meltwater streams and gravitational mass flows. The common occurrence of mass-transport deposits at the base of the gullies (Fig. 5.2j; see also Fig. 3.4g) suggests that mass-flow events are more commonly responsible for their formation.

Within the fjord basins troughs may occur as curvilinear to sinuous features, with the largest up to 40 m deep, ∼16 km long, and 800 m wide and following the contours of a bedrock ridge. They are interpreted as submarine channels associated with meltwater drainage (section 4.4.1; cf. e.g. Booth & Hallet, 1993; Vaughan *et al.*, 2012).

8. Iceberg ploughmarks

Elongate but curvilinear furrows in Lomfjorden are U- or V-shaped in cross-section and are often associated with a circular depression and an upstanding rim on one side (Fig. 5.2l). These furrows are shorter than 1 km, shallower than 1 m, and only about 30 m wide and they are randomly orientated to form criss-cross patterns in places. These landforms are interpreted as iceberg ploughmarks formed from the keels of grounded icebergs that erode and re-deposit the seafloor sediments (e.g. Belderson *et al.*, 1973; Barnes & Lien, 1988; Dowdeswell *et al.*, 1993). Their random orientation is a consequence of the frequently changing direction of iceberg drift paths due to wind and water currents (e.g. Solheim & Pfirman, 1985; Dowdeswell & Bamber, 2007; Mugford & Dowdeswell, 2010). The upstanding rim and circular depression on one side of a furrow probably represent pushed-up sediment and in-situ melting of the icebergs, respectively.

9. Pockmarks

Large craters are circular to elongate in plan-view, U- or V-shaped in cross-section, and have maximum diameters of around 100 m. They are up to 15 m deep and often occur in clusters, particularly in association with mass-flow deposits. On seismic reflection profiles these features show distinct draw-down of surrounding reflections and acoustic masking beneath the crater (see Fig. 4.5). These craters are interpreted as pockmarks, which form from the upwards migration of pore fluids. They are especially common in areas where active gas seepage occurs along tectonic faults and where pore fluids are expelled from rapidly deposited sediments (e.g. Harrington, 1985; Rogers *et al.*, 2006; Forwick *et al.*, 2009; Roy *et al.*, 2014, 2015). The latter is considered the more likely formation mechanism in the study area, because of their close association with sedimentary lobes (cf. Syvitski, 1997; Hovland *et al.*, 2002; Roy *et al.*, 2015).

5.5.1.2 Broader Arctic region

While the submarine geomorphology on many continental shelves and in fjords of West Spitsbergen has been well-mapped over recent decades, the glacigenic landform assemblages

in other High-Arctic fjords are less well understood due to a lack of high-resolution swath-bathymetric data from these regions. Nevertheless, some inferences can be made from detailed observations on both the sedimentology and the terrestrial landscapes within these fjords (e.g. Gilbert, 1978; Powell, 1981; Gilbert, 1982; Ó Cofaigh *et al.*, 1999). Furthermore, fjords have become increasingly more accessible due to a warming climate leading to reduced sea ice cover, and necessary data are thus more easily obtainable, aided by improved research technologies. As a result, submarine geomorphological evidence is emerging from other areas of the world, including fjords of East Spitsbergen, the Canadian Arctic, and Greenland (e.g. Dowdeswell *et al.*, 2016d; and references therein). The distribution of the different types of landforms is shown in Table 5.4.

Little is known about the seafloor morphology in front of fjord-terminating Alaskan tidewater glaciers. Swath-bathymetric data[2] from several fjords only reveal the occurrence of one channel (Fig. 5.3d, e), possibly formed from slumps and/or slides, and several large fjord-transverse ridges (Fig. 5.3f–k). The latter, based on the generally scarce appearance of bedrock features, their transverse orientation, and their preferred occurrence at fjord narrowings, are inferred to represent recessional moraines formed during a temporary stabilisation of the terminus of a receding ice mass. This is supported indirectly by work by Powell (1981), who inferred the presence of recessional moraines, annual push moraines, eskers, turbidity-current channels, and lobate debris flows from observations of associated lithofacies (coarse-grained diamict, "diamictic pockets", sand and gravel, fine-grained (pebbly) mud, and laminated sand and mud) in many fjords in Alaska. Turbidity-current channels evolve from slumps as the sediment erodes the underlying seafloor, or from meltwater underflows, and were also documented in Queen Inlet, Alaska (Hoskin & Burrell, 1972; Carlson, 1989).

Landforms in other West Spitsbergen fjords are similar to those observed in Ymerbukta, Trygghamna, Kongsfjorden, and Magdalenefjorden and most landform assemblages comprise glacial lineations, terminal moraines and debris lobes, and recessional or De Geer moraines (Table 5.4). Additionally, crevasse-squeeze ridges and eskers are present in some of the fjords (e.g. Ottesen & Dowdeswell, 2006; Ottesen *et al.*, 2008; Flink *et al.*, 2015). Crevasse-squeeze ridges are 1–3 m high ridges, commonly arranged in a rhombohedral pattern, that form when a glacier experiences a period of stillstand after advance, thus permitting soft subglacial sediment to be squeezed upwards into basal crevasses (e.g. Solheim & Pfirman, 1985; Boulton, 1986). Because such ridges often occur in front of surge-type glaciers, glaciers that experience climatically-independent cyclic switches between advance and retreat (Meier & Post, 1969), they have been suggested to be diagnostic of surge activity (Sharp, 1985; Ottesen & Dowdeswell, 2006; Farnsworth *et al.*, 2016).

Research from fjords in Nordaustlandet and East Spitsbergen has revealed the presence of several common submarine glacigenic features (Table 5.4). For East Spitsbergen, these include streamlined bedforms and a terminal moraine in Vaigattbogen (Ottesen *et al.*, 2005), glacial lineations, terminal moraines and associated debris lobes, as well as crevasse-squeeze ridges in Mohnbukta (Flink *et al.*, 2016a), and medial moraines and iceberg ploughmarks in Hambergbukta in southeast Spitsbergen (Noormets *et al.*, 2016a,b). Medial moraines form from concentrated debris entrainment and subsequent folding at the confluence zone of two glaciers (Hambrey *et al.*, 1999; Noormets *et al.*, 2016b). From the bathymetric data of Hambergbukta,

[2]Swath-bathymetric data available from the National Oceanic and Atmospheric Administration in the United States, online at https://maps.ngdc.noaa.gov/viewers/bathymetry, were visualised and interpreted as part of this study.

the appearance of recessional/De Geer moraines is also implied (cf. Noormets *et al.*, 2016b). Recessional features are absent in Mohnbukta, suggesting that the ice margin was at or close to flotation during its retreat through the bay (Flink *et al.*, 2016a).

Streamlined bedforms in the form of crag-and-tails and glacial lineations are also present in fjords around Nordaustlandet, particularly in Rijp- and Duvefjorden in the north, and in front of the large surge-type glacier Bråsvellbreen in the southwest. Here, they commonly appear in conjunction with transverse ridges, interpreted as De Geer moraines and/or recessional features and iceberg ploughmarks (Solheim & Pfirman, 1985; Fransner *et al.*, 2017). Large terminal

Table 5.4: *Distribution of landforms and lithofacies in fjords across the northern hemisphere. Regime refers to the classification of glacimarine environments according to Dowdeswell* et al. *(1998). Meltwater/Iceberg = relative annual meltwater/iceberg flux. Note that flux needs to be looked at with respect to total glaciated area, so values for Greenland may be higher than for Svalbard, but still mean relatively lower flux. Red numbers indicate the ratio between the two. Where not given as specific values, quantifications are estimated based on IRD flux relative to the amount of meltwater-derived mud. *values refer to debris flux from the two means. Sea ice, where data are available, is given in duration in months and estimated otherwise. LF = Lithofacies, see also Table 5.5. References are selected examples only. For further information, see also chapters 2–5, and Marienfeld (1992), Andrews* et al. *(1994), Bigg (1999), Ottesen* et al. *(2008), as well as Dowdeswell* et al. *(2016d) and references therein.*

Location	Regime	Sea ice	Meltwater	Icebergs	Landforms	LF	References
SE Alaska	cool-temperate mild sub-polar	low	very high 730 $km^3\ a^{-1}$ ~10–100*	moderate? ~1*	Recessional moraines? eskers turbidity-current channels mass-flow deposits	LF2 LF3 LF4 LF5	Powell (1981); Royer (1983) Gilbert (1983) Mackiewicz *et al.* (1984) Cowan *et al.* (1988) Powell & Molnia (1989) Cowan (1992)
W Spitsbergen	sub-polar	seasonal	high 25 ± 5 $km^3\ a^{-1}$ ~4	low 4 ± 1 $km^3\ a^{-1}$ 1	streamlined bedforms terminal moraines mass-flow deposits recessional/AP moraines De Geer moraines crevasse-squeeze ridges gullies, channels, eskers iceberg ploughmarks medial moraines	LF2 LF3 LF4	Elverhøi *et al.* (1980, 1983) Dowdeswell & Dowdeswell (1989) Hunter *et al.* (1996) Zajaczkowski *et al.* (2004) Ottesen & Dowdeswell (2006) Forwick *et al.* (2010) Forwick & Vorren (2011)
E Spitsbergen	sub-polar	8–9	high 25 ± 5 $km^3\ a^{-1}$ ~4	low 4 ± 1 $km^3\ a^{-1}$ 1	streamlined bedforms terminal moraines mass-flow deposits gullies, medial moraines recessional moraines De Geer moraines crevasse-squeeze ridges iceberg ploughmarks	LF2 LF3 LF4 LF5	www.npolar.no Hagen *et al.* (2003) Ottesen *et al.* (2005) Førland *et al.* (2009) Flink *et al.* (2016a) Noormets *et al.* (2016b) Flink *et al.* (2017)
Nordaustlandet	sub-polar	8–9	high 25 ± 5 $km^3\ a^{-1}$ ~4	low 4 ± 1 $km^3\ a^{-1}$ 1	streamlined bedforms terminal moraines mass-flow deposits recessional/AP moraines De Geer moraines channels iceberg ploughmarks	LF2 LF3 LF4	Solheim & Pfirman (1985) Solheim (1986, 1991) Dowdeswell *et al.* (1998) Hagen *et al.* (2003) Førland *et al.* (2009) Flink *et al.* (2017) Fransner *et al.* (2017)
Canada	sub-polar	10–11	moderate	low?	streamlined bedforms De Geer moraines mass-flow deposits turbidity-current channels eskers, medial moraines mass-flow deposits	LF2 LF3 LF4	Gilbert (1978, 1982) Syvitski *et al.* (1989) Dowdeswell *et al.* (1998) Batchelor *et al.* (2016) Dowdeswell *et al.* (2016b,c) Lajeunesse (2016)
W Greenland	sub-polar– polar?	seasonal	moderate? 51 $km^3\ a^{-1}$ 1	high 100–200 $km^3\ a^{-1}$ 2	streamlined bedforms mass-flow deposits channels transverse moraines	LF2 LF3 LF4 LF5	Echelmeyer *et al.* (1992) Buch (2002); Mernild *et al.* (2010) Hogan *et al.* (2011, 2012) Dowdeswell *et al.* (2014)
E Greenland	(sub-)polar	multi-year sikkussaqs	low 1	high 100–150 $km^3\ a^{-1}$ 2–4	turbidity-current channels gullies iceberg ploughmarks	LF2 LF3 LF4 LF5	Dowdeswell *et al.* (1994b,a) Jennings & Weiner (1996) Syvitski *et al.* (1996) Ó Cofaigh *et al.* (2001)

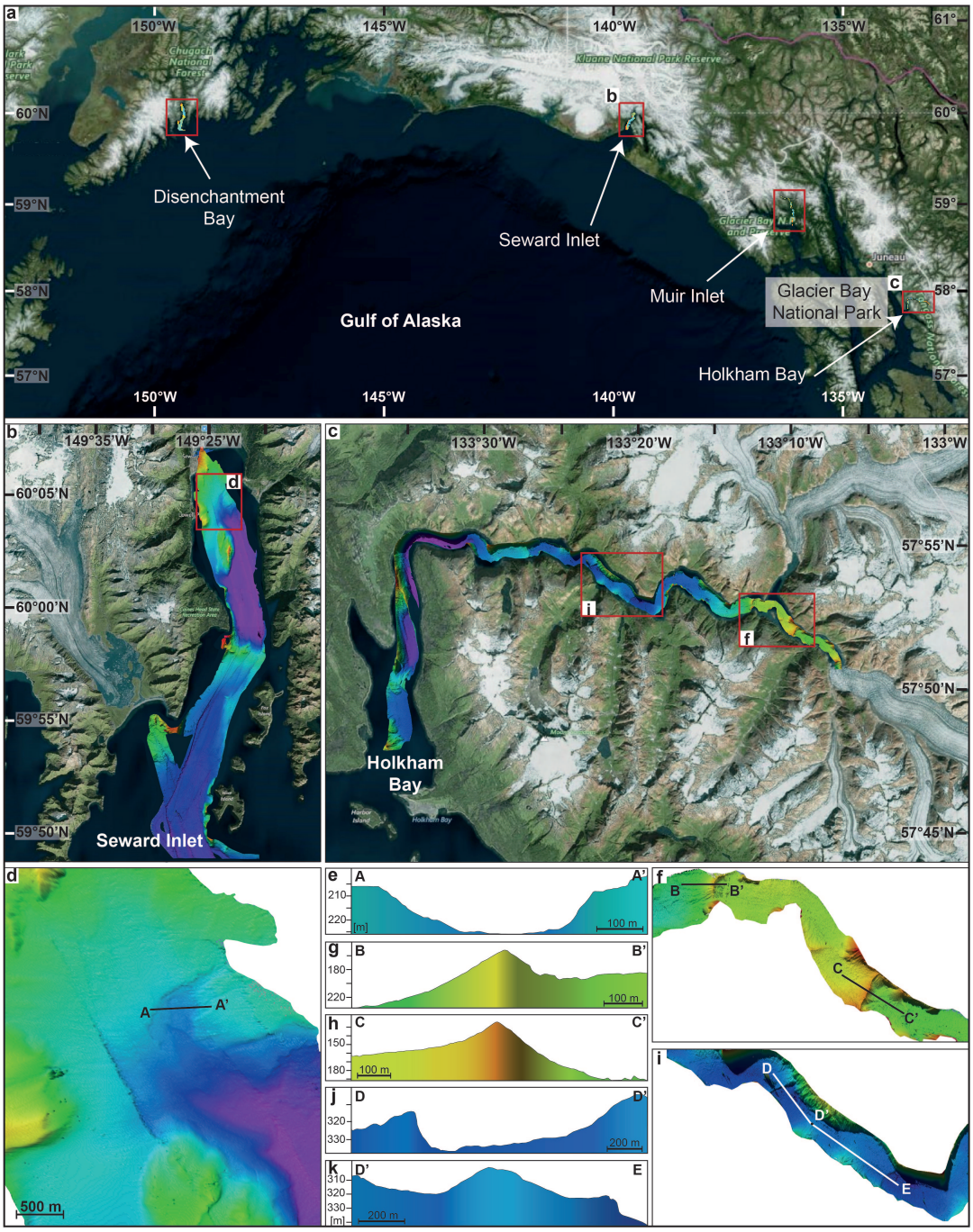

Figure 5.3: *a) Overview of the northern Gulf of Alaska and the swath-bathymetric data investigated here. Satellite data are courtesy of BingMaps and swath-bathymetric data are publically available from the National Oceanic and Atmospheric Administration in the United States. Examples of the seafloor of Seward Inlet and Holkham Bay are shown in b) and c), respectively. d) Channel in Seward Inlet with cross-sectional profile A–A' shown in e). f) Detail image of the inner part of Holkham Bay with cross-sectional profiles B–B' and C–C' across transverse ridges displayed in g) and h). i) Detail image of the central part of Holkham Bay with cross-sectional profile D–D'–E across transverse features shown in j) and k).*

moraines with associated debris lobes as well as "rhombohedral" ridges, inferred to be crevasse-squeeze ridges, also occur in front of Bråsvellbreen (Solheim & Pfirman, 1985; Solheim, 1991). In Wahlenbergfjorden in West Nordaustlandet a paleo-ice stream and several tidewater glaciers formed landform assemblages with crag-and-tails and glacial lineations, terminal moraines and debris lobes, De Geer moraines, crevasse-squeeze ridges, eskers, which are positive-relief infills

of subglacial meltwater channels, submarine channels and iceberg ploughmarks (Flink *et al.*, 2017), suggesting that the tidewater glaciers there behaved generally similar to those in West Spitsbergen (cf. Ottesen & Dowdeswell, 2006; Ottesen *et al.*, 2008; Flink *et al.*, 2015).

Observations in Canada show that streamlined bedforms, including ice-moulded and striated bedrock, crag-and-tails and (mega-scale) glacial lineations occur in many fjords and are often related to fast ice flow during the LGM (e.g. Ó Cofaigh *et al.*, 1999; Bennett *et al.*, 2016; Dowdeswell *et al.*, 2016a; MacLean *et al.*, 2016). Slump scars, mass flow deposits ("mounds"), ice-proximal fans, medial moraines and (turbidity-current) channels have also been observed in several fjords (Lewis *et al.*, 1977; Gilbert, 1978, 1982; Ó Cofaigh *et al.*, 1999; Dowdeswell *et al.*, 2016b,c) and recessional moraines were described from fjords in southwest Newfoundland (Shaw *et al.*, 2000; Shaw, 2003). A complete landform assemblage in Belcher Inlet, Devon Island (for location see Fig. 5.1a), comprises glacial lineations, ice-sculpted bedrock, rock drumlins, grounding-zone wedges, De Geer moraines, gullies, sediment lobes, and iceberg ploughmarks (Batchelor *et al.*, 2016). Grounding-zone wedges are asymmetrical sedimentary depocentres, that form from continued sediment delivery to the grounding zone of temporarily stillstanding ice masses and are therefore often present in previously glaciated areas (Ó Cofaigh *et al.*, 2005; Ottesen *et al.*, 2007; Dowdeswell & Fugelli, 2012; Batchelor & Dowdeswell, 2015). However, they are large-scale features generally formed from ice streams or large outlet glaciers, so they appear more commonly on the continental shelf rather than in fjords.

In terms of landforms and landform assemblages, not much is known about Greenland fjords. The only landforms documented from fjords in East Greenland are bedrock pinnacles, turbidity-current channels, and gullies (Syvitski *et al.*, 1996; Dowdeswell *et al.*, 2010b, 2016e; Evans & Dowdeswell, 2016). A smooth seafloor implies that glacial sediments may mask previously formed landforms in some of the fjords, a theory that is somewhat supported by the presence of drumlins, glacial lineations and iceberg ploughmarks on the continental shelf in front of Kangerdlugssuaq Fjord (Dowdeswell *et al.*, 2010b). Similarly, the landforms documented from the Uummannaq Fjord System just north of Disko Bay and the Vaigat Strait in West Greenland are masked by a relatively thick post-glacial sediment cover. Landforms visible on swath-bathymetric data from there are crag-and-tails, drumlins, and glacial lineations, a large fjord-transverse ridge interpreted to mark the maximum position of Rink Isbræ (one of the fjord-head glaciers) during the Little Ice Age, several sedimentary lobes interpreted as debris flows, and a turbidity-current channel (Dowdeswell *et al.*, 2014).

5.5.2 Glacimarine sediments and associated processes in High-Arctic fjords

5.5.2.1 Spitsbergen and West Greenland

The sub-bottom profiler data obtained from the different fjords provide evidence for the occurrence of a total of six acoustic facies, AF1–AF6. All facies occurred in all fjords, with AF1, as bedrock, forming the acoustic basement. An overview of the acoustic facies, their lithological composition and their main characteristics are shown in Table 5.5. The distribution of the associated lithofacies is indicated in Table 5.4, while selected core logs from the study area are shown in Figure 5.4.

AF2 is acoustically (semi-)transparent with few chaotic internal reflections (Table 5.5). Internal reflections only occur at the top of the facies, where they can be of high amplitude, although generally weakening with depth. AF2 is bounded by an opaque and hummocky upper reflection and either forms or overlies the acoustic basement. The acoustic appearance of AF2 is consistent with uniformly mixed material of a diamictic composition (Stewart & Stoker,

1990) and has previously been interpreted as glacial till (e.g. Forwick & Vorren, 2009; section 3.4.2). Although glacial till in the study area was not sampled in the sediment cores, the sandy diamicts of LF2a (Table 5.5) have the same acoustic appearance on sub-bottom profiler data. These sediments are very poorly sorted, have a muddy to sandy matrix, a high concentration of clasts with random orientations, and a variable but high shear strength. They are interpreted as iceberg turbates (cf. Vorren *et al.*, 1983; Marienfeld, 1992; Dowdeswell *et al.*, 1994b) formed from concentrated input of IRD and partial iceberg scouring at the core site, and as mass-flow deposits, particularly when intercalated with muddy lenses (section 4.4.3.3).

AF3 is acoustically (semi-)transparent with few but chaotic internal reflections and strong top and bottom reflections. It occurs as lens-shaped pockets, conformably drapes the underlying

Table 5.5: *Summary of the common acoustic facies and associated lithofacies in the study area. Examples are shown for usual appearance of each facies on core logs and on x-radiographs (dense areas appear dark). General physical properties are described. As LF2b was not sampled in the sediment cores, physical properties and an example of its appearance on x-radiographs were obtained from Ó Cofaigh* et al. *(2013). In the case of LF5, the lithofacies may have more than one acoustic appearance.*

Acoustic facies	LF	Colour Code	Log (Clay, Silt, Sand)	X-Ray	Description	Properties	Interpretation
	LF2a				sandy, massive matrix-supported diamict, structureless	variable shear strength (<80 kPa), low water content (<20 %), random clast orientation	glacier outwash; slumps; "iceberg turbate"
AF2	LF2b				LF4a with deformation structures	generally high shear strength (>40 ka), low water content, preferred clast orientation	grounding line meltout, subglacial till
AF3 AF4b AF3	LF3			Mud	massive, poorly sorted sand	shear strength not applicable, low water content (~20 %), internally massive or graded, occasional flame/load structures, no clasts	mass-flow deposits; turbidites; glacier outwash
AF4a	LF4a				homogeneous mud	very low shear strength (~5 kPa), moderate water content (20-40 %), no internal structures, variable clast amounts	suspension settling; low-density turbidites; usually ice-distal
	LF4b				bioturbated mud	low shear strength (5-10 kPa), high water content (40-50 %), bioturbation traces and shells common, occasional clasts	
AF3 AF4b	LF4c				stratified/ laminated mud	low shear strength (5-20 kPa), moderate water content (20-40 %), internally stratified, often rhythmically laminated, few clasts	controlled suspension rainout; ice-proximal
	LF4d				stratified/laminated mud with sandy beds/lenses	low shear strength (10-20 kPa), low water content (20-30 %), internally stratified, very few clasts	suspension rainout; turbidites; ice-proximal
	LF4e				pebbly mud	low shear strength (5-20 kPa), low water content (20-40 %), no internal structures	suspension rainout with high IRD input; ice-distal
AF5	LF5				Stratified mud with diamict layers	low shear strength (5-10 kPa), moderate water content (~40 %), internally stratified	(seasonal) rainout from suspension and meltout from icebergs/ sea ice

stratigraphy and occasionally onlaps onto bedrock highs. Lithologically, AF3 is composed of massive, usually well-sorted sand bodies with sharp lower contacts, containing fine to coarse sand (LF3; Fig. 5.4, Table 5.5). AF3/LF3 is interpreted as the deposits from mass-flow events. The sand generally lacks clasts and macro-/micro-fossils (e.g. bioturbation, shells, foraminifera tests), but may appear normally graded up-sequence, show cross-bedding or convoluted structures. Thinner and finer sand laminae or beds are thought to represent deposits from smaller-scale mass flows, such as turbidites or low-density mass flows, while thicker packages relate to larger-scale events like slumps and slides. In the case of the former, the thin sandy beds appear intercalated into the marine mud (Fig. 5.4), and the acoustic signature changes to stratified (LF4d, Table 5.5). Possible triggers for the gravitational mass flows are continuously high sediment accumulation causing slope failure, local earthquakes, isostasy-related seismic activity, and pressurised pores in sediment as a consequence of sea level variations or gas escape (Gilbert, 1983; Prior *et al.*, 1984; Forwick & Vorren, 2012).

AF4 can be divided into two subfacies, AF4a, which is acoustically transparent with few internal reflections, and AF4b which appears acoustically stratified with parallel sets of one transparent and one strong, opaque reflection (Table 5.5). Both subfacies have a draping geometry and conformably overlie AF1, AF2, or AF3. AF4 is the most common in the study area and represents the different subfacies of LF4. LF4 comprises fine-grained mud with a variable silt and clay content, is well sorted, has a high water content and a low shear strength. It occurs in various colours ranging from brown to greenish to grey. Based on internal structures and association with other lithofacies, LF4 can be subdivided into LF4a to LF4e (Fig. 5.4, Table 5.5). The mud of LF4a is internally massive and homogeneous with no internal structures; LF4b is similar to LF4a but shows traces of bioturbation; LF4c is stratified mud that occurs intercalated with thin beds of LF3; LF4d is laminated or stratified with stratification arising from minor changes in density, likely related to grain size; and LF4e is pebbly mud with a very high clast concentration (Fig. 5.4, Table 5.5). All five subfacies can contain variable amounts of clasts and coarser components and may show black mottles. AF4b was sampled by an additional lithofacies, LF5, where the mud of LF4 occurs interstratified with diamictic layers (Fig. 5.4, Table 5.5).

LF4 is interpreted as the product of suspension settling from turbid meltwater plumes. Changes in internal structure, colour and clast content are related to variations in meltwater flux, particle release from the meltwater plume, depositional energy, and ice rafting activity. The characteristics and the distribution of LF4 in the investigated fjords from Spitsbergen and West Greenland can be used to draw the following conclusions about glacimarine environments: (1) massive, often bioturbated mud is commonly found in ice-distal settings with a low depositional energy and low sediment accumulation rates (LF4a, LF4b; Table 5.5; see also Gilbert, 1978; Ó Cofaigh & Dowdeswell, 2001). (2) Conversely, sharp-based mm- to cm-thick massive silt beds are likely the product of low-density turbidity currents (LF4d; see also Mackiewicz *et al.*, 1984; Cai *et al.*, 1997). (3) Stratified mud is indicative of glacier-proximal settings with (a) sandy beds in mud attesting to the frequent occurrence of turbidites or other mass-flow events (LF4d; Table 5.5; see also Gilbert, 1982; Hein & Syvitski, 1992; Gilbert *et al.*, 1993; Forwick & Vorren, 2009), and (b) (cyclically) stratified silt and clay attesting to seasonal or diurnal changes in meltwater flux, particle release from the water column, or meltwater source, particularly in areas where several glaciers terminate in a fjord (LF4c, d; Table 5.5; see also Syvitski *et al.*, 1989; Powell, 1990; Cowan, 1992; Cai *et al.*, 1997; Forwick *et al.*, 2010; Szczuciński & Zajaczkowski, 2012). (4) The amount of clasts embedded in the mud is related to ice rafting,

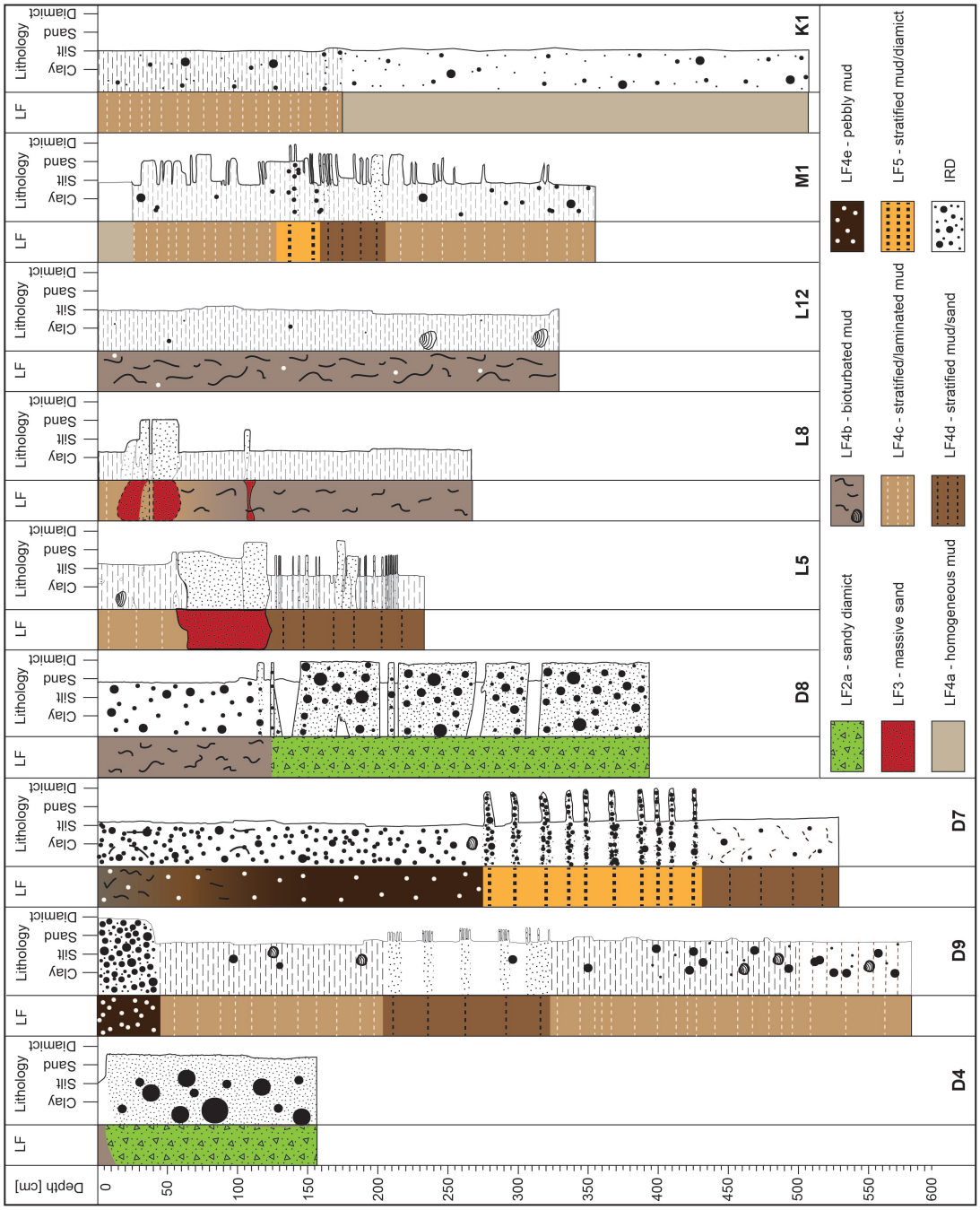

Figure 5.4: *a) Selected core logs from the study areas representing proximal to distal conditions from left to right. LF = Lithofacies log. For location of individual core sites see Figure 5.1d–h. The letter D annotates cores from Disko Bay, L from Lomfjorden, M from Magdalenefjorden, and K from Kongsfjorden.*

with few lonestones indicative either of low iceberg flux or prolonged retention of IRD within bergs and sea ice, possibly due to colder conditions, and high clast amounts (LF4e; Table 5.5) indicative of increased calving, more sea ice, or enhanced iceberg melt. (5) When occurring rhythmically stratified with diamictic beds the muds can imply the presence of sea ice, because a couplet of mud and diamicton is thought to form over the course of one year, with diamicts representing sea ice-derived IRD (section 4.4.3.3; cf. Jennings & Weiner, 1996; Syvitski *et al.*, 1996; Cowan *et al.*, 1997; Hogan *et al.*, 2016). Nevertheless, concentrated diamictic layers are not necessarily seasonal in all instances; they can also stem from more punctual occurrences, such

as overturning icebergs, or simply from periods of increased ice rafting and iceberg melting or reduced meltwater supply. (6) In general, the amount of glacimarine mud appears to be roughly proportional to the availability of meltwater, i.e. the more meltwater or the higher its flux, the more mud is deposited. However, the amount of mud in a fjord is further controlled by other factors (see section 5.6.5 below). (7) Mottles or black layers within the mud are monosulphide layers indicative of increased biological activity caused, for example, by diatom blooms in spring (see also Elverhøi *et al.*, 1980).

The acoustic facies and the lithofacies identified in the study area attest to the occurrence of three main sedimentary processes in the glacimarine realm of Spitsbergen and West Greenland. These are suspension rainout, ice rafting, and gravitational mass flows. Meltout directly from the ice margin is also implied by the presence of AF2, or what is inferred to be glacial till.

5.5.2.2 Broader Arctic region

Although variations occur in, for example, sediment colour, grain size distribution, internal structure and particularly distribution of the lithofacies within the fjord basins, the lithofacies defined for the study area also occur in other glacimarine systems. The general distribution of lithofacies within the fjords of the northern hemisphere was summarised in Table 5.4; note, however, that similar to the types of landforms, not all lithofacies necessarily appear in every fjord.

The lithological record in Alaskan fjords is dominated by fine-grained mud, that formed by settling from suspension in meltwater plumes. According to the different processes active during its deposition (see also section 5.6.5 below) the mud appears massive (LF4a), bioturbated (LF4b), or laminated/stratified (LF4c/d). Cyclically laminated mud (LF4c) is one of the most common lithofacies observed in the fjords there, and comprises couplets of a fine-grained sand or silt layer grading upwards into a poorly sorted mud layer. These so-called cyclopels and cyclopsams are deposited from tidally-controlled suspension settling, where sorting and grading are a function of the different settling velocities of individual particles (see also section 5.6.5 below; e.g. Mackiewicz *et al.*, 1984; Cowan & Powell, 1990; Cowan, 1992; Ó Cofaigh & Dowdeswell, 2001). Mud layers interbedded with sharply-bounded sand horizons are indicative of suspension settling, which is regularly interrupted by turbidity currents. The latter are particularly common during periods of high meltwater discharge, when sandy layers form, whereas the muddy layers tend to form during winter in a lower-energy depositional environment (e.g. Powell, 1981; Gilbert, 1983; Cai *et al.*, 1997). Clasts in the sedimentary record are interpreted as IRD and attest to the presence of some icebergs in the fjords (e.g. Powell & Molnia, 1989). Where clasts appear in concentrated diamict layers, which are interbedded with fine-grained mud layers, seasonally-controlled deposition is implied (e.g. Cai *et al.*, 1997; Cowan *et al.*, 1997). Directly at the glacier front sediments are generally coarser, and often appear in the form of a chaotic diamict (LF2) or imbricate boulder gravels, thought to form from the local accumulation of supraglacial debris, or from the load carried in meltwater jets and streams, which is deposited as glacial outwash (Powell, 1981, 1990). Because the concentration of coarse-grained sediment in meltwater plumes reduces down-fjord, sediments tend to become finer with increasing distance from the ice margin (cf. e.g. Dowdeswell, 1987; Dowdeswell & Cromack, 1991). Bioturbation is considered negligible in many Alaskan fjords, because sediment accumulation rates are too high to provide an appropriate living environment for such organisms (e.g. Mackiewicz *et al.*, 1984; Cowan & Powell, 1990).

Fine-grained mud deposited from suspension settling is the dominant lithofacies also in

fjords of Svalbard, Canada, and West Greenland, and in ice-proximal areas of East Greenland fjords (e.g. Elverhøi *et al.*, 1983; Gilbert *et al.*, 1993; Syvitski *et al.*, 1996; Ó Cofaigh *et al.*, 2001; Forwick *et al.*, 2010; Hogan *et al.*, 2011). Different internal structures may prevail in different areas, depending on the variables influencing the depositional environment (see also section 5.6.5 below). Cyclically laminated muds, for instance, are less common in other Arctic fjords than they are in Alaska, which is possibly related to variable tidal influence across the geographic regions. Nevertheless, stratified sand and mud from alternating turbidity currents and suspension settling are a common lithofacies in the ice-proximal areas of most fjords (sections 2.4.3, 3.4.4, 4.4.3, and 4.4.3.3; e.g. Lemmen, 1990; Gilbert *et al.*, 1993; Forwick & Vorren, 2009). Laminated mud is abundant in the fjords and attests to recurring changes in the depositional environment. Bioturbated muds are often found in ice-distal areas, where the mud is usually diffusely stratified or homogeneous and can be finer than in proximal areas (e.g. Elverhøi *et al.*, 1983; Hein & Syvitski, 1992; Forwick *et al.*, 2010). Pebbly mud differs in the quantity of contained clasts, which can yield information about relative iceberg flux. In East Greenland, for example, diamictic sediments of LF2a are ubiquitous, and are thought to be the result of increased meltout of debris from icebergs and sea ice (e.g. Marienfeld, 1992; Dowdeswell *et al.*, 1994b; Syvitski *et al.*, 1996; Smith & Andrews, 2000). The presence of massive, poorly sorted material, including massive and wispy laminated mud, massive sand, and diamict, provides evidence for the occurrence of gravitational mass flows, such as slumps, slides, turbidity currents and liquefied mass flows in many fjords, including Alaska, particularly where slide scars, channels and sedimentary lobes or mounds have been observed in the geomorphological record (see also sections 3.4.1 and 3.4.4; e.g. Powell, 1981; Syvitski & Hein, 1991; Gilbert *et al.*, 1993; Forwick & Vorren, 2007, 2012).

5.6 Discussion

5.6.1 Glacigenic landform-sediment assemblages in High-Arctic fjords

Figure 5.5 shows selected landform-sediment assemblages from West Greenland and Spitsbergen fjords as identified in this thesis. It is notable, that the types of landforms and lithofacies are not only comparable between fjords in Spitsbergen and between Spitsbergen and West Greenland, but that they are remarkably similar in glaciated fjords across the entire northern hemisphere (see Table 5.4). This implies, that the depositional processes in tidewater glacier settings are also similar.

The data presented throughout this thesis show that the submarine morphology of glaciated fjords is commonly characterised by (1) (streamlined) bedrock highs, (2) (mega-scale) glacial lineations, (3) crag-and-tails/drumlins, (4) terminal moraines often associated with (5) large debris lobes on their distal flanks, (6) recessional moraines, (7) De Geer moraines, (8) iceberg ploughmarks, (9) submarine channels and gullies, (10) mass-transport deposits, and (11) pockmarks. Glacial landforms formed from subglacial, ice-marginal, or glacimarine processes (landform types 2–8), and non-glacial landforms formed mainly from other processes (landforms 9–11) are distinguished. Although bedrock highs are not technically a glacial landform, their streamlined nature in many areas indicates that they were at least partially modified by overriding glacier ice and can thus be classified as partly glacigenic. These observations indicate that the main formation mechanisms for glacial landforms are (1) deposition directly at the glacier grounding line, either though meltout of englacial debris or through pushing

and thrusting and related slope failure, (2) erosion and re-deposition of subglacial debris, (3) sediment infill of cavities, either by deposition from meltwater (eskers) or by upwards-squeezing into basal crevasses (crevasse-squeeze ridges), and (4) erosion and/or deposition by meltwater.

The large similarities in landforms across glacimarine environments is perhaps not surprising considering that certain ice dynamics produce certain types of landforms and glaciers generally only undergo cycles of advance and retreat with intermittent stillstands. Streamlined bedforms, for instance, occur in many presently glaciated fjords where fast ice flow was related to glacier surge behaviour or ice streaming (sections A.5.1, 2.4.1, 3.4.1; e.g. Ottesen *et al.*, 2005, 2008; Dowdeswell *et al.*, 2010b, 2014; Flink *et al.*, 2015, 2016a, 2017). Terminal moraines and debris lobes appear to be present everywhere where glaciers or ice streams experienced a longer period of stillstand at their positions of maximum ice extent (sections A.5.1, 2.4.1; e.g. Boulton *et al.*, 1996; Plassen *et al.*, 2004; Ottesen & Dowdeswell, 2006; Baeten *et al.*, 2010; Forwick & Vorren, 2011; Burton *et al.*, 2016). Likewise, where recessional moraines or well-developed suites of De Geer moraines are present, ice retreat is likely to have been episodic (e.g. Solheim & Pfirman, 1985; Boulton, 1986; Hogan *et al.*, 2010; Flink *et al.*, 2016b). Accordingly, in fjords where ice flow was slow, or where ice retreated continuously without pause, glacial lineations and recessional features may be absent. This suggests, that while there can be a certain variety in the distribution of landforms within different fjords, the types of landforms one can expect to find are likely to be the same.

A notable similarity exists also in the types of lithofacies observed across the different

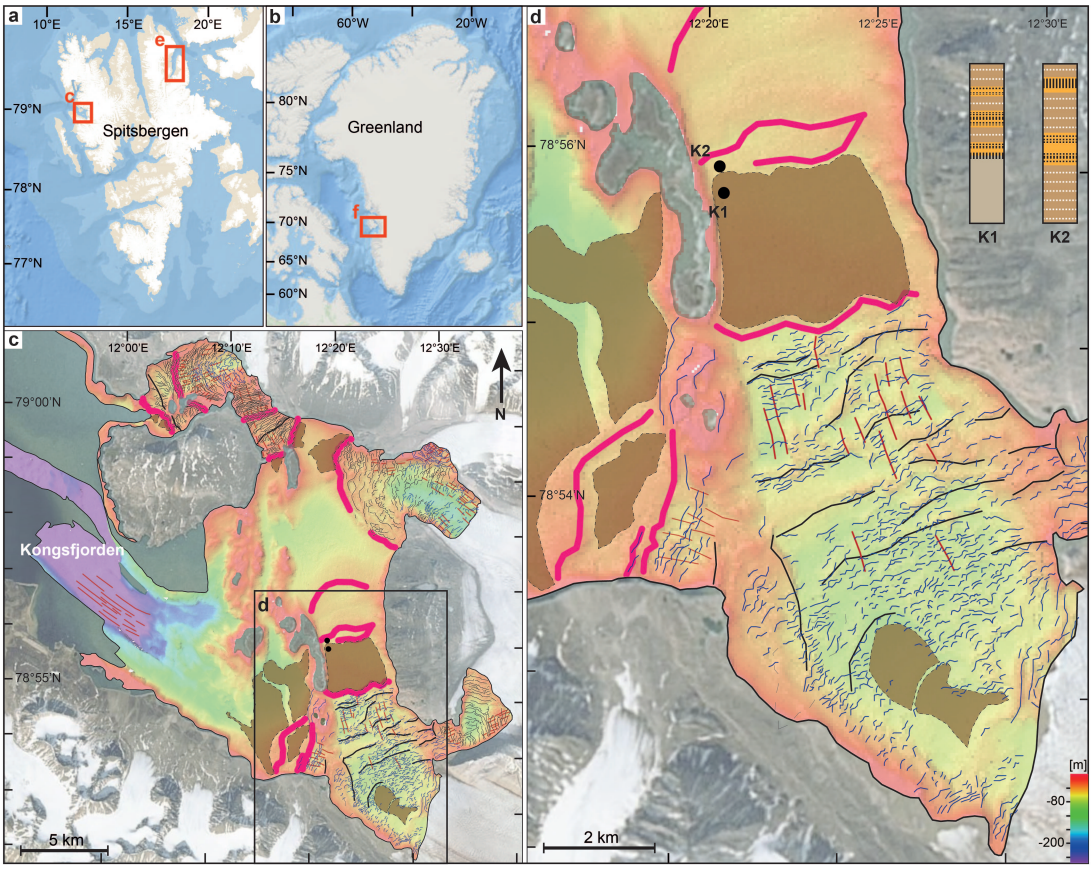

Figure 5.5: *a) Overview map of Spitsbergen showing the location of subfigures c, e and f. b) Overview map of Greenland, showing location of subfigure g). c) Overview of the landform assemblages in Kongsfjorden, with d) showing the landform-sediment assemblage in front of the Kronebreen/Kongsvegen ice margin. For lithofacies information see also Table 5.5.*

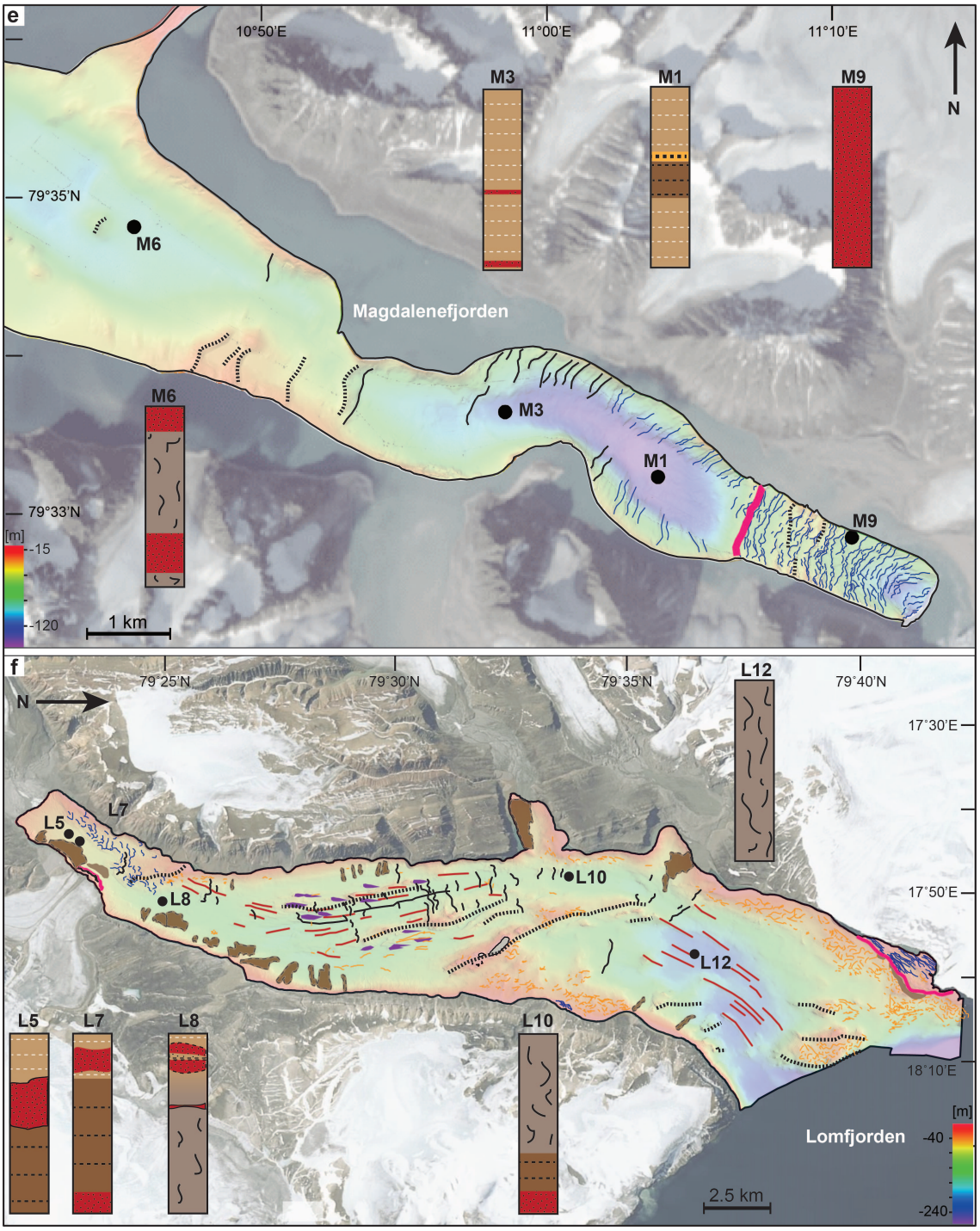

Figure 5.5 *(cont.): Landform-sediment-assemblages in e) Magdalenefjorden and f) Lomfjorden. For location see a) and for lithofacies information see Table 5.5.*

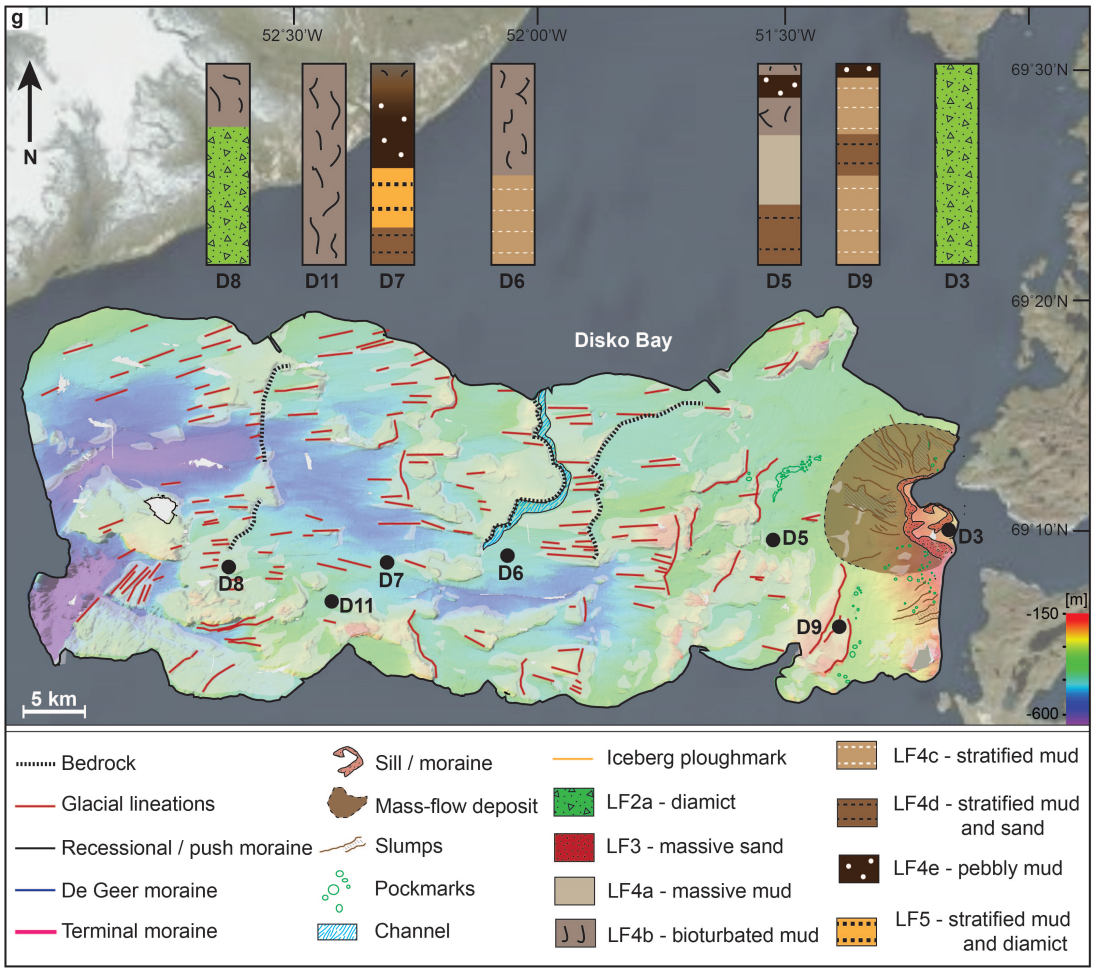

Figure 5.5 *(cont.): g) Landform-sediment assemblage in Disko Bay, West Greenland. For exact location see a) and for lithofacies information see also Table 5.5.*

glacimarine environments, which, likewise, implies that there is a certain generality in the glacimarine sedimentary processes and their associated products in High-Arctic fjords across different climatic regimes. Indeed, the sedimentary processes identified in the study area have also been documented from a range of other fjords (e.g. Gilbert, 1978, 1982; Elverhøi *et al.*, 1983; Powell & Molnia, 1989; Syvitski & Hein, 1991; Hein & Syvitski, 1992; Jennings & Weiner, 1996; Syvitski *et al.*, 1996; Cowan *et al.*, 1997; Ó Cofaigh *et al.*, 2001; Forwick *et al.*, 2010). I therefore define the following principal sedimentary processes in High-Arctic fjords: (1) suspension settling from meltwater and the water column, including the settling of bedload at the location of meltwater efflux, (2) IRD meltout from icebergs and sea ice, and (3) sediment gravity flows, including turbidity currents, slumps, and fluidised or liquefied flows. The latter can play an important role in the depositional processes, as gravity flows not only act to supply sediment to the fjords by rockfall and slope failures along the coast (e.g. Howe *et al.*, 2010), but also to rework already deposited sediment, thereby modifying the stratigraphic record. Sediment reworking has also been attributed to iceberg ploughing, where the grounded keels of icebergs scour the seafloor (e.g. Marienfeld, 1992; Dowdeswell *et al.*, 1994b). In some fjords, the meltout of glacial debris was found to also occur directly at the glacier grounding line, a process, which tends to deposit a stiff glacial till (cf. e.g. Powell, 1981; Powell & Molnia, 1989; Forwick & Vorren, 2009, 2011). The local importance of aeolian sediments on the depositional environments was noted in some Canadian fjords, as

such material can be blown onto the sea ice cover in winter and then melt out as characteristic quartz layers in the following summer (Gilbert, 1978, 1982; Syvitski & Hein, 1991). Further information on glacimarine sedimentary processes and the associated products in High-Arctic fjords can be found in, for example, Powell (1981), Elverhøi *et al.* (1980, 1983), Dowdeswell (1987), Powell & Molnia (1989), Ó Cofaigh & Dowdeswell (2001), and Howe *et al.* (2010).

5.6.2 A conceptual model for sedimentary processes and products in front of fjord-terminating tidewater glaciers

Based on the above, we present a new conceptual model summarising the glacimarine sedimentary processes and associated products in front of contemporary tidewater glacier margins (Fig. 5.6). Although the idea of conceptualising landform and sediment assemblages in front of fjord-terminating tidewater glaciers is not novel, and there are similarities between the model presented here and those developed previously, existing models are often based on limited data and are hence too regional in focus (e.g. Ottesen *et al.*, 2008; Forwick & Vorren, 2011). Furthermore, the majority were developed more than a decade ago (e.g. Powell, 1981; Dowdeswell *et al.*, 1998; Plassen *et al.*, 2004; Ottesen & Dowdeswell, 2006) and therefore do not include the continuously growing body of evidence from contemporary glacimarine environments across the Arctic (chapters A–4; e.g. Baeten *et al.*, 2010; Dowdeswell *et al.*, 2010a; Kempf *et al.*, 2013; Flink *et al.*, 2015; Dowdeswell *et al.*, 2016d; Hogan *et al.*, 2016; Flink *et al.*, 2017; Fransner *et al.*, 2017).

The updated model presented here not only includes both landforms and sedimentary processes and products, but also integrates data from glacimarine environments across the entire northern hemisphere. It is intended to serve as a comprehensive template for the interpretation of glacier-derived sediments and landforms in fjords. Note, however, that due to the complexity of different controls acting on glacimarine environments, there is still some variety in glacial geomorphology and sedimentation across different areas of the world. This is further discussed in section 5.6.5.

5.6.3 Landform assemblages and their implications

While the types of landforms identified in the study area commonly occur in High-Arctic fjords, not every landform necessarily occurs in every fjord, and their distribution therefore leads to significant differences in glacigenic landform assemblages. In Nordvestfjord in East Greenland, for example, the only landform visible on the seafloor is a large turbidity-current channel (Dowdeswell *et al.*, 2016e). Similarly, recessional moraines appear to be the only type of landform in many Alaskan fjords (see Fig. 5.3). Likewise, the main type of glacial landform in Disko Bay in West Greenland are crag-and-tails, although some individual channels, pockmarks, and mass-flow deposits occur in the innermost bay (Fig. 5.5, section 4.4.1; see also Hogan *et al.*, 2012). Conversely, tidewater glaciers in West Spitsbergen usually form entire suites of landforms with similar types of landforms present in different fjords. In the majority of West Spitsbergen fjords the following features are present: (1) streamlined glacial lineations, (2) terminal moraines, (3) lobe-shaped debris flows, and (4) small, transverse moraine ridges (Fig. 5.5, sections A.5.1 and 2.4.1; e.g. Plassen *et al.*, 2004; Ottesen & Dowdeswell, 2006; Ottesen *et al.*, 2008). However, additional landforms, such as crevasse-squeeze ridges, crag-and-tails or eskers occur in some fjords, while in others (e.g. Magdalenefjorden and Lomfjorden; see sections 2.4.1, 3.4.1) terminal moraines are, if not absent, at least very poorly developed.

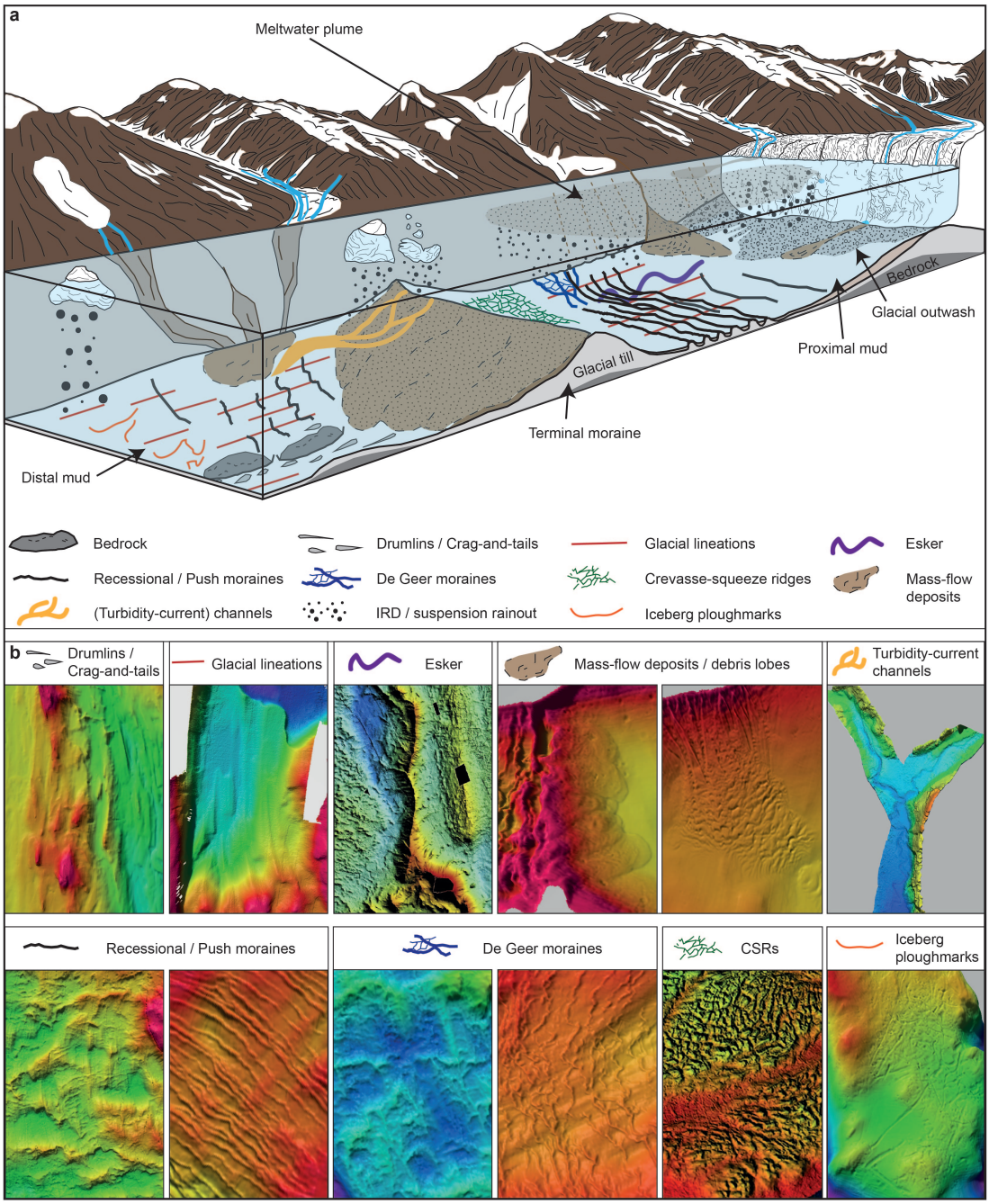

Figure 5.6: *Conceptual model for the sedimentary processes and associated products in front of fjord-terminating tidewater glaciers. The extended legend in the lower half of the figure shows examples of the appearance of these landforms on bathymetric data. Examples for eskers, turbidity-current channels and crevasse-squeeze ridges are modified from Ottesen* et al. *(2008), Dowdeswell* et al. *(2016e), and Ottesen & Dowdeswell (2006), respectively.*

This highlights inter-fjord variability in tidewater glacier dynamics and the resulting landform-sediment assemblages.

5.6.3.1 De Geer moraines

One of the most striking differences between the landform assemblages observed in the seven fjords investigated for this study and those observed in other Spitsbergen fjords is the appearance of De Geer moraines rather than defined annual push moraines or well developed

crevasse-squeeze ridges, even though the latter two landforms are common components of tidewater glacier assemblages in Svalbard (e.g. Solheim & Pfirman, 1985; Plassen *et al.*, 2004; Ottesen & Dowdeswell, 2006; Ottesen *et al.*, 2008; Flink *et al.*, 2015, 2017). Although the De Geer moraines observed in Kongsfjorden, Magdalenefjorden, Ymerbukta and Trygghamna, and Lomfjorden are similar to annual push moraines in many respects, the variable orientation of their crests, their cross-cutting relationships and their, in places, considerable discontinuity all suggest that the De Geer moraines are not simply the product of winter stillstands or re-advances. This is supported by the fact that, at least in front of those glaciers that last advanced during the Little Ice Age, annual formation should have led to the development of a minimum of ∼100 individual ridges (cf. Mangerud & Landvik, 2007). The much lower number (around 40 in both Magdalenefjorden and Trygghamna) suggests either irregular sea ice development (cf. Boulton, 1986; Ottesen & Dowdeswell, 2006), or that moraine formation occurs at more irregular intervals than once a year.

It was suggested above (section 5.5.1.1) that the formation of De Geer moraines in the study area is related to a combination of glacier push and crevasse-squeezing. Crevasse-squeeze ridges (CSRs) have been suggested to form during a glacier's transitional phase at surge termination, when the glacier reaches its maximum surge extent, is in a stable position, and can "sink into its bed" before commencing retreat (Sharp, 1985). The small, transverse push moraines on the other hand have been suggested to form each year during winter, when calving and further retreat are inhibited by the presence of shorefast sea ice (Boulton, 1986). Considering that CSRs are thought to be surge-diagnostic and have been used as a tool to identify surge-type glaciers (Farnsworth *et al.*, 2016), their absence even in front of the known surge-type glaciers in Kongsfjorden is notable. The rarity of well-developed annual push moraines is equally unusual (cf. Ottesen & Dowdeswell, 2006; Ottesen *et al.*, 2008). Instead, the appearance of De Geer moraines in front of nearly all the glaciers in the investigated fjords suggests that while the processes required to form both types of landforms were active to some degree, conditions for the proper development of either were not ideal.

A certain variability in glacier substrate could favour the formation of CSRs in those fjords with softer, more saturated sediments, which are more easily deformable and are hence more prone to squeezing (e.g. Boulton *et al.*, 1996; Evans & Rea, 1999). Another factor potentially controlling the formation of De Geer moraines over CSRs or annual push moraines is time. Generally, the more time there is for the formation of a specific landform, the better-developed the feature. This is true for terminal and recessional moraines as well as debris lobes, all of which are likely to be larger when the stillstand lasted longer (cf. e.g. Boulton, 1986); similarly, subglacial channels are likely to become deeper and more defined, the longer water erodes them. Applying this theory to the De Geer moraines, this would imply that proper CSRs did not form because the transitional phase the glaciers experienced after their re-advances was insufficiently long. Equally, the presence of a crevasse-squeeze component in the De Geer moraines would then mean that, in contrast to 'normal' annual push moraines, phases of stillstand during glacier retreat were longer than one winter season, and are therefore not necessarily tied to sea ice formation. This is based on the fact that phases of stillstand were long enough for processes of crevasse-squeezing to become active, and is supported by the fact that the number of De Geer moraines in front of most glaciers does not correlate with the number of years elapsed since the glaciers were at their maximum positions. It is possible therefore, that crevasse-squeeze ridges are not diagnostic of surge activity as previously thought, but are rather a landform indicative of a prolonged transitional phase after glacier advance. I also infer that while some characteristics

of the De Geer moraines are similar to annual push moraines, the De Geer moraines form much less frequently than once per year.

5.6.3.2 Implications for regional tidewater glacier dynamics

While we distinguish between De Geer moraines and annual push moraines as separate types of landforms and assume that time regulates the formation of one landform over the other, the occurrence of either landform in some fjords but not others could be explained by individual ice dynamics. Nevertheless, there remains the question why some glaciers appear to halt once a year during winter to form one push moraine, whereas others seem to halt less frequently and for longer, thus forming the De Geer moraines. As there are often large uncertainties with regards to annual ice front positions and/or the ages of individual moraines, one possibility is that glaciers thought to halt annually experienced less frequent stillstands than previously thought. Another possibility is that annually formed moraines were not perfectly preserved over time, with glaciers obliterating previous landforms by re-advancing across them during a particularly cold winter. Notwithstanding this, if that were the case I would expect signs of overriding ice to be present in the geomorphological record, which is not always the case (see Magdalenefjorden and Trygghamna; section 2.4.1). Both scenarios suggest that while certain ice dynamics are indicated by the landform assemblages in front of tidewater glaciers, it is difficult to reconstruct detailed dynamics and ages of formation without suitable evidence (i.e. radiocarbon dates, satellite imagery).

As it is assumed that the relationship between glacier bed and glacier plays an important role for moraine formation, another possibility could be intermittent periods of ungrounding, where the glacier loses contact with its bed. This could, for example, be caused by increased inflow of warm water into the fjord, promoting subglacial melt. The latter mechanism could theoretically also lead to the development of a floating ice shelf, where the glacier deposits a moraine at its grounding line but remains at that position until the floating tongue has calved off and the glacier continues to retreat. If the period of calving of the floating tongue takes three years, for instance, during which the grounding line remained stationary, this would account for a discrepancy between the number of moraines formed (one) and the number of years elapsed (three). Variations could also occur due to differences in local sediment accumulation rates between fjords, causing tidewater glaciers with a higher sediment yield to experience longer phases of stillstand during which they form De Geer moraines, whereas termini fluctuations of glaciers with lower sediment availability would only be subject to climatic controls, i.e. seasonal changes (cf. Powell, 1991).

Topographic controls can also influence glacier retreat (e.g. Powell, 1991; Ó Cofaigh, 1998; Benn *et al.*, 2007b; Briner *et al.*, 2009). One example of this is the fjord width, which, in the context of the small ridges, could promote formation of De Geer moraines in narrower fjords, which can temporarily stabilise the ice margin, whereas annual push moraines could form in wider fjords when ice retreat is unhampered (cf. Åkesson, 2016). Indeed, Magdalenefjorden, Ymerbukta, Trygghamna, and Lomfjorden all seem to be up to half the width of Borebukta, Rindersbukta, Yoldiabukta, Tempelfjorden, and Van Keulenfjorden, from where annual formation has been inferred for small transverse ridges (Ottesen & Dowdeswell, 2006; Ottesen *et al.*, 2008; Flink *et al.*, 2015). With regards to sediment availability, accumulation rates in Kongsfjorden, Lomfjorden and Magdalenefjorden only appear to be higher than in Van Keulenfjorden, whereas rates for Tempelfjorden and Yoldiabukta appear to be relatively similar (see sections A.5.5, 2.4.3.2, 3.4.5, and 4.4.3.2; cf. Plassen *et al.*, 2004; Forwick *et al.*, 2010;

Kempf *et al.*, 2013). This may suggest that topography exerts a larger control on the formation of landforms than sediment yield. It is important to keep in mind, however, that the SARs are based on an assumption of linear accumulation over long periods of time. Furthermore, they are rarely directly comparable between fjords due to their strong dependence on distance to the glacier margin (see section 5.6.5 below). Thus, in order to test the relationship between De Geer moraine formation and increased sediment yield, SARs would have to be acquired at a much higher resolution, in similar sediments, as close to the annual moraines and De Geer moraines as possible, and at roughly the same distances from current glacier margins.

5.6.4 Sedimentary processes and associated lithofacies

It was established above that suspension settling from meltwater and the water column, meltout of glacial debris from the glacier front, sea ice and icebergs, and sediment reworking by gravitational mass flows and iceberg keels are the main sedimentary processes active in glacimarine fjord settings. Accordingly, most of the lithofacies types are generally similar. Stratified to massive mud is a component of the lithological record in all fjords, not just in Spitsbergen and West Greenland, but also in Alaska, Canada and East Greenland. Likewise, sharp-based sands, interpreted as turbidites or other mass-flow deposits occur nearly everywhere, particularly in areas close to the ice margins. IRD is also present in all fjords. However, the sediment cores from the study areas (see chapters 2–5) reveal differences in the structure, composition and distribution of the lithofacies, not only in fjords of the same region or adjacent fjords, but even within a single fjord basin. Cyclically laminated muds, which are thought to reflect seasonal or diurnal changes in sediment delivery, only occur in Magdalenefjorden. Similarly, the stratified mud and diamict of LF5 is confined to the lithological record of Disko Bay, and was not recovered in the adjacent Vaigat Strait, although this could be due to the restricted depth of sediment recovery (max. 6 m). Turbidites are common in Lomfjorden, Magdalenefjorden, and Disko Bay, but occur in the shallow inner part of Lomfjorden, in a deep basin in the central fjord in Magdalenefjorden, and in what is now technically an ice-distal environment in Disko Bay. Conversely, turbidites appear to be absent in Kongsfjorden, even in ice-proximal sediment. Large-scale mass-flow deposits are very common along the fjord walls of both Lomfjorden and Ymerbukta, but are much less common in the adjacent Trygghamna or in Magdalenefjorden. Diamictic sediments are almost entirely absent from the fjords in Spitsbergen but occur in West Greenland. Indeed, the clast concentration in general appears to be much higher in West Greenland than in the Spitsbergen fjords (see Fig. 5.4). Bioturbated mud is present in all cores from Disko Bay, but is confined to the outer part of Lomfjorden in the Spitsbergen fjords.

Differences in the nature of the sediments can also be observed when comparing the fjords in the study areas to those in Alaska, Canada and East Greenland. Cyclically laminated muds in Alaska, for instance, have often been related to tidal influences controlling particle release from the meltwater plume (cf. Mackiewicz *et al.*, 1984; Cowan & Powell, 1990; Cowan, 1992), whereas stratified or laminated muds in many other Arctic fjords are commonly related to (seasonal) changes in meltwater flux, biological productivity, or sediment source (cf. Elverhøi *et al.*, 1983; Plassen *et al.*, 2004; Forwick *et al.*, 2010). So while the main mechanism forming the stratified muds, i.e. suspension rainout from meltwater, is the same, and the general end product, i.e. fine-grained glacimarine mud, is the same, slight variations in the depositional environment and the factors controlling sedimentation can lead to different lithofacies characteristics. The

same holds true for turbidites and other mass-transport deposits. Typically turbidites are graded, can show load clasts or flame structures and ripple lamination or cross-bedding (e.g. Stow & Shanmugam, 1980; Gilbert, 1982; Cai *et al.*, 1997). On the other hand, turbidites can also be massive and predominantly sandy (e.g. Gilbert *et al.*, 1993; Mackiewicz *et al.*, 1984; Cai *et al.*, 1997). Furthermore, large-scale mass-transport deposits such as slumps and slides and debris flows can have a variable lithological composition, depending on their provenance. In submarine settings they tend to comprise a chaotic mixture of glacimarine sediments, i.e. massive mud, sand and/or clasts. Nevertheless, while the composition is roughly the same, mass-transport lithofacies can be markedly different in the sedimentary record of fjords. For example, in Disko Bay, a sandy diamict of LF2a in VC08 was interpreted as a mass-transport deposit, while a debris lobe sampled from Kongsfjorden contained mainly massive mud with several clasts (LF4a). In contrast, mass-transport deposits in Lomfjorden are devoid of clasts and only contain massive sand, at least in the sampled gravity cores (Fig. 5.4, cf. ∼130 cm to core bottom in D8, ∼60–110 cm in L5, and 165 cm to core bottom in K1; see also sections A.5.3, 3.4.4).

Another example of variable lithofacies characteristics despite similar sedimentary processes is the clast concentration in the sediments. In Alaska, diamicts commonly occur close to the ice margin, and occasional lonestones in the glacimarine mud sequences attest to the presence of some icebergs. Although ice-proximal coarse-grained diamicts have not been described from Spitsbergen fjords, occasional lonestones are also interpreted as IRD. Conversely, pebbly muds and diamicts in Disko Bay are interpreted to be deposited exclusively as IRD. Similarly, the sedimentary record in several East Greenland fjords shows a majority of massive diamicton, while mud derived purely from meltwater is scarce (e.g. Dowdeswell *et al.*, 1994a,b, 2000). This shows, that while the meltout of IRD from icebergs and possibly sea ice is actively contributing to the lithological record in all settings, the relative importance of it varies. This can even be seen within single fjords, such as in Spitsbergen, where ice rafting in proximal areas is usually swamped by very high accumulation rates of meltwater-derived fines. However, it becomes relatively more important towards distal areas, where sediment concentrations in the meltwater plumes dissipate and accumulation rates decrease (e.g. Elverhøi *et al.*, 1983; Dowdeswell *et al.*, 1998).

5.6.5 Controls on glacimarine sedimentation in front of fjord-terminating tidewater glaciers

The results presented in this thesis show that ice dynamics and the relative importance of individual sedimentary processes are spatially highly variable across different fjords, even when the latter are situated in the same geographic region. This suggests that the final landform-sediment assemblages deposited in front of fjord-terminating tidewater glaciers are not dependent on geographic location and thus climate alone, but are also influenced by a range of external factors. The following paragraphs and Figure 5.7 attempt to summarise these factors and their exceedingly complex interrelations.

The controls that affect glacimarine environments and sedimentation are manifold, and include tectonics, sea-level change, and climate as important global controls, which are further affected by several local influences (Fig. 5.7; Powell & Molnia, 1989; Powell, 1991). Tectonics can influence glacier dynamics in many ways, as they primarily control the morphology of a glacier and its catchment area. Topography of a glacier and its surrounding areas has, for

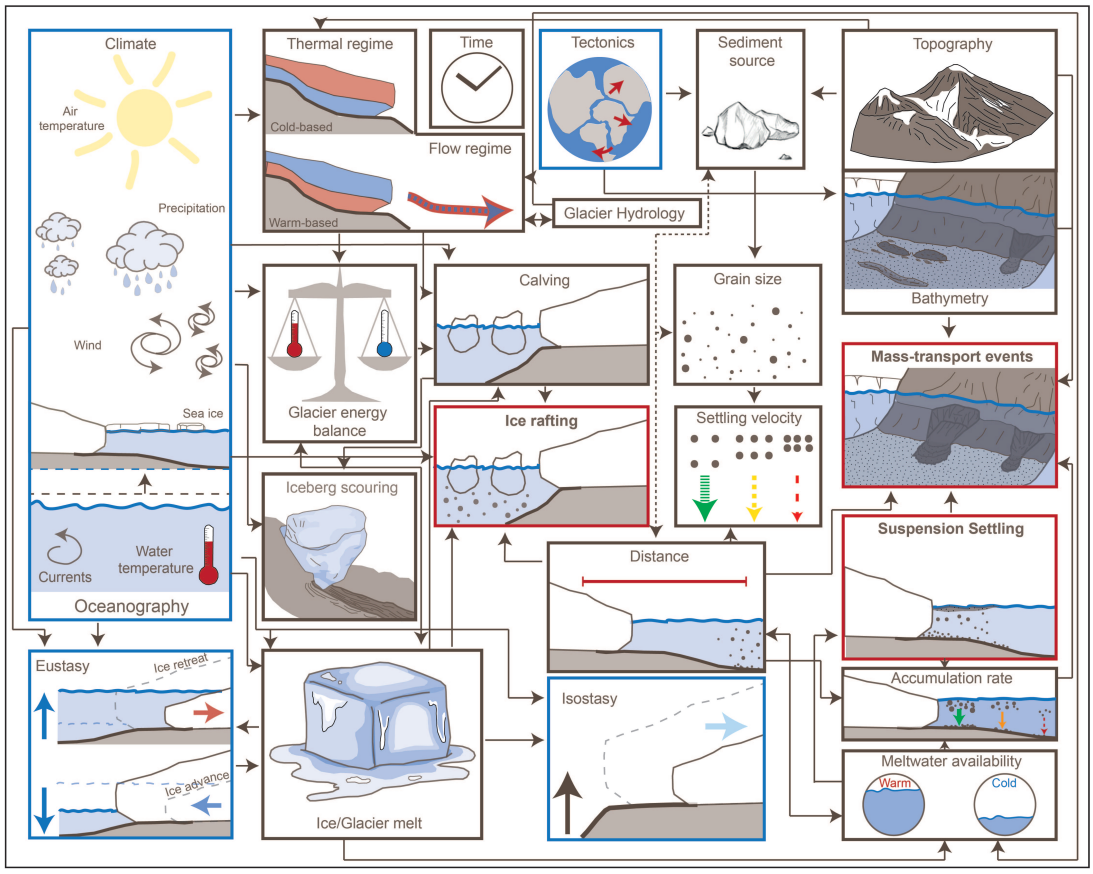

Figure 5.7: *Conceptual model summarising the main glacimarine sedimentary processes (red boxes) identified in High-Arctic fjords and the global (blue boxes) and regional controls (brown boxes) that influence them. Note that arrows are missing for time because it is an important factor relating to nearly all of the processes.*

example, been shown to have a major effect on the glacier's energy balance, which, in turn, is closely related to ice melt (Fig. 5.7; e.g. Arnold *et al.*, 2006). Moreover, the types of rock present in the catchment area define (a) how easily a glacier can produce "rock flour" (e.g. Powell & Molnia, 1989), i.e. erode the underlying substrate, and (b) which type of sediment will be delivered to the fjord basins (e.g. granitic material, carbonate rock flour, sandstones etc.; Forwick *et al.*, 2010; Rasmussen & Thomsen, 2013; Streuff, 2013). Tectonics can also modify an existing sedimentary record by faulting and folding, or by triggering earthquakes, which in turn, have been related to increased mass-flow activity in Spitsbergen (Forwick & Vorren, 2012). Another landform type whose formation can be facilitated by tectonics are pockmarks, which favourably form in areas where tectonic faulting allows the upward migration of gaseous fluids (e.g. Forwick & Vorren, 2009; Roy *et al.*, 2014). Note, however, that although certain glacimarine processes, such as high sediment accumulation rates or the formation of glacigenic debris flows, may aid their formation, pockmarks are non-glacial in origin.

Isostasy and eustasy have been suggested to influence ice margin position, which, in turn, can influence glacial landform assemblages (e.g. Boulton, 1990; Powell, 1991; Oerlemans & Nick, 2006; Benn *et al.*, 2007a). While it is unlikely that isostasy accounts for differences between adjacent fjords, as the adjustment is usually regionally-integrated, it could explain differences in landform-sediment assemblages across geographically widespread areas. The occurrence of turbidity-current channels could, for example, be related to an increased occurrence of earthquake-triggered mass flows due to ongoing isostatic adjustment. Like isostasy, eustasy is a

global phenomenon and thus affects all investigated areas equally. While it is highly important for regulating the types of landforms being formed (e.g. ice-contact delta vs. terrestrial moraine), sea-level changes are non-instantaneous but happen over longer time scales, and are therefore unlikely to cause differences in landform-sediment assemblages that were formed at roughly the same time. Nevertheless, if a landform assemblage in Spitsbergen were to form much later than one in Greenland, the formation of landforms could then be influenced by eustasy.

Climate is a very important factor when looking at glacial regimes, as it governs air temperature, ocean currents and thus water temperatures, precipitation, and winds, all of which have an effect on glacimarine sedimentation (Fig. 5.7). It also contributes significantly to glacier mass balance by modulating accumulation and ablation within a glacier, and can determine whether a glacier is cold-based, polythermal, or warm-based (e.g. Dowdeswell *et al.*, 1997; Benn & Evans, 2010). Climate thereby regulates ice flow to some degree, which can cause variations in landforms deposited. The thermal regime can also influence the types of landforms deposited in a fjord, as was shown in fjords in Canada by the presence of predominantly lateral and proglacial meltwater channels inferred to be deposited by cold-based ice, and ice-moulded bedrock, moraines and grounding-line fans inferred to be deposited by warm-based glaciers (Ó Cofaigh *et al.*, 1999). In very cold, dry areas, such as Antarctica, glaciers tend to be cold-based, and precipitation is generally low, leading to very restricted meltwater and rainwater runoff, causing sedimentation from icebergs and directly from the glacier to be the predominant sedimentary process (Powell & Molnia, 1989; Dowdeswell *et al.*, 1998). Conversely, in areas where air temperatures and precipitation volumes are high, such as in Alaska, ample amounts of rain- and meltwater supply fine-grained sediment to the fjords, which rains out from suspension at such high rates, that the component from icebergs and sea ice is swamped (e.g. Cowan *et al.*, 1988; Boulton, 1990; Dowdeswell *et al.*, 1998). This was the basis for a conceptual model, classifying glacimarine environments according to climate into meltwater-dominated and iceberg-dominated settings (Dowdeswell *et al.*, 1998). However, while warmer temperatures may amplify glacier melt and associated meltwater flux, the latter can also be regulated by glacier hydrology and flow regime (Fig. 5.7). Fast-flowing glaciers, for example, tend to create more friction at the glacier bed than those that move more slowly, and therefore produce higher amounts of subglacial meltwater (Bell, 2008; Alexander *et al.*, 2013). Faster-flowing glaciers are also more prone to form glacial lineations at their bed. Furthermore, subglacial melting and hence meltwater flux can be enhanced by pressure melting underneath thick ice, even within cold-based glaciers, and additional environmental factors such as solar and atmospheric radiation, latent heat released by internal processes in the ice, and geothermal heat (e.g. Kayashta *et al.*, 2003; Benn & Evans, 2010).

Basal melting can, in turn, facilitate (partial) ungrounding of the ice margin, thereby causing variability in the development of proglacial landforms. The absence of recessional features in a fjord, for example, can be accounted for by an ungrounded ice margin, particularly if retreat is happening extremely rapidly (cf. Dowdeswell *et al.*, 2008; Ó Cofaigh *et al.*, 2008; Flink *et al.*, 2017). The presence of a floating tongue would prevent contact of the glacier with its bed, thus precluding the formation of moraines underneath the tongue.

While the paths of turbid meltwater plumes and icebergs are controlled primarily by wind and ocean currents (e.g. Dowdeswell & Bamber, 2007; Andreassen *et al.*, 2008; Mugford & Dowdeswell, 2010), the location of meltwater deposits may change as a control of the position of meltwater efflux from the glacier (cf. e.g. Pfirman & Solheim, 1989; Trusel *et al.*, 2010; Kehrl

et al., 2011). Notwithstanding this, the distribution of sediment within a fjord is also largely controlled by climate-independent factors, such as the Coriolis force (e.g. Dowdeswell, 1987; Howe *et al.*, 2010), and fjord morphology (e.g. Powell & Molnia, 1989). Indeed, topography has been recognised as an important factor influencing local ice dynamics and sedimentary deposition. Among these controls are both the bathymetry of the fjord, but also the glacier's underlying topography (Fig. 5.7). As glacier flow is partially controlled by basal drag (the resistance of the glacier bed to ice flow), the presence of many "sticky spots" will hamper glacier flow, an effect further enhanced by an uneven and undersaturated glacier bed (Alley, 1993; Stokes *et al.*, 2007; Benn & Evans, 2010). Incidentally, the nature of the glacier substrate also plays a role in landform formation, as softer, more saturated sediments are more easily deformable and therefore can facilitate the development of glacial lineations and CSRs (cf. e.g. Clark *et al.*, 2003; Ottesen & Dowdeswell, 2006; MacLachlan *et al.*, 2010). The absence of those landforms in some fjords could thus be explained by variability in the composition of the glacier bed. Given the relationship between bumps in the glacier bed and ice flow behaviour, bedrock highs in a fjord can temporarily stabilise a glacier margin as it retreats, by serving as so-called pinning points (e.g. Warren, 1991; Ó Cofaigh *et al.*, 1999). Temporary stabilisation can then be accompanied by the formation of large glacial outwash fans, debris lobes, and turbidite deposits (cf. e.g. Boulton, 1986; Powell, 1991). Bathymetric highs can also facilitate the redistribution of glacimarine sediments into the deeper parts of the fjord (cf. Hogan *et al.*, 2012), as their slopes are normally too steep to permit the accumulation of thick sedimentary sequences.

Fjord width and water depth are further controls that have been suggested to influence glacier margin stability and they can also regulate the distribution of the meltwater plume. Considering that sediment concentration in meltwater plumes and hence sediment accumulation rates decrease with increasing distance from the ice margin (e.g. Elverhøi *et al.*, 1983; Syvitski *et al.*, 1996), and that a meltwater plume, once exiting the glacier and rising, spreads radially along the surface of the water column (e.g. Mugford & Dowdeswell, 2011), it is reasonable to assume, that a wider, more open fjord would promote the spreading of a meltwater plume and hence the distribution of its suspension load over a wider area (section 4.5.4). Additionally, wider fjords tend to be more exposed to wind or ocean currents, which may alter the lithological record by reworking the deposited sediments. In contrast, in narrower fjords, the meltwater plume is confined to a relatively small space, allowing it to extend over long distances, and to deliver fine-grained mud also into areas far away from the glacier margin, particularly during periods of higher meltwater flux (e.g. Dowdeswell & Cromack, 1991). The process of plume dispersal and an associated re-distribution of suspended particles can actually be observed on aerial imagery from many Svalbard fjords (Fig. 5.8). The presence of a sill or another large, fjord-transverse obstacle, such as a moraine, can be of importance here, as, in some cases, trapping of sediment has been observed behind a morphological barrier (cf. e.g. Syvitski *et al.*, 1996; Kempf *et al.*, 2013). As a result, accumulation of sediments is likely to be spatially variable within a fjord.

Fjord width also plays an important role for glacial dynamics, as ice margins tend to retreat faster in wider embayments, whereas narrow fjords can both provide pinning points for the glacier to halt at, and slow ice retreat owing to increased lateral drag (cf. e.g. Warren & Glasser, 1992; Benn *et al.*, 2007b; Benn & Evans, 2010; Åkesson, 2016). Similarly, deeper water generally promotes faster retreat, whereas shallower water slows down the glacier (e.g. Benn *et al.*, 2007a; Kehrl *et al.*, 2011). This is partly due to ungrounding of the glacier front in bathymetric overdeepenings, where subglacial melt and, accordingly, faster retreat can be

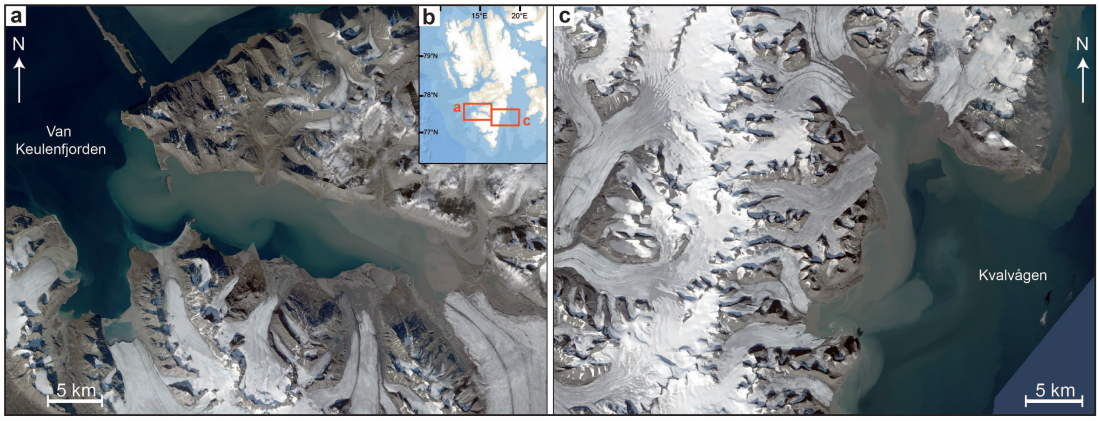

Figure 5.8: *Examples of the distribution of meltwater plumes exiting tidewater glaciers in Spitsbergen from a) van Keulenfjorden, and b) Kvalvågen. Aerial imagery is taken from TopoSvalbard, courtesy of the Norwegian Polar Institute. Note how the colour of the meltwater varies from more opaque in narrower confinements to more transparent in wider embayments, indicating the dispersal of the carried suspension load.*

promoted by the inflow of warm, more saline seawater into the basin underneath the glacier (O'Leary & Christoffersen, 2013; Straneo & Heimbach, 2013; Rignot *et al.*, 2016). Water depth can also control the distribution of landforms; one example of this are iceberg ploughmarks, which only occur where keel depths are larger than water depths (cf. Dowdeswell & Forsberg, 1992; Solheim, 1997).

Water depth can, in turn, be influenced by sedimentation at the glacier grounding line. Several studies have shown that the retreat velocity of a glacier margin decreased when sediment accumulation at the grounding line was high, as the associated shoaling waters effectively inhibited calving (e.g. Powell, 1991; Benn *et al.*, 2007a; Kehrl *et al.*, 2011). Tidewater glaciers with a higher sediment yield could therefore experience longer phases of stillstand than those where sediment availability is scarce, causing variability in the landforms, particularly regarding size. Sediment yield can also have an effect on the visibility of glacial landforms on swath-bathymetric data, as sediment draping could bury previously formed landforms, particularly in ice-proximal locations. Sediment yield in a glacier can be highly variable and changes according to factors such as bedrock erodability (partially promoted by a warmer climate), topography and the glacier's ability to erode and entrain debris (e.g. Hallet *et al.*, 1996; Benn & Evans, 2010). Surging glaciers have been documented to not only show some of the highest erosion rates, but also to be very rich in glacial debris due to their rapid movement, their commonly crevassed nature, their ability to thrust forwards ice and glacial debris, and their tendency to override and re-entrain debris deposited during a previous surge (cf. e.g. Clapperton, 1975; Sharp *et al.*, 1994; Hambrey *et al.*, 1996, 1999). Moreover, meltwater flux is commonly increased during and directly after a surge (e.g. Gilbert *et al.*, 2002; Zajaczkowski *et al.*, 2004), which also amplifies sediment delivery to fjords with surging glaciers at their heads.

The fact that the nature of the catchment area has some impact on the type of sediment deposited in the fjords is clearly shown in the sediment characteristics. The colour is variable and is usually influenced by the bedrock geology (cf. Andrews & Principato, 2002; Rasmussen & Thomsen, 2013). Devonian red sandstones cropping out over large parts of Spitsbergen, for example, cause mud deposited in the inner parts of Kongsfjorden to be of a characteristic reddish-brown/pink colour (cf. Rasmussen & Thomsen, 2013). Conversely, the greyish-green colour in sediments in the outer fjords is probably related to increasingly carbonate-rich material, derived either from carbonate rocks eroded on the island (Kongsfjorden; Streuff, 2013), or from the increasing abundance of organic fauna in hemipelagic sediments (Lomfjorden; cf.

Wilson & Austin, 2002). Mineralogical analyses have indeed shown a close relationship between the geology of the glacier's hinterland and the fjord floor sediments, and can even be used as tracers for sediment provenance (e.g. Forwick *et al.*, 2010; Andrews, 2011; Andrews & Eberl, 2012; Streuff, 2013).

As discussed in section 5.6.3, time is another important factor, particularly with regards to landform morphology and size, with longer stillstands leading to the development of a larger, more defined end moraine (cf. e.g. Boulton, 1986). The same holds true for proglacial outwash fans or ice-marginal debris flows; the development of trough-mouth fans at the front of many ice streams terminating at the edge of continental shelves during the LGM provides clear evidence for this (e.g. Laberg & Vorren, 1995; King *et al.*, 1998).

A range of other factors also influence glacimarine sedimentation. These include the location of meltwater efflux at the glacier front, the sediment concentration within a meltwater stream (which in turn depends on the erodability of the glacier bed), sea water characteristics, iceberg availability, the nature of the glacier grounding line, and the flow energy in a meltwater stream (cf. e.g. Powell, 1981; Gilbert, 1983; Cowan & Powell, 1990; Syvitski, 1993; Szczuciński & Zajaczkowski, 2012). Changing locations of meltwater stream effluxes at Kongsbreen/Kronebreen, have, over time, led to the deposition of several bathymetric highs (Trusel *et al.*, 2010; Kehrl *et al.*, 2011), which presumably mainly contain glacial outwash facies. Sediment concentrations within meltwater plumes tend to decrease with increasing distance from the glacier margin, as they progressively lose momentum (Pfirman & Solheim, 1989; Syvitski, 1989). As a consequence, coarse-grained debris is usually deposited close to the ice margin, whereas finer mud is transported in suspension for longer distances (e.g. Dowdeswell, 1987; Boulton, 1990; Powell, 1991; Ó Cofaigh & Dowdeswell, 2001). This has direct implications for the sedimentary record, not only for predominant grain size at a given location in a fjord, but also for sediment accumulation rates, which have been observed to decrease exponentially away from the ice margin (Elverhøi *et al.*, 1983; Sexton *et al.*, 1992; Syvitski *et al.*, 1996). In cyclically laminated lithofacies slower accumulation in distal areas is particularly obvious, because individual couplets comprise increasingly thinner laminae with increasing distance from the source (e.g. Mackiewicz *et al.*, 1984). Moreover, greater distances from the ice margin can, for instance, lead to the formation of bioturbated facies and the absence or lower frequency of turbidity currents. Nevertheless, the greater the distance to the ice margin, the smaller the influence of the meltwater plume on the depositional environment. Accordingly, the appearance of predominantly coarser grains is common in very distal areas, where IRD or sand from gravitational mass flows are no longer swamped by the meltwater-derived fines (section 4.4.3; e.g. Gilbert, 1978; Dowdeswell & Dowdeswell, 1989; Boulton, 1990; Cai *et al.*, 1997; Barrie & Conway, 2002). Seawater characteristics, particularly oceanographic currents, control sedimentation as stronger currents may cause particles to be retained in suspension for a longer time period than normal. Tidal currents are of particular importance in this context, as the release of suspension load from meltwater plumes is often subject to the diurnal changes between high and low tide (Mackiewicz *et al.*, 1984; Cowan, 1992). Such currents can also lead to the re-entrainment of already settled grains into suspension, thus altering the stratigraphic and lithological record (e.g. Cowan & Powell, 1990; Ó Cofaigh & Dowdeswell, 2001). Iceberg availability directly controls the abundance of IRD in a fjord and also impacts the landform record by forming iceberg ploughmarks thereby reworking the seafloor sediments, if iceberg keels are sufficiently deep. The meltwater flux is important because it strongly influences the depositional environment. Turbid meltwater plumes for instance produce different lithofacies

compared to those deposited from hemipelagic sedimentation, and overflows produce different lithofacies to underflows (Mackiewicz *et al.*, 1984). The turbidity of a meltwater plume can, again, be influenced by the distance to the ice margin. The latter may also encourage formation of turbidity-current channels (Powell, 1981). In addition to grain-size, the settling velocity of sediment particles can also be affected by the degree of clay particle flocculation and the oceanographic circulation patterns in the water column, thus causing differences in the lithological deposits (e.g. Gilbert, 1982; Ó Cofaigh & Dowdeswell, 2001; Szczuciński & Zajaczkowski, 2012).

In summary, the principal sedimentary processes, and, accordingly, the associated lithofacies in glacimarine environments of Spitsbergen and West Greenland are strikingly similar to those documented in high-latitude fjords elsewhere, but ice dynamics and the relative importance of individual sedimentary processes can be different even for adjacent glaciers and fjords. The seemingly random distribution of landform- and lithofacies-types across High-Arctic fjords therefore provides evidence that the composition of landform assemblages, i.e. which landform types co-exist, and the final lithological product, i.e. whether muds will be stratified or rhythmic or massive, is not only modulated by geographic location and thus climate, but is rather more dependent on an exceedingly complex system of locally variable external factors.

5.7 Conclusions

- Modern tidewater glaciers form a variety of landform types. These include ice flow-parallel landforms such as streamlined bedrock, glacial lineations, drumlins and crag-and-tails, which normally form during ice advance. Terminal moraines and associated debris lobes on their distal flanks form after advance has ceased, and commonly mark the position of maximum glacier extent. During retreat a number of recessional features can form, among which are most commonly larger recessional moraines, and smaller De Geer moraines, annual push moraines and/or crevasse-squeeze ridges. Eskers and (in some cases turbidity-current) channels are indicative of large quantities of meltwater and its erosive power in the fjords. Similarly, iceberg ploughmarks develop where calved icebergs are present and have keels deep enough to scour the sea-bottom. Gravitational mass-flow events are more common in some fjords than in others and their occurrence can be aided by regional tectonics and continuously high sediment accumulation rates. The common landform types, alongside the common lithofacies in High-Arctic fjords were summarised in a conceptual model.

- The glacimarine sedimentary processes in front of tidewater glaciers are identical across a wide range of geographic locations and generally include (1) the deposition of sediments carried in glacial meltwater, occurring through rainout from suspension and through settling from bedload, (2) the rainout of coarser-grained IRD from icebergs and sea ice, (3) the meltout of glacial debris directly at the glacier grounding line, and (4) the deposition of sediment from gravitational mass flows. The latter act both as a source for debris in fjords and as an agent for sediment reworking. Reworking also occurs through the keels of icebergs, if present. These processes generally lead to the accumulation of fine-grained glacimarine mud, coarser-grained, heterogeneous pebbly muds and diamicts, and sharp-based sands.

- The principal sedimentary processes are locally controlled by external factors which not only account for variations in the internal structure, the sorting, and the colour of the resulting lithofacies, but also in the occurrence and distribution of landforms within a fjord. While

climate plays some role in controlling glacial growth and decay, thus regulating ice dynamics but also meltwater and iceberg flux to some degree, its effect on the sedimentary processes and products in front of fjord-terminating tidewater glaciers appears to be less important than previously thought. This is particularly obvious in, for instance, the occurrence of stratified mud and diamict in West and East Greenland and in Alaska, which shows that ice rafting can be equally important in these settings despite their contrasting classification as temperate and polar glacimarine. Similarly, the abundance of meltwater-derived mud observed in West Greenland and the predominance of laminated muds from suspension settling in some fjords of East Greenland show that the influence of meltwater on glacimarine sedimentation is not necessarily related to geographic location or climate.

- Glacier dynamics can be highly diverse even within geographically adjacent fjords and are not exclusively governed by climatic influences. They should therefore not be generalised across larger areas, but should be assessed individually.

Chapter 6

Concluding remarks

6.1 Main findings

This study investigated the landforms and lithofacies in seven fjords in Spitsbergen and West Greenland in order to reconstruct the Holocene glacimarine environments in front of modern fjord-terminating tidewater glaciers. Using acoustic and lithological data glacial landforms and lithofacies were identified and compared to those in fjords of Alaska, the Canadian Arctic and other Svalbard and Greenland fjords. The landforms and lithofacies in High-Arctic fjords were summarised in a new conceptual model for contemporary tidewater glacier sedimentation and include twelve types of landforms and nine different lithofacies. The landforms are (1) (streamlined) bedrock highs, (2) (mega-scale) glacial lineations, (3) crag-and-tails/drumlins, (4) terminal moraines often associated with (5) large debris lobes on their distal flanks, (6) recessional moraines, (7) De Geer moraines, (8) crevasse-squeeze ridges, (9) iceberg ploughmarks, (10) gullies and submarine channels, the latter sometimes filled to form eskers, (11) mass-transport deposits, and (12) pockmarks. The lithofacies are (1) massive, (2) bioturbated, (3) stratified/laminated, and (4) pebbly glacimarine mud, (5) stratified mud and sand, (6) stratified mud and diamict, (7) poorly sorted, massive sand, (8) massive, matrix-supported diamict, and (9) diamict with deformation structures.

From these observations it can be deduced that the main formation mechanisms for submarine glacial landforms are (1) deposition directly at the glacier grounding line by meltout, pushing, and thrusting of glacial debris and related slope failure, (2) erosion and re-deposition of subglacial debris by entrainment, transport, and subsequent meltout, (3) erosion of sediment by meltwater, with the former being re-deposited by suspension settling and mass-transport events, and (4) sediment infill of cavities by the settling of material carried in glacial meltwater streams or by upwards-squeezing into basal crevasses.

From the lithofacies, the following principal glacimarine sedimentary processes are inferred: (1) sediment rainout from glacial meltwater, (2) meltout from icebergs and sea ice and (3) meltout directly from the glacier grounding line, and (4) sediment deposition from gravitational mass flows. Sediment reworking occurs through mass flows and iceberg scouring. A certain variability in the occurrence of specific landform types and the internal structure of particular lithofacies suggests that these general processes are influenced by a range of local controls and that climate is not the pivotal factor controlling tidewater-glacier sedimentation.

Radiocarbon and Lead/Caesium dates allowed for the calculation of sediment accumulation rates. These were highest directly after a surge of Kongsvegen, where deposition occurred as fast as 30 cm a^{-1}. In the other fjords, SARs were much lower, ranging from 0.02 cm a^{-1} in ice-distal areas to 2.9 cm a^{-1} in more proximal regions. A SAR of 3.3 cm a^{-1} was observed in a submarine basin in Magdalenefjorden, which could reflect relatively proximal conditions during deposition or, more likely, enhanced sediment accumulation aided by gravitational

processes into the basin. The dates further provided constraints on the timing of individual ice dynamics, and in some cases allowed for the estimation of retreat velocities of the ice margins during deglaciation. In Kongsfjorden, a surge of the conjoined Kongsvegen and Kronebreen ice margins was confirmed for around 1948. A date of around 320 a BP from Magdalenefjorden provided a time frame for a glacier re-advance associated with the Little Ice Age cooling. In Lomfjorden, the radiocarbon dates obtained from ice-distal sediment in the outer fjord enabled the constraint of a minimum deglaciation age, whereas radiocarbon dates from Disko Bay provided further information on the mode of retreat of Jakobshavn Isbræ through the bay.

The examples of landforms and lithofacies observed in different fjords of the northern hemisphere, along with the detailed analyses carried out in this study, suggest that while the principal sedimentary processes and products in glacimarine settings are similar across wide geographic areas, one cannot generalise glacimarine environments according to climate alone. This study shows that while warming air and ocean temperatures are certain to promote subaerial and subglacial melt, the response of a glacier to climate can be highly individual, and is dependent on the intricate system of different influences, that make a glaciated fjord unique.

6.2 Future work

This study emphasises the spatial and temporal variability of tidewater glacier dynamics across the northern hemisphere and highlights the need for future studies, such as:

- to investigate an increasing number of tidewater glaciers, particularly those that drain Earth's remaining ice sheets, as it will only be possible to gain a better idea of their potential future behaviour with a comprehensive knowledge of their past dynamics;
- to correlate reconstructed glacier dynamics with past climatic events in order to better understand how the glaciers previously reacted to a changing climate. Again, a particular focus on the fast-flowing outlet glaciers of Greenland and Antarctica in this context might provide a better understanding of the potential ramifications of global warming, as these glaciers are intrinsically linked to ice sheet stability and, therefore, sea level rise;
- to research whether the glaciers in the southern hemisphere behave similarly to those in the northern hemisphere by taking a closer look at the glacial landforms, dynamics and sediments in Antarctica and Patagonia;
- to develop increasingly detailed reconstructions of past ice sheet extents and their dynamics in order to encourage more accurate predictions of future ice sheet behaviour. While a lot of work is already being done in this respect, the work from Lomfjorden and Magdalenefjorden shows that current models of the Svalbard-Barents Sea Ice Sheet are, in many areas, based on estimations and need to be re-evaluated as further evidence emerges;
- to try and quantify the degree of control the numerous external factors actually have on glacimarine sedimentation. This could potentially be done by trying to isolate certain parameters and thereby estimate the relative importance of individual controls.

Chapter A

Submarine landform assemblages and sedimentary processes related to glacier surging in Kongsfjorden, Svalbard

Streuff, K.; Forwick, M.; Szczuciński, W.; Andreassen, K.; Ó Cofaigh, C. (2015): Submarine landform assemblages and sedimentary processes related to glacier surging in Kongsfjorden, Svalbard. *Arktos* (2015)1:14. DOI: 10.1007/s41063-015-0003-y.

Abstract

High-resolution swath-bathymetric data from inner Kongsfjorden, Svalbard, reveal characteristic landform assemblages formed during and after surges of tidewater glaciers, and provide new insights into the dynamics of surging glaciers. Glacier front oscillations and overriding related to surge activity lead to the formation of overridden moraines, glacial lineations of two types, terminal moraines, associated debris lobes and De Geer moraines. In contrast to submarine landform assemblages from other Svalbard fjords, the occurrence of two kinds of glacial lineations and the presence of De Geer moraines suggest variability in the landforms produced by surge-type tidewater glaciers. All the landforms in inner Kongsfjorden were deposited during the last c. 150 years. Lithological and acoustic data from the innermost fjord reveal that suspension settling from meltwater plumes as well as ice rafting are dominant sedimentary processes in the fjord, leading to the deposition of stratified glacimarine muds with variable numbers of clasts. Reworking of sediments by glacier surging results in the deposition of sediment lobes containing massive glacimarine muds. Two sediment cores reveal minimum sediment accumulation rates related to the Kongsvegen surge from 1948; these were 30 cm a^{-1} approximately 2.5 km beyond the glacier front shortly after surge termination, and rapidly dropped to an average rate of 1.8 cm a^{-1} in ∼1950, during glacier retreat.

A.1 Introduction

Glacier surges are cyclic switches between active and passive phases, during which the ice front may either advance rapidly (active), stagnate (transition), or retreat slowly (passive/quiescent phase; e.g. Meier & Post, 1969; Sharp, 1985; Raymond, 1987; Dowdeswell *et al.*, 1995; Gilbert *et al.*, 2002). They generally occur independently of climate and are triggered internally through, for example, changes in glacier hydrology or basal thermal regime (Meier & Post, 1969; Kamb, 1987; Raymond, 1987; Sharp, 1988). Surges are common on Svalbard, where they have a generally longer duration than elsewhere, with active phases of between 4 and 10 years and quiescent phases of between 50 and 500 years (Dowdeswell *et al.*, 1991; Murray *et al.*, 1998;

Benn & Evans, 2010). Many Svalbard glaciers have been identified as surge-type (e.g. Liestøl, 1969; Dowdeswell *et al.*, 1991; Hagen, 1993; Plassen *et al.*, 2004; Ottesen & Dowdeswell, 2006; Ottesen *et al.*, 2008), with surges well-documented from the past c. 180 years, but only two older examples (Paulabreen and Nathorstbreen; Liestøl, 1969; Hagen, 1993; Hald *et al.*, 2001; Kristensen *et al.*, 2009; Kempf *et al.*, 2013).

Glacier surges lead to the formation of characteristic landform assemblages, which are revealed when the glaciers retreat (e.g. Sharp, 1985; Solheim, 1991; Boulton *et al.*, 1996; Evans & Rea, 1999; Evans *et al.*, 1999; Evans, 2003; Ottesen & Dowdeswell, 2006; Ottesen *et al.*, 2008). Landforms related to glacier surges in submarine settings have been described from several Spitsbergen fjords (Boulton *et al.*, 1996; Plassen *et al.*, 2004; Ottesen & Dowdeswell, 2006; Ottesen *et al.*, 2008; Baeten *et al.*, 2010; Flink *et al.*, 2015). The landform models suggested thus far include overridden recessional moraines, (mega-scale) glacial lineations, terminal moraines with associated sediment lobes on their distal slopes, eskers, annual push moraines and crevasse-squeeze ridges, the latter suggested to be the only feature diagnostic of a glacier surge (Sharp, 1985; Ottesen *et al.*, 2008). The high detail preserved in submarine environments offers invaluable insights into the processes controlling landform genesis, and, together with lithological records from sediment cores, enables a better understanding of tidewater glacier sedimentation and dynamics (e.g. Boulton *et al.*, 1996; Ottesen & Dowdeswell, 2006; Ottesen *et al.*, 2008).

In this paper we present acoustic data (multibeam swath-bathymetry and high-resolution seismic data) and lithological analyses of two sediment cores from inner Kongsfjorden, Svalbard. We describe and interpret submarine landform assemblages and deposits related to glacier surges and show that such assemblages are more diverse than previously suggested.

A.2 Study area

Kongsfjorden is located on northwestern Spitsbergen, the largest island of the Svalbard archipelago. It is the southern branch of the Kongsfjorden-Krossfjorden fjord system (78°50'N, 11°40'E, and 79°04'N, 12°40'E; Fig. A.1). Kongsfjorden and Krossfjorden merge towards the open sea, where a large submarine trough, Kongsfjordrenna, channelled fast-flowing ice streams during the last glacial (e.g. Ottesen *et al.*, 2005; Ingólfsson & Landvik, 2013). Kongsfjorden is approximately 20 km long and between 4 and 10 km wide. It covers an area of $\sim$ 210 km^2, and has a volume of 29.4 km^3 (Ito & Kudoh, 1997). Water depths range from 350 m in the outer and central parts to <100 m in the inner fjord. A detailed review on Kongsfjorden's climate and oceanography was provided by Svendsen *et al.* (2002).

Seven tidewater glaciers terminate in Kongsfjorden: Løvlandbreen and Svansbreen form one tidewater front with Blomstrandbreen in the north of the fjord (Fig. A.1) and will be summarised by the term "Blomstrandbreen" throughout this paper. Conwaybreen, Kongsbreen and Kronebreen dominate the east of the fjord with Kongsbreen terminating as two tidewater margins, one north and one south of Ossian Sarsfjellet (Fig. A.1). Kongsvegen flows into the fjord from the south-east, adjacent to Kronebreen (Fig. A.1). Three of these glaciers have been documented to be of surge-type, with Kronebreen and Kongsvegen experiencing respective surges in 1869 and 1948, and Blomstrandbreen surging in 1960 (Liestøl, 1988; Hagen, 1993).

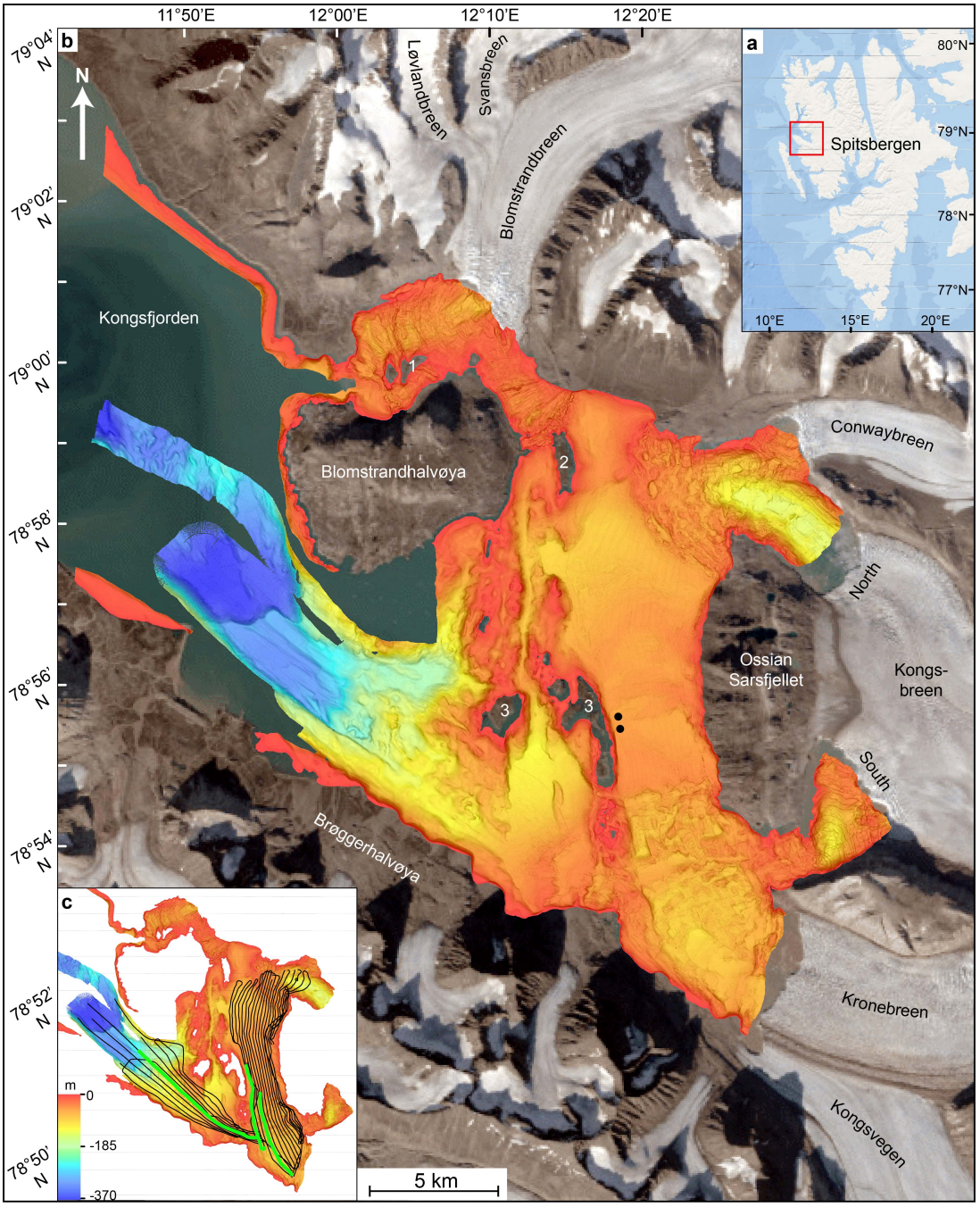

Figure A.1: *a) Map of Spitsbergen with red rectangle indicating the extent of b) swath-bathymetric data available for this study and surrounding areas. 1=Breøyane, 2=Gerdøya, 3=Løvenøyane. Black dots indicate the locations of the two sediment cores 10JM-GlaciBar-GC01 (south) and 10JM-GlaciBar-GC02 (north). Satellite imagery was downloaded from Svalbardkartet, courtesy of the Norwegian Polar Institute. c) Locations and extent of available chirp lines, with bright green lines showing the location of profiles in Fig. A.6. The colour scale indicates water depth and refers to both, b) and c).*

A.3 Glacial history

The glacial history of the Svalbard archipelago during and since the Late Weichselian is documented to have occurred in three main stages: (a) ice advance, (b) full glaciation during the Last Glacial Maximum (LGM), and (c) ice retreat (see e.g. Elverhøi *et al.*, 1995; Landvik *et al.*, 1998; Jessen *et al.*, 2010).

During initial advance, ice extended beyond the present coastline, reaching the shelf break between ∼24 and 23.5 ka BP (Landvik *et al.*, 1998; Jessen *et al.*, 2010). Fast-flowing ice streams drained the Svalbard-Barents Sea Ice-Sheet via the main fjord systems on Svalbard, including Kongsfjorden (e.g. Ottesen *et al.*, 2005, 2007; Ingólfsson & Landvik, 2013). A terminal moraine at the shelf break in southern Kongsfjordrenna was inferred to reflect maximum ice extent during the Late Weichselian (Ottesen *et al.*, 2007). Deglaciation of the shelf and fjords on West Spitsbergen began around 20.5 ka BP and was interrupted by multiple glacier halts and/or re-advances (e.g. Ottesen *et al.*, 2007; Baeten *et al.*, 2010; Jessen *et al.*, 2010; Forwick *et al.*, 2009; Forwick & Vorren, 2011; Kempf *et al.*, 2013). The deglaciation of Kongsfjorden proper was documented as a two-stage recession initiated ∼13 ka BP, leading to ice-free conditions by approximately 9 ka BP (Lehman & Forman, 1992). Recent findings by Henriksen *et al.* (2014), however, show that the ice stream in Kongsfjorden had retreated to the fjord mouth by 16.6 ka BP, and that the deglaciation of the areas west of Blomstrandhalvøya was already complete before 14.4 ka BP.

Asynchronous re-growth of Svalbard glaciers occurred after c. 9 ka BP (e.g. Forwick & Vorren, 2007; Forwick *et al.*, 2009; Baeten *et al.*, 2010; Forwick *et al.*, 2010). Maximum Late Holocene glacier extents occurred either due to climatic cooling during the Little Ice Age or due to glacier surges (e.g. Liestøl, 1969; Dowdeswell *et al.*, 1991; Hagen, 1993; Plassen *et al.*, 2004; Ottesen & Dowdeswell, 2006; Mangerud & Landvik, 2007; Ottesen *et al.*, 2008; Kempf *et al.*, 2013).

A.4 Material and methods

Swath-bathymetry, sub-bottom profiler (chirp) data and sediment cores acquired in autumn 2010 with R/V Jan Mayen (now R/V Helmer Hanssen) from inner Kongsfjorden provide the basis for this study (Fig. A.1). A Kongsberg Maritime Simrad EM 300 multibeam echo sounder was used to acquire the bathymetric data (max. resolution of 5 m). The instrument operated at a frequency of approximately 30 kHz and was calibrated using p-wave velocities for the water column obtained from CTD (conductivity, temperature, depth) measurements. The bathymetric data were supplemented with multibeam data from the Norwegian Hydrographic Survey gridded to a max. resolution of 5 m and visualised and interpreted using the Fledermaus v7 3D Visualization and Analysing Software. Chirp data are exclusively available for the innermost part of Kongsfjorden (Fig. A.1c), where profiles were recorded using a hull-mounted EdgeTech 3300-HM sub-bottom profiler operating at a pulse mode of 2-12 kHz and 3 ms, while the ping rate was set to 1.9 Hz. The profiles were processed in the EdgeTech Software and interpreted using SMT The Kingdom Suite.

Two gravity cores, 10JM-GlaciBar-GC01 (GC01) and 10JM-GlaciBar-GC02 (GC02), were retrieved with a 1900 kg heavy gravity corer with a 6 m long barrel. After retrieval the cores were divided into sections of up to 1 m in length and were subsequently stored at +4°C. The core sites are located ∼310 m apart from each other, with GC01 (78°55'50"N, 12°20'49"E; 50 m water depth; 286 cm length) recovered from the top of a sediment wedge (representing a debris lobe deposited from a glacier surge, see section A.5.3 below), and GC02 (78°55'59"N, 12°20'36"E; 53 m water depth; 339 cm length) from c. 130 m beyond this wedge (Fig. A.1b). The p-wave velocity of the sediments was measured in 1 cm increments using a GEOTEK multi-sensor core logger (MSCL) at UiT - The Arctic University of Norway prior to opening of the cores. Lithological logs are based on visual descriptions of the sediment surfaces as well as

x-radiographs taken with a Philips Macrotank (5 mA; 80 kV; exposure times: 100 s to 4 min). Colour images were acquired with a Jai L-107CC 3CCD RGB Line Scan Camera installed on an Avaatech XRF core scanner. Sediment samples (∼1 g every 10 cm) were measured with a Beckman Coulter LS13320 Laser Diffraction Particle Size Analyzer to obtain information on grain size distribution. Prior to measurements each sample was dissolved in 50 ml of water and homogenised in a shaker.

Sediment accumulation rates (SARs) for the last century were determined through complementary ^{210}Pb and ^{137}Cs analyses, as previously used for Svalbard fjords (Svendsen *et al.*, 2002; Zajaczkowski *et al.*, 2004; Zaborska *et al.*, 2006; Szczuciński *et al.*, 2009). Activities of both isotopes were measured with gamma spectroscopy using a Canberra GX2520 high-purity coaxial germanium detector at the Institute of Geology, Adam Mickiewicz University in Poznań, Poland. For this, sediment samples of about 20 g were taken from 10 cm thick intervals, dried and ground. Obtained activities were decay-corrected to the date of sampling, and the results are presented with a two-sigma standard deviation uncertainty range. From the decrease of excess ^{210}Pb activities with sediment depth, SARs could be calculated (following McKee *et al.*, 1983). Excess ^{210}Pb activities were determined by taking the average supported activity from the sample below the region of radioactive decay, and subtracting it from the total activity. The independent SAR assessment was made using the first occurrence of ^{137}Cs as a marker of the early 1950s (taken as 1952), its maximum activity peak as ∼1962 and the younger secondary activity peak as Chernobyl-related 1986 (e.g. Robbins & Edgington, 1975; Appleby, 2008). However, due to the possible loss of the core top sediment during the coring process, sediment mixing, variations in SARs and low activities of excess ^{210}Pb, the calculated SARs should be treated as approximate values.

A digital terrain model (DTM) from 2009 with a vertical resolution of 5 m (Delmodell 5m 2009_13822_33, courtesy of the Norwegian Polar Institute, provided on geodata.npolar.no) was supplemented with satellite imagery available on Google Earth (August 2015) and visualised in Esri ArcMap 10.2. Superficial crevasses were then mapped on all tidewater glaciers in Kongsfjorden within ∼1 km of the current glacier fronts.

A.5 Results and interpretations

A.5.1 Seafloor morphology

Landforms occurring in Kongsfjorden are described and interpreted in the following section. Their distribution is shown in Figure A.2.

A.5.1.1 Large transverse ridges – overridden moraines

10–30 m high ridges are orientated generally transverse to the direction of ice flow and occur in front of Kronebreen/Kongsvegen and Blomstrandbreen (Fig. A.2b). They are up to 300 m wide and around 1 km long. Their crests are round, smooth, cross-cut by streamlined bedforms (section A.5.1.2) and are overprinted by small sharp-crested transverse ridges (section A.5.1.4).

The large ridges are very similar to transverse ridges from Borebukta (Ottesen & Dowdeswell, 2006) and are thus interpreted to be moraines deposited by a tidewater glacier during an earlier phase of stagnation or retreat. These ridges were then overridden during a subsequent advance, leading to the formation of the streamlined bedforms described in section A.5.1.2. The occurrence of several of these moraines in front of Kronebreen and Kongsvegen (Figs. A.2b and A.3a) suggests that here they represent recessional moraines

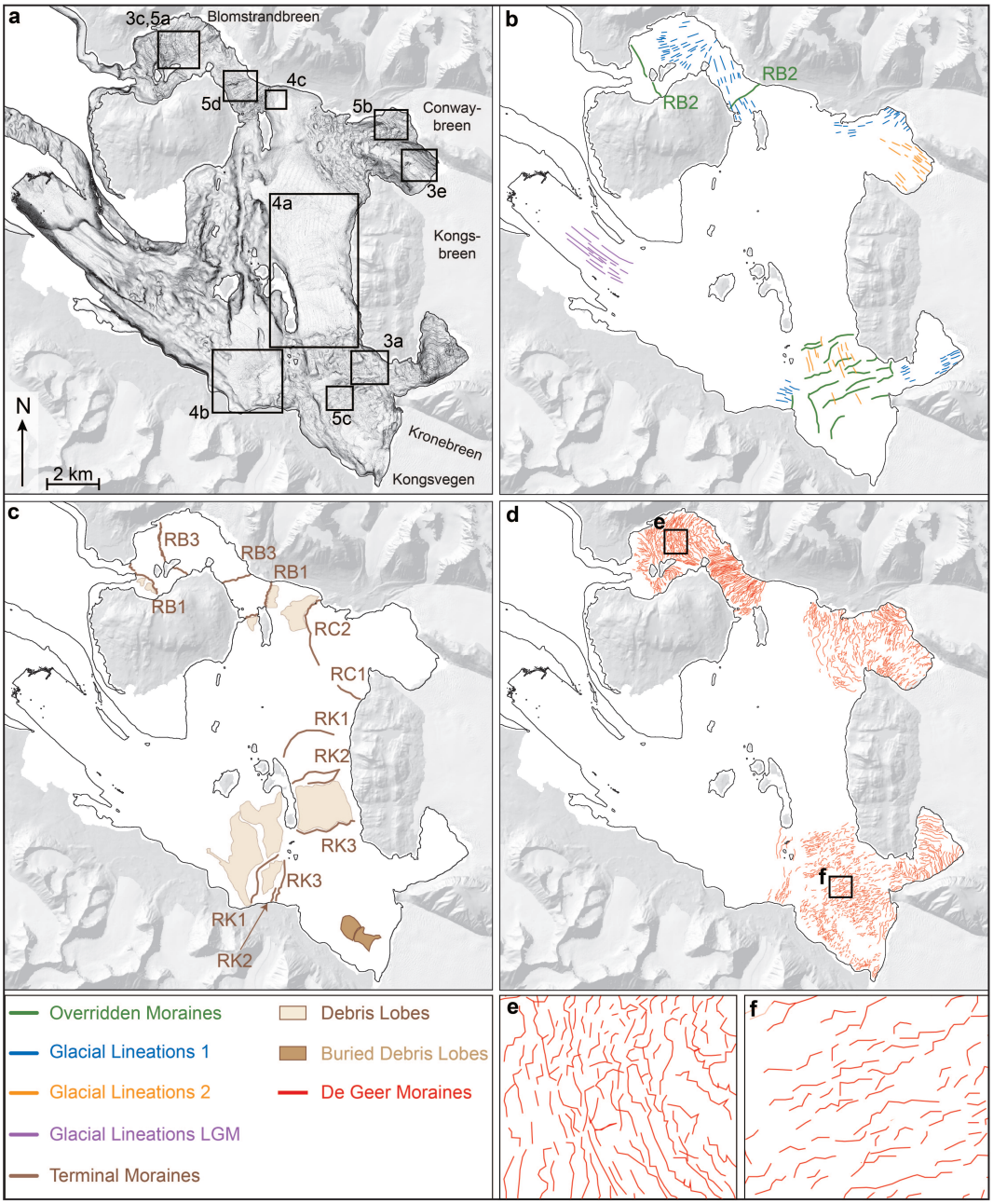

Figure A.2: *a) Overview of the bathymetric relief and indication of the locations for subsequent figures; b) Map of overridden moraines and glacial lineations; c) Map of terminal moraines and debris lobes. The bathymetric high refers to work from Trusel* et al. *(2010) and Kehrl* et al. *(2011); d) Map of De Geer moraines in the fjord, with indications of locations of the detail figures e) and f). Maps in this chapter were created using a Svalbard DTM, available online from the Norwegian Polar Institute.*

deposited from repeated stillstands during overall retreat of the glacier. The single ridge in front of Blomstrandbreen (RB2, Fig. A.2b), however, probably represents a terminal moraine (cf. section A.5.1.3 below) from an earlier advance.

A.5.1.2 Streamlined bedforms – glacial lineations

Two types of streamlined bedforms are distinguished: (1) sets of parallel, 8 m high, 20-80 m wide, and up to 2 km long smooth-crested grooves and ridges, aligned parallel to the direction of

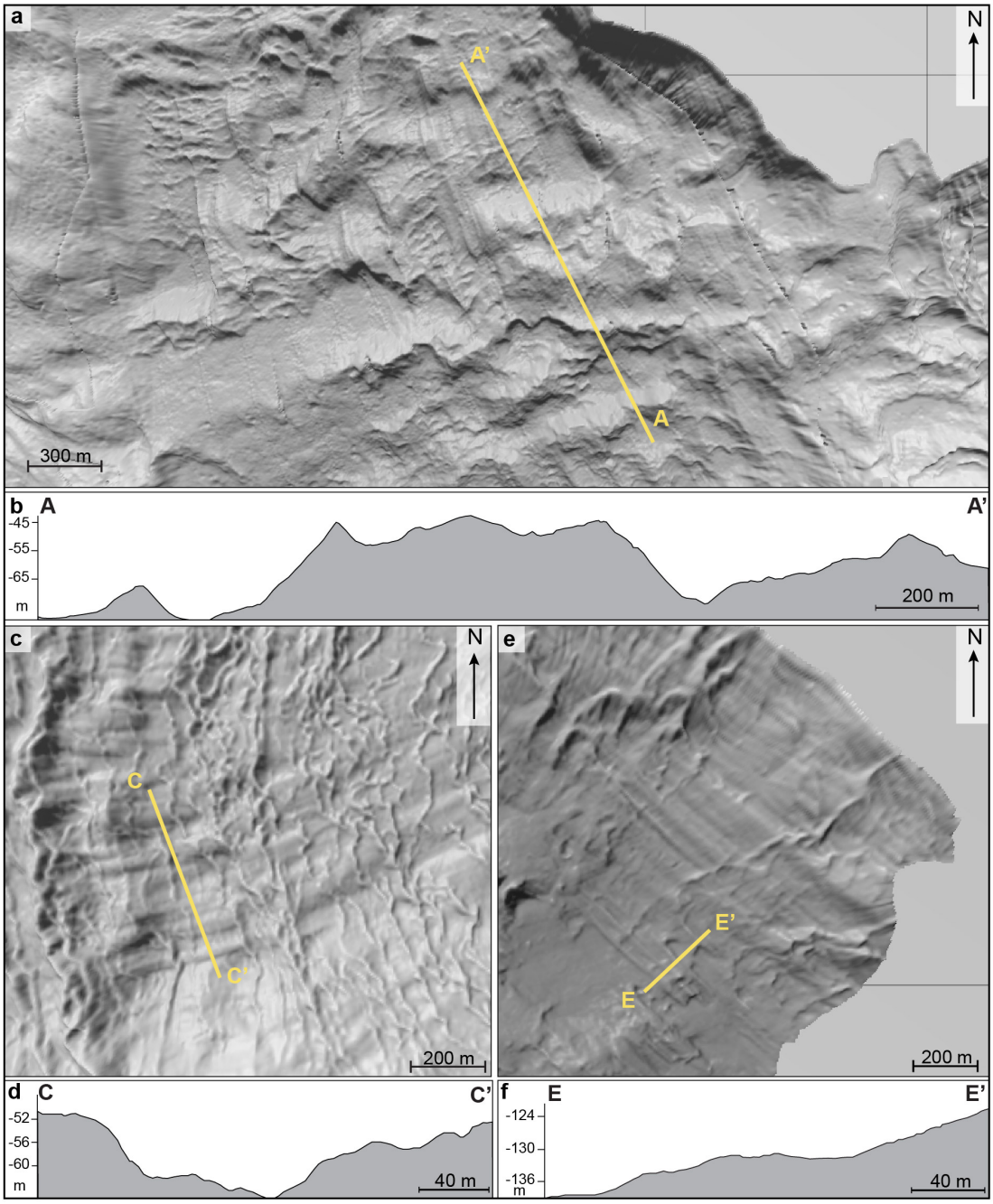

Figure A.3: *The locations of all subfigures are outlined in Fig. A.2a. a) Shaded-relief image of the bathymetry showing overridden moraines in front of Kronebreen/Kongsvegen, which are overprinted by streamlined bedforms and small transverse ridges. b) Profile A-A' from proximal to distal across overridden moraines. c) Groove-ridge features in front of Blomstrandbreen with the profile C-C' across them shown in d). e) Small streamlined ridges in front of Kongsbreen North. The profile E-E' across them is shown in f).*

ice flow (Figs. A.2b, A.3c) and (2) sets of parallel, ∼2 m high, ∼20 m wide and up to 600 m long sharp-crested grooves and ridges, also aligned parallel to the direction of ice flow and spaced at variable distances between 50 and 300 m (Figs. A.2b, A.3e). These latter features are confined to the areas in front of Kongsbreen North and Kronebreen/Kongsvegen, whereas the smoother groove-ridge features occur in front of Blomstrandbreen, Conwaybreen and Kongsbreen South. Similar features also appear in the outer fjord where they were likely formed during the last

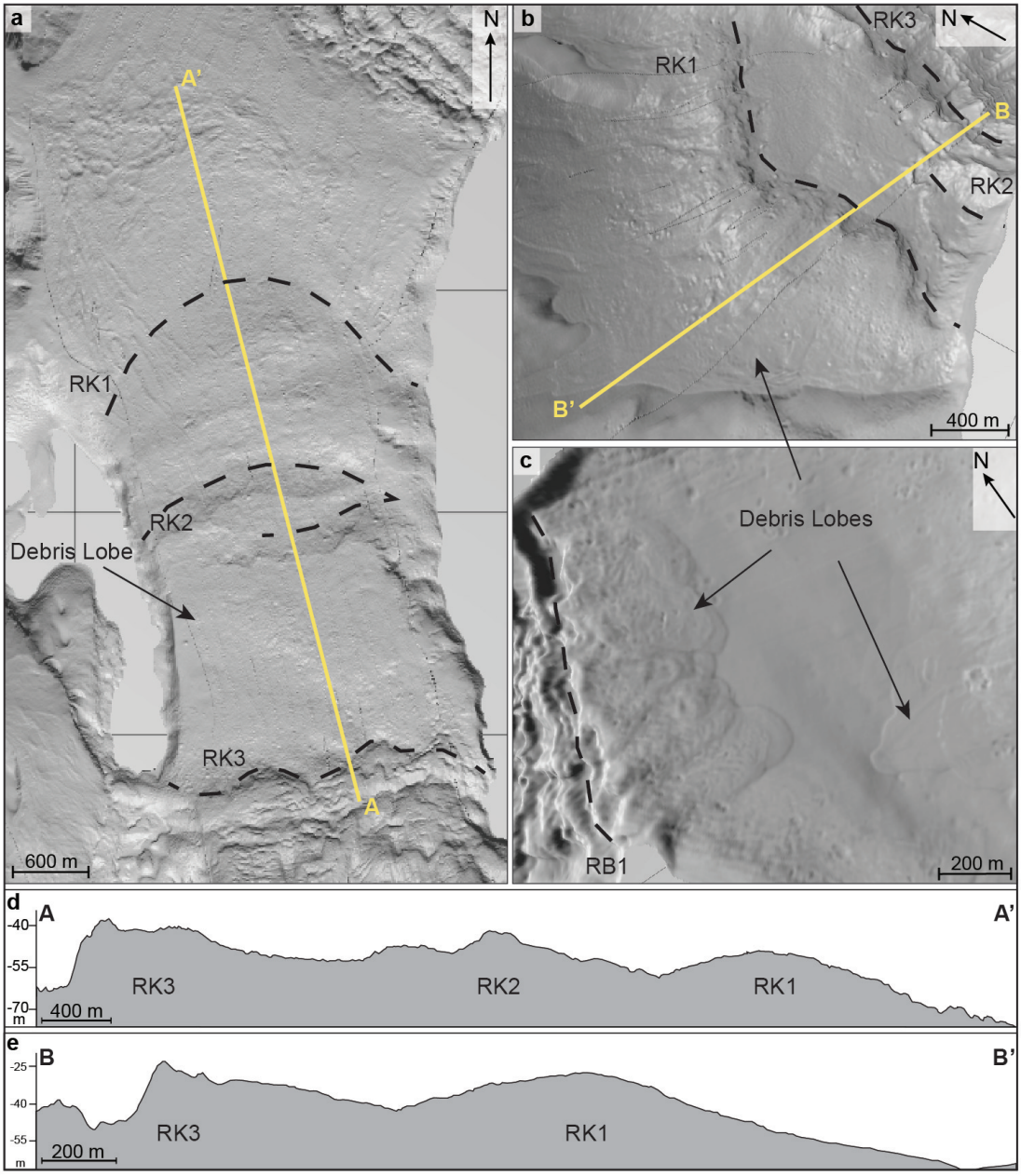

Figure A.4: *The locations of all subfigures are outlined in Fig. A.2a. a) Shaded-relief image of the bathymetry showing three terminal moraines in front of Kronebreen/Kongsvegen (RK1, RK2 and RK3), with RK1 marking the most distal moraine. b) Terminal moraines RK1, 2 and 3 west of Kronebreen/Kongsvegen. The large debris lobe associated with RK1 is also visible. c) Debris lobes off Blomstrandbreen's and Conwaybreen's outermost moraines, RB1 and RC2. Water depths range from -15 to -50 m. d) and e) show profiles A-A' and B-B', respectively, across RK1, RK2 and RK3 from proximal to distal.*

glacial (Fig. A.2b; MacLachlan *et al.*, 2010). With the exception of these latter features, all streamlined bedforms in Kongsfjorden are overprinted by small, transverse ridges (see section A.5.1.4).

The two types of streamlined bedforms in Kongsfjorden are interpreted to be glacial lineations. Based on appearance and dimensions, the grooves and ridges are similar to (mega-scale) glacial lineations (MSGLs; e.g. Clark, 1994; Stokes & Clark, 2002; Ottesen *et al.*, 2005; Ottesen & Dowdeswell, 2006; Andreassen *et al.*, 2007; Baeten *et al.*, 2010; Flink *et al.*, 2015),

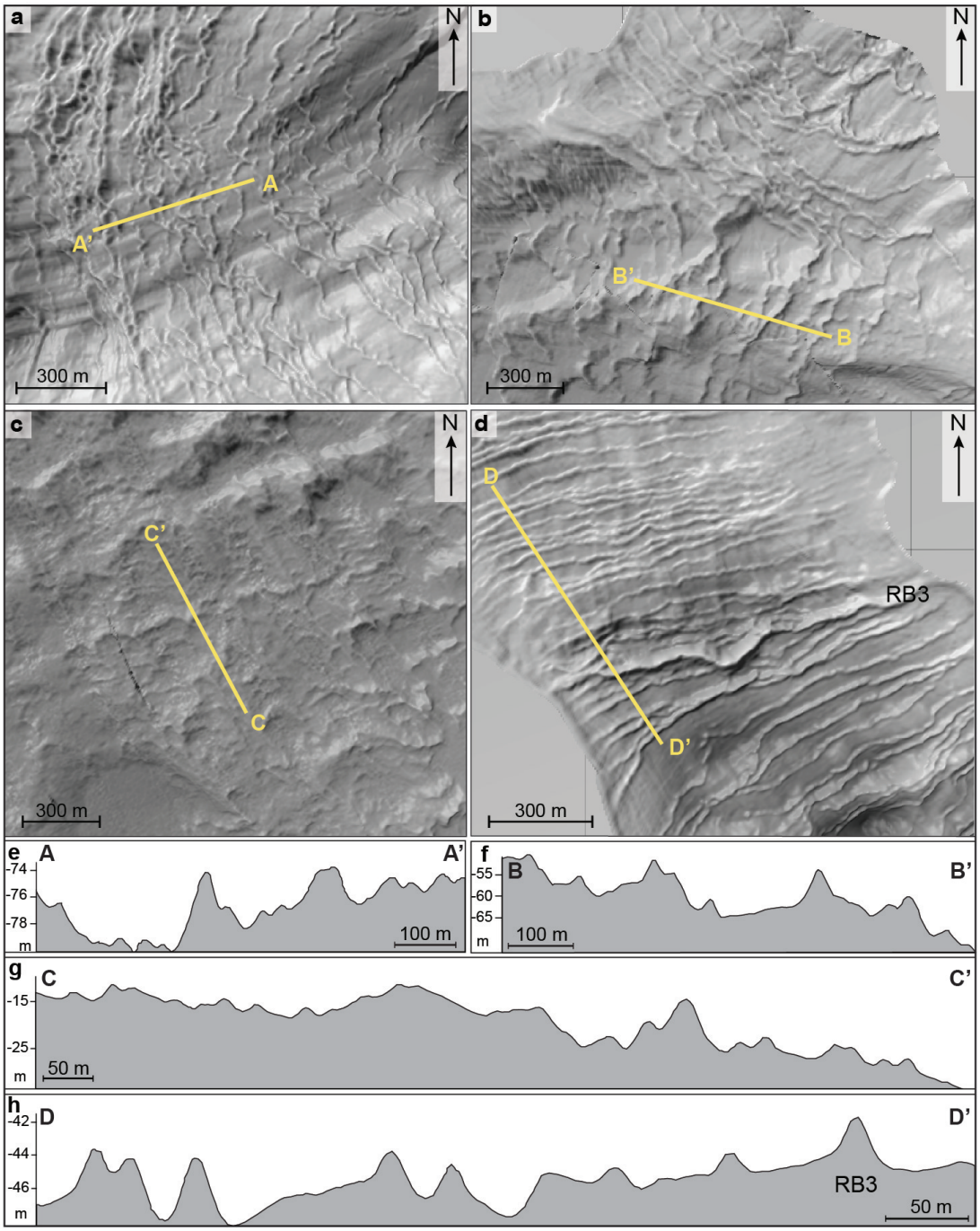

Figure A.5: *The locations of all subfigures are outlined in Fig. A.2a. Shaded-relief image of the bathymetry showing the different appearance of De Geer moraines in Kongsfjorden in front of a) Blomstrandbreen, b) Conwaybreen, c) Kronebreen/Kongsvegen and d) southeast of Blomstrandbreen. d) also shows the large moraine ridge RB3. Cross-sectional profiles across the features from proximal to distal are shown in e), f), g) and h) respectively.*

which are closely associated with fast ice flow (King *et al.*, 2009). Even though lineations in Kongsfjorden are much shorter (max. 2 km) than MSGLs described from elsewhere (up to 70 km; Clark, 1993), the majority have elongation ratios of 10:1 or greater, technically classifying them as MSGLs. We infer that the Kongsfjorden lineations resulted from the same processes forming MSGLs, i.e. fast ice flow (e.g. Stokes & Clark, 2002), when processes of erosion and re-deposition deform soft subglacial sediments into sets of grooves and ridges (cf. e.g. Tulaczyk

et al., 2001; Ó Cofaigh *et al.*, 2005; Ottesen *et al.*, 2008; King *et al.*, 2009). In Kongsfjorden fast ice flow was probably due to the onset of the active phase of a glacier's surge-cycle. We note, however, that the differences in size and crest morphology between the two lineation types in Kongsfjorden indicates that their formation probably occurred under slightly different conditions. This issue is further discussed in section A.6 below.

All glacial lineations in inner Kongsfjorden are inside the respective glaciers' maximum extents, so we interpret them to have formed within the last ∼150 years (see section A.6.2 below).

A.5.1.3 Large transverse ridges and lobe-shaped deposits – terminal moraines and debris lobes

Seven large transverse ridges occur in Kongsfjorden, three in front of Blomstrandbreen (RB1, RB2 (overridden), RB3; numbered from distal to proximal, Fig. A.2b,c), two in front of Conwaybreen and Kongsbreen North (RC1 and RC2) and three in front of Kronebreen and Kongsvegen (RK1, RK2 and RK3; Fig. A.2c). They are 15–35 m high, between 500 and 2000 m long and several hundred meters wide (Fig. A.4). Ridges in front of Blomstrandbreen and Kronebreen/Kongsvegen are separated into several segments by the surrounding islands (Fig. A.2c). The ridges occur at distances of between 3 and 9 km from the present ice margins and are characterised by generally steeper proximal and gentler distal flanks (Fig. A.4d,e). RB3 differs from the other ridges by being symmetrical in cross-section and narrower (max. 100 m); it also has a much sharper crest (see Fig. A.5d). With the exception of RB3 and RC1 the ridges occur in close association with lobe-shaped deposits on their distal flanks (Figs. A.2c, A.4b,c). These lobes occur as single deposits (up to 360 m wide and 600 m long) or in sets of (partly superimposed) tongue-shaped landforms. The latter can cover areas of up to 5 km^2. The lobes typically occur at water depths between 15 and 50 m, but one lobe in the southwestern part of the fjord extends down to c. 110 m.

In front of the Kronebreen/Kongsvegen ice margin two lobes have very similar characteristics, but are dissociated from terminal moraines (Fig. A.2c). They are separated by an approximately 3 m high elevation. Both features are located directly at the glacier margin and cover areas of 0.06 km^2 (380 x 160 m^2) and 0.04 km^2 (500 x 85 m^2), respectively. Chirp data reveal that these features are buried beneath stratified sediments (cf. section A.5.2, Fig. A.6c).

The large transverse ridges are inferred to be terminal moraines marking the maximum extent of, in most cases several, glacier advances. These ridges could be of glaciotectonic origin and reflect pushed-up, folded and/or thrust sub- or proglacial sediments, as described for other areas on Svalbard (e.g. Solheim & Pfirman, 1985; Boulton, 1986; Boulton *et al.*, 1996; Plassen *et al.*, 2004; Ottesen & Dowdeswell, 2006; Ottesen *et al.*, 2008; MacLachlan *et al.*, 2010). We suggest that the lobe-shaped landforms are debris lobes that represent either (1) a product of downslope mass transport of glacigenic sediment deposited from quasi-continuous slope failure on the distal side of the moraine during or after maximum ice extent, or (2) glacier-outwash fans formed by meltwater-related processes during maximum extent of the glacier (e.g. Boulton *et al.*, 1996; Plassen *et al.*, 2004; Ottesen *et al.*, 2008; Kristensen *et al.*, 2009). The sedimentary lobes in front of Kronebreen/Kongsvegen were probably formed from continuously high sediment supply from meltwater streams (cf. Trusel *et al.*, 2010; Kehrl *et al.*, 2011) and may indicate that the Kronebreen/Kongsvegen margin experienced a prolonged stillstand close to its 2010 position.

A.5.1.4 Small, predominantly transverse ridges – De Geer moraines

Numerous small ridges, that are 1–5 m high, several hundred meters long, and around 30 m wide (Figs. A.2d, A.5), are observed in Kongsfjorden. Although generally transverse and (sub-)parallel to each other, they have variable orientations and, in some cases, have a "saw-tooth" pattern in planform (Fig. A.2e,f). Individual ridges cross-cut each other in places, are spaced at irregular intervals between 5 and 100 m and can exhibit branching. They occur in water depths down to 150 m and have mostly sharp, symmetrical crests (Fig. A.5). Some ridges are longer and straighter than others, may extend across the entire width of the fjord and have slightly sinuous crests orientated exclusively perpendicular to the direction of ice flow (Fig. A.5d). About 55 of these latter ridges occur in the fjord basin southeast of Blomstrandbreen, where they have been deposited between the outermost terminal moraine and the current ice front (Fig. A.2d). 45 ridges or segments thereof extend between the outermost moraine and the current ice front of Conwaybreen, whereas about 30 ridges were deposited in the proximal basin of Kongsbreen South (Fig. A.2d). In front of Kronebreen/Kongsvegen, most of the small ridges are around 1 m high and show weakly defined crests and frequent changes in orientation (Figs. A.5c,g).

Based on their dimensions and morphology the small ridges are interpreted as De Geer moraines (e.g. De Geer, 1940; Zilliacus, 1989). De Geer moraines form subaquatically and typically occur as sets of transverse, parallel, irregularly spaced ridges that are around 3 m high, several hundred m long and up to 30 m wide (Zilliacus, 1989; Lundqvist, 2000). Two main mechanisms have been proposed for their formation: (1) the ridges are annual end moraines composed of subglacial sediment pushed up at the glacier grounding line (e.g. De Geer, 1940; Boulton, 1986; Sollid, 1989; Larsen *et al.*, 1991; Blake, 2000); (2) they are the product of sediment squeezed into basal crevasses (e.g. Hoppe, 1957; Strömberg, 1965; Zilliacus, 1989; Beaudry & Prichonnet, 1991). In Svalbard, similar ridges have been interpreted as either annual push moraines, created in front of tidewater glaciers by pushing during small winter re-advances, or as crevasse-squeeze ridges (Sharp, 1985; Ottesen & Dowdeswell, 2006; Ottesen *et al.*, 2008; Flink *et al.*, 2015). As glaciers are believed to be especially crevassed when in the active phase of a surge cycle, the crevasse-squeeze ridges have been suggested to be the only landform definitively indicative of surge activity (Sharp, 1985; Ottesen & Dowdeswell, 2006). Following the recommendation of Lundqvist (1981), we interpret the small ridges in Kongsfjorden as De Geer moraines. Although they could have been formed by either of the two suggested mechanisms (see above), we favour formation related to crevasse-squeezing. This issue is further discussed in section A.6 below.

A.5.2 Seismostratigraphy

Chirp data reveal four acoustic facies in inner Kongsfjorden, AF1–AF4 (Fig. A.6). AF4 is stratigraphically oldest and is characterised by (semi-)transparent, acoustically massive reflections. It occasionally crops out along steeper slopes (Fig. A.6). The thickness of AF4 ranges from 1–10 ms (two-way travel time – TWT), which converts to about 1–8 m, respectively (using 1500 m s^{-1} for all facies, the p-wave velocity determined from MSCL measurements). These are minimum thicknesses, however, as the maximum penetration of the echo sounder signal is ∼26 ms TWT, i.e. ∼20 m. AF3 is acoustically similar to AF4 and shows transparent and massive reflections. However, AF3 appears thicker than AF4 (min. 10–20 ms or 8–15 m thick) and has a wedge-like shape (as indicated by brown polygons in Fig. A.6). AF3 only occurs on slopes, specifically the distal sides of terminal moraines, and

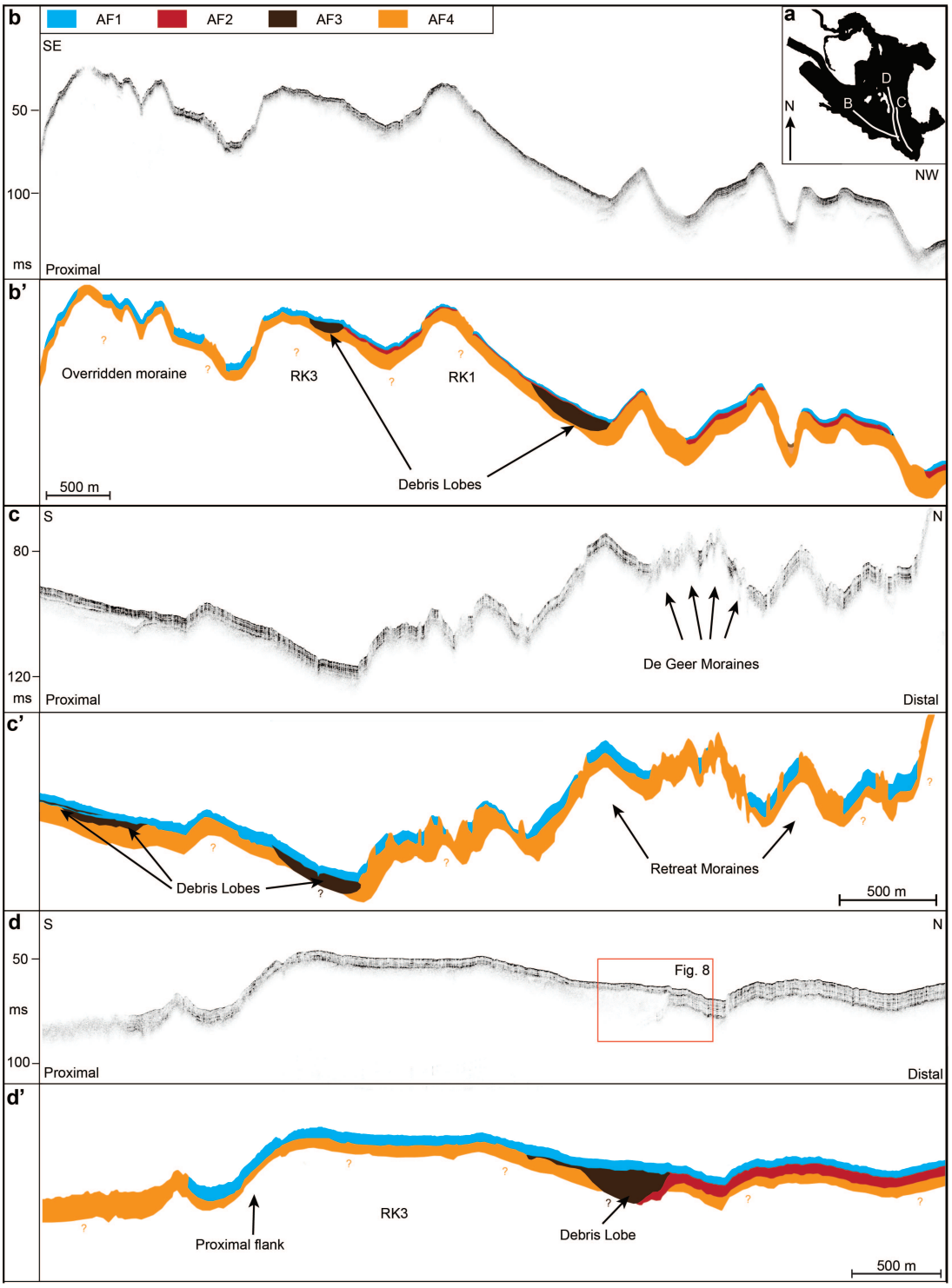

Figure A.6: *a) Black polygon showing the extent of the bathymetric data with white lines indicating the locations of b), c), and d); b) Chirp line 10JM-GlaciBar025 with the acoustic facies interpretation in b'). The y-axis displays two-way travel time (TWT) in ms. Proximal and distal refer to the proximity to the Kronebreen/Kongsvegen ice margin; c) Chirp line 10JM-GlaciBar038 with facies interpretation in c'; d) Chirp line 10JM-GlaciBar055 with facies interpretation in d'). Red rectangle indicates the extent of Figure A.8.*

close to the Kronebreen/Kongsvegen ice margin. It appears thicker at the foot of the slopes, where it generally onlaps onto AF4. However, on the distal side of RK3 it onlaps onto AF2

(Fig. A.6b,d). AF2 is acoustically stratified with laterally (semi-)continuous, opaque, parallel reflections of variable strength (Fig. A.6b,d). The facies is bounded by a variably strong, opaque, semi-continuous reflection at its top, which is largely parallel to the seabed, and a weaker semi-continuous reflection at its base. AF2 is around 5 ms (∼4 m) thick and shows a downlapping character in some areas in Kongsfjorden (Fig. A.6b,d). AF1 is similar to AF2, with parallel, (semi-)continuous, opaque and parallel reflections. It is bounded by the seabed on top (Fig. A.6). We thus infer AF1 to be youngest. The thickness of AF1 ranges from 1 ms (∼1 m) in distal and steep areas to max. 5 ms (∼4 m) in ice-proximal areas. Both AF1 and AF2 are abundant in Kongsfjorden and are particularly common in bathymetric depressions, where, together, they can be up to 11 ms (8 m) thick.

The stratigraphic relationship between the facies varies locally. In ice-distal areas and away from the terminal moraines AF4 directly underlies AF2, which, in turn, directly underlies AF1 (Fig. A.6b,d). In the ice-proximal area of Kronebreen/Kongsvegen, however, AF1 directly overlies AF4 (Fig. A.6). The differing relationship of AF3 to the other facies in the fjord suggests variable timing of deposition. Generally AF3 overlies AF4 and is thus considered younger. In the case of RK3, however, AF3 onlaps onto AF2 (Fig. A.6d), indicating that at this locality AF3 is also younger than AF2.

The acoustically massive appearance of AF4 (and AF3) is suggested to reflect a mixed lithological composition. This, together with the facies' distribution within the fjord, leads us to interpret AF4 as acoustic basement. As this facies dominates on steeper slopes and in hummocky terrain (Fig. A.6), and numerous glacier advances occurred, it is likely that the acoustic basement is comprised of bedrock or glacigenic sediments (cf. Forwick & Vorren, 2011), the latter possibly representing glacitectonite (sensu Evans *et al.*, 2006) or subglacial till (see also Elverhøi *et al.*, 1983). From its onlapping character, its wedge-like shape and its close association with distal moraine slopes we infer that AF3 represents the debris lobes described in section A.5.1.3. AF3 is acoustically similar to sediment wedges from other Spitsbergen fjords (e.g. Plassen *et al.*, 2004; Ottesen & Dowdeswell, 2006; Ottesen *et al.*, 2008), thus supporting our interpretations. The acoustic stratification of AF1 and AF2 reflects repeated changes in the physical properties of the sediments most probably related to changes in grain size in a glacier-proximal environment (e.g. Plassen *et al.*, 2004; Forwick *et al.*, 2010; Forwick & Vorren, 2011). The differences in thickness between AF1 and AF2 are explained by varying durations of deposition. In the case of Kongsvegen, which surged in 1948 (Hagen, 1993), the uppermost sediments between the terminal surge moraine and the glacier front, i.e. AF1, accumulated over a maximum of 62 years (1948–2010), while the sediments of AF1 and AF2 beyond the surge moraine (RK3) accumulated over a much longer time period (>100 years since the last advance, see Fig. A.6d). The variable thickness of AF1 is probably related to the distance from the ice margin: in ice-proximal areas sedimentation rates are usually high, whereas they decrease exponentially with increasing distance from the glacier margin (e.g. Elverhøi *et al.*, 1983). We infer the bottom reflector of AF1 to represent the surge surface of 1948, and the bottom reflector of AF2 to represent the surge surface from 1869, when Kronebreen surged (cf. Elverhøi *et al.*, 1983; Hagen, 1993). The increased thicknesses of AF1 and AF2 in bathymetric depressions might indicate elevated sediment input from the surrounding slopes. AF1, AF2 and AF3 have been sampled in the two sediment cores and their origin is discussed further in the next section.

A.5.3 Lithology

A total of three lithofacies are distinguished: LF3 is found at the base of GC02 (205–339 cm; Fig. A.7a) and is inferred to be the oldest facies. It contains lighter and darker sharp-based layers of (reddish) brown clayey silt, that are a few millimetres to several centimetres thick. Scattered clasts occur throughout. LF2 is a matrix-supported, soft and water-rich diamict occurring at the base of GC01 (165–286 cm). It has a sharp upper boundary and contains abundant clasts distributed in a matrix of massive clayey silt. LF1 forms the uppermost, and therefore youngest facies in both sediment cores and extends from 0–165 cm in GC01 and from 0–205 cm in GC02 (Fig. A.7a). LF1, like LF3, contains stratified clayey silt; however, the clast content is much higher. Clasts occur in concentrated layers or clusters or as randomly distributed lonestones (Fig. A.7a). The boundary between LF3 and LF1 in core GC02 is transitional.

We suggest that LF3 and LF1 were deposited in a glacimarine environment where sedimentation occurred from suspension settling (mud) and ice rafting (clasts). This is in accordance with similar findings from Elverhøi *et al.* (1980, 1983). Ice rafting probably occurred mainly from icebergs, but some contribution by sea ice is likely. The stratification of LF3 and LF1 is probably related to recurring changes in the sediment source with varying contributions of meltwater from Kronebreen and Kongsvegen. Such variations could be due to changes in the glaciers' hydrology or seasonal variations in the rate of sediment delivery and discharge (cf. e.g. Szczuciński & Zajaczkowski, 2012). Based on the high water content, the massive internal structure and the variable grain size, we interpret the sediments of LF2 as reworked glacimarine sediments.

Measurements of the ^{137}Cs activity in the two sediment cores show a presence of ^{137}Cs in the upper 110 cm of both cores, with maximum activity at approximately 85 cm. A secondary peak of ^{137}Cs activity appears in the uppermost 15 cm of GC02 (Fig. A.7b). The ^{210}Pb measurements reveal excess ^{210}Pb in the upper 150 cm of both cores. These activities show an irregular profile in both cores, but generally decrease with depth (Fig. A.7b).

The results of the ^{137}Cs activity measurements indicate that the upper 110 cm in both cores, i.e. large parts of LF1, have likely been deposited after ∼1950. Results further indicate that a sediment depth of approximately 85 cm in both cores is attributed to an age of 1962 AD (Fig. A.7b). We thus infer that LF1 was deposited after the Kongsvegen surge in 1948 and reflects an increasingly ice-distal environment during glacier retreat. As LF1 directly overlies LF2 in GC01, we deduce that the reworked sediments of LF2 were deposited as one of the debris flows described in section A.5.1.3 and represent the sediment lobe associated with RK1 (Figs. A.6, A.8). The stratigraphic relationship from the chirp data suggests the debris lobe from the 1948 Kongsvegen surge to be younger than LF3 (see section A.5.4). We suggest, therefore, that the base of LF3 was deposited during quiescent-phase conditions after the previous surge, and its uppermost parts during the active phase of the 1948 surge. The relatively low number of clasts in LF3 could be explained by either a reduction in ice rafting or by high suspension rainout which swamped the contribution from IRD. The latter is most likely, as the high calving intensity of Kronebreen (0.2247 km^3 a^{-1}; Błaszczyk *et al.*, 2009), the configuration of local ocean and wind currents and the warm water temperatures resulting from increased inflow of Atlantic water are at odds with a low IRD delivery to the core sites (cf. Svendsen *et al.*, 2002; Howe *et al.*, 2003; Jernas *et al.*, 2013).

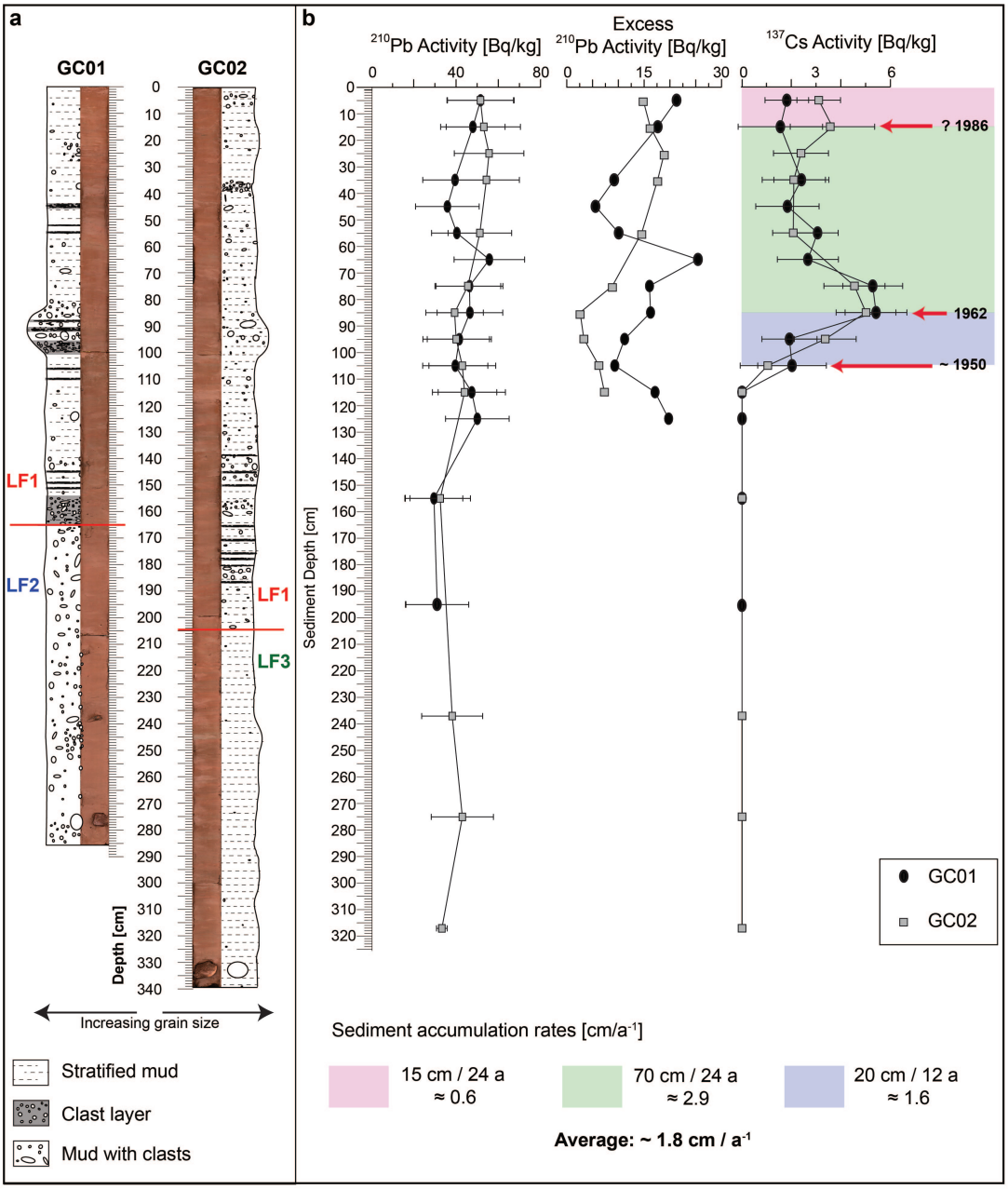

Figure A.7: *a) Logs and colour images of the sediments in the two cores GC01 and GC02. b) Total ^{210}Pb, excess ^{210}Pb and ^{137}Cs activity profiles for the sediment cores. Vertical error bars represent depth range of the sample, whereas horizontal error bars indicate 2-sigma measurement uncertainties. The derived age model provides approximate average sediment accumulation rates shown by the different colours in the ^{137}Cs-plot.*

A.5.4 Correlation of seismo- and lithostratigraphy

We correlate facies AF3 with LF2 (reworked glacimarine sediment deposited from debris flows triggered by surge activity), facies AF2 with LF3 (glacimarine muds deposited during glacier advance), and facies AF1 with LF1 (glacimarine muds deposited during glacier retreat; Fig. A.8). The hiatus from AF1 to AF4 in the proximal parts of Kongsvegen/Kronebreen (Fig. A.6) indicates that the sediments of LF3 (AF2) were likely eroded here, probably as a result of glacial advance during the Kongsvegen surge.

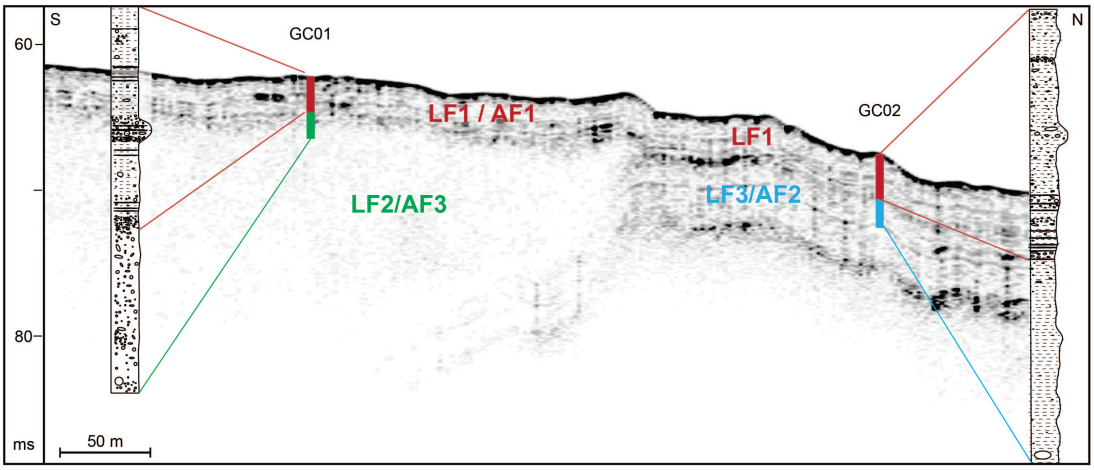

Figure A.8: *Detail figure of chirp line 10JM-GlaciBar055 showing location and penetration of the lithofacies within the GC01 and GC02. LF1, LF2 and LF3 correlate with the acoustic facies AF1, AF3 and AF2, respectively.*

A.5.5 Sediment accumulation rates

The age-depth relationship in both cores shows that the majority of LF1 was deposited with a calculated average SAR of 1.8 cm a^{-1} (Fig. A.7b). The results of the ^{137}Cs activity measurements also indicate that the upper 15 cm in GC02 have probably been deposited since the Chernobyl-accident in 1986, which suggests a low SAR of 0.6 cm a^{-1} for this portion of LF1. In fact, ^{210}Pb activity measurements suggest non-steady sedimentation conditions and thus variable SARs due to the irregular profile of excess ^{210}Pb. The measurements also show a minimum SAR for the uppermost 150 cm in both cores of ~1.5 cm a^{-1}, which is in accordance with the ^{137}Cs dating. Note, however, that all rates presented here are minimum SARs, because the cores were taken with a gravity corer and the uppermost portion of the sediment cover may have been lost during sampling. This could, for example, explain the especially low SAR for the upper 15 cm of LF1.

The overall decrease in excess ^{210}Pb activity with depth in both cores (see Fig. A.7b) is related to its radioactive decay with time. Despite the fact that generally excess ^{210}Pb is measurable in sediments up to c. 100 years old (Koide *et al.*, 1972), no excess ^{210}Pb could be detected in sediments older than c. 60 years in both cores (Fig. A.7b). This could be due to the presence of sediments older than 100 years that were reworked and re-deposited, or due to very high SARs causing dilution of the excess ^{210}Pb. The latter is particularly likely, because the top of the sediment lobe deposited during the Kongsvegen surge in 1948 was inferred to be located at 165 cm in core GC01, while a sediment depth of 110 cm dates to 1950 (according to the ^{137}Cs dating), thus suggesting a SAR of ~30 cm a^{-1} (i.e. one order of magnitude higher than the SARs after 1950). It should be noted that this is a minimum SAR as the exact time of deposition of the sediment lobe remains unknown. We ascribe this high accumulation rate to the proximity of the glacier front, which, based on the distance between terminal moraine and core site, was located approximately 2.5 km from the core site. According to Trusel *et al.* (2010) and Kehrl *et al.* (2011), recent SARs at the immediate fronts of Kongsvegen and Kronebreen are >1 m a^{-1}. As exceptionally high discharge of turbid meltwater is common during and immediately after glacier surges (e.g. Elverhøi *et al.*, 1983; Gilbert *et al.*, 2002; Björnsson *et al.*, 2003), a former SAR of about 30 cm a^{-1} at the core site seems reasonable. Such high accumulation rates are also in accordance with the low number of IRD in LF3, which was linked to high input

of fine-grained material from meltwater plumes, masking the contribution of IRD (see section A.5.3). As the rate of sedimentation from suspension in glacimarine settings usually decreases exponentially with distance (Elverhøi *et al.*, 1983; Farrow *et al.*, 1983; Syvitski *et al.*, 1989; Cowan & Powell, 1991; Szczuciński & Zajaczkowski, 2012), the relatively rapid decline of SARs later on may be related to rapid glacier retreat and the increasing distance between core sites and sediment source. This effect may have been enhanced by trapping of sediments within the basin between the terminal moraine and the retreating glacier front (cf. Kempf *et al.*, 2013).

A.6 Discussion

A.6.1 Surge signatures in Kongsfjorden and comparison with other Spitsbergen fjords

Each tidewater glacier in Kongsfjorden formed (1) glacial lineations during an advancing phase of fast ice flow, (2) terminal moraines when reaching maximum ice extent, (3) associated debris lobes on the moraines' distal slopes, and (4) De Geer moraines after the termination of the advance. In front of Blomstrandbreen and Kronebreen/Kongsvegen, overridden moraines reflect a terminal moraine and recessional moraines, respectively, which were modified during a later re-advance.

The observed assemblages are generally consistent with those observed for terrestrial surge-type glaciers (e.g. Evans & Rea, 1999; Evans & Twigg, 2002) and are also similar to submarine landform assemblages described for surge-type glaciers in other Spitsbergen fjords. This shows that the depositional models proposed by Plassen *et al.* (2004), Ottesen & Dowdeswell (2006), Ottesen *et al.* (2008) and Flink *et al.* (2015) are largely applicable also in Kongsfjorden. However, the occurrence of two different types of glacial lineations in the same fjord, as well as the presence of De Geer moraines appears to be unique to Kongsfjorden.

A.6.1.1 Various types of glacial lineations

Features similar to the smoother grooves and ridges from Kongsfjorden also occur in other Svalbard fjords, including Billefjorden (Baeten *et al.*, 2010), Lomfjorden, and Ymerbukta (see sections 2.4.1 and 3.4.1 below). Conversely, glacial lineations from Borebukta (Ottesen & Dowdeswell, 2006), Van Keulenfjorden, Rindersbukta (Ottesen *et al.*, 2008), and Tempelfjorden (Forwick *et al.*, 2010; Flink *et al.*, 2015), are more comparable to the sharp-crested lineations from Kongsfjorden. Thus the formation processes for the latter were probably similar to those for MSGL, even though the lineations in Kongsfjorden are of a much smaller scale. Possible explanations for this could be e.g. a less deformable substratum beneath the glacier, slower ice flow, shorter advances leaving insufficient time for the formation of larger features, or thinner glacier ice. Such differences between the individual glaciers could also account for the presence of both types of glacial lineations in Kongsfjorden.

A.6.1.2 De Geer moraines

De Geer moraines have been variously described in the literature (De Geer, 1940; Zilliacus, 1989; Lundqvist, 2000), but in fjords on Svalbard similar ridges have always been interpreted as either annual push moraines deposited during overall glacier retreat or as crevasse-squeeze ridges formed after surge termination (Solheim & Pfirman, 1985; Boulton *et al.*, 1996; Ottesen & Dowdeswell, 2006; Ottesen *et al.*, 2008; Flink *et al.*, 2015). Based on their dimensions and morphology, some of the De Geer moraines in Kongsfjorden appear similar to annual push moraines described from e.g. Borebukta and Yoldiabukta in Spitsbergen (Ottesen & Dowdeswell, 2006). This is the case especially for the areas in front of Blomstrandbreen, Conwaybreen, and Kongsbreen South, where the longer, more continuous ridges could have been deposited from, and reflect the shape of, the grounding line (Fig. A.5b,d). However, the number of De Geer moraines in front of the different glaciers is inconsistent with the number of elapsed years since the formation of the outermost moraine. Assuming that glacier retreat began shortly after moraine formation (cf. Flink *et al.*, 2015), the 55 ridges in front

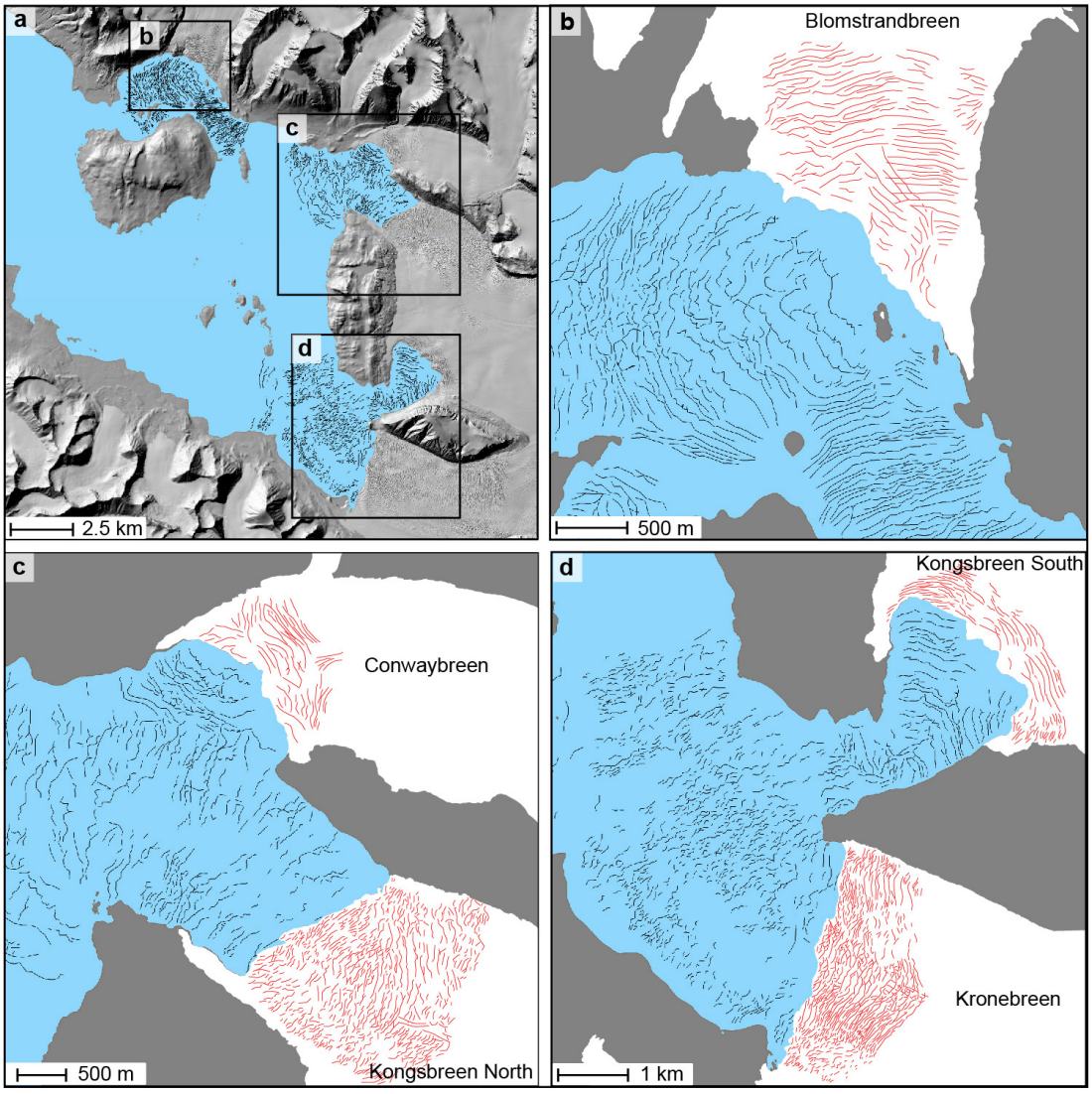

Figure A.9: *a) Map of De Geer moraines in Kongsfjorden with rectangles showing locations of b), c) and d). B), c), and d) show maps of De Geer moraines in front of (black lines) and crevasses on top of the glaciers (red lines).*

of Blomstrandbreen suggest the outermost moraine (RK1) to be formed in 1955. However, RK1 is probably considerably older, as the glacier front was at least 1.5 km further inland in 1956 (see also section A.6.2 below). Furthermore, we would expect c. 113 ridges in front of Conwaybreen (rather than the observed 45), and c. 46 (rather than the observed 30) ridges in front of Kongsbreen South. We thus conclude that if the De Geer moraines in Kongsfjorden were formed from the same mechanism as (annual) push moraines from other fjords, the ridges in Kongsfjorden were formed at more irregular timescales (i.e. not annually).

In places the Kongsfjorden ridges exhibit a saw-tooth pattern in planform, which could be related to formation by a combination of longitudinal crevasse infill and sediment pushing at the glacier snout (Sharp, 1984; Evans & Twigg, 2002; Evans & Orton, 2014; Evans *et al.*, 2015). This could suggest that both processes were active in Kongsfjorden, and that the De Geer moraines thus reflect a combination of recessional push moraines and crevasse-squeeze ridges.

Although both, formation as end moraines or as crevasse-squeeze ridges, is possible, the almost perfect symmetry between proximal and distal slopes, the occasional cross-cutting of the ridges, a generally discontinuous character, and a largely similar pattern between crevasses and De Geer moraines (Fig. A.9) suggest most of the moraines in Kongsfjorden to derive from crevasse-squeezing. Moreover, on the bathymetry data, the majority of the De Geer moraines appear more consistent with crevasse-squeeze ridges (rather than annual retreat moraines) from Van Keulenfjorden, Rindersbukta (Ottesen *et al.*, 2008) and Tempelfjorden (Flink *et al.*, 2015). In planform their pattern of distribution also compares with crevasse-squeeze ridges from terrestrial surge-type glaciers (Evans & Rea, 1999, 2003), thus further supporting a crevasse-squeeze origin.

Based on the above observations, we therefore suggest that the majority of the De Geer moraines in Kongsfjorden resemble crevasse-squeeze ridges. Nonetheless there are also elements which are compatible with formation of some of the ridges as retreat moraines. This indicates that De Geer moraines associated with surging glaciers in Spitsbergen fjords form by a variety of processes and thus that submarine landform assemblages in front of surge-type glaciers are more diverse than previously described (cf. e.g. Plassen *et al.*, 2004; Ottesen & Dowdeswell, 2006; Ottesen *et al.*, 2008; Flink *et al.*, 2015).

A.6.2 Timing of landform formation

From correlation of the terminal moraines with known ice front positions (Liestøl, 1988), we infer that all the submarine glacial landforms in inner Kongsfjorden were deposited throughout the past 150 years. Registered surge years are 1869 for Kronebreen, 1948 for Kongsvegen and 1960 for Blomstrandbreen (Hagen, 1993). RK1 was deposited around 1869 (Fig. A.10) and probably marks the maximum extent of the Kronebreen surge. RK3 fits the 1948 position, when Kongsvegen surged (Fig. A.10). RC1 also dates back to 1869, indicating that the Kronebreen surge caused a simultaenous advance of Kongsbreen North. RK2 and RC2 are close to ice front positions from 1897 (Fig. A.10). Neither Kongsbreen nor Conwaybreen are documented to be of surge-type (Hagen, 1993), hence it is possible that these moraines were deposited from a climatically induced advance during the Little Ice Age (LIA). However, the LIA is documented to have ended ∼1900 AD (cf. Mangerud & Landvik, 2007) and temperatures were probably warmer already in 1897, making a purely climatic advance unlikely. Furthermore, the similarity between the landforms in front of Conwaybreen and Kongsbreen with those in front of the surge-type glaciers (Blomstrandbreen, Kronebreen and Kongsvegen) could suggest that Kongsbreen did surge. The presence of De Geer moraines between RC2 and the present glacier

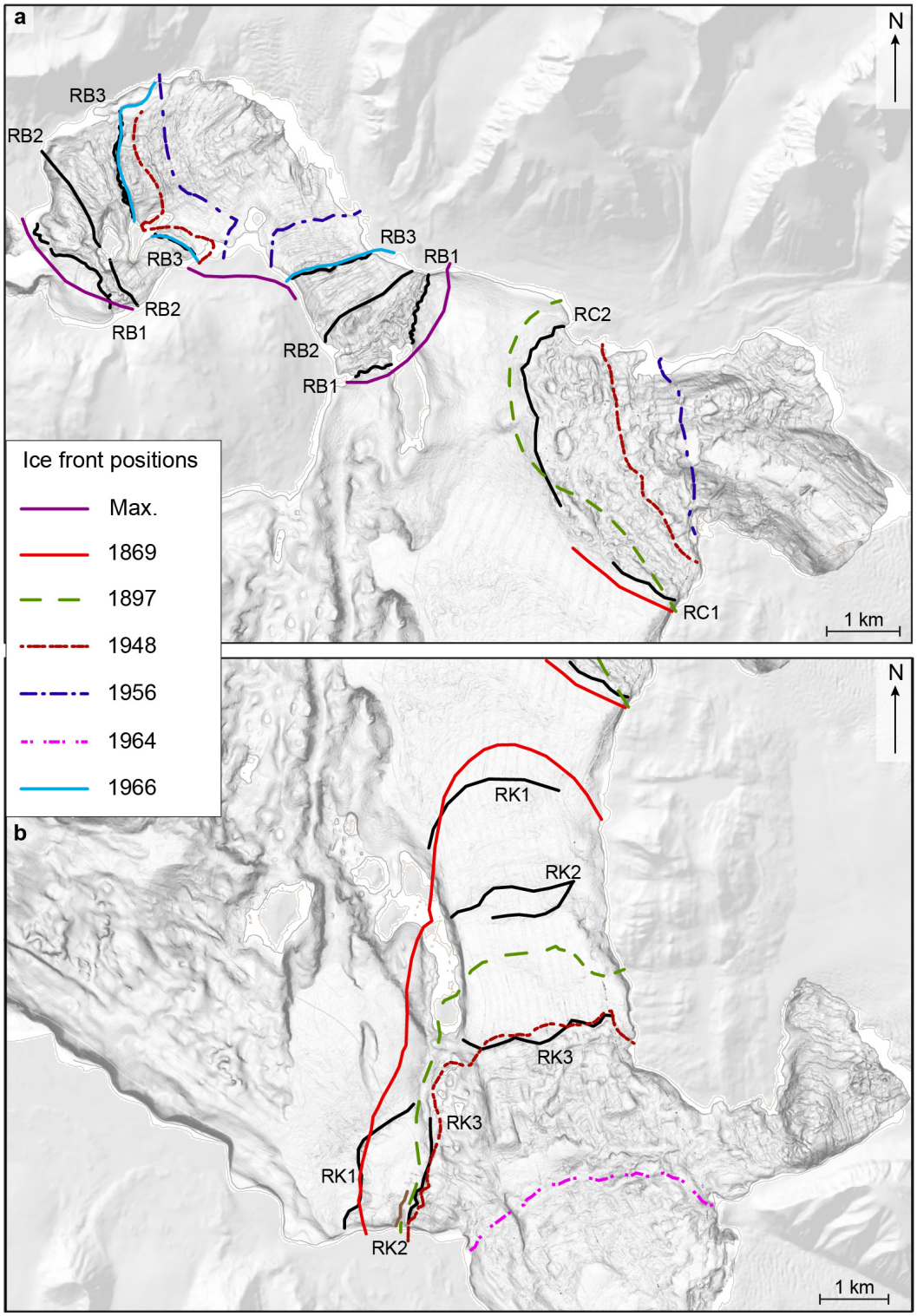

Figure A.10: *Terminal moraines in Kongsfjorden with respect to glacier front positions reconstructed by Liestøl (1988) in front of a) Blomstrandbreen (RB1, 2, 3) and Conwaybreen/Kongsbreen North (RC1, 2), and b) Kronebreen/Kongsvegen (RK1, 2, 3). Max refers to the unknown year of Blomstrandbreen's maximum extent (cf. Liestøl, 1988)*

fronts supports this and we thus infer that a Kongsbreen surge is the more likely scenario.

The ice front positions from 1956 and 1966, as well as the fact that Blomstrandbreen

advanced ∼600 m during its active surge phase (Liestøl, 1988) strongly suggest RB3 to be the terminal surge moraine from 1960 (Fig. A.10). Although the exact chronology of deposition of RB1 and RB2 is still pending, the overridden character of RB2 indicates that it is older than RB1.

We conclude that the geomorphological evidence from the landform assemblages in Kongsfjorden is consistent with surging, especially because (1) the positions of the terminal moraines largely coincide with the glacier front positions documented for respective surge years (cf. Liestøl, 1988), (2) the likely presence of De Geer moraines resembling crevasse-squeeze ridges is considered as possibly surge-diagnostic, (3) glacial lineations in front of all the glaciers indicate fast ice flow, a characteristic of the active phase of a surge cycle (Meier & Post, 1969), and (4) overridden moraines in front of Blomstrandbreen and Kronebreen/Kongsvegen are the product of multiple advances.

A.7 Conclusions

Multibeam and seismic investigations in inner Kongsfjorden reveal a variety of landforms that formed as a result of glacier surges during the past c. 150 years. These include (1) overridden (recessional) moraines from previous ice advance(s), (2) glacial lineations of two types: (a) smooth and (b) sharp-crested groove-ridge features of different sizes, both formed when basal sediments are deformed as a consequence of a rapidly advancing glacier. (3) Large transverse ridges mark the maximum glacier extent during a surge event and were deposited at the end of surges of Kronebreen in 1869, Kongsvegen in 1948, and Blomstrandbreen in 1960. Terminal moraines in front of Conwaybreen/Kongsbreen North and Kongsbreen South/Kronebreen/Kongsvegen coincide with glacier front positions from ∼1897, and suggest a Kongsbreen surge for that year. The distal flanks of most of the terminal moraines are characterised by the occurrence of (4) lobe-shaped debris flows resulting from sediment failure or pushing of sediments at the glacier front during the late stages of advance or shortly after. The formation of (5) De Geer moraines, occurred following surge termination and is linked to either crevasse-squeezing during the glacier's stagnant transitional phase and/or to sediment push from small re-advances/halts during overall retreat.

Suspension settling from meltwater plumes and ice rafting are the dominant sedimentary processes in the fjord, leading to the deposition of stratified glacimarine muds with variable numbers of clasts. Reworking of sediments by glacier surging results in the deposition of sediment lobes containing massive silty clay with frequent clasts. Minimum sediment accumulation rates were ∼30 cm a^{-1} approximately 2.5 km beyond the front of Kongsvegen after it reached its maximum surge extent in 1948, but rapidly decreased to an average rate of 1.8 cm a^{-1} around 1950.

Acknowledgements

This work, as part of the PetroMaks project "Glaciations in the Barents Sea area (GlaciBar)", was funded by the Research Council of Norway (RCN), Statoil, Det Norske oljeselskap ASA and BG group Norway (grant 200672). It also contributes to the Research School in Arctic Marine Geology and Geophysics (AMGG) and to the Centre of Excellence "Arctic Gas Hydrate, Environment and Climate (CAGE)" at the Department of Geology, UiT – The Arctic University of Norway. CAGE is funded by RCN (grant 223259). The project was further funded by the People Programme (Marie Curie Actions) of the European Union's Seventh Framework

Programme FP7/2007-2013/ under REA grant agreement n^{o}317217. Measurements of sediment accumulation rates were supported by grant IP2010040970 from the Polish Ministry of Science and Higher Education and grant 2013/10/E/ST10/00166 from the Polish National Science Center. We thank the captain and crew of R/V Helmer Hanssen (previously Jan Mayen) and Steinar Iversen for collecting and processing the data and are grateful to Monica Winsborrow and Rune Mattingsdal for collecting the sediment cores. Denise Christina Rüther and Lilja Rún Bjarnadóttir's assistance with the use of the software was greatly appreciated and Beata Sternal kindly helped with the laboratory analyses.

Author contributions

This chapter in its current form is based on a team effort of the individual co-authors. Data acquisition was organised by Karin Andreassen, who made the data accessible to me and supervised me during my master's thesis. The majority of analyses and interpretations including the visualisation of acoustic data and the description and sub-sampling of sediment cores were carried out by the lead author, who also prepared all figures and the large majority of the text. Matthias Forwick and Colm Ó Cofaigh did most of the reviewing, providing feedback and suggestions for improvement on the manuscript, particularly in its final stages. Karin Andreassen helped with earlier stages of the manuscript providing feedback on the text and figures and providing advice when I needed it. Witold Szczuciński at the University of Pozńan in Poland was in charge of the Lead/Caesium dating and analysed the samples I prepared according to his instructions. Witold also provided the first draft of the text section describing the dating method in this paper. Two anonymous reviewers helped improve the manuscript by providing several suggestions for editing. Author contributions to the manuscript in its current form are estimated as follows (not considering data acquisition processes): Katharina Streuff 85%, Matthias Forwick 5%, Witold Szczuciński 4%, Karin Andreassen 3%, and Colm Ó Cofaigh 3%.

Bibliography

2017 (03). *meteoblue*.

2017 (January). *U.S. Climate Data: Temperature – Precipitation – Sunshine – Snowfall*. Online.

2017 (03). *USA Today: Climate of Baffin Island*.

Aagaard, K., & Coachman, L. K. 1968. The East Greenland Current north of Denmark Strait: part I. *Arctic*, 181–200.

Aagaard, K., Foldvik, A., & Hillman, S. R. 1987. The West Spitsbergen Current: disposition and water mass transformation. *Journal of Geophysical Research: Oceans*, **92**(C4), 3778–3784.

Åkesson, H. 2016. On the impact of fjord geometry on grounding line stability. *In: American Geophysical Union Fall Meeting*.

Alexander, D. J., Davies, T. R. H., & Shulmeister, J. 2013. Basal melting beneath a fast-flowing temperate tidewater glacier. *Annals of Glaciology*, **54**(63), 265–271.

Alley, R., Clark, P., Huybrechts, P., & Joughin, I. 2005. Ice-sheet and sea-level changes. *Science*, **310**(5747), 456–460.

Alley, R. B. 1993. In search of ice-stream sticky spots. *Journal of Glaciology*, **39**(133), 447–454.

Andersen, E., Dokken, T., Elverhøi, A., Solheim, A., & Fossen, I. 1996. Late Quaternary sedimentation and glacial history of the western Svalbard continental margin. *Marine Geology*, **133**(3-4), 123–156.

Andersen, O. 1981. The annual cycle of temperature, salinity, currents and water masses in Disko Bugt and adjacent waters, West Greenland. *Meddelelser on Grønland, Bioscience*, **5**.

Anderson, J., Kennedy, D., Smith, M., & Domack, E. 1991. Sedimentary facies associated with Antarcticas floating ice masses. *Geological Society of America Special Papers*, **261**, 1–26.

Andreassen, K., Ødegaard, C., & Rafaelsen, B. 2007. Imprints of former ice streams, imaged and interpreted using industry three-dimensional seismic data from the south-western Barents Sea. *Pages 151–169 of:* Davies, R. J., Posamentier, H. W., Wood, L. J., & Cartwright, J. A. (eds), *Seismic Geomorphology: Applications to Hydrocarbon Exploration and Production*, vol. 277. The Geological Society London.

Andreassen, K., Laberg, J., & Vorren, T. 2008. Seafloor geomorphology of the SW Barents Sea and its glaci-dynamic implications. *Geomorphology*, **97**(1-2), 157–177.

Andreassen, K., Winsborrow, M., Bjarnadóttir, L., & Rüther, D. 2014. Ice stream retreat dynamics inferred from an assemblage of landforms in the northern Barents Sea. *Quaternary Science Reviews*, **92**(APEX II: Arctic Palaeoclimate and its Extremes), 246–257.

Andresen, C., McCarthy, D., Dylmer, C., Seidenkrantz, M., Kuijpers, A., & Lloyd, J. 2010. Interaction between subsurface ocean waters and calving of the Jakobshavn Isbræ during the late Holocene. *The Holocene*, 1–14.

Andrews, J., Milliman, J., Jennings, A., Rynes, N., & Dwyer, J. 1994. Sediment thicknesses and Holocene glacial marine sedimentation rates in three east Greenland fjords (ca. 68° N). *The Journal of Geology*, **102**(6), 669–683.

Andrews, J. T. 2011. Unraveling sediment transport along glaciated margins (the northwestern Nordic Seas) using quantitative x-ray diffraction of bulk (< 2mm) sediment. *In: Sediment Transport-Flow and Morphological Processes.* InTech.

Andrews, J. T., & Eberl, D. D. 2012. Determination of sediment provenance by unmixing the mineralogy of source-area sediments: the SedUnMix program. *Marine Geology*, **291**, 24–33.

Andrews, J. T., & Principato, S. M. 2002. Grain-size characteristics and provenance of ice-proximal glacial marine sediments. *Glacier-Influenced Sedimentation on High-Latitude Continental Margins. Geological Society of London, Special Publications*, **203**, 305–324.

Andrews, J. T., Smith, L. M., Preston, R., Cooper, T., & Jennings, A. E. 1997. Spatial and temporal patterns of iceberg rafting (IRD) along the East Greenland margin, ca. 68° N, over the last 14 cal. ka. *Journal of Quaternary Science*, **12**(1), 1–13.

Appleby, P. 2008. Three decades of dating recent sediments by fallout radionuclides: a review. *The Holocene*, **18**(1), 83–93.

Arnold, N. S., Rees, W. G., Hodson, A. J., & Kohler, J. 2006. Topographic controls on the surface energy balance of a high Arctic valley glacier. *Journal of Geophysical Research: Earth Surface*, **111**(F2).

Ashley, G., & Smith, N. 2000. Marine sedimentation at a calving glacier margin. *The Geological Society of America Bulletin*, **112**(5), 657–667.

Baeten, N., Forwick, M., Vogt, C., & Vorren, T. 2010. Late Weichselian and Holocene sedimentary environments and glacial activity in Billefjorden, Svalbard. *Geological Society, London, Special Publications*, **344**(1), 207–223.

Bamber, J., Alley, R., & Joughin, I. 2007. Rapid response of modern day ice sheets to external forcing. *Earth and Planetary Science Letters*, **257**(1), 1–13.

Barnes, P., & Lien, R. 1988. Icebergs rework shelf sediments to 500 m off Antarctica. *Geology*, **16**(12), 1130–1133.

Barrie, J. V., & Conway, K. W. 2002. Contrasting glacial sedimentation processes and sea-level changes in two adjacent basins on the Pacific margin of Canada. *Geological Society, London, Special Publications*, **203**(1), 181–194.

Batchelor, C., & Dowdeswell, J. 2015. Ice-sheet grounding-zone wedges (GZWs) on high-latitude continental margins. *Marine Geology*, **363**, 65–92.

Batchelor, C. L., Dowdeswell, J. A., Dowdeswell, E. K., Todd, B. J., & Sharp, M. J. 2016. A tidewater glacier landform assemblage in Belcher Inlet, Canadian Arctic. *Pages 155–158 of:* Dowdeswell, J. A., Canals, M., Jakobsson, M., Todd, B. J., Dowdeswell, E. K., & Hogan, K. A. (eds), *Atlas of submarine glacial landforms.* Geological Society Memoir, no. 46. The Geological Society London.

Beaudry, L. M., & Prichonnet, G. 1991. Late Glacial De Geer moraines with glaciofluvial sediment in the Chapais area, Québec (Canada). *Boreas*, **20**(4), 377–394.

Belderson, R. H., Kenyon, N. H., & Wilson, J. B. 1973. Iceberg plough marks in the northeast Atlantic. *Palaeogeography, Palaeoclimatology, Palaeoecology*, **13**(3), 215–224.

Bell, R. E. 2008. The role of subglacial water in ice-sheet mass balance. *Nature Geoscience*, **1**, 297–304.

Benn, D., & Evans, D. 2010. *Glaciers and Glaciation.* 2 edn. Hodder Education.

Benn, D., Warren, C., & Mottram, R. 2007a. Calving processes and the dynamics of calving glaciers. *Earth-Science Reviews*, **82**(3-4), 143–179.

Benn, D. I., Hulton, N. R. J., & Mottram, R. H. 2007b. 'Calving laws','sliding laws' and the stability of tidewater glaciers. *Annals of glaciology*, **46**(1), 123–130.

Bennett, R., MacLean, B., Blasco, S., & Hughes Clarke, J. E. 2016. Glacial lineations in Navy Board Inlet, Nunavut, Canada. *Pages 49–50 of:* Dowdeswell, J. A., Canals, M., Jakobsson, M., Todd, B. J., Dowdeswell, E. K., & Hogan, K. A. (eds), *Atlas of submarine glacial landforms.* Geological Society Memoir, no. 46. The Geological Society London.

Bennike, O. 2000. Palaeoecological studies of Holocene lake sediments from west Greenland. *Palaeogeography, Palaeoclimatology, Palaeoecology*, **155**(3), 285–304.

Bigg, G. R. 1999. An estimate of the flux of iceberg calving from Greenland. *Arctic, Antarctic, and Alpine Research*, **31**(2), 174–178.

Bindschadler, R. 1984. Jakobshavns Glacier drainage basin: a balance assessment. *Journal of Geophysical Research: Oceans*, **89**(C2), 2066–2072.

Bjarnadóttir, L. R., Rüther, D. C., Winsborrow, M. C. M., & Andreassen, K. 2013. Grounding-line dynamics during the last deglaciation of Kveithola, W Barents Sea, as revealed by seabed geomorphology and shallow seismic stratigraphy. *Boreas*, **42**(1), 84–107.

Björnsson, H., Pálsson, F., Sigurðsson, O., & Flowers, G. 2003. Surges of glaciers in Iceland. *Annals of Glaciology*, **36**(1), 82–90.

Blake, K. 2000. Common origin for De Geer moraines of variable composition in Raudvassdalen, northern Norway. *Journal of Quaternary Science*, **15**(6), 633–644.

Błaszczyk, M., Jania, J. A., & Hagen, J. O. 2009. Tidewater glaciers of Svalbard: Recent changes and estimates of calving fluxes. *Polish Polar Research*, **30**(2), 85–142.

Blatter, H., & Hutter, K. 1991. Polythermal conditions in Arctic glaciers. *Journal of Glaciology*, **37**, 261–269.

Booth, D. B., & Hallet, B. 1993. Channel networks carved by subglacial water: Observations and reconstruction in the eastern Puget Lowland of Washington. *Geological Society of America Bulletin*, **105**(5), 671–683.

Boulton, G. 1986. Push-moraines and glacier-contact fans in marine and terrestrial environments. *Sedimentology*, **33**(5), 667–698.

Boulton, G. 1990. Sedimentary and sea level changes during glacial cycles and their control on glacimarine facies architecture. *Geological Society, London, Special Publications*, **53**, 15–52.

Boulton, G., Van Der Meer, J., Hart, J., Beets, D., Ruegg, G., Van Der Wateren, F., & Jarvis, J. 1996. Till and moraine emplacement in a deforming bed surge – an example from a marine environment. *Quaternary Science Reviews*, **15**(10), 961–987.

Briner, J. P., Bini, A. C., & Anderson, R. S. 2009. Rapid early Holocene retreat of a Laurentide outlet glacier through an Arctic fjord. *Nature Geoscience*, **2**(7), 496–499.

Buch, E. 2002. *Present oceanographic conditions in Greenland waters.* Danish Meteorological Institute Copenhagen.

Burton, D. J., Dowdeswell, J. A., Hogan, K. A., & Noormets, R. 2016. Marginal fluctuations of a Svalbard surge-type tidewater glacier, Blomstrandbreen, since the Little Ice Age: a record of three surges. *Arctic, Antarctic, and Alpine Research*, **48**(2), 411–426.

Cai, J., Powell, R., Cowan, E., & P., Carlson. 1997. Lithofacies and seismic-reflection interpretation of temperate glacimarine sedimentation in Tarr Inlet, Glacier Bay, Alaska. *Marine Geology*, **143**(1-4), 5–37.

Cappelen, J., Jørgensen, B. V., & Laursen, E. V. 2001. *The observed climate of Greenland, 1958–99.* Tech. rept. 00–18. Danish Meteorological Institute.

Caress, D. W., & Chayes, D. N. 1996. Improved processing of Hydrosweep DS multibeam data on the R/V Maurice Ewing. *Marine Geophysical Research*, **18**(6), 631–650.

Carlson, P. R. 1989. Seismic reflection characteristics of glacial and glacimarine sediment in the Gulf of Alaska and adjacent fjords. *Marine Geology*, **85**(2-4), 391–416.

Chalmers, J., Pulvertaft, T., Marcussen, C., & Pedersen, A. 1999. New insight into the structure of the Nuussuaq Basin, central West Greenland. *Marine and Petroleum Geology*, **16**(3), 197–224.

Chauhan, T., Rasmussen, T. L., & Noormets, R. 2016. Palaeoceanography of the Barents Sea continental margin, north of Nordaustlandet, Svalbard, during the last 74 ka. *Boreas*, **45**(1), 76–99.

Christoffersen, P., Piotrowski, J. A., & Larsen, N. K. 2005. Basal processes beneath an Arctic glacier and their geomorphic imprint after a surge, Elisebreen, Svalbard. *Quaternary Research*, **64**(2), 125–137.

Clapperton, C. M. 1975. The debris content of surging glaciers in Svalbard and Iceland. *Journal of Glaciology*, **14**(72), 395–406.

Clark, C. 1993. Mega-scale glacial lineations and cross-cutting ice-flow landforms. *Earth Surface Processes and Landforms*, **18**(1), 1–29.

Clark, C. 1994. Large-scale ice-moulding: a discussion of genesis and glaciological significance. *Sedimentary Geology*, **91**(1-4), 253–268.

Clark, C., Tulaczyk, S., Stokes, C., & Canals, M. 2003. A groove-ploughing theory for the production of mega-scale glacial lineations, and implications for ice-stream mechanics. *Journal of Glaciology*, **49**(165), 240–256.

Clark, C., Hughes, A., Greenwood, S., Spagnolo, M., & Ng, F. 2009. Size and shape characteristics of drumlins, derived from a large sample, and associated scaling laws. *Quaternary Science Reviews*, **28**(7-8), 677–692.

Clark, C. D., Hughes, A. L. C., Greenwood, S. L., Jordan, C., & Sejrup, H. P. 2012. Pattern and timing of retreat of the last British-Irish Ice Sheet. *Quaternary Science Reviews*, **44**, 112–146.

Corbett, L., Young, N., Bierman, P., Briner, J., Neumann, T., Rood, D., & Graly, J. 2011. Paired bedrock and boulder ^{10} Be concentrations resulting from early Holocene ice retreat near Jakobshavn Isfjord, western Greenland. *Quaternary Science Reviews*, **30**(13), 1739–1749.

Cottier, F., Nilsen, F., Skogseth, R., Tverberg, V., Skarðhamar, J., & Svendsen, H. 2010. Arctic fjords: a review of the oceanographic environment and dominant physical processes. *Geological Society, London, Special Publications*, **344**, 35–50.

Cowan, E., & Powell, R. 1990. Suspended sediment transport and deposition of cyclically interlaminated sediment in a temperate glacial fjord, Alaska, USA. *Geological Society, London, Special Publications*, **53**, 75–89.

Cowan, E., & Powell, R. 1991. Ice-proximal sediment accumulation rates in a temperate glacial fjord, southeastern Alaska. *Geological Society of America Special Papers*, **261**, 61–74.

Cowan, E., Powell, R., & Smith, N. 1988. Rainstorm-induced event sedimentation at the tidewater front of a temperate glacier. *Geology*, **16**(5), 409–412.

Cowan, E., Cai, J., Powell, R., Clark, J., & Pitcher, J. 1997. Temperate glacimarine varves: an example from Disenchantment Bay, southern Alaska. *Journal of Sedimentary Research*, **67**(3), 536–549.

Cowan, E. A., Seramur, K. C., Cai, J., & Powell, R. D. 1999. Cyclic sedimentation produced by fluctuations in meltwater discharge, tides and marine productivity in an Alaskan fjord. *Sedimentology*, **46**(6), 1109–1126.

Cowan, Ellen A. 1992. Meltwater and tidal currents: controls on circulation in a small glacial fjord. *Estuarine, Coastal and Shelf Science*, **34**(4), 381–392.

Crossen, K. J. 1991. Structural control of deposition by Pleistocene tidewater glaciers, Gulf of Maine. *Geological Society of America Special Papers*, **261**, 127–136.

Dallmann, W., Ohta, Y., Elvevold, S., & Blomeier, D. 2002. *Bedrock map of Svalbard and Jan Mayen*. Norsk Polarinstitutt, Temakart No. 33.

De Geer, G. 1940. *Geochronologia suecica principles*. Vol. 18. Almqvist & Wiksells.

Dionne, J. C. 1987. Tadpole rock (rocdrumlin): a glacial streamline moulded form. *Page 159 of: Drumlin Symposium. Rotterdam: Balkema*, vol. 149.

Domack, E., Jacobson, E., Shipp, S., & Anderson, J. 1999. Late Pleistocene–Holocene retreat of the West Antarctic Ice-Sheet system in the Ross Sea: Part 2 – sedimentologic and stratigraphic signature. *Geological Society of America Bulletin*, **111**(10), 1517–1536.

Domack, E. W. 1984. Rhythmically bedded glaciomarine sediments on Whidbey Island, Washington. *Journal of Sedimentary Research*, **54**(2).

Dowdeswell, E. K., Todd, B. J., & Dowdeswell, J. A. 2016a. Crag-and-tail features: convergent ice flow through Eclipse Sound, Baffin Island, Arctic Canada. *Pages 55–56 of:* Dowdeswell, J. A., Canals, M., Jakobsson, M., Todd, B. J., Dowdeswell, E. K., & Hogan, K. A. (eds), *Atlas of submarine glacial landforms*. Geological Society Memoir, no. 46. The Geological Society London.

Dowdeswell, E. K., Todd, B. J., & Dowdeswell, J. A. 2016b. Ice-proximal fans in Dexterity Fjord, Buchan Gulf, Baffin Island, Canadian Arctic. *Pages 89–90 of:* Dowdeswell, J. A., Canals, M., Jakobsson, M., Todd, B. J., Dowdeswell, E. K., & Hogan, K. A. (eds), *Atlas of submarine glacial landforms*. Geological Society Memoir, no. 46. The Geological Society London.

Dowdeswell, E. K., Todd, B. J., & Dowdeswell, J. A. 2016c. Submarine medial moraines and convergent ice flow, Scott Inlet, Baffin Island, Arctic Canada. *Pages 193–194 of:* Dowdeswell, J. A., Canals, M., Jakobsson, M., Todd, B. J., Dowdeswell, E. K., & Hogan, K. A. (eds), *Atlas of submarine glacial landforms*. Geological Society Memoir, no. 46. The Geological Society London.

Dowdeswell, J. A. 1987. Processes of glacimarine sedimentation. *Progress in Physical Geography*, **11**(1), 52–90.

Dowdeswell, J. A., & Bamber, J. 2007. Keel depths of modern Antarctic icebergs and implications for sea-floor scouring in the geological record. *Marine Geology*, **243**(1-4), 120–131.

Dowdeswell, J. A, & Cromack, M. 1991. Behavior of a glacier-derived suspended sediment plume in a small Arctic inlet. *The Journal of Geology*, **99**(1), 111–123.

Dowdeswell, J. A., & Dowdeswell, E. 1989. Debris in Icebergs and Rates of Glaci-Marine Sedimentation: Observations from Spitsbergen and a Simple Model. *The Journal of Geology*, **97**(2), 221–231.

Dowdeswell, J. A., & Forsberg, C. 1992. The size and frequency of iceberg and bergy bits derived from tidewater glaciers in Kongsfjorden, northwest Spitsbergen. *Polar Research*, **2**, 81–91.

Dowdeswell, J. A., & Fugelli, E. M. G. 2012. The seismic architecture and geometry of grounding-zone wedges formed at the marine margins of past ice sheets. *Geological Society of America Bulletin*, **124**(11-12), 1750–1761.

Dowdeswell, J. A., & Ottesen, D. 2016. Eskers formed at the beds of modern surge-type tidewater glaciers in Spitsbergen. *Pages 83–84 of:* Dowdeswell, J. A., Canals, M., Jakobsson, M., Todd, B. J., Dowdeswell, E. K., & Hogan, K. A. (eds), *Atlas of submarine glacial landforms*. Geological Society Memoir, no. 46. The Geological Society London.

Dowdeswell, J. A., Hamilton, G., & Hagen, J. O. 1991. The duration of the active phase of surge-type glaciers: contrasts between Svalbard and other regions. *Journal of Glaciology*, **37**(127), 388–400.

Dowdeswell, J. A., Villinger, H., Whittington, R. J., & Marienfeld, P. 1993. Iceberg scouring in Scoresby Sund and on the East Greenland continental shelf. *Marine Geology*, **111**(1-2), 37–53.

Dowdeswell, J. A., Uenzelmann-Neben, G., Whittington, R. J., & Marienfeld, P. 1994a. The Late Quaternary sedimentary record in Scoresby Sund, East Greenland. *Boreas*, **23**(4), 294–310.

Dowdeswell, J. A., Whittington, R. J., & Marienfeld, P. 1994b. The origin of massive diamicton facies by iceberg rafting and scouring, Scoresby Sund, East Greenland. *Sedimentology*, **41**(1), 21–35.

Dowdeswell, J. A., Hodgkins, R., Nuttall, A., Hagen, J. O., & Hamilton, G. 1995. Mass balance change as a control on the frequency and occurrence of glacier surges in Svalbard, Norwegian High Arctic. *Geophysical Research Letters*, **22**(21), 2909–2912.

Dowdeswell, J. A., Hagen, J. O., Björnsson, H., Glazovsky, A. F., Harrison, W. D., Holmlund, P., Jania, J., Koerner, R. M., Lefauconnier, B., Ommanney, C. S. L., *et al.* 1997. The mass balance of circum-Arctic glaciers and recent climate change. *Quaternary research*, **48**(1), 1–14.

Dowdeswell, J. A., Elverhøi, A., & Spielhagen, R. 1998. Glacimarine sedimentary processes and facies on the Polar North Atlantic margins. *Quaternary Science Reviews*, **17**(1-3), 243–272.

Dowdeswell, J. A., Whittington, R., Jennings, A., Andrews, J., Mackensen, A., & Marienfeld, P. 2000. An origin for laminated glacimarine sediments through sea-ice build-up and suppressed iceberg rafting. *Sedimentology*, **47**.

Dowdeswell, J. A., Ottesen, D., Evans, J., 'Ø Cofaigh, C., & Anderson, J. B. 2008. Submarine glacial landforms and rates of ice-stream collapse. *Geology*, **36**(10), 819–822.

Dowdeswell, J. A., Hogan, K., Evans, J., Noormets, R., Ó Cofaigh, C., & Ottesen, D. 2010a. Past ice-sheet flow east of Svalbard inferred from streamlined subglacial landforms. *Geology*, **38**(2), 163–166.

Dowdeswell, J. A., Evans, J., & Ó Cofaigh, C. 2010b. Submarine landforms and shallow acoustic stratigraphy of a 400 km-long fjord-shelf-slope transect, Kangerlussuaq margin, East Greenland. *Quaternary Science Reviews*, **29**(25), 3359–3369.

Dowdeswell, J. A., Hogan, K., Ó Cofaigh, C., Fugelli, E., Evans, J., & Noormets, R. 2014. Late Quaternary ice flow in a West Greenland fjord and cross-shelf trough system: submarine landforms from Rink Isbrae to Uummannaq shelf and slope. *Quaternary Science Reviews*, **92**, 292–309.

Dowdeswell, J. A., Canals, M., Jakobsson, M., Todd, B. J., Dowdeswell, E. K., & Hogan, K. A. (eds). 2016d. *Atlas of Submarine Glacial Landforms: Modern, Quaternary and Ancient.* Geological Society Memoir, no. 46. The Geological Society London.

Dowdeswell, J. A., Batchelor, C. L., Hogan, K. A., & Schenke, H.-W. 2016e. Nordvestfjord: a major East Greenland fjord system. *Pages 43–44 of:* Dowdeswell, J. A., Canals, M., Jakobsson, M., Todd, B. J., Dowdeswell, E. K., & Hogan, K. A. (eds), *Atlas of submarine glacial landforms.* Geological Society Memoir, no. 46. The Geological Society London.

Dowdeswell, J. A., Dowdeswell, E., & Rodrigo, C. 2016f. Pockmarks in the fjords of Chilean Patagonia. *Pages 109–110 of:* Dowdeswell, J. A., Canals, M., Jakobsson, M., Todd, B. J., Dowdeswell, E. K., & Hogan, K. A. (eds), *Atlas of submarine glacial landforms.* Geological Society Memoir, no. 46. The Geological Society London.

Echelmeyer, K., Clarke, T., & Harrison, W. 1991. Surficial glaciology of Jakobshavns Isbræ, West Greenland: Part I: Surface morphology. *Journal of Glaciology*, **37**(127), 368–382.

Echelmeyer, K., Clarke, T., & Harrison, W. 1992. Surficial glaciology of Jakobshavns Isbræ, West Greenland: Part II. Ablation, accumulation and temperature. *Journal of Glaciology*, **38**(128), 169–181.

Elverhøi, A., Liestøl, O., & Nagy, J. 1980. Glacial erosion, sedimentation and microfauna in the inner part of Kongsfjorden, Spitsbergen. *Norsk Polarinstitutt Skrifter*, **172**, 33–58.

Elverhøi, A., Lønne, Ø., & Seland, R. 1983. Glaciomarine sedimentation in a modern fjord environment, Spitsbergen. *Polar Research*, **1**(2), 127–150.

Elverhøi, A., Fjeldskaar, W., Solheim, A., Nyland-Berg, M., & Russwurm, L. 1993. The Barents Sea Ice Sheet – A model of its growth and decay during the last ice maximum. *Quaternary Science Reviews*, **12**(10), 863–873.

Elverhøi, A., Andersen, E., Dokken, T., Hebbeln, D., Spielhagen, R., Svendsen, J., & Forsberg, C. 1995. The growth and decay of the Late Weichselian ice sheet in western Svalbard and adjacent areas based on provenance studies of marine sediments. *Quaternary Research*, **44**(3), 303–316.

Elverhøi, A., Harbitz, C.B., Dimakis, P., Morhrig, D., Marr, J., & G., Parker. 2000. On the dynamics of subaqueous debris flows. *Oceanography*, **13**(3).

Evans, D. 2003. Ice-marginal terrestrial landsystems: active temperate glacier margins. *Pages 12–43 of: Glacial Landsystems.* Arnold, London.

Evans, D., & Orton, C. 2014. Heinabergsjökull and Skalafellsjökull, Iceland: active temperate piedmont lobe and outwash head glacial landsystem. *Journal of Maps*, **11**(3), 415–431.

Evans, D., & Rea, B. 1999. Geomorphology and sedimentology of surging glaciers: a land-systems approach. *Annals of Glaciology*, **28(1)**, 75–82.

Evans, D., & Rea, B. 2003. Surging glacier landsystem. *Chap. Glacial Landsystems, pages 259–288 of:* Evans, D. (ed), *Glacial Landsystems*. Arnold, London.

Evans, D., & Twigg, D. 2002. The active temperate glacial landsystem: a model based on Breiðamerkurjökull and Fjallsjökull, Iceland. *Quaternary Science Reviews*, **21(20)**, 2143–2177.

Evans, D., Lemmen, D. R., & Rea, B. 1999. Glacial landsystems of the southwest Laurentide Ice Sheet: modern Icelandic analogues. *Journal of Quaternary Science*, **14(7)**, 673–691.

Evans, D., Ewertowski, M., & Orton, C. 2015. Fláajökull (north lobe), Iceland: active temperate piedmont lobe glacial landsystem. *Journal of Maps*.

Evans, D. J. A., Phillips, E.R., Hiemstra, J.F., & Auton, C.A. 2006. Subglacial till: formation, sedimentary characteristics and classification. *Earth-Science Reviews*, **78**(1), 115–176.

Evans, J., & Dowdeswell, J. A. 2016. Submarine gullies and an axial channel in glacier-influenced Courtauld Fjord, East Greenland. *Pages 103–104 of:* Dowdeswell, J. A., Canals, M., Jakobsson, M., Todd, B. J., Dowdeswell, E. K., & Hogan, K. A. (eds), *Atlas of submarine glacial landforms*. Geological Society Memoir, no. 46. The Geological Society London.

Farnsworth, W. R., Ingólfsson, Ó., Retelle, M., & Schomacker, A. 2016. Over 400 previously undocumented Svalbard surge-type glaciers identified. *Geomorphology*, **264**, 52–60.

Farrow, G., Syvitski, J., & Tunnicliffe, V. 1983. Suspended particulate loading on the macrobenthos in a highly turbid fjord: Knight Inlet, British Columbia. *Canadian Journal of Fisheries and Aquatic Sciences*, **40**(S1), s273–s288.

Flink, A. E., Noormets, R., Kirchner, N., Benn, D. I., Luckman, A., & Lovell, H. 2015. The evolution of a submarine landform record following recent and multiple surges of Tunabreen glacier, Svalbard. *Quaternary Science Reviews*, **108**, 37–50.

Flink, A. E., Noormets, R., Fransner, O., Hogan, K. A., O'Regan, M., & Jakobsson, M. 2017. Past ice flow in Wahlenbergfjorden and its implications for late Quaternary ice sheet dynamics in northeastern Svalbard. *Quaternary Science Reviews*.

Flink, A. E., Noormets, R., Hill, P., & Kirchner, N. 2016a. Glacial dynamics in Mohnbukta east Spitsbergen inferred from the submarine landform record. *In: PAST Gateways, 4th international conference*.

Flink, A. E., Noormets, R., & Kirchner, N. 2016b. Annual moraine ridges in Tempelfjorden, Spitsbergen. *Pages 75–76 of:* Dowdeswell, J. A., Canals, M., Jakobsson, M., Todd, B. J., Dowdeswell, E. K., & Hogan, K. A. (eds), *Atlas of submarine glacial landforms*. Geological Society Memoir, no. 46. The Geological Society London.

Førland, E. J., Haugen, J. E., Isaksen, K., Sorteberg, A., & Ådlandsvik, B. 2009. Climate development in North Norway and the Svalbard region during 1900–2100. *Rapportserie Norsk Polarinstitutt*.

Forman, S.L. 1990. Post-glacial relative sea-level history of northwestern Spitsbergen, Svalbard. *Geological Society of America Bulletin*, **102**, 1580–1590.

Forsberg, C. F., Solheim, A., Elverhøi, A., Jansen, E., Channell, J. E. T., & Andersen, E. S. 1999. The depositional environment of the western Svalbard margin during the Late Pliocene and the Pleistocene: Sedimentary facies changes at Site 9. *Page 233 of: Proceedings of the Ocean Drilling Program: Scientific results*, vol. 162. The Program.

Forwick, M., & Vorren, T. 2007. Holocene mass-transport activity and climate in outer Isfjorden, Spitsbergen: marine and subsurface evidence. *The Holocene*, **17(6)**, 707–716.

Forwick, M., & Vorren, T. 2009. Late Weichselian and Holocene sedimentary environments and ice rafting in Isfjorden, Spitsbergen. *Paleogeography, Paleoclimatology, Paleoecology*, **280(1)**, 258–274.

Forwick, M., & Vorren, T. 2011. Stratigraphy and deglaciation of the Isfjorden area, Spitsbergen. *Norwegian Journal of Geology*, **90**, 163–179.

Forwick, M., & Vorren, T. O. 2012. Submarine Mass Wasting in Isfjorden, Spitsbergen. *Pages 711–722 of:* Yamada, Y., Kawamura, K., Ikehara, K., Ogawa, Y., Urgeles, R., Mosher, D., Chaytor, J., & Strasser, M. (eds), *Submarine mass movements and their consequences*, vol. 31. Springer Springer+ Business Media.

Forwick, M., Baeten, N., & Vorren, T. 2009. Pockmarks in Spitsbergen fjords. *Norwegian Journal of Geology*, **89**(1/2), 65–77.

Forwick, M., Vorren, T., Hald, M., Korsun, S., Roh, Y., Vogt, C., & Yoo, K. 2010. Spatial and temporal influence of glaciers and rivers on the sedimentary environment in Sassenfjorden and Tempelfjorden, Spitsbergen. *Geological Society, London, Special Publications*, **344(1)**, 163–193.

Fransner, O., Noormets, R., Flink, A. E., Hogan, K., O'Regan, M., & Jakobsson, M. 2017. Glacial landforms and their implications for glacier dynamics in Rijpfjorden and Duvefjorden, northern Nordaustlandet, Svalbard. *Journal of Quaternary Science*.

Funder, S., & Hansen, L. 1996. *The Greenland ice sheet – a model for its culmination and decay during and after the Last Glacial Maximum*. Geological Society of Denmark.

Funder, S., Kjellerup, K., Kjær, K., & Ó Cofaigh, C. 2011. The Greenland ice sheet during the past 300,000 years: a review. *Quaternary Glaciations - Extent and Chronology. Part IV: A closer look.: Developments in Quaternary Science*, **15**, 699–713.

Gilbert, R. 1978. Observations on oceanography and sedimentation at Pangnirtung Fiord, Baffin Island. *Atlantic Geology*.

Gilbert, R. 1982. Contemporary sedimentary environments on Baffin Island, NWT, Canada: Glaciomarine processes in fiords of eastern Cumberland Peninsula. *Arctic and Alpine Research*, **14**(1), 1–12.

Gilbert, R. 1983. Sedimentary processes of Canadian Arctic fjords. *Sedimentary Geology*, **36(2–4)**, 147–175.

Gilbert, R. 1990. Sedimentation in Expedition Fiord, Axel Heiberg Island, Northwest Territories. *Géographie physique et Quaternaire*, **44**(1), 71–76.

Gilbert, R., Naldrett, D. L., & Horvath, V. 1990. Holocene sedimentary environment of Cambridge Fiord, Baffin Island, Northwest Territories. *Sedimentology of Arctic Fiords*, **27**, 271–280.

Gilbert, R., Aitken, A., & Lemmen, D. 1993. The glacimarine sedimentary environment of Expedition Fiord, Canadian High Arctic. *Marine Geology*, **110**(3), 257–273.

Gilbert, R., Nielsen, N., Möller, H., Desloges, J., & Rasch, M. 2002. Glacimarine sedimentation in Kangerdluk (Disko Fjord), West Greenland, in response to a surging glacier. *Marine Geology*, **191**, 1–18.

Gowan, E. J., Fransner, O. J., & Dowdeswell, J. A. 2016. ICESHEET 1.0: a program to produce paleo-ice sheet reconstructions with minimal assumptions. *Geoscientific Model Development*, **9**(5), 1673.

Greenwood, S. .L, & Clark, C. D. 2009. Reconstructing the last Irish Ice Sheet 2: a geomorphologically-driven model of ice sheet growth, retreat and dynamics. *Quaternary Science Reviews*, **28**(27), 3101–3123.

Grobe, H. 1987. A simple method for the determination of ice-rafted debris in sediment cores. *Polarforschung*, **57 (3)**, 123–126.

Hagen, J. 1993. *Glacier atlas of Svalbard and Jan Mayen.* Vol. 129. Norsk Polarinstitutt Middelelser.

Hagen, J. O., Kohler, J., Melvold, K., & Winther, J.-G. 2003. Glaciers in Svalbard: mass balance, runoff and freshwater flux. *Polar Research*, **22**(2), 145–159.

Hald, M., Dahlgren, T., Olsen, T.-E., & Lebesbye, E. 2001. Late Holocene paleoceanography in Van Mijenfjorden, Svalbard. *Polar Research*, **20(1)**, 23–35.

Hald, M., Ebbesen, H., Forwick, M., Godtliebsen, F., Khomenko, L., Korsun, S., & Vorren, T. 2004. Holocene paleoceanography and glacial history of the West Spitsbergen area, Euro-Arctic margin. *Quaternary Science Reviews*, **23(20)**, 2075–2088.

Hallet, B., Hunter, L., & Bogen, J. 1996. Rates of erosion and sediment evacuation by glaciers: A review of field data and their implications. *Global and Planetary Change*, **12**(1-4), 213–235.

Hambrey, M. 1994. *Glacial Environments.* CRC Press.

Hambrey, M. J., & McKelvey, B. 2000. Major Neogene fluctuations of the East Antarctic ice sheet: Stratigraphic evidence from the Lambert Glacier region. *Geology*, **28**(10), 887–890.

Hambrey, M. J., Dowdeswell, J. A., Murray, T., & Porter, P. R. 1996. Thrusting and debris entrainment in a surging glacier: Bakaninbreen, Svalbard. *Annals of Glaciology*, **22**(1), 241–248.

Hambrey, M. J., Bennett, M. R., Dowdeswell, J. A., Glasser, N. F., & Huddart, D. 1999. Debris entrainment and transfer in polythermal valley glaciers. *Journal of Glaciology*, **45**(149), 69–86.

Hamilton, G., & Dowdeswell, J. 1996. Controls of glacier surging in Svalbard. *Journal of Glaciology*, **42**, 157–168.

Harrington, P. K. 1985. Formation of pockmarks by pore-water escape. *Geo-Marine Letters*, **5**(3), 193–197.

Hein, F., & Syvitski, J. 1992. Sedimentary environments and facies in an Arctic basin, Itirbilung Fjord, Baffin Island, Canada. *Sedimentary Geology*, **81(1–2)**, 17–45.

Henriksen, M., Alexanderson, H., Landvik, J. Y., Linge, H., & Peterson, G. 2014. Dynamics and retreat of the Late Weichselian Kongsfjorden ice stream, NW Svalbard. *Quaternary Science Reviews*, **92**, 235–245.

Hofmann, J., Knutz, P., Nielsen, T., & Kuijpers, A. 2016. Seismic architecture and evolution of the Disko Bay trough-mouth fan, central West Greenland margin. *Quaternary Science Reviews*, **147**, 69–90.

Hogan, K., Dix, J., Lloyd, J., Long, A., & Cotterill, C. 2011. Seismic stratigraphy records the deglacial history of Jakobshavn Isbræ, West Greenland. *Journal of Quaternary Science*, **26(7)**, 757–766.

Hogan, K., Dowdeswell, J., & Ó Cofaigh, C. 2012. Glacimarine sedimentary processes and depositional environments in an embayment fed by West Greenland ice streams. *Marine Geology*, **311**, 1–16.

Hogan, K., Ó Cofaigh, C., Jennings, A., Dowdeswell, J., & Hiemstra, J. 2016. Deglaciation of a major palaeo-ice stream in Disko Trough, West Greenland. *Quaternary Science Reviews*, **147**, 5–26.

Hogan, K. A., Dowdeswell, J. A., Noormets, R., Evans, J., & Ó Cofaigh, C. 2010. Evidence for full-glacial flow and retreat of the Late Weichselian Ice Sheet from the waters around Kong Karls Land, eastern Svalbard. *Quaternary Science Reviews*, **29**(25), 3563–3582.

Holland, D., Thomas, R., De Young, B., Ribergaard, M., & Lyberth, B. 2008. Acceleration of Jakobshavn Isbræ triggered by warm subsurface ocean waters. *Nature Geoscience*, **1**, 659–664.

Hoppe, G. 1957. Problems of glacial morphology and the Ice Age. *Geografiska Annaler*, 1–18.

Hoskin, C. M., & Burrell, D. C. 1972. Sediment transport and accumulation in a fjord basin, Glacier Bay, Alaska. *The Journal of Geology*, 539–551.

Hovland, M., & Judd, A. G. 1988. *Seabed pockmarks and seepages: impact on geology, biology and the marine environment.*

Hovland, M, Gardner, J. V., & Judd, A. G. 2002. The significance of pockmarks to understanding fluid flow processes and geohazards. *Geofluids*, **2**(2), 127–136.

Howat, I., Ahn, Y., Joughin, I., Van Den Broeke, M., Lenaerts, J., & Smith, B. 2011. Mass balance of Greenland's three largest outlet glaciers, 2000–2010. *Geophysical Research Letters*, **38**(12).

Howe, J., Moreton, S., Morri, C., & Morris, P. 2003. Multibeam bathymetry and the depositional environments of Kongsfjorden and Krossfjorden, western Spitsbergen, Svalbard. *Polar Research*, **22 (2)**, 301–316.

Howe, J., Austin, W., Forwick, M., Paetzel, M., Harland, R., & Cage, A. 2010. Fjord systems and archives: a review. *Geological Society London, Special Publications*, **344(1)**, 5–15.

Hubbard, A., Bradwell, T., Golledge, N., Hall, A., Patton, H., Sugden, D., Cooper, R., & Stoker, M. 2009. Dynamic cycles, ice streams and their impact on the extent, chronology and deglaciation of the British–Irish ice sheet. *Quaternary Science Reviews*, **28**(7), 758–776.

Hughes, A. L. C., Gyllencreutz, R., Lohne, Ø. S., Mangerud, J., & Svendsen, J. I. 2016. The last Eurasian ice sheets–a chronological database and time-slice reconstruction, DATED-1. *Boreas*, **45**(1), 1–45.

Hunt, A. G., & Malin, P. E. 1998. Possible triggering of Heinrich events by ice-load-induced earthquakes. *Nature*, **393**, 155–158.

Hunter, L. E., Powell, R. D., & Lawson, D. E. 1996. Flux of debris transported by ice at three Alaskan tidewater glaciers. *Journal of Glaciology*, **42**(140), 123–135.

Ingólfsson, Ó., & Landvik, J. 2013. The Svalbard-Barents Sea ice-sheet – historical, current and future perspectives. *Quaternary Science Reviews*, **64**, 33–60.

Ingólfsson, Ó., Farnsworth, W., Schomacker, A., Håkansson, L., & Allaart, L. 2016. Younger Dryas-Holocene glacial advance in De Geerbukta, NE Spitsbergen: climate controlled, or glacial system turning to Holocene mode. *In: PAST Gateways Abstracts*.

Ito, H., & Kudoh, S. 1997. Characteristics of water in Kongsfjorden, Svalbard. *Proceedings of the NIPR symposium on polar meteorology and glaciology*, **11**, 211–232.

Jennings, A., Walton, M., Ó Cofaigh, C., Kilfeather, A., Andrews, J., Ortiz, J., De Vernal, A., & Dowdeswell, J. 2013. Paleoenvironments during Younger Dryas – Early Holocene retreat of the Greenland Ice Sheet from outer Disko Trough, central west Greenland. *Journal of Quaternary Science*, **2652**, 1–14.

Jennings, A. E, & Weiner, N. J. 1996. Environmental change in eastern Greenland during the last 1300 years: evidence from foraminifera and lithofacies in Nansen Fjord, 68 °N. *The Holocene*, **6**(2), 179–191.

Jernas, P., Klitgaard-Kristensen, D., Husum, K., Wilson, L., & Koç, N. 2013. Palaeoenvironmental changes of the last two millennia on the western and northern Svalbard shelf. *Boreas*, **42**(1), 236–255.

Jessen, S., Rasmussen, T., Nielsen, T., & Solheim, A. 2010. A new Late Weichselian and Holocene marine chronology for the western Svalbard slope 30000-0 cal years BP. *Quaternary Science Reviews*, **29(9)**, 1301–1312.

Jones, G. A., & Keigwin, L. D. 1988. Evidence from Fram Strait (78 N) for early deglaciation. *Nature*, **336**(6194), 56–59.

Joughin, I., Abdalati, W., & Fahnestock, M. 2004. Large fluctuations in speed on Greenland's Jakobshavn Isbrae glacier. *Nature*, **432**(7017), 608–610.

Joughin, I., Das, S., King, M., Smith, B., Howat, I., & Moon, T. 2008. Seasonal speedup along the western flank of the Greenland Ice Sheet. *Science*, **320**(5877), 781–783.

Joughin, I., Smith, B., Shean, D., & Floricioiu, D. 2014. Brief Communication: Further summer speedup of Jakobshavn Isbræ. *The Cryosphere*, **8**, 209–214.

Kamb, B. 1987. Glacier surge mechanism based on linked cavity configuration of the basal water conduit system. *Journal of Geophysical Research: Solid Earth*, **92**(B9), 9083–9100.

Kayashta, R. B., Ageta, Y., Nakawo, M., Fujita, K., Sakai, A., & Matsuda, Y. 2003. Positive degree-day factors for ice ablation on four glaciers in the Nepalese Himalayas and Qinghai-Tibetan Plateau. *Bulletin of Glaciological Research*, **20**, 7–14.

Kehrl, L., Hawley, R., Powell, R., & Brigham-Grette, J. 2011. Glacimarine sedimentation processes at Kronebreen and Kongsvegen, Svalbard. *Journal of Glaciology*, **57(205)**, 841–847.

Kelley, S., Briner, J., & Young, N. 2013. Rapid ice retreat in Disko Bugt supported by ^{10}Be dating of the last recession of the western Greenland Ice Sheet. *Quaternary Science Reviews*, **82**, 13–22.

Kempf, P., Forwick, M., Laberg, J., & Vorren, T. 2013. Late Weichselian – Holocene sedimentary palaeoenvironment and glacial activity in the high-Arctic van Keulenfjorden, Spitsbergen. *The Holocene*, **23(11)**, 1607–1618.

Kilfeather, A., Ó Cofaigh, C., Lloyd, J., Dowdeswell, J., Xu, S., & Moreton, S. 2011. Ice-stream retreat and ice-shelf history in Marguerite Trough, Antarctic Peninsula: Sedimentological and foraminiferal signatures. *Geological Society of America Bulletin*, **123**(5-6), 997–1015.

King, E., Hindmarsh, R., & Stokes, C. 2009. Formation of mega-scale glacial lineations observed beneath a West Antarctic ice stream. *Nature Geoscience*, **2(8)**, 585–588.

King, E. L., Haflidason, H., Sejrup, H. P., & Løvlie, R. 1998. Glacigenic debris flows on the North Sea Trough Mouth Fan during ice stream maxima. *Marine Geology*, **152**(1), 217–246.

Kirchner, N., Ahlkrona, J., Gowan, E. J., Lötstedt, P., Lea, J. M., Noormets, R., von Sydow, L., Dowdeswell, J. A., & Benham, T. 2016. Shallow ice approximation, second order shallow ice approximation, and full Stokes models: A discussion of their roles in palaeo-ice sheet modelling and development. *Quaternary Science Reviews*, **135**, 103–114.

Kleiber, H. P., Knies, J., & Niessen, F. 2000. The Late Weichselian glaciation of the Franz Victoria Trough, northern Barents Sea: ice sheet extent and timing. *Marine Geology*, **168**(1), 25–44.

Knudsen, N., Yde, J., & Gasser, G. 2007. Suspended sediment transport in glacial meltwater during the initial quiescent phase after a major surge event at Kuannersuit Glacier, Greenland. *Geografisk Tidsskrift-Danish Journal of Geography*, **107**(1), 1–7.

Knutz, P. C., Sicre, M.-A., Ebbesen, H., Christiansen, S., & Kuijpers, A. 2011. Multiple-stage deglacial retreat of the southern Greenland Ice Sheet linked with Irminger Current warm water transport. *Paleoceanography*, **26**(3).

Koç, N., Klitgaard-Kristensen, D., Hasle, K., Forsberg, C.F., & Solheim, A. 2002. Late glacial palaeoceanography of Hinlopen Strait, northern Svalbard. *Polar Research*, **21**(2), 307–314.

Kohler, J., James, T. D., Murray, T.and Nuth, C.and Brandt O., Barrand, N., Aas, H., & Luckman, A. 2007. Acceleration in thinning rate on western Svalbard glaciers. *Geophysical Research Letters*, **34**(18).

Koide, M., Soutar, A., & Goldberg, E. D. 1972. Marine geochronology with ^{210}Pb. *Earth and Planetary Science Letters*, **14**(3), 442–446.

Kristensen, L., Benn, D., Hormes, A., & Ottesen, D. 2009. Mud aprons in front of Svalbard surge moraines: Evidence of subglacial deforming layers or proglacial glaciotectonics? *Geomorphology*, **111(3)**, 206–221.

Kubischta, F., Knudsen, K. L., Kaakinen, A., & Salonen, V.-P. 2010. Late quaternary foraminiferal record in Murchisonfjorden, Nordaustlandet, Svalbard. *Polar Research*, **29**(3), 283–297.

Kuenen, P. 1948. Slumping in the Carboniferous rocks of Pembrokeshire. *Quarterly Journal of the Geological Society*, **104**(1-4), 365–385.

Laberg, J., & Vorren, T. 1995. Late Weichselian submarine debris flow deposits on the Bear Island trough-mouth fan. *Marine Geology*, **127**(1), 45–72.

Lajeunesse, P. 2016. Long continuous dendritic eskers offshore of Southampton Island, northern Hudson Bay. *Pages 87–88 of:* Dowdeswell, J. A., Canals, M., Jakobsson, M., Todd, B. J., Dowdeswell, E. K., & Hogan, K. A. (eds), *Atlas of submarine glacial landforms*. Geological Society of London.

Landvik, J. 1994. The last glaciation of Germania Land and adjacent areas, northeast Greenland. *Journal of Quaternary Science*, **9**(1), 81–92.

Landvik, J., Bondevik, S., Elverhøi, A., Fjeldskaar, W., Mangerud, J., Salvigsen, O., Siegert, M. J., Svendsen, J.-I., & O., Vorren T. 1998. The last glacial maximum of Svalbard and the Barents Sea area: ice sheet extent and configuration. *Quaternary Science Reviews*, **17(1-3)**, 43–75.

Landvik, J., Brook, E., Gualtieri, L., Raisbeck, G., Salvigsen, O., & Yiou, F. 2003. Northwest Svalbard during the last glaciation: Ice-free areas existed. *Geology*, **31**(10), 905–908.

Landvik, J., Ingólfsson, Ó., Mienert, J., Lehman, S., Solheim, A., Elverhøi, A., & Ottesen, D. 2005. Rethinking Late Weichselian ice-sheet dynamics in coastal NW-Svalbard. *Boreas*, **34(1)**, 7–24.

Landvik, J. Y., Hjort, C., Mangerud, J., Moller, P., & Salvigsen, O. 1995. The Quaternary record of eastern Svalbard-an overview. *Polar Research*, **14**(2), 95–104.

Lane, T. P., Roberts, D. H., Rea, B. R., Ó Cofaigh, C., Vieli, A., & Rodés, A. 2014. Controls upon the Last Glacial maximum deglaciation of the northern Uummannaq ice stream system, West Greenland. *Quaternary Science Reviews*, **92**, 324–344.

Larsen, E., Longva, O., & Follestad, B. A. 1991. Formation of De Geer moraines and implications for deglaciation dynamics. *Journal of Quaternary Science*, **6**(4), 263–277.

Larsen, J., & Pulvertaft, T. 2000. *The structure of the Cretaceous-Palaeogene sedimentary-volcanic area of Svartenhuk Halvø, central West Greenland*. Vol. 188. Geological Survey of Denmark and Greenland, Ministry of Environment and Energy.

Lehman, S., & Forman, S. 1992. Late Weichselian glacier retreat in Kongsfjorden, west Spitsbergen, Svalbard. *Quaternary Research*, **37(2)**, 139–154.

Lemmen, D. S. 1990. Glaciomarine sedimentation in Disraeli Fiord, high arctic Canada. *Marine Geology*, **94**(1), 9–22.

Lewis, C. F. M., Blasco, S. M., Bornhold, B. D., Hunter, J. A. M., Judge, A. S., Kerr, J. W., McLaren, P., & Pelletier, B. R. 1977. Marine geological and geophysical activities in Lancaster Sound and adjacent fiords. *Current Research, Part A, Geological Survey of Canada, Paper*, 495–506.

Liestøl, O. 1969. Glacier surges in west Spitsbergen. *Canadian Journal of Earth Sciences*, **6**, 895–898.

Liestøl, O. 1988. The glaciers in the Kongsfjorden area, Spitsbergen. *Norske geografiske Tidsskrifter*, **42**, 231–238.

Linch, L. D., & Dowdeswell, J. A. 2016. Micromorphology of diamicton affected by iceberg-keel scouring, Scoresby Sund, East Greenland. *Quaternary Science Reviews*, **152**, 169–196.

Lloyd, J. 2006. Late Holocene environmental change in Disko Bugt, west Greenland: interaction between climate, ocean circulation and Jakobshavn Isbrae. *Boreas*, **35**, 35–49.

Lloyd, J., Park, L., Kuijpers, A., & Moros, M. 2005. Early Holocene palaeoceanography and deglacial chronology of Disko Bugt, West Greenland. *Quaternary Science Reviews*, **24**, 1741–1755.

Lloyd, J., Moros, M., Perner, K., Telford, R., Kuijpers, A., Jansen, E., & McCarthy, D. 2011. A 100 yr record of ocean temperature control on the stability of Jakobshavn Isbrae, West Greenland. *Geology*, **39(9)**, 867–870.

Long, A., & Roberts, D. 2003. Late Weichselian deglacial history of Disko Bugt, West Greenland, and the dynamics of the Jakobshavns Isbrae ice stream. *Boreas*, **32**(1), 208–226.

Long, A., Roberts, D., & Dawson, S. 2006. Early Holocene history of the west Greenland Ice Sheet and the GH-8.2 event. *Quaternary Science Reviews*, **25**(9), 904–922.

Long, A. J., Strzelecki, M. C., Lloyd, J. M., & Bryant, C. L. 2012. Dating High Arctic Holocene relative sea level changes using juvenile articulated marine shells in raised beaches. *Quaternary Science Reviews*, **48**, 61–66.

Lønne, I. 1997. Facies characteristics of a proglacial turbiditic sand-lobe at Svalbard. *Sedimentary Geology*, **109**(1), 13–35.

Lønne, I., & Mangerud, J. 1991. An Early or Middle Weichselian sequence of proglacial, shallow marine sediments on western Svalbard. *Boreas*, **20**(2), 85–104.

Lovell, H., Fleming, E. J., Benn, D. I., Hubbard, B., Lukas, S., Rea, B. R., Noormets, R., & Flink, A. E. 2015. Debris entrainment and landform genesis during tidewater glacier surges. *Journal of Geophysical Research: Earth Surface*, **120**(8), 1574–1595.

Lovell, T. V. 2000. As climate changes, so do glaciers. *Proceedings of the National Academy of Sciences of the United States of America*, **97**(4), 1351–1354.

Lundqvist, J. 1981. Moraine morphology. Terminological remarks and regional aspects. *Geografiska Annaler. Series A. Physical Geography*, 127–138.

Lundqvist, J. 2000. Palaeoseismicity and De Geer Moraines. *Quaternary International*, **68**, 175–186.

Mackiewicz, N., Powell, R., Carlson, P., & Molnia, B. 1984. Interlaminated ice-proximal glacimarine sediments in Muir Inlet, Alaska. *Marine Geology*, **57**(1-4), 113–147.

MacLachlan, S., Howe, J., & Vardy, M. 2010. Morphodynamic evolution of Kongsfjorden-Krossfjorden, Svalbard, during the Late Weichselian and the Holocene. *Geological Society London, Special Publications*, **344(1)**, 195–205.

MacLean, B., Blasco, S., Bennett, R., Hughes Clarke, J. E., & Patton, E. 2016. Mega-scale glacial lineations, Peel Sound, Canadian Arctic Archipelago. *Pages 47–48 of:* Dowdeswell, J. A., Canals, M., Jakobsson, M., Todd, B. J., Dowdeswell, E. K., & Hogan, K. A. (eds), *Atlas of submarine glacial landforms*. Geological Society Memoir, no. 46. The Geological Society London.

Mangerud, J., & Landvik, J. 2007. Younger Dryas cirque glaciers in western Spitsbergen: smaller than during the Little Ice Age. *Boreas*, **36(3)**, 278–285.

Mangerud, J., Bolstad, M., Elgersma, A., Helliksen, D., Landvik, J. Y., Lønne, I., Lycke, A. K., Salvigsen, O., Sandahl, T., & Svendsen, J. I. 1992. The last glacial maximum on Spitsbergen, Svalbard. *Quaternary Research*, **38**(1), 1–31.

Mangerud, J., Dokken, T., Hebbeln, D., Heggen, B., Ingólfsson, Ó., Landvik, J.Y., Mejdahl, V., J.I., Svendsen, & Vorren, T.O. 1998. Fluctuations of the Svalbard-Barents Sea Ice Sheet during the last 150 000 years. *Quaternary Science Reviews*, **17**, 11–42.

Mangerud, J.I. 1972. Radiocarbon dating of marine shells, including a discussion of apparent age of recent shells from Norway. *Boreas*, **1**, 143–172.

Marienfeld, P. 1991. Holozäne Sedimentationsentwicklung im Scoresby Sund, Ost–Grönland. **96**, 162.

Marienfeld, P. 1992. Postglacial sedimentary history of Scoresby Sund, East Greenland. *Polarforschung*, **60**(3), 181–195.

McCarthy, D. 2011. *Late Quaternary ice-ocean interactions in central West Greenland.* Ph.D. thesis, Department of Geography, University of Durham, UK.

McKee, B.A., Nittrouer, C.A., & DeMaster, D.J. 1983. Concepts of sediment deposition and accumulation applied to the continental shelf near the mouth of the Yangtze River. *Geology*, **11**, 631–633.

Meier, M., & Post, A. 1969. What are glacier surges? *Canadian Journal of Earth Sciences*, **6**, 807–817.

Meier, M., & Post, A. 1987. Fast tidewater glaciers. *Journal of Geophysical Research: Solid Earth*, **92**(B9), 9051–9058.

Mernild, S. H., Liston, G. E., Steffen, K., & Chylek, P. 2010. Meltwater flux and runoff modeling in the ablation area of Jakobshavn Isbræ, West Greenland. *Journal of Glaciology*, **56**(195), 20–32.

Møller, H., Jensen, K., Kuijpers, A., Aagaard-Sørensen, S., Seidenkrantz, M-S., Prins, M., Endler, R., & Mikkelsen, N. 2006. Late-Holocene environment and climatic changes in Ameralik Fjord, southwest Greenland: evidence from the sedimentary record. *The Holocene*, **16**(5), 685–695.

Moon, T., & Joughin, I. 2008. Changes in ice front position on Greenland's outlet glaciers from 1992 to 2007. *Journal of Geophysical Research: Earth Surface*, **113**(F2).

Moros, M., Kuijpers, A., Snowball, I., Lassen, S., Bäckström, D., Gingele, F., & McManus, J. 2002. Were glacial iceberg surges in the North Atlantic triggered by climatic warming? *Marine Geology*, **192**(4), 393–417.

Moros, M., Jensen, K., & Kuijpers, A. 2006. Mid-to late-Holocene hydrological and climatic variability in Disko Bugt, central West Greenland. *The Holocene*, **16**(3), 357–367.

Mugford, R. I., & Dowdeswell, J. A. 2010. Modeling iceberg-rafted sedimentation in high-latitude fjord environments. *Journal of Geophysical Research: Earth Surface*, **115**(F3).

Mugford, R. I., & Dowdeswell, J. A. 2011. Modeling glacial meltwater plume dynamics and sedimentation in high-latitude fjords. *Journal of Geophysical Research: Earth Surface*, **116**(F1).

Mulder, T., & Alexander, J. 2001. The physical character of subaqueous sedimentary density flows and their deposits. *Sedimentology*, **48**(2), 269–299.

Murray, T., Dowdeswell, J. A., Drewry, D. J., & Frearson, I. 1998. Geometric evolution and ice dynamics during a surge of Bakaninbreen, Svalbard. *Journal of Glaciology*, **44**(147), 263–374.

Nick, F., Vieli, A., Howat, I., & Joughin, I. 2009. Large-scale changes in Greenland outlet glacier dynamics triggered at the terminus. *Nature Geoscience*, **2**(2), 110–114.

Nielsen, T., Laier, T., Kuijpers, A., Rasmussen, T., Mikkelsen, N., & Nørgård-Pedersen, N. 2014. Fluid flow and methane ooccurrence in the Disko Bugt area offshore West Greenland: indications for gas hydrates? *Geo-Marine Letters*, **34**(6), 511–523.

Noormets, R., Kirchner, N., Flink, A. E., & Dowdeswell, J. A. 2016a. Possible iceberg-produced submarine terraces in Hambergbukta, Spitsbergen. *Pages 101–102 of:* Dowdeswell, J. A., Canals, M., Jakobsson, M., Todd, B. J., Dowdeswell, E. K., & Hogan, K. A. (eds), *Atlas of submarine glacial landforms.* Geological Society Memoir, no. 46. The Geological Society London.

Noormets, R., Kirchner, N., & Flink, A. E. 2016b. Submarine medial moraines in Hambergbukta, southeastern Spitsbergen. *Pages 61–62 of:* Dowdeswell, J. A., Canals, M., Jakobsson, M., Todd, B. J., Dowdeswell, E. K., & Hogan, K. A. (eds), *Atlas of submarine glacial landforms.* Geological Society Memoir, no. 46. The Geological Society London.

Ó Cofaigh, C. 1998. Geomorphic and sedimentary signatures of early Holocene deglaciation in High Arctic fiords, Ellesmere Island, Canada: implications for deglacial ice dynamics and thermal regime. *Canadian Journal of Earth Sciences*, **35**(4), 437–452.

Ó Cofaigh, C., & Dowdeswell, J. 2001. Laminated sediments in glacimarine environments: diagnostic criteria for their interpretation. *Quaternary Science Reviews*, **20**(13), 1411–1436.

Ó Cofaigh, C., Lemmen, D. S., Evans, D. J. A., & Bednarski, J. 1999. Glacial landform–sediment assemblages in the Canadian High Arctic and their implications for late Quaternary glaciation. *Annals of Glaciology*, **28**(1), 195–201.

Ó Cofaigh, C., Dowdeswell, J., & Grobe, H. 2001. Holocene glacimarine sedimentation, inner Scoresby Sund, East Greenland: the influence of fast-flowing ice-sheet outlet glaciers. *Marine Geology*, **175**(1), 103–129.

Ó Cofaigh, C., Dowdeswell, J., Allen, C., Hiemstra, J., Pudsey, C., Evans, J., & Evans, D. 2005. Flow dynamics and till genesis associated with a marine-based Antarctic paleo-ice stream. *Quaternary Science Reviews*, **24**(5-6), 709–740.

Ó Cofaigh, C., Dowdeswell, J. A., Evans, J., & Larter, R. D. 2008. Geological constraints on Antarctic palaeo-ice-stream retreat. *Earth Surface Processes and Landforms*, **33**(4), 513–525.

Ó Cofaigh, C., Dowdeswell, J., Jennings, A., Hogan, K., Kilfeather, A., Hiemstra, J., Noormets, R., Evans, J., McCarthy, D., Andrews, J., Lloyd, J., & Moros, M. 2013. An extensive and dynamic ice sheet on the West Greenland shelf during the last glacial cycle. *Geology*, **41**(2), 219–222.

Oerlemans, J., & Nick, F. 2006. Modelling the advance–retreat cycle of a tidewater glacier with simple sediment dynamics. *Global and Planetary Change*, **50**(3), 148–160.

O'Leary, M, & Christoffersen, P. 2013. Calving on tidewater glaciers amplified by submarine frontal melting. *The Cryosphere*, **7**(1), 119.

Ottesen, D., & Dowdeswell, J. 2006. Assemblages of submarine landforms produced by tidewater glaciers in Svalbard. *Journal of Geophysical Research*, **111**, F01016.

Ottesen, D., & Dowdeswell, J. 2009. An inter-ice stream glaciated margin: submarine landforms and a geomorphic model based on marine-geophysical data from Svalbard. *Geological Society of America Bulletin*, **121(11/12)**, 1647–1665.

Ottesen, D., Dowdeswell, J., & Rise, L. 2005. Submarine landforms and the reconstruction of fast-flowing ice streams within a large Quaternary ice sheet: the 2500-km-long Norwegian-Svalbard margin (57°– 80°N). *Geological Society of America Bulletin*, **117**, 1033–1050.

Ottesen, D., Dowdeswell, J., Landvik, J., & Mienert, J. 2007. Dynamics of the Late-Weichselian ice sheet on Svalbard inferred from high-resolution sea-floor morphology. *Boreas*, **36**, 286–306.

Ottesen, D., Dowdeswell, J., Benn, D., Kristensen, L., Christiansen, H., Christensen, O., & Vorren, T. 2008. Submarine landforms characteristic of glacier surges in two Spitsbergen fjords. *Quaternary Science Reviews*, **27(15)**, 1583–1599.

Patton, H., Andreassen, K., Bjarnadóttir, L. R., Dowdeswell, J. A., Winsborrow, M., Noormets, R., Polyak, L., Auriac, A., & Hubbard, A. 2015. Geophysical constraints on the dynamics and retreat of the Barents Sea ice sheet as a paleobenchmark for models of marine ice sheet deglaciation. *Reviews of Geophysics*, **53**(4), 1051–1098.

Perner, K., Moros, M., Snowball, I., Lloyd, J., Kuijpers, A., & Richter, T. 2013. Establishment of modern circulation patterns at c. 6000 cal a BP in Disko Bugt, central West Greenland: Opening of the Vaigat Strait. *Journal of Quaternary Science*, **28**(5), 480–489.

Pettersson, R. 2004. *Dynamics of the cold surface layer of polythermal Storglaciären.* Ph.D. thesis, Institutionen för naturgeografi och kvartärgeologi.

Pfirman, S., & Solheim, A. 1989. Subglacial meltwater discharge in the open-marine tidewater glacier environment: observations from Nordaustlandet, Svalbard archipelago. *Marine Geology*, **86**, 265–281.

Pfirman, S. L., Bauch, D., & Gammelsrød, T. 1994. The northern Barents Sea: water mass distribution and modification. *The polar oceans and their role in shaping the global environment*, 77–94.

Plassen, L., Vorren, T., & Forwick, M. 2004. Integrated acoustic and coring investigations of glacigenic deposits in Spitsbergen fjords. *Polar Research*, **23(1)**, 89–110.

Powell, R. 1981. A model for sedimentation by tidewater glaciers. *Annals of Glaciology*, **2**, 129–134.

Powell, R. 1990. Glacimarine processes at grounding-line fans and their growth to ice-contact deltas. *Geological Society, London, Special Publications*, **53**(1), 53–73.

Powell, R., & Molnia, B. 1989. Glacimarine sedimentary processes, facies and morphology of the south-southeast Alaska shelf and fjords. *Marine Geology*, **85**(2), 359–390.

Powell, R., Dawber, M., McInnes, J., & Pyne, A. 1996. Observations of the grounding-line area at a floating glacier terminus. *Annals of Glaciology*, **22**(1), 217–223.

Powell, R. D. 1991. Grounding-line systems as second-order controls on fluctuations of tidewater termini of temperate glaciers. *Geological Society of America Special Papers*, **261**, 75–94.

Powell, R. D., & Domack, E. 1995. Modern glaciomarine environments. *Glacial environments*, **1**, 445–486.

Prior, D. B., Bornhold, B. D., & Johns, M. W. 1984. Depositional characteristics of a submarine debris flow. *The Journal of Geology*, 707–727.

Rasch, M. 2000. Holocene relative sea-level changes in Disko Bugt, West Greenland. *Journal of Coastal Research*, **16**, 306–315.

Rasmussen, T. L., & Thomsen, E. 2013. Pink marine sediments reveal rapid ice melt and Arctic meltwater discharge during Dansgaard–Oeschger warmings. *Nature communications*, **4**.

Rasmussen, T. L., Forwick, M., & Mackensen, A. 2012. Reconstruction of inflow of Atlantic Water to Isfjorden, Svalbard during the Holocene: Correlation to climate and seasonality. *Marine Micropaleontology*, **94-95**, 80–90.

Raymond, C. 1987. How do glaciers surge? A review. *Journal of Geophysical Research: Solid Earth (1978-2012)*, **92(B9)**, 9121–9134.

Rebesco, M., Liu, Y., Camerlenghi, A., Winsborrow, M., Laberg, J. S., Caburlotto, A., Diviacco, P., Accettella, D., Sauli, C., Wardell, N., *et al.* 2011. Deglaciation of the western margin of the Barents Sea Ice Sheet – a swath bathymetric and sub-bottom seismic study from the Kveithola Trough. *Marine Geology*, **279**(1), 141–147.

Reimer, P., Bard, E., Bayliss, A., Beck, J., Blackwell, P., Ramsey, C., Buck, C., Cheng, H., Edwards, R., Friedrich, M., Grootes, P., Guilderson, T., Haflidason, H., Hajdas, I., Hatté, C., Heaton, T., Hoffmann, D., Hogg, A., Hughen, K., Kaiser, F., Kromer, B., Manning, S., Niu, M., Reimer, R., Richards, D., Scott, E., Southon, J., Staff, R., Turney, C., & van der Plicht, J. 2013. IntCal13 and Marine13 Radiocarbon Age Calibration Curves 0–50,000 Years cal BP. *Radiocarbon*, **55**(4), 1869–1887.

Ribergaard, M., & Buch, E. 2008. Oceanographic investigations off west Greenland 2007. *NAFO Scientific Council Documents*, **7**(003).

Rignot, E., & Kanagaratnam, P. 2006. Changes in the velocity structure of the Greenland Ice Sheet. *Science*, **311**(5763), 986–990.

Rignot, E., Koppes, M., & Velicogna, I. 2010. Rapid submarine melting of the calving faces of West Greenland glaciers. *Nature Geoscience*, **3**(3), 187–191.

Rignot, E, Fenty, I, Xu, Y, Cai, C, Velicogna, I, Cofaigh, C Ó, Dowdeswell, JA, Weinrebe, Wilhelm, Catania, G, & Duncan, D. 2016. Bathymetry data reveal glaciers vulnerable to ice-ocean interaction in Uummannaq and Vaigat glacial fjords, west Greenland. *Geophysical Research Letters*, **43**(6), 2667–2674.

Rinterknecht, V., Gorokhovich, Y., Schaefer, J., & Caffee, M. 2009. Preliminary ^{10}Be chronology for the last deglaciation of the western margin of the Greenland Ice Sheet. *Journal of Quaternary Science*, **24**(3), 270–278.

Robbins, J. A., & Edgington, D. N. 1975. Determination of recent sedimentation rates in Lake Michigan using Pb-210 and Cs-137. *Geochimica et Cosmochimica Acta*, **Acta 39**, 285–304.

Roberts, D., & Long, A. 2005. Streamlined bedrock terrain and fast ice flow, Jakobshavns Isbrae, West Greenland: implications for ice stream and ice sheet dynamics. *Boreas*, **34**(1), 25–42.

Robinson, S. 1993. Lithostratigraphic applications for magnetic susceptibility logging of deep-sea sediment cores: examples from ODP Leg 115. *Geological Society, London, Special Publications*, **70**(1), 65–98.

Rogers, J. N., Kelley, J. T., Belknap, D. F., Gontz, A., & Barnhardt, W. A. 2006. Shallow-water pockmark formation in temperate estuaries: a consideration of origins in the western gulf of Maine with special focus on Belfast Bay. *Marine Geology*, **225**(1), 45–62.

Roy, S., Senger, K., Braathen, A., Noormets, R., Hovland, M., & Olaussen, S. 2014. Fluid migration pathways to seafloor seepage in inner Isfjorden and Adventfjorden, Svalbard. *Norwegian Journal of Geology*, **94**, 99–119.

Roy, S., Hovland, M., Noormets, R., & Olaussen, S. 2015. Seepage in Isfjorden and its tributary fjords, West Spitsbergen. *Marine Geology*, **363**, 146–159.

Royer, T. C. 1983. Observations of the Alaska Coastal Current. *Pages 9–30 of: Coastal oceanography*. Springer.

Schumann, K., Völker, D., & Weinrebe, W. 2012. Acoustic mapping of the Ilulissat Ice Fjord mouth, west Greenland. *Quaternary Science Reviews*, **40**, 78–88.

Schytt, V. 1969. Some comments on glacier surges in eastern Svalbard. *Canadian Journal of Earth Sciences*, **6**(4), 867–873.

Seidenkrantz, M.-S., Aagaard-Sørensen, S., Sulsbrück, H., Kuijpers, A., Jensen, K., & Kunzendorf, H. 2007. Hydrography and climate of the last 4400 years in a SW Greenland fjord: implications for Labrador Sea palaeoceanography. *The Holocene*, **17**(3), 387–401.

Seidenkrantz, M.-S., Ebbesen, H., Aagaard-Sørensen, S., Moros, M., Lloyd, J., Olsen, J., Knudsen, M., & Kuijpers, A. 2013. Early Holocene large-scale meltwater discharge from Greenland documented by foraminifera and sediment parameters. *Palaeogeography, Palaeoclimatology, Palaeoecology*, **391**, 71–81.

Senger, K., Roy, S., Braathen, A., Buckley, S. J., Bælum, K., Gernigon, L., Mjelde, R., Noormets, R., Ogata, K., Olaussen, S., Planke, S., Ruud, B., & Tveranger, J. 2013. Geometries of doleritic intrusions in central Spitsbergen, Svalbard: an integrated study of an onshore-offshore magmatic province with implications for CO2 sequestration. **93**, 143–146.

Seramur, K. C., Powell, R. D., & Carlson, P. R. 1997. Evaluation of conditions along the grounding line of temperate marine glaciers: an example from Muir Inlet, Glacier Bay, Alaska. *Marine Geology*, **140**(3), 307–327.

Sevestre, H., & Benn, D. I. 2015. Climatic and geometric controls on the global distribution of surge-type glaciers: implications for a unifying model of surging. *Journal of Glaciology*, **61**(228), 646–662.

Sexton, D. J., Dowdeswell, J. A., Solheim, A., & Elverhøi, A. 1992. Seismic architecture and sedimentation in northwest Spitsbergen fjords. *Marine Geology*, **103**(1), 53–68.

Shanmugam, G., Lehtonen, L., Straume, T., Syvertsen, S., Hodgkinson, R., & Skibeli, M. 1994. Slump and debris-flow dominated upper slope facies in the Cretaceous of the Norwegian and

northern North Seas (61-67 N): Implications for sand distribution. *AAPG bulletin*, **78**(6), 910–937.

Sharp, M. 1984. Annual moraine ridges at Skálafellsjökull, south-east Iceland. *Journal of Glaciology*, **30**, 104.

Sharp, M. 1985. Crevasse-fill-ridges - a landform type characteristic of surging glaciers? *Geografiska Annaler. Series A. Physical Geography*, **67(3/4)**, 213–220.

Sharp, M. 1988. Surging glaciers: behaviour and mechanisms. *Progress in Physical Geography*, **12(3)**, 349–370.

Sharp, M., Jouzel, J., Hubbard, B., & Lawson, W. 1994. The character, structure and origin of the basal ice layer of a surge-type glacier. *Journal of Glaciology*, **40**(135), 327–340.

Shaw, J. 2003. Submarine moraines in Newfoundland coastal waters: implications for the deglaciation of Newfoundland and adjacent areas. *Quaternary International*, **99–100**, 115–134.

Shaw, J., Grant, D. R., Guilbault, J.-P., Anderson, T. W., & Parrott, D. R. 2000. Submarine and onshore end moraines in southern Newfoundland: implications for the history of late Wisconsinan ice retreat. *Boreas*, **29**(4), 295–314.

Sheldon, C., Jennings, A., Andrews, J., Ó Cofaigh, C., Hogan, K., Dowdeswell, J., & Seidenkrantz, M-S. 2016. Ice stream retreat following the LGM and onset of the west Greenland current in Uummannaq Trough, west Greenland. *Quaternary Science Reviews*, **147**, 27–46.

Ślubowska, M. A., Koç, N., Rasmussen, T. L., & Klitgaard-Kristensen, D. 2005. Changes in the flow of Atlantic water into the Arctic Ocean since the last deglaciation: evidence from the northern Svalbard continental margin, 80° N. *Paleoceanography*, **20**(4).

Ślubowska-Woldengen, M., Rasmussen, T., Koç, N., Klitgaard-Kristensen, D., Nilsen, F., & Solheim, A. 2007. Advection of Atlantic Water to the western and northern Svalbard shelf since 17,500 cal yr BP. *Quaternary Science Reviews*, **26**(3-4), 463–478.

Smith, A. M. 1997. Basal conditions on Rutford ice stream, West Antarctica, from seismic observations. *Journal of Geophysical Research: Solid Earth*, **102**(B1), 543–552.

Smith, L. M., & Andrews, J. T. 2000. Sediment characteristics in iceberg dominated fjords, Kangerlussuaq region, East Greenland. *Sedimentary Geology*, **130**(1), 11–25.

Solheim, A. 1986. Submarine evidence of glacier surges. *Polar Research*, **4**(1), 91–95.

Solheim, A. 1991. The depositional environment of surging sub-polar tidewater glaciers. *Norsk Polarinstitutt Skrifter*, **194**, 1–97.

Solheim, A. 1997. Depth-dependent iceberg plough marks in the Barents Sea. *Pages 138–139 of:* Davies, T. A., Bell, T., Cooper, A. K., Josenhans, H., Polyak, L., Solheim, A., Stoker, M. S., & Stravers, J. A. (eds), *Glaciated Continental Margins*. Springer.

Solheim, A., & Pfirman, S. 1985. Sea-floor morphology outside a grounded, surging glacier; Bråsvellbreen, Svalbard. *Marine Geology*, **65**, 127–143.

Sollid, J. L. 1989. Comments on the genesis of De Geer moraines. *Norsk Geografisk Tidsskrift-Norwegian Journal of Geography*, **43**(1), 45–47.

Spagnolo, M., Clark, C., Hughes, A., Dunlop, P., & Stokes, C. 2010. The planar shape of drumlins. *Sedimentary Geology*, **232**(3–4), 119–129.

Stevens, R. 1990. Proximal and distal glacimarine deposits in southwestern Sweden: contrasts in sedimentation. *Geological Society, London, Special Publications*, **53**(1), 307–316.

Stewart, F. S., & Stoker, M. S. 1990. Problems Associated with Seismic Facies Analysis of Diamicton-Dominated, Shelf Glacigenic Sequences. *Geo-Marine Letters*, **10**, 151–156.

Stokes, C., & Clark, C. 2002. Are long subglacial bedforms indicative of fast ice flow? *Boreas*, **31(3)**, 239–249.

Stokes, C., Spagnolo, M., & Clark, C. 2011. The composition and internal structure of drumlins: complexity, commonality, and implications for a unifying theory of their formation. *Earth-Science Reviews*, **107**(3), 398–422.

Stokes, C. R., Clark, C. D., Lian, O. B., & Tulaczyk, S. 2007. Ice stream sticky spots: a review of their identification and influence beneath contemporary and palaeo-ice streams. *Earth-Science Reviews*, **81**(3), 217–249.

Stokes, C. R., Tarasov, L., Blomdin, R., Cronin, T. M., Fisher, T. G., Gyllencreutz, R., Hättestrand, C., Heyman, J., Hindmarsh, R. C. A., Hughes, A. L. C., Jakobsson, M., Kirchner, N., Livingstone, S., Margold, M., Murton, J. B., Noormets, R., Peltier, W. R., Peteet, D. M., Piper, D. J. W., Preussner, F.and Renssen, H., Roberts, D. H., Roche, D. R., SaintAnge, F., Stroeven, A. P., & Teller, J. T. 2015. On the reconstruction of palaeo-ice sheets: recent advances and future challenges. *Quaternary Science Reviews*, **125**, 15–49.

Stow, D. A. V., & Shanmugam, G. 1980. Sequence of structures in fine-grained turbidites: comparison of recent deep-sea and ancient flysch sediments. *Sedimentary Geology*, **25**(1-2), 23–42.

Straneo, F., & Heimbach, P. 2013. North Atlantic warming and the retreat of Greenland's outlet glaciers. *Nature*, **504**(7478), 36–43.

Straneo, F., Hamilton, G., Sutherland, D., Stearns, L., Davidson, F., Hammill, M., Stenson, G., & Rosing-Asvid, A. 2010. Rapid circulation of warm subtropical waters in a major glacial fjord in East Greenland. *Nature Geoscience Letters*, **3**, 182–186.

Streuff, K. 2013. *Landform assemblages in inner Kongsfjorden, Svalbard: Evidence of recent glacial (surge) activity.* M.Phil. thesis, University of Tromsø.

Streuff, K., Forwick, M., Szczuciński, W., Andreassen, K., & Ó Cofaigh, C. 2015. Landform assemblages in inner Kongsfjorden, Svalbard: evidence of recent glacial (surge) activity. *Arktos*, **1**(1).

Streuff, K., Ó Cofaigh, C., Noormets, R., & Lloyd, J. 2017. Submarine landforms and glacimarine sedimentary processes in Lomfjorden, east Spitsbergen. *Marine Geology*.

Streuff, K., Ó Cofaigh, C., Noormets, R., & Lloyd, J. subm.. Submarine landform assemblages and sedimentary processes in front of Spitsbergen tidewater glaciers. *Marine Geology Special Publications*.

Strömberg, B. 1965. Mappings and geochronological investigations in some moraine areas of south-central Sweden. *Geografiska Annaler. Series A, Physical Geography*, **47**(2), 73–82.

Stuiver, M., & Reimer, P. 1993. Extended ^{14}C data base and revised Calib 3.0 ^{14}C age calibration program. *Radiocarbon*.

Svendsen, H., Beszczynska-Møller, A., Hagen, J., Lefauconnier, B., Tverberg, V., Gerland, S., Ørbæk, J. B., Bischof, K., Papucci, C., Zajaczkowski, M., Azzolini, R., Bruland, O., Wiencke, C., Winther, J.-G., & Dallmann, W. 2002. The physical environment of Kongsfjorden-Krossfjorden, an Arctic fjord system in Svalbard. *Polar Research*, **21(1)**, 133–166.

Svendsen, J. I., & Mangerud, J. 1992. Paleoclimatic inferences from glacial fluctuations on Svalbard during the last 20 000 years. *Climate Dynamics*, **6**(3-4), 213–220.

Svendsen, J. I., Astakhov, V. I., Bolshiyanov, D. Y., Demidov, I., Dowdeswell, J. A., Gataullin, V., Hjort, C., Hubberten, H. W., Larsen, E., Mangerud, J., Melles, M., Möller, P., Saarnisto, M., & Siegert, M. J. 1999. Maximum extent of the Eurasian ice sheets in the Barents and Kara Sea region during the Weichselian. *Boreas*, **28**(1), 234–242.

Svendsen, J. I., Gataullin, V., Mangerud, J., & Polyak, L. 2004. The glacial history of the Barents and Kara Sea region. *Developments in Quaternary Sciences*, **2**, 369–378.

Svendsen, J.I., Mangerud, J., Elverhøi, A., Solheim, A., & Schüttenhelm, R. 1992. The Late Weichselian glacial maximum on western Spitsbergen inferred from offshore sediment cores. *Marine Geology*, **104**(1–4), 1–17.

Svendsen, J.I., Elverhøi, A., & Mangerud, J. 1996. The retreat of the Barents Sea Ice Sheet on the western Svalbard margin. *Boreas*, **25**(4), 244–256.

Syvitski, J., & Murray, J. 1981. Particle interaction in fjord-suspended sediment. *Marine Geology*, **39**(3), 215–242.

Syvitski, J. P. 1997. Water-escape sea floor depressions. *Pages 160–161 of: Glaciated Continental Margins*. Springer.

Syvitski, J. P. M. 1989. On the deposition of sediment within glacier-influenced fjords: oceanographic controls. *Marine Geology*, **85**(2), 301–329.

Syvitski, J. P. M. 1993. Glaciomarine environments in Canada: an overview. *Canadian Journal of Earth Sciences*, **30**(2), 354–371.

Syvitski, J. P. M., & Hein, F. J. 1991. *Sedimentology of an Arctic Basin: Itirbilung Fiord, Baffin Island, Northwest Territories*. Geological Survey of Canada.

Syvitski, J. P. M., & Shaw, J. 1995. Sedimentology and geomorphology of fjords. *Developments in sedimentology*, **53**, 113–178.

Syvitski, J. P. M., Farrow, G. E., Atkinson, R. J. A., Moore, P. G., & Andrews, J. T. 1989. Baffin Island fjord macrobenthos: bottom communities and environmental significance. *Arctic*, 232–247.

Syvitski, J.P.M., Andrews, J.T., & Dowdeswell, J.A. 1996. Sediment deposition in an iceberg-dominated glacimarine environment, East Greenland: basin fill implications. *Global and Planetary Change*, **12**, 251–270.

Szczuciński, W., & Zajaczkowski, M. 2012. Factors controlling downward fluxes of particulate matter in glacier-contact and non-glacier contact settings in a subpolar fjord (Billefjorden, Svalbard). *International Association of Sedimentology, Special Publication*, **44**, 369–386.

Szczuciński, W., Zajaczkowski, M., & Scholten, J. 2009. Sediment accumulation rates in subpolar fjords – impact of post-Little Ice Age glacier retreat, Billefjorden, Svalbard. *Estuarine, Coastal and Shelf Science*, **85**, 345–356.

Thomas, R, Frederick, E, Krabill, W, Manizade, S, & Martin, C. 2009. Recent changes on Greenland outlet glaciers. *Journal of Glaciology*, **55**(189), 147–162.

Thompson, T. G., & Barkey, K. T. 1938. Observations on fjord waters. *EOS Archives: Earth & Space Science News*, **19**.

Trusel, L., Powell, R., Cumpston, R., & Brigham-Grette, J. 2010. Modern glacimarine processes and potential future behaviour of Kronebreen and Kongsvegen polythermal tidewater glaciers, Kongsfjorden, Svalbard. *Geological Society of London Special Publications*, **344**, 89–102.

Tulaczyk, S., Scherer, R., & Clark, C. 2001. A ploughing model for the origin of weak tills beneath ice streams: a qualitative treatment. *Quaternary Internationals*, **86**, 59–70.

Van der Veen, C. J. 1999. Crevasses on glaciers 1. *Polar Geography*, **23**(3), 213–245.

Vaughan, D. G., Corr, H. F. J., Bindschadler, R. A., Dutrieux, P., Gudmundsson, G. H., Jenkins, A., Newman, T., Vornberger, P., & Wingham, D. J. 2012. Subglacial melt channels and fracture in the floating part of Pine Island Glacier, Antarctica. *Journal of Geophysical Research: Earth Surface*, **117**(F3).

Velle, J. 2012. *Holocene sedimentary environments in Smeerenburgfjorden, Spitsbergen.* M.Phil. thesis, University of Tromsø.

Vorren, T. O., Hald, M., Edvardsen, M., & Lind-Hansen, O. W. 1983. Glacigenic sediments and sedimentary environments on continental shelves: general principles with a case study from the Norwegian shelf. *Glacial Deposits in North-West Europe. Balkema, Rotterdam*, 61–73.

Walder, J., & Hallet, B. 1979. Geometry of former subglacial water channels and cavities. *Journal of Glaciology*, **23**(89), 335–346.

Warren, C. R. 1991. Terminal environment, topographic control and fluctuations of West Greenland glaciers. *Boreas*, **20**(1), 1–15.

Warren, C. R., & Glasser, N. F. 1992. Contrasting response of South Greenland glaciers to recent climatic change. *Arctic and Alpine Research*, 124–132.

Weidick, A. 1968. Observations on some Holocene glacier fluctuations in West Greenland. *Meddelelser on Grønland*, **165**(6), 202.

Weidick, A. 1994. Historical fluctuations of calving glaciers in south and West Greenland. *Rapport Grønlands Geologiske Undersølgelse*, **161**, 73–79.

Weidick, A. 1996. *The Paleo-Eskimo Cultures of Greenland. New Perspectives in Greenlandic Archaeology.* Danish Polar Center, Copenhagen. Chap. Neoglacial changes of ice cover and sea level in Greenland–a classical enigma, pages 257–270.

Weidick, A., & Bennike, O. 2007. Quaternary glaciation history and glaciology of Jakobshavn Isbræ and the Disko Bugt region, West Greenland: a review. *Geological Survey of Denmark and Greenland Bulletin*, **14**, 13.

Wilson, L. J., & Austin, W. E. N. 2002. Millennial and sub-millennial-scale variability in sediment colour from the Barra Fan, NW Scotland: implications for British ice sheet dynamics. *Glacier-Influenced Sedimentation on High-Latitude Continental Margins. Geological Society of London, Special Publications*, **203**, 349–365.

Winsborrow, M. C. M., Andreassen, K., Corner, G. D., & Laberg, J. S. 2010. Deglaciation of a marine-based ice sheet: Late Weichselian palaeo-ice dynamics and retreat in the southern Barents Sea reconstructed from onshore and offshore glacial geomorphology. *Quaternary Science Reviews*, **29**(3), 424–442.

Woodworth-Lynas, C. M. T., & Guigné, J. Y. 1990. Iceberg scours in the geological record: examples from glacial Lake Agassiz. *Geological Society, London, Special Publications*, **53**(1), 217–233.

Young, N., Briner, J., Axford, Y., Csatho, B., Babonis, G., Rood, D., & Finkel, R. 2011a. Response of a marine-terminating Greenland outlet glacier to abrupt cooling 8200 and 9300 years ago. *Geophysical Research Letters*, **38**(24).

Young, N., Briner, J., Stewart, H., Axford, Y., Csatho, B., Rood, D., & Finkel, R. 2011b. Response of Jakobshavn Isbræ, Greenland, to Holocene climate change. *Geology*, **39**(2), 131–134.

Young, N., Briner, J., Rood, D., Finkel, R., Corbett, L., & Bierman, P. 2013. Age of the Fjord Stade moraines in the Disko Bugt region, western Greenland, and the 9.3 and 8.2 ka cooling events. *Quaternary Science Reviews*, **60**, 76–90.

Zaborska, A., Pempkowiak, J., & Papucci, C. 2006. Some sediment characteristics and sedimentation rates in an Arctic fjord (Kongsfjorden, Svalbard). *Annual Environmental Protection*, **8**, 79–96.

Zajaczkowski, M., Szczuciński, W., & Bojanowski, R. 2004. Recent changes in sediment accumulation rates in Adventfjorden, Svalbard. *Oceanologia*, **46**, 217–231.

Zilliacus, H. 1989. Genesis of De Geer moraines in Finland. *Sedimentary geology*, **62**(2), 309–317.

Zwally, H., Abdalati, W., Herring, T., Larson, K., Saba, J., & Steffen, K. 2002. Surface melt-induced acceleration of Greenland ice-sheet flow. *Science*, **297**(5579), 218–222.